

**Economic and Environmental Assessment of Large-scale Electro-chemical
and Flywheel Energy Storage Systems for Stationary Applications**

by

Md Mustafizur Rahman

A thesis submitted in partial fulfillment of the requirements for the degree of

Doctor of Philosophy

in

Engineering Management

Department of Mechanical Engineering
University of Alberta

© Md Mustafizur Rahman, 2022

Abstract

There are few cost and environmental feasibility assessments of energy storage systems for utility-scale applications. The development of techno-economic and environmental performance indicators is crucial to make an informed decision on future development and deployment of energy storage technologies. This thesis aims to address the knowledge and literature gaps in economic and environmental aspects of energy storage systems for stationary applications. Scientific principles-based techno-economic and life cycle assessment models were developed for seven energy storage technologies: sodium-sulfur (Na-S), lithium-ion (Li-ion), valve-regulated lead-acid (VRLA), nickel-cadmium (Ni-Cd), vanadium redox flow (VRF), steel rotor flywheel, and composite rotor flywheel. Four stationary application scenarios were evaluated. These are bulk energy storage, transmission and distribution investment deferral, frequency regulation, and support of voltage regulation. With the rapidly growing number of electric vehicles, vehicle-to-grid (V2G) technology can play an important role in stabilizing electricity grids. An assessment is necessary to develop performance metrics for the V2G system and compare it with stationary energy storage systems. Therefore, a special case for an electro-chemical energy storage system, V2G, was investigated to evaluate its techno-economic feasibility in Canadian weather conditions. The system components were designed in such a way that the power and energy of each application scenario are met. Then, cost functions were developed, followed by estimation of the life cycle cost and the levelized cost of storage (LCOS). The environmental assessment involves building material and energy inventories and translating them to net energy ratio (NER) and life cycle greenhouse gas (GHG) emissions values.

The LCOS ranges from \$199-\$941/MWh for the Na-S, \$180-\$1032/MWh for the Li-ion, \$410-\$1184/MWh for the VRLA, \$802-\$1991/MWh for the Ni-Cd, and \$267-\$3794/MWh for the VRF, depending on the application scenario. The life cycle GHG emissions range from 715-784 kg-CO₂eq/MWh for Na-S, 625-659 kg-CO₂eq/MWh for Li-ion, 749-803 kg-CO₂eq/MWh for VRLA, 742-806 kg-CO₂eq/MWh for Ni-Cd, and 800-963 kg-CO₂eq/MWh for VRF. Because they have a longer cycle life, lower capital cost, and higher energy density, Li-ion and Na-S energy storage systems outperform other battery storage technologies.

The composite rotor flywheel has a higher LCOS (\$189.94/MWh) than the steel rotor flywheel (\$146.41/MWh), mainly due to the higher composite material cost compared to steel. However, with respect to the life cycle GHG emissions, the composite rotor flywheel has a higher performance (48.9-95.0 kg-CO₂eq/MWh) than the steel rotor (75.2-121.4 kg-CO₂eq/MWh), mainly due to the higher operational energy consumption in the steel rotor flywheel to compensate for the frictional loss.

In the techno-economic assessment of the V2G system, the weather conditions in four Canadian provinces were considered. The LCOS values for the V2G system range from \$176.97/MWh in Quebec to \$233.08/MWh in Ontario when it is used for energy arbitrage. When the V2G system is used for frequency regulation, the LCOS values range from \$271.42/MWh in Quebec to \$329.93/MWh in Ontario. The LCOS varies by province mainly because of differences in electricity prices and average ambient temperatures.

The framework developed in this research can be used for assessment of other energy pathways. Insights from the study will help industry and electric utility companies understand the economic and environmental performances of electro-chemical and flywheel energy storage systems and ultimately help them make informed policy and investment decisions.

Preface

This thesis is an original intellectual work by Md Mustafizur Rahman under the supervision of Dr. Amit Kumar.

Chapter 2 of this thesis is a combination of a review paper and a book chapter. Sections 2.1-2.4 and 2.6-2.7 have been published as Rahman MM, Oni AO, Gemechu E, Kumar A. Assessment of energy storage technologies: A review. *Energy Conversion and Management*. 2020, 223:113295. Section 2.5 is based on Rahman MM, Oni AO, Gemechu E, Kumar A. Environmental impact assessments of compressed air energy storage systems: A review. In: Fokaides PA, Morsink-Georgali PZ, Kylili Angeliki, editors. *Environmental Assessment of Renewable Energy Conversion Technologies*, Elsevier Inc., Amsterdam, The Netherlands, 2022. I am the principal author of these publications; AO Oni, E Gemechu, and A Kumar provided intellectual guidance and support with the manuscript composition.

Chapter 3 has been published as Rahman MM, Oni AO, Gemechu E, Kumar A. The development of techno-economic models for the assessment of utility-scale electro-chemical battery storage systems. *Applied Energy*. 2021, 283:116343. I was responsible for conceptualization, methodology, investigation, validation, and writing the original draft. AO Oni and E Gemechu validated the results and reviewed the manuscript. A Kumar was the supervisory author and was involved with funding acquisition and conceptualization.

Chapter 4 has been published as Rahman MM, Gemechu E, Oni AO, Kumar A. The greenhouse gas emissions' footprint and net energy ratio of utility-scale electro-chemical energy storage systems. *Energy Conversion and Management*. 2021, 244:114497. I was responsible for conceptualization, methodology, model development, formal analysis, validation, and writing the

original draft. E Gemechu and AO Oni were involved in validation and writing (reviewing and editing). A Kumar provided supervisory oversight and intellectual guidance with model development and manuscript composition.

Chapter 5 has been published as Rahman MM, Gemechu E, Oni AO, Kumar A. The development of a techno-economic model for the assessment of the cost of flywheel energy storage systems for utility-scale stationary applications. *Sustainable Energy Technologies and Assessments*. 2021, 47:101382. I am the principal author and was responsible for conceptualization, methodology, model development, formal analysis, validation, and writing the original draft. E Gemechu, AO Oni, and A Kumar provided intellectual guidance and support with the manuscript composition.

Chapter 6 has been published as Rahman MM, Gemechu E, Oni AO, Kumar A. Energy and environmental footprints of flywheels for utility-scale energy storage applications. *e-Prime*, 2021, 1:100020. I was responsible for concept formulation, data collection and model development, model validation, and writing the original draft. E Gemechu and AO Oni were involved in model validation, and manuscript review and editing. A Kumar contributed by reviewing the results and editing the manuscript.

Chapter 7 has been submitted as Rahman MM, Gemechu E, Oni AO, Kumar A. The development of a techno-economic model for assessment of cost of energy storage for vehicle-to-grid applications in a cold climate to Energy. I was responsible for conceptualization, methodology, model development, formal analysis, validation, and writing the original draft. E Gemechu and AO Oni contributed by reviewing and editing the manuscript. A Kumar was the supervising author and was involved in concept development and the review of the manuscript.

This thesis is dedicated
to my parents, Md. Sakendar Ali and Zinnate Zahan Moslima Khatun,
my wife, Nafisa Ashraf, my son, Ayman Nusair,
and my sister, Sika Mustaki,
for their unconditional love, belief, support, and encouragement

Acknowledgements

First, I would like to thank God Almighty for affording me the health, intellect, and fortitude required to conduct this research. I would like to express my sincere gratitude to my supervisor, Dr. Amit Kumar, for his mentorship and guidance throughout this research. My Ph.D. thesis would not have been accomplished without his invaluable supervision that helped to achieve my research goals. Dr. Kumar made an indelible mark on me as a student, and I regard our relationship to be a life-long gift. I would like to thank my supervisory committee members, Dr. Yunwei (Ryan) Li and Dr. Ge Li, for their insightful comments and questions, which helped me to broaden my research from various perspectives.

I would like to acknowledge the NSERC Energy Storage Technology (NEST) Network, the University of Alberta, the NSERC/Cenovus/Alberta Innovates Associate Industrial Research Chair in Energy and Environmental Systems Engineering, and the Cenovus Energy Endowed Chair in Environmental Engineering for the financial support provided to carry out this research.

I would like to thank Dr. Eskinder Gemechu and Dr. Abayomi Olufemi Oni for providing intellectual guidance and support throughout this research. I appreciate their efforts in reviewing the research models and the manuscripts. I am thankful to Astrid Blodgett for editing my research papers and the thesis. Many thanks to Caitlin Aspland for her support in administrative matters. I am also grateful to Gail Dowler for helping me with administrative information at different stages of my graduate program. I would like to acknowledge my colleagues in the Sustainable Energy Research Group (SERG) for their support.

I would like to convey sincere appreciation to the University of Alberta Sustainability Scholar Council and Lafarge Canada Inc. for giving me the first professional exposure to work and contribute to the Canadian energy sector. Special thanks to William Gowdy, my mentor at Lafarge, for providing me with insightful suggestions and helpful advice during my internship as a Sustainability Scholar.

I would like to extend my sincerest gratitude towards my parents, Md. Sakendar Ali and Zinnate Zahan Moslima Khatun, and my in-laws, Md. Ashraful Alam and Nadira Sultana, for their belief in me and endless prayers. To my dearest wife, Nafisa Ashraf, thank you for your unending love and support, for all the late nights and early mornings. Thanks for all the delicious food you made for me. Most of all, thank you for being my best friend. I owe you everything. The best gift of my life, my son, Ayman Nusair, thanks for being such an awesome kid. Special thanks to my younger sister, Sika Mustaki, for sending me festival gifts over the last four years. I would like to acknowledge my uncles Dr. Md. Afsar Siddiquee, Md. Ali Reza Siddiquee, and Md. Ahsan Kibria Siddiquee for encouraging me to pursue my higher studies abroad and fulfill my dreams.

Table of contents

Abstract.....	ii
Preface.....	iv
Acknowledgements.....	vii
Table of contents.....	ix
List of tables.....	xiv
List of figures.....	xvi
List of abbreviations	xix
Chapter 1: Introduction.....	1
1.1. Background.....	1
1.2. Literature review and research gap.....	4
1.3. Research motivation.....	9
1.4. Research objectives.....	10
1.5. Scope and limitations of the thesis.....	11
1.6. Organization of the thesis	12
Chapter 2: Assessment of energy storage technologies: A review.....	14
2.1. Introduction.....	14
2.2. An overview of energy storage technologies.....	17
2.2.1. Mechanical storage.....	21
2.2.2. Electro-chemical storage.....	22
2.2.3. Hydrogen and thermal storage	24
2.3. Review of the techno-economic assessments of energy storage technologies	28
2.3.1. Cost models.....	28
2.3.2. Economic performance of various ESSs.....	32
2.3.2.1. Mechanical storage	32
2.3.2.2. Electro-chemical storage	42
2.3.2.3. Hydrogen storage	55
2.3.2.4. Thermal storage.....	56
2.3.3. Future cost estimates.....	62
2.4. Review of the life cycle assessments of energy storage technologies.....	63

2.4.1. Goal and scope definition.....	63
2.4.2. Inventory analysis	66
2.4.3. Impact assessment.....	68
2.5. Land footprint of energy storage systems.....	99
2.6. Identified gaps and recommendations	100
2.6.1. Economy of scale	100
2.6.2. Consistency in cost estimation	101
2.6.3. LCA system boundary and data sources	101
2.6.4. Need for uncertainty analysis.....	102
2.6.5. LCA of emerging energy storage technologies.....	103
2.7. Conclusion	104
Chapter 3: The development of techno-economic models for the assessment of utility-scale electro-chemical battery storage systems.....	106
3.1. Introduction.....	106
3.2. Model development	110
3.2.1. Modeling approach.....	110
3.2.1.1. Stationary application scenario development.....	113
3.2.1.2. System boundary and sizing	114
3.2.1.3. Techno-economic model.....	121
3.2.1.4. Sensitivity and uncertainty analyses.....	125
3.3. Results and discussion	125
3.3.1. Technical analysis	125
3.3.2. Economic analysis.....	129
3.3.3. The effect of discharge duration on the TIC and LCOS	134
3.3.4. Sensitivity and uncertainty analyses	135
3.3.5. Comparison with other energy storage technologies	141
3.4. Conclusion	143
Chapter 4: The greenhouse gas emissions' footprint and net energy ratio of utility-scale electro-chemical energy storage systems.....	146
4.1. Introduction.....	146
4.2. Method.....	150

4.2.1. Application scenario development	151
4.2.2. System design.....	153
4.2.3. Life cycle assessment.....	155
4.2.3.1. Goal and scope definition.....	155
4.2.3.2. Inventory analysis	156
4.2.3.2.1. Material production	156
4.2.3.2.2. Manufacturing	159
4.2.3.2.3. Operation.....	161
4.2.3.2.4. End-of-life (EOL).....	161
4.2.3.2.5. Transportation	162
4.2.3.4. Sensitivity and uncertainty analyses	163
4.3. Results and discussion	164
4.3.1. Net energy ratio (NER)	164
4.3.2. Life cycle GHG emissions	167
4.3.3. Sensitivity and uncertainty analyses	173
4.4. Conclusion	178
Chapter 5: The development of a techno-economic model for the assessment of the cost of flywheel energy storage systems for utility-scale stationary applications.....	179
5.1. Introduction.....	179
5.2. Modeling method.....	184
5.2.1. Input parameter categorization.....	186
5.2.2. System design and sizing	186
5.2.3. Components' cost development	191
5.2.4. Cost estimation.....	193
5.2.5. Sensitivity and uncertainty analyses	196
5.3. Results and discussion	198
5.3.1. Total investment cost (TIC)	198
5.3.2. Annual life cycle cost (ALCC).....	200
5.3.3. Levelized cost of storage (LCOS).....	202
5.3.4. Sensitivity and uncertainty analyses	207
5.4. Conclusion	212

Chapter 6: Energy and environmental footprints of flywheels for utility-scale energy storage applications	214
6.1. Introduction.....	214
6.2. Modeling method.....	218
6.2.1. Goal and scope	219
6.2.1.1. FES system description	222
6.2.2. System design.....	223
6.2.3. Inventory analysis	225
6.2.3.1. Material production.....	225
6.2.3.2. Manufacturing.....	229
6.2.3.3. Operation	233
6.2.3.4. End-of-life	233
6.2.3.5. Transportation.....	234
6.2.4. Sensitivity and uncertainty analyses	235
6.3. Results and discussion	235
6.3.1. Net energy ratio.....	236
6.3.2. Life cycle GHG emissions	238
6.3.3. Sensitivity and uncertainty analyses	243
6.4. Conclusion	247
Chapter 7: The development of a techno-economic model for assessment of cost of energy storage for vehicle-to-grid applications in a cold climate	249
7.1. Introduction.....	249
7.2. Methods.....	253
7.2.1. Vehicle-to-grid technical analysis.....	255
7.2.2. Cost estimation.....	259
7.2.3. Techno-economic model development	262
7.3. Results and discussion	264
7.3.1. Economic analysis.....	265
7.3.2. Effect of ambient temperature on available energy	269
7.3.3. Sensitivity and uncertainty analyses' results.....	271
7.4. Conclusion	273

Chapter 8: Conclusions and recommendations for future research	276
8.1. Conclusions.....	276
8.1.1. Techno-economic and life cycle assessment of electro-chemical energy storage systems	277
8.1.2. Techno-economic and life cycle assessment of flywheel energy storage systems	280
8.1.3. Assessment of vehicle-to-grid systems	283
8.2. Recommendations for future work	285
8.2.1. Assessment of alternative and emerging energy storage systems.....	285
8.2.2. Life cycle assessment model enhancement.....	286
8.2.3. Life cycle sustainability assessment.....	286
8.2.4. Assessment of second-life batteries	286
8.2.5. Techno-economic model enhancement.....	287
Bibliography	288
Appendix A.....	341
Appendix B	351
Appendix C	368
Appendix D.....	386
Appendix E	388
List of publications	396

List of tables

Table 2.1: Rated installed capacity (GW) and number of projects for various energy storage technologies around the world [12]	19
Table 2.2: Number of projects in operation by storage type for different services [12].....	20
Table 2.3: Technical parameters of different energy storage technologies	26
Table 2.4: Cost items of various energy storage systems [24, 25, 28, 69, 94, 105, 176, 184-194]	31
Table 2.5: A summary of TEAs of mechanical storage systems	35
Table 2.6: A summary of TEAs of electro-chemical storage systems.....	44
Table 2.7: A summary of TEAs of hydrogen and thermal storage systems	57
Table 2.8: A summary of LCAs of energy storage technologies.....	74
Table 2.9: Land footprint of different energy storage technologies	100
Table 3.1: Scenario assumptions.....	114
Table 3.2: Technical parameters used to design the storage systems	117
Table 3.3: Technical and cost inputs used for the VRF battery system.....	120
Table 3.4: Input data for investment cost estimation and LCOS calculation	121
Table 3.5: Battery cost data used for model development.....	122
Table 3.6: PCS characteristics and cost data	124
Table 3.7: List of technical outputs from the models	127
Table 3.8: List of technical outputs from the VRF ESS model	128
Table 3.9: Comparison of cost outputs for different electro-chemical ESSs.....	130
Table 3.10: Total investment cost (TIC) model for 1-8 hours of discharge in S1 (50 MW).....	134
Table 4.1: Assumptions used in the stationary application scenarios.....	152
Table 4.2: Technical inputs used to design the energy storage systems.....	154
Table 4.3: Energy densities considered for various electro-chemical batteries.....	157
Table 4.4: Energy requirements for manufacturing electro-chemical batteries.....	160
Table 5.1: Design parameters used in the techno-economic model.....	188
Table 5.2: Economic parameters used to calculate the levelized cost of storage	195

Table 5.3: Input parameters for sensitivity and uncertainty analyses	197
Table 5.4: Cost summary for 20 MW/5MWh flywheel energy storage systems.....	206
Table 6.1: Technical assumptions used for the FESSs	224
Table 6.2: The material inventory for steel rotor and composite rotor FESSs	227
Table 6.3: Developed energy inventory for the manufacturing phase.....	230
Table 6.4: Recovery rate, specific energy, and emission factors for different metals	234
Table 7.1: Technical parameters used for the techno-economic assessment.....	257
Table 7.2: Parameters used to calculate various cost items	261
Table 7.3: The maximum and minimum values of the input parameters used in the sensitivity and uncertainty analyses	264

List of figures

Figure 2.1: Classification of energy storage systems based on the form of energy stored [115].	18
Figure 2.2: The top ten countries by installed capacity of ESSs [12].....	19
Figure 2.3: ESS's generalized total life cycle cost structure	31
Figure 2.4: General LCA system boundary considered for energy storage systems	66
Figure 3.1: Developed techno-economic modeling methodology used in this study	112
Figure 3.2: Main components of an electro-chemical energy storage system with energy flows	115
Figure 3.3: Annual life cycle cost for electro-chemical ESSs	132
Figure 3.4: The levelized cost of storage developed in this study in the four scenarios	133
Figure 3.5: The levelized cost of storage with variations in discharge duration, Scenario 1	135
Figure 3.6: Sensitivity analysis for the TIC in the Na-S ESS for bulk energy storage.....	136
Figure 3.7: Sensitivity analysis for the LCOS in the Na-S ESS for bulk energy storage.....	137
Figure 3.8: Uncertainty analysis for the LCOS for bulk energy storage (S1)	139
Figure 3.9: Uncertainty analysis for the LCOS for T&D investment deferral (S2)	139
Figure 3.10: Uncertainty analysis for the LCOS for frequency regulation (S3).....	140
Figure 3.11: Uncertainty analysis for the LCOS for support for voltage regulation (S4)	140
Figure 3.12: LCOSs for different ESSs for a discharge duration of 8 hours	143
Figure 4.1: Methodological framework	151
Figure 4.2: System boundary for electro-chemical energy storage systems.....	156
Figure 4.3: Overview map of the supply chain routes for the batteries and power conversion system	163
Figure 4.4: Net energy ratio (NER) for electro-chemical energy storage technologies	167
Figure 4.5: Comparative life cycle GHG emissions of five electro-chemical ESSs	172
Figure 4.6: Sensitivity analysis for the GHG emissions of the Li-ion ESS for bulk energy storage (S1).....	175
Figure 4.7: Uncertainty analysis for the net energy ratio.....	176
Figure 4.8: Uncertainty analysis for the life cycle GHG emissions	177
Figure 5.1: Overview of the modeling framework	185

Figure 5.2: Capital cost curve for a motor-generator.....	192
Figure 5.3: Capital cost curve for a vacuum pump.....	192
Figure 5.4: Capital cost curve for a power converter.....	193
Figure 5.5: Equipment cost distribution for the flywheel energy storage systems.....	200
Figure 5.6: Annual life cycle cost for flywheel energy storage systems	202
Figure 5.7: Change of the levelized cost of storage (LCOS) with rated capacity of the storage plant. y and x in the equations represent the LCOS (\$/MWh) and the rated capacity (MW), respectively	207
Figure 5.8: Morris sensitivity analysis for the levelized cost of storage for composite rotor flywheel storage.....	209
Figure 5.9: Morris sensitivity analysis for the levelized cost of storage for steel rotor flywheel storage.....	210
Figure 5.10: Total investment cost uncertainty analysis.....	211
Figure 5.11: Levelized cost of storage uncertainty analysis.....	211
Figure 6.1: Life cycle assessment framework for a flywheel energy storage system.....	219
Figure 6.2: System boundary for FESSs.....	221
Figure 6.3: Life cycle energy requirements for FESSs.....	238
Figure 6.4: Life cycle GHG emissions of FESSs	241
Figure 6.5: Cradle-to-gate GHG emissions for various energy storage technologies used for frequency regulation.	243
Figure 6.6: Uncertainty analysis for the net energy ratio.....	246
Figure 6.7: Uncertainty analysis for the life cycle GHG emissions	246
Figure 7.1: Vehicle-to-grid (V2G) techno-economic assessment framework	254
Figure 7.2: Schematic of a vehicle-to-grid system	256
Figure 7.3: Temperature ranges in four Canadian provinces throughout the year. Values were estimated using information from a database [517].....	259
Figure 7.4: Annual life cycle costs for V2G applications.....	266
Figure 7.5: Levelized cost of storage in four provinces in Canada	267
Figure 7.6: Levelized cost of storage for several battery energy storage technologies	269
Figure 7.7: Effect of ambient temperature on electricity available for the V2G applications....	270

Figure 7.8: Sensitivity analysis for the levelized cost of storage for energy arbitrage	272
Figure 7.9: Levelized cost of storage uncertainty analysis	273
Figure 8.1: Comparative reassessment of five electro-chemical energy storage systems' (a) levelized cost of storage and (b) life cycle GHG emissions	280
Figure 8.2: Comparative assessment of flywheel energy storage systems' (a) levelized cost of storage and (b) life cycle GHG emissions	283
Figure 8.3: Levelized cost of storage in four provinces in Canada	285

List of abbreviations

AC	Alternating current
A-CAES	Adiabatic compressed air energy storage
AULO	Agricultural and urban land occupation
BES	Bulk energy storage
BOP	Balance of plant
BP	Bridging power
CAES	Compressed air energy storage
CC	Climate change
C-CAES	Conventional compressed air energy storage
CED	Cumulative energy demand
CoC	Contingency cost
CSP	Concentrated solar power
DC	Direct current
DCF	Discounted cash flow
DOD	Depth of discharge
EA	Energy arbitrage
EF	Emission factor
EM	Energy management
EOL	End-of-life
EPDM	Ethylene propylene diene monomer
ER	Energy requirements
ESS	Energy storage system
EV	Electric vehicle
FES	Flywheel energy storage
FESS	Flywheel energy storage system
FFD	Fossil fuel depletion
FR	Frequency regulation
FWE	Freshwater eutrophication

FWET	Freshwater ecotoxicity
GHG	Greenhouse gas
GREET	Greenhouse gases, Regulated Emissions, and Energy use in Transportation
GWP	Global warming potential
HT	Human toxicity
HX	Heat exchanger
IRENA	International Renewable Energy Agency
ISC	Increase of self-consumption
ISO	International Organization for Standardization
LAES	Liquid air energy storage
LB	Load balancing
LCA	Life cycle assessment
LCAS	Levelized cost added by storage
LCC	Life cycle cost
LCOE	Levelized cost of electricity
LCOS	Levelized cost of storage
LCSA	Life cycle sustainability assessment
LFP	Lithium iron phosphate
Li-ion	Lithium-ion
LMO	Lithium manganese oxide
LMP	Lithium metal polymer
LR	Learning rate
MIC	Miscellaneous items cost
MRD	Mineral resource depletion
MSW	Municipal solid waste
NaNiCl	Sodium nickel chloride
Na-S	Sodium-sulfur
NdFeB	Neodymium iron boron
NER	Net energy ratio
Ni-Cd	Nickel-cadmium
NMC	Lithium nickel manganese cobalt

NO	Network operation
O&M	Operation and maintenance
OD	Ozone depletion
PAN	Polyacrylonitrile
Pb-A	Lead-acid
PCS	Power conversion system
PE	Primary energy
PEM	Proton exchange membrane
PHS	Pumped hydro storage
PMF	Particulate matter formation
POF	Photochemical oxidant formation
PQ	Power quality
PR	Primary regulation
PS	Peak shaving
PV	Photovoltaic
PVC	Polyvinyl chloride
PVSC	Photovoltaic self-consumption
PVT	Photovoltaic thermal
RC	Replacement cost
RD	Resources depletion
REB	Reducing electricity bill
RI	Renewable integration
RPD	Reducing peak demand
RPM	Revolutions per minute
RS	Renewables support
RUST	Regression, Uncertainty, and Sensitivity Tool
S1	Scenario 1: Bulk energy storage
S2	Scenario 2: T&D investment deferral
S3	Scenario 3: Frequency regulation
S4	Scenario 4: Support of voltage regulation
SD	Smooth demand

SF	Scale factor
SO	System operation
SU	Storage unit
SVR	Support of voltage regulation
TA	Terrestrial acidification
T&D	Transmission and distribution
TCC	Total capital cost
TDC	Total direct cost
TEA	Techno-economic assessment
TEC	Total equipment cost
TES	Thermal energy storage
TIC	Total investment cost
TS	Time-shift
UPS	Uninterruptible power supply
USDOE	United States Department of Energy
V2G	Vehicle-to-grid
V ₂ O ₅	Vanadium pentoxide
VRF	Vanadium redox flow
VRFB	Vanadium redox flow battery
VRLA	Valve-regulated lead-acid
Zn-Br	Zinc-bromine

Chapter 1: Introduction¹

1.1. Background

Electricity and heat production is one of the greenhouse gas (GHG)-intensive sectors, responsible for 31% of global emissions [1]. Electricity demand, moreover, is expected to increase by 57% by 2050 [2] and, with it, the GHG emissions' contribution. Thus, the energy sector needs a deep decarbonization by transitioning to renewable energy to meet the global reduction targets set by the Paris Agreement, which aims to keep the global temperature rise to well below 2°C [3]. Renewable energy grew 39% between 2014 and 2018; solar and wind experienced huge growths of 61% and 275%, respectively, during the last 5 years [4]. It is projected that the renewable energy capacity will increase by more than 60% by 2026 from 2020 levels [5]. While these renewable sources have many environmental advantages, they also come with some challenges due to their intermittency [6]. Increasing their shares in the grid creates stability problems, as these sources disrupt the conventional methods used in daily planning and operations [7]. Energy storage systems (ESSs) can play an important role both in mitigating grid stability challenges and facilitating the integration of renewables to the grid, thus ensuring deep decarbonization of the electricity sector [8, 9].

An ESS stores electricity from renewable and non-renewable sources in a different form and converts it back when required [10]. ESSs can be classified as mechanical (e.g., pumped hydro, compressed air, flywheel), electrical (e.g., supercapacitor), electro-chemical (e.g. lithium-ion, lead-acid, etc.), and thermal (e.g., sensible heat, latent heat, etc.) [11]. The global installed ESS

¹ Part of this chapter is based on a book chapter. The chapter has been published as Environmental impact assessments of compressed air energy storage systems: A review. In: Fokaides PA, Morsink-Georgali PZ, Kylili Angeliki, editors. Environmental Assessment of Renewable Energy Conversion Technologies, Elsevier Inc., Amsterdam, The Netherlands, 2022.

capacity was 181 GW in 2018, of which about 96% is pumped hydro storage (PHS) [12]. PHS pumps water from a lower to a higher reservoir when there is low energy demand and allows water to flow to the lower reservoir and generate electricity when the demand is high. PHS is among the most mature energy storage technologies. It is characterized by long lifetime and low cost of storage for large-scale applications [13]. PHS is site-constrained, as it is attached to hydropower [14]. Compressed air energy storage systems (CAESs) and thermal ESSs are other mature technologies. A CAES system stores electricity in the form of the potential elastic energy of air and air is released from the storage medium and used in a gas-fired turbine to produce electricity during high demand. Problems with a CAES are that it uses natural gas and has low efficiency [15, 16]. In a thermal ESS, the heat from the solar or waste stream is stored in molten salt during low demand periods. When demand is high, the heat transfer fluid extracts heat from the molten salt to produce superheated steam, which is then used to generate electricity using steam turbines. PHS, CAES, and thermal ESS are used for long-duration applications (e.g., time-shift) and are not suitable for short-duration applications such as frequency regulation or support of voltage regulation. Electro-chemical battery technologies, such as valve-regulated lead-acid, lithium-ion, sodium-sulfur, nickel-cadmium, and flow batteries, are more versatile than PHS, CAES, and thermal ESS as they can be used for any short- or long-duration application.

The electric vehicle (EV) is an application of electro-chemical batteries, in that it can be used as energy storage to provide several services in the electricity network including frequency regulation [17], energy arbitrage [18], and load-leveling [19]. The connection between the grid and EVs can be facilitated through vehicle-to-grid (V2G) technology. With the rapidly growing number of electric vehicles, V2G technology can play an important role in stabilizing electricity grids.

However, research that focuses on the V2G's economic feasibility in different applications is scarce.

Short-duration applications, such as frequency regulation and voltage leveling, are crucial for the safety and reliability of electricity networks. Large-scale flywheels could be an attractive option for short-duration utility applications given their fast response time, longer cycle life, and large power discharge. Because of the recent developments in flywheel bearing and rotor material, it is projected that the flywheel energy storage market will increase by about 77% between 2019 and 2027 [20, 21].

Electro-chemical and flywheel ESSs can play a key role in achieving a high penetration of renewables by providing flexibility to the electricity grid and improving its reliability and efficiency. The choice of ESS depends largely on its economic viability and environmental sustainability. Unlike mature storage technologies such as PHS, CEAS, and thermal ESS, information on the economic and environmental performances of electro-chemical batteries and flywheel storage systems for utility applications is limited. This can be a barrier to the development of feasible business models for electro-chemical and flywheel ESSs and to making an informed decision. This research develops techno-economic and life cycle assessment (LCA) models that allow a system-based evaluation of electro-chemical and flywheel ESSs for short- and long-duration applications. The techno-economic model uses design and cost parameters associated with an ESS over its lifetime to determine its life cycle cost as a levelized cost of storage (LCOS). Scale factors were developed to define the cost implications of a change in storage capacity. The LCA model was developed by accounting for the material and energy inputs and outputs in the life cycle stages of an ESS from raw material extraction to the end-of-life to measure the energy and environmental performances in terms of net energy ratio and GHG emissions.

1.2. Literature review and research gap

There are some studies on the techno-economic implications of ESSs. Most studies performed comparative assessments, for example, flywheel with PHS, CAES, and several electro-chemical batteries [22, 23] or with supercapacitor and superconducting magnetic energy storage [24]. The studies by Schoenung [25] and Schoenung and Eyer [26] used data collected from various sources to estimate and compare the costs and benefits of different types of electro-chemical storage technologies. Abrams et al. [27] developed a framework to evaluate the cost-effectiveness of lead acid (Pb-A) and lithium-ion (Li-ion) using data from manufacturers. Nikolaidis and Poullikkas [22] compared the performances of flywheel energy storage systems (FESSs), PHS, and CAES based on the power capital cost. Schmidt et al. [23] projected the LCOE to 2050 for various mechanical and electro-chemical ESSs. Zakeri and Syri [28] and Li et al. [29] compared the economic competitiveness of flywheels, Li-ion, and Pb-A. Although these studies provide useful information on the economic performance of various energy storage technologies in stationary applications, there are limitations. Most of the assessments use a top-down approach. A top-down approach uses aggregated data and provides opaque results without sharing the details [30]. Due to the lack of process specifics, this approach cannot capture the full interaction between the technical parameters and economic outputs. For example, the studies by Schoenung [25] and Schoenung and Eyer [26] used aggregated capital cost data without considering equipment design and sizing. The bottom-up approach, on the other hand, uses engineering principles to calculate the installed ESS capacity, design the components, and estimate the costs of components [31]. The bottom-up approach is transparent, and the results are easily reproducible.

Another important aspect that has not been well addressed in the literature is how economies of scale change the techno-economic performance of an ESS or how to find the optimal capacity at

which the cost per unit output is lowest. A few studies developed scale factors for large-scale PHS and CAES systems and showed there is a cost advantage for large-capacity plants because of economies of scale. For example, Kapila et al. [31] found scale factors of 0.53, 0.87, and 0.88, respectively, for PHS, conventional CAES, and adiabatic CAES. To the best of the author's knowledge, scale factors have not been developed for electro-chemical and flywheel ESSs in the existing literature.

A key research gap that should be addressed is the techno-economic feasibility of V2G systems in different applications. The Bank of Canada projects that the EV market will reach about 120 million by 2030 [32]. This drastic increase will put a significant load on electricity grids, impacting their daily operations [33]. The combined effects of increased renewable penetration and a large number of EVs in the electricity networks will result in a power imbalance between demand and supply [34]. Problems such as frequency variation and voltage fluctuation will occur, which can harm the electricity network's economic and stability performance [35, 36]. One way to manage these problems is to use EVs as aggregated energy storage systems, transforming them from electric loads to energy resources. There are a few studies that attempt to assess a V2G technology for stationary applications. For example, Noori et al. [37] and Zhao et al. [38] conducted assessments of the net revenue of V2G systems for five independent system operators in the United States. Rodríguez-Molina et al. [39] developed a cost-benefit model for a V2G system and found that EVs can obtain additional revenue by selling electricity to the grid.

Although existing studies provide some information on various cost items, they have limitations. Because the energy storage market is competitive and costs fluctuate, there is no common indicator that can be used to compare the economic performance of V2G applications with stationary battery storage systems. The LCOS needs to be developed for V2G technology. The advantage of this

indicator is that it does not use any location-specific profit/loss function but indicates a price that should be applied to cover all the expenses over the lifetime of a system and can be used as a location-independent performance indicator. In addition, the impact of extremely cold weather on the V2G system's economic performance was not evaluated in earlier studies. According to Donkers et al. [40] and Yuksel and Michalek [41], extremely cold weather can adversely influence an EV's performance. This is mainly because cold temperature reduces battery capacity significantly, thereby reducing the battery efficiency and increasing energy consumption to heat the vehicle cabin. To the best of the author's knowledge, no study considers extreme cold weather conditions to evaluate the LCOS for V2G applications.

Cost estimates of a technology inherently differ from one study to the next given the differences in input parameters, modeling approach, and assumptions, among others. These differences should be reflected in the output results through sensitivity analysis and quantifying the uncertainty. However, most existing studies are limited to point estimates and fail to provide a cost range that considers multiple assumptions and input parameters. A wide range of capital costs is reported in the literature; for example, according to Akinyele and Rayudu [42], the capital cost of a FESS can be from \$1000-\$5000/kW and \$250-\$350/kWh. There are uncertainties not only in cost inputs but also in technical parameters and assumptions. For instance, Li-ion battery efficiency is reported in two studies as 85% [43] and 95% [28]. Studies that attempt to understand the techno-economic performance of storage systems should be supported with detailed sensitivity and uncertainty analyses.

LCAs of electro-chemical ESSs focus on comparative assessments, for example, vanadium redox flow (VRF) with Li-ion [44], aluminium ion (Al-ion) with Li-ion [45], and VRF with lead-acid (Pb-A) and sodium-sulfur (Na-S) [46]. Two studies compared the environmental footprints of

different Li-ion batteries [47, 48]. However, none of these studies provides a relative ranking of battery technologies in different applications considering the impacts of operational characteristics in the use phase. Few studies investigate the environmental performances of electro-chemical ESSs in different stationary applications. Ryan et al. [49] conducted an LCA of three types of Li-ion batteries to estimate cumulative energy demand (CED), global warming potential (GWP), and acidification for frequency regulation. Jones et al. [50] evaluated the GWP of Li-ion and VRF storage systems for black start, renewables support, reserve, and balancing. Baumann et al. [51] assessed the GWP of Li-ion, valve-regulated lead-acid (VRLA), VRF, and NaNiCl for renewables support, primary regulation, time-shift, and increase of self-consumption. In addition to the GWP, two studies estimated a wide range of environmental impacts, such as human toxicity, particulate matter formation, freshwater ecotoxicity, etc. [52, 53]. These studies provide useful information on the environmental performance of electro-chemical ESSs. However, life cycle inventory analysis and impact assessment in these studies relied on generic databases, which might not be applicable for a specific project or application, as material and energy inventories can vary by application and jurisdiction [11]. While one cannot avoid using generic inventory data, especially for background systems, primary data can be accurately estimated by applying fundamental engineering principles to size the storage systems and develop the material and energy inventories for different applications. In addition, these studies overlooked the environmental impacts arising from the use of the power conversion system (PCS). To the best of the author's knowledge, none of the earlier LCA studies included the PCS in the system boundary to evaluate the energy use and resulting GHG emissions in the material production and manufacturing of the PCS. Moreover, some studies omitted one or more life cycle stages, for example, dismantling and transportation of

dismantled components. Excluding any of these aspects when comparing different energy storage technologies can generate misleading results.

While there are a few LCA studies on FESSs, none include all the components and the full supply chain from material production to end-of-life (EOL). Torell [54] performed an LCA of lead-acid (PbA) batteries and FESSs focusing on the material production, transportation, and operation phases. Although the study provides some information on the carbon footprint, details of assumptions, data sources, and model development are missing. A similar study [55] estimated the carbon footprint of a FESS for an uninterruptible power supply application. The study focuses on material production for a steel rotor flywheel. A study by the Beacon Power Corporation [56] compares the GHG emissions of a 20 MW FES plant with natural gas, coal, and PHS. The authors estimated only the GHG emissions from the use of some electricity to compensate for the energy loss in the operation phase without considering the other life cycle stages. While those studies are helpful to understand the inventory for the material production and operation phases, many important aspects are not covered.

There are no LCA studies that assess the environmental performances of composite rotor FESSs. Research on composite rotor FESSs mainly evaluates cost performance. As composite rotor flywheels have become popular for their low weight and low space requirement, it is worth investigating the energy and GHG emission characteristics of the system and comparing them with those of conventional steel rotor FESSs. Most LCA studies on FESSs estimate the carbon footprint of the flywheel rotor, which is the heart of the FESS. Other key components such as the bearings, vacuum system, motor/generator, and power conversion system (PCS) are not fully studied. Leaving out the energy required to produce these components may lead to a misleading conclusion.

Most earlier studies did not include sensitivity and uncertainty analyses, an important part of the assessment. According to ISO 14040, an LCA should have sensitivity and uncertainty analyses to improve the reliability of models and results by identifying the most influential parameters and providing a probable range of results [57]. LCA involves data collection and assumptions in building inventories (material and energy inputs) for all the life cycle phases and determining the environmental impacts associated with each input. For the same input, different sources may have different values. It is important to identify the variables that most impact the results. Furthermore, to understand the probable range of results from the interactions of the input variables with a range, uncertainty analysis is required. Sensitivity and uncertainty analyses can handle variations in assumptions and data; however, they were not included in the existing LCA studies of ESSs.

1.3. Research motivation

The followings were the impetus for this research:

- There has been little work done on the economic and environmental feasibilities of energy storage systems for stationary applications;
- The need for bottom-up techno-economic and life cycle assessment models that considers the interactions among technical parameters, cost items, and specific energy to evaluate the economic and environmental footprints of energy storage systems;
- The need to understand the relative ranking of energy storage systems based on their environmental performances in various applications;
- There is not enough information on the cost of using battery-based electric vehicles for utility applications in cold climates;

- Economic and environmental policies for the deployment of ESSs in the power grid are needed, and to formulate these it is necessary to estimate the investment cost, net energy ratio, and life cycle GHG emissions; and
- To identify the areas where costs and GHG emissions could be reduced, it is necessary to understand the sensitivity of various parameters on the cost of storage and life cycle GHG emissions in each unit operation.

1.4. Research objectives

The overall objective of this thesis is to develop bottom-up techno-economic and LCA models to estimate the economic and environmental footprints of large-scale electro-chemical and flywheel energy storage systems for stationary applications. The specific objectives of this research are to:

- Provide a detailed overview on the recent developments in utility-scale energy storage technologies;
- Apply engineering principles to design various components of energy storage systems;
- Evaluate the total investment cost, annual life cycle cost, and levelized cost of energy storage;
- Develop scale factors and economies of scale for a wide range of capacities;
- Develop material and energy inventories for all the life cycle stages from material production to end-of-life;
- Evaluate the net energy ratio and life cycle GHG emissions considering all the life cycle stages from material production to end-of-life; and
- Perform sensitivity and uncertainty analyses to identify important input parameters and provide a range of estimates.

1.5. Scope and limitations of the thesis

This research develops scientific-principles-based techno-economic and LCA models for the five most promising electro-chemical and two flywheel energy storage systems for large-scale stationary applications. The electro-chemical energy storage systems are sodium-sulfur, lithium-ion, valve-regulated lead-acid, nickel-cadmium, and vanadium redox flow. The two flywheel energy storage systems are low-speed steel rotor and high-speed composite rotor. In addition, because of the rapid increase in electric vehicles, the techno-economic feasibility of lithium-ion-based vehicle-to-grid system was also analyzed.

Four economic and environmental performance metrics were developed including total investment cost, levelized cost of storage, net energy ratio, and life cycle GHG emissions. The vital cost parameters, such as capital cost, replacement cost, operation and maintenance cost, and charging cost, were considered in the techno-economic assessment. The LCA system boundary includes all the unit operations in the energy storage supply chain from material production, manufacturing, transportation, and end-of-life.

The LCOS developed in this research are based on the duration of discharge and number of cycles which can vary by application. Therefore, a comparison of different ESSs based on the LCOS should be done for similar applications.

The decommissioning costs were not considered in the techno-economic assessment because of the lack of data. Although most inventories were developed using engineering principles, some data related to component costs, energy use, and emission factors were taken from published sources. This study conducts a case study for Alberta-based energy storage systems; however, the developed techno-economic and life cycle assessment frameworks are valid for other jurisdictions

with some adjustments in economic input data, emission factors, transportation distance, and charging cost.

The scope and limitations of this study are discussed further in Chapters 2-7.

1.6. Organization of the thesis

This thesis has eight chapters and is in a paper-based format. It is comprised of papers intended to be read independently and hence some concepts, assumptions, and data are repeated. Below is a summary of each chapter.

Chapter 2 reviews in detail the available techno-economic assessments and LCAs of stationary energy storage systems. It includes information on the current status of large-scale energy storage systems. Furthermore, an up-to-date inventory of cost and environmental footprints of mechanical, electro-chemical, hydrogen, and thermal energy storage systems is presented.

Chapter 3 discusses the development of comprehensive bottom-up models to assess the techno-economic feasibility of five electro-chemical energy storage systems – sodium-sulfur, lithium-ion, valve-regulated lead-acid, nickel-cadmium, and vanadium redox – for different stationary applications. The total investment cost and levelized cost of storage are presented for the electro-chemical energy storage systems along with a cost comparison with mechanical and thermal energy storage systems.

Chapter 4 describes the development of the LCA models to quantify the net energy ratio and the life cycle GHG emissions of sodium-sulfur, lithium-ion, valve-regulated lead-acid, nickel-cadmium, and vanadium redox for utility-scale stationary applications.

Chapter 5 presents a comparative techno-economic assessment of large-scale steel rotor and composite rotor flywheel energy storage systems for frequency regulation. In this study, cost functions for the system components were developed and then the total investment cost and levelized cost of storage were calculated.

Chapter 6 describes the investigation of the net energy ratio and life cycle GHG emissions of large-scale steel rotor and composite rotor flywheel energy storage systems for frequency regulation through LCA. The LCA model includes the system's supply chain: material production, manufacturing, transportation, and end-of-life.

Chapter 7 examines the techno-economic feasibility of vehicle-to-grid applications in a cold climate. A case study for four Canadian provinces – Alberta, Ontario, British Columbia, and Quebec – was conducted. The levelized cost of storage was developed for time-shift and frequency regulation.

Chapter 8 summarizes the key research findings and provides a list of recommendations for future research.

Chapter 2: Assessment of energy storage technologies: A review²

2.1. Introduction

Global electricity generation is heavily dependent on fossil fuel-based energy sources such as coal, natural gas, and liquid fuels. There are two major concerns with the use of these energy sources: the impending exhaustion of fossil fuels, predicted to run out in less than 100 years [58], and the release of greenhouse gases (GHGs) and other pollutants that adversely affect ecosystem services and human health [59-61]. Environmental regulations have set GHG emission reduction targets in several sectors [3, 62, 63]. Renewable energy is a promising source that can play a vital role in mitigating GHG emissions and fulfilling global energy demand [64-67]. Among the renewable energy sources, globally solar and wind have shown remarkable growth, from 182 GW in 2009 to 660 GW in 2015 [68]. However, their integration into the existing power network has challenges in terms of efficiency, stability, and reliability, as most renewable sources are intermittent by nature [69-74]. This intermittency could be mitigated by incorporating energy storage systems (ESSs) in the power grid [75-79].

An ESS is a system that converts energy from one form, usually electricity, to another form that can be reserved in a storage medium and then converted back to electricity when required [10, 80].

An ESS stores electricity when demand is low and discharges when demand is high, providing

² This chapter is a combination of a review paper and a book chapter. The review paper has been published as Rahman MM, Oni AO, Gemechu E, Kumar A. Assessment of energy storage technologies: A review. *Energy Conversion and Management*. 2020;223:113295. The book chapter has been published as Rahman MM, Oni AO, Gemechu E, Kumar A. Environmental impact assessments of compressed air energy storage systems: A review. In: Fokaides PA, Morsink-Georgali PZ, Kylili Angeliki, editors. *Environmental Assessment of Renewable Energy Conversion Technologies*, Elsevier Inc., Amsterdam, The Netherlands, 2022.

great operational flexibility to the electrical grid and mitigated intermittency [81-84]. Transportation, portable devices, and the power network are the typical application areas for an energy storage system [85-89].

Several studies have addressed the technical and economic aspects of energy storage technologies. Most of these studies reviewed the technical characteristics [6, 90-94], the sizing of various ESSs [42, 95-99], and challenges associated with their applications [8, 100-104]. These studies help us understand technical properties, such as efficiency, energy and power densities, depth of discharge, lifetime, etc., and to determine the size of energy storage technologies for renewable sources like solar and wind. Techno-economic assessments (TEAs) of energy storage technologies evaluate their performance in terms of capital cost, life cycle cost, and levelized cost of energy in order to determine how to develop and deploy them in the power network. Battke et al. reviewed the impact of uncertainty in the inputs on the life cycle costs of electro-chemical storage systems, focusing on four types of battery systems, lithium-ion, lead-acid, sodium-sulfur, and vanadium redox flow [105]. The review did not include mechanical, hydrogen, or thermal energy storage technologies. A review article by Zakeri and Syri looked into a number of studies and performed a TEA of energy storage technologies along with uncertainty analysis [28]. The authors provided useful information on various cost components. However, the study does not include information on energy use or the environmental impacts of each technology. A recent study by Koochi-Fayegh and Rosen [106] includes a thorough review on the technical aspects and applications of different ESSs. The review presents a brief discussion on the economics of ESSs but no detailed information on cost parameters and how they are used in TEA. Nor were the environmental aspects included in the review.

Given the growing environmental concerns and policy regulations, the quantification of energy consumption and environmental footprints has become increasingly important in the deployment of energy systems in the power network. Understanding the trade-off between the economic viability and environmental performance of an ESS is crucial in order to make decisions towards sustainability. Life cycle assessment (LCA) is a useful tool to quantify the environmental performance of a product or a system from cradle-to-grave. LCA is based on ISO 14040 [57] and IOS 14044 [107] from the International Organization for Standardization (ISO), which provides guidelines and a methodological framework. LCA has four phases: goal and scope definition, inventory analysis, impact assessment, and interpretation. LCA of ESSs involves estimating energy use and emissions as well as particulate matter at various stages, from material extraction, manufacturing, transportation, and operation to final decommissioning [108-112]. A recent paper by Pellow et al. [113] reviewed the environmental impacts of lithium-ion (Li-ion) batteries in various applications including stationary and transportation. But the review does not include a comparative environmental assessment of different energy storage types.

There is a scarcity of review articles that provide useful information on the life cycle energy use and GHG emissions associated with different energy storage technologies focusing on utility-scale stationary applications. Moreover, many cost numbers presented in the earlier review articles are not up-to-date. A study that looks extensively into ESSs' development and their economic and environmental performances is needed. This chapter, therefore, aims to provide a comprehensive review of state-of-the-art energy storage technologies and their applications. This review integrates both the economic and the environmental aspects of ESSs for stationary applications in the power network and provides a database that incorporates the latest cost and emissions numbers of energy storage technologies. Finally, knowledge gaps in this area of research are identified and

recommendations are made. The literature review includes peer-reviewed journal papers, conference proceedings, and scientific reports from governments and non-governmental organizations.

The specific objectives of this chapter are to:

- Provide a detailed overview on recent developments in utility-scale energy storage technologies;
- Extensively review and compare the techno-economic performance of various energy storage systems;
- Critically review the methods used in the literature to evaluate the environmental sustainability of energy storage technologies;
- Review the life cycle environmental performance of different utility-scale energy storage systems; and
- Identify knowledge gaps in the literature relevant to the techno-economic and life cycle assessments of utility-scale energy storage systems.

This chapter is organized into five sections. Section 2.2 provides an overview on the status of energy storage technologies around the world. Sections 2.3 and 2.4 provide critical reviews and discuss the techno-economic and life cycle assessments of different energy storage technologies, respectively. Land footprints of different energy storage systems are discussed in section 2.5. Section 2.6 outlines the research gaps and recommendations for future research.

2.2. An overview of energy storage technologies

Although energy storage technologies can be categorized by storage duration, response time, and function [10, 114], the most popular method is by the form of energy stored, broadly classified

into mechanical, electro-chemical, chemical, electrical, and thermal [69, 115-117]. Figure 2.1 presents a classification of energy storage technologies based on the form of energy stored.

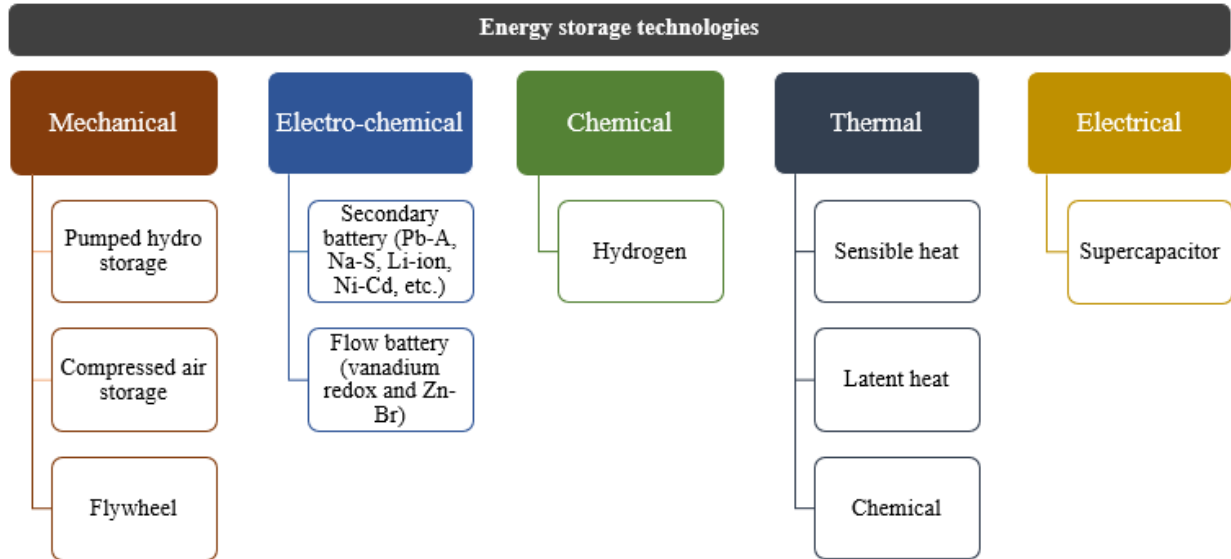


Figure 2.1: Classification of energy storage systems based on the form of energy stored

[115]

With increased renewable energy penetration in power grids, the use of energy storage devices has become increasingly common. According to the United States Department of Energy (USDOE) [12], the capacity of ESSs increased by 24% from 2010 to 2017. In 2017, the worldwide capacity of ESSs was about 171 GW from 1267 operational projects [12]. Table 2.1 shows the rated capacity and number of projects for each ESS type based on project status. Of 171 GW, China has the largest installed energy storage capacity (32 GW), followed by Japan (29 GW), and the US (24 GW). However, the number of operational projects in the US is 494, the highest in the world. China and Japan have 94 and 90 projects, respectively, operating for various power grid applications [12]. Figure 2.2 shows the cumulative ESS capacity and the number of projects in the top 10 countries in the world by installed capacity.

Table 2.1: Rated installed capacity (GW) and number of projects for various energy storage technologies around the world [12]

Technology	Operational	Offline /under repair	Contracted	Announced	De-commissioned	Under construction
Mechanical storage*	166.20 (372)	0.28 (2)	2.31 (11)	11.63 (26)	0.08 (3)	5.95 (7)
Electro-chemical	2.03 (695)	0.05 (3)	0.95 (67)	0.63 (136)	0.09 (40)	0.70 (10)
Chemical storage#	0.01 (7)	-	0.003 (3)	0.001 (1)	0.00007 (1)	-
Thermal storage	3.21 (193)	0.21 (1)	0.13 (3)	0.16 (5)	-	0.12 (2)

* Includes pumped hydro, compressed air, and flywheel storage systems.

Only hydrogen storage is considered.

Values in parenthesis represent the number of projects.

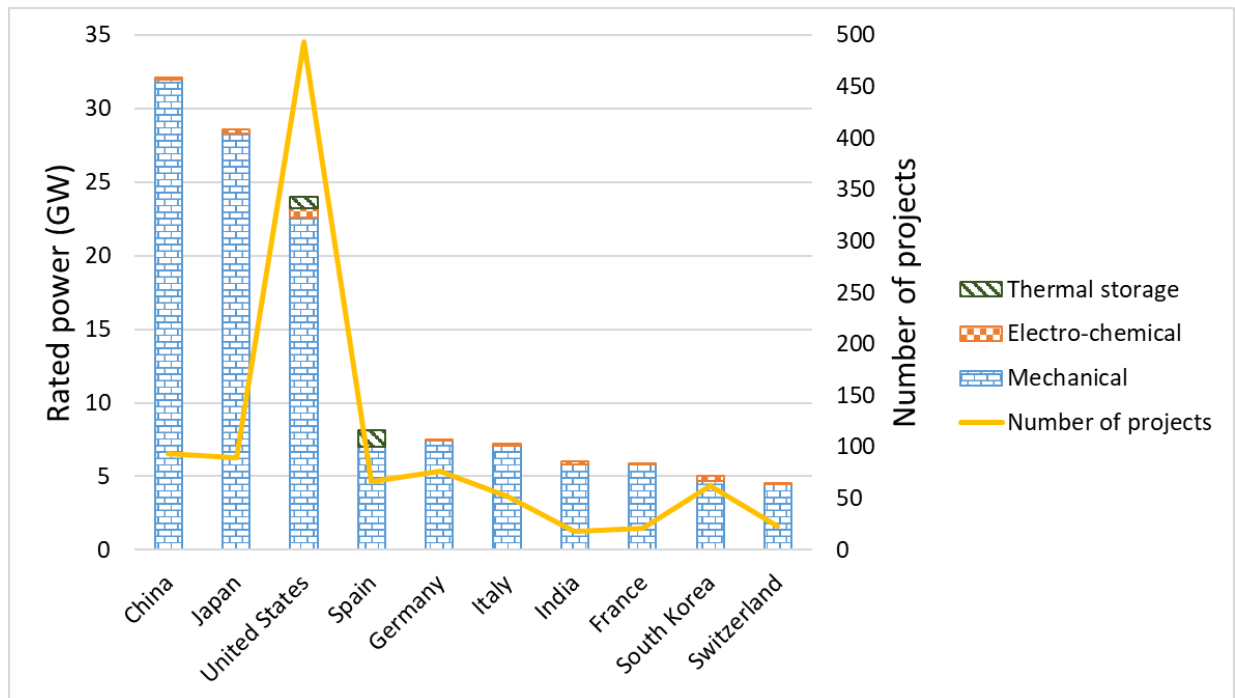


Figure 2.2: The top ten countries by installed capacity of ESSs [12]

Energy storage devices are used in the power grid for a variety of applications including electric energy time-shift, electric supply capacity, frequency and voltage support, and electricity bill management [12]. The number of projects in operation by storage type for different services is provided in Table 2.2. Although mechanical storage systems have the largest share in the world's installed capacity, these systems are mainly used in electrical energy time-shift (314 projects) and electric supply capacity (282 projects) (see Table 2.2). Electro-chemical batteries, such as lithium-ion (Li-ion), sodium-sulfur (Na-S), vanadium redox flow (VRF), and lead-acid (Pb-A) are used for all the services an ESS can provide.

Table 2.2: Number of projects in operation by storage type for different services [12]

Service	Mechanical storage	Electro-chemical storage	Chemical storage	Thermal storage
Electric energy time-shift	314	197	-	75
Electric supply capacity	282	79	-	66
Renewables capacity firming	12	204	6	54
Frequency regulation	77	168	1	4
Electricity bill management	3	119	-	119
Renewables energy time-shift	15	139	3	57
Voltage support	46	133	-	-
On-site renewable generation shifting	1	135	1	9
Electric supply reserve capacity- spinning	92	52	-	-
On-site power	4	90	-	-
Grid-connected commercial (reliability and quality)	2	64	-	3
Electricity bill management with renewables	3	77	1	2
Transportation services	-	51	2	-

Service	Mechanical storage	Electro-chemical storage	Chemical storage	Thermal storage
Distribution upgrade due to solar	-	46	-	-
Grid-connected residential (reliability)	-	35	-	3
Ramping	4	40	1	1
Load following (tertiary balancing)	26	50	1	-
Microgrid capability	2	92	-	1
Black start	1	36	-	-
Transmission congestion relief	1	24	1	3
Transmission support	-	17	-	3
Electric supply reserve capacity- non-spinning	1	20	-	17

2.2.1. Mechanical storage

Among the mechanical storage systems, the pumped hydro storage (PHS) system is the most developed commercial storage technology and makes up about 94% of the world's energy storage capacity [12]. As of 2017, there were 322 PHS projects around the globe with a cumulative capacity of 164.63 GW. The rated capacity of PHS varies from 100-2000 MW [28]. It has high efficiency, long discharge duration and cycle life that makes it suitable for bulk energy applications.

Compressed air energy storage (CAES) can be classified as conventional and adiabatic. The operation principles of conventional and adiabatic CAES systems along with the other ESSs can be found in Appendix A in section A.1. The world's first conventional CAES plant was built in Germany in 1978 with a capacity of 290 MW [118]. According to the USDOE, 660 kW adiabatic CAES plant is the only operational plant in the world, located in Toronto, Canada. A 5 MW/10

MWh adiabatic CAES plant in Strathalbyn, South Australia, Australia is under construction and expected to be in operation in 2020 [12].

The installed capacity of flywheel energy storage (FES) system is 931 MW [12]. Flywheels are usually used in frequency regulation, integration of renewable energy systems [119], and hybrid energy systems [120, 121]. They have a very high efficiency (80-90%), short response time, and long lifetime (see Table 2.3), making them favorable to use. The world's largest capacity flywheel, located in Culham, United Kingdom and used for frequency regulation, can supply up to 400 MW (2 large flywheels) for 30 seconds [12].

2.2.2. Electro-chemical storage

Electro-chemical battery storage systems have the third highest installed capacity of 2.03 GW [12] (see table 2.1). The most widely used utility-scale electro-chemical batteries are lead-acid, lithium-ion, sodium-sulfur, nickel-cadmium, and flow batteries [122-124]. Among the battery technologies, Li-ion has the highest market share with a capacity of 1.66 GW, followed by sodium-based batteries (204.32 MW) and flow batteries (71.94 MW) [12].

The Pb-A batteries are used for services like micro-grids, hybrid energy systems, spinning reserve, bulk energy storage, frequency regulation, etc. [10]. According to DOE, the largest Pb-A project, 10 MW, is in Phoenix, Arizona, USA [12]. While the Pb-A batteries have high efficiency, typically 70-80% (see Table 2.3), and lower capital cost, the main drawbacks of this technology are its short lifetime and intensive maintenance requirement. The lifetime is limited by the depth of discharge (DOD) and operating temperature, typically -5 to +40°C [125]. The improved Pb-A battery, the advanced valve-regulated lead-acid battery (VRLA), can overcome these limitations. The lifetime of the VRLA is about ten times longer than the old Pb-A battery [90]. Although the power

conversion system and balance of plant costs of conventional Pb-A and VRLA batteries are within the same range, the cost of the storage section could be 25-35% higher for the advanced one [26].

The Li-ion battery dominates the energy storage market. High efficiency, longer life cycle, and high power and energy density helped this technology grow rapidly [8]. High capital cost remains the biggest challenge for the use of these batteries in commercial-scale ESSs [8]. According to the DOE database, the world's largest Li-ion battery storage was commissioned in 2017, in South Australia with power and energy capacities of 100 MW and 129 MWh, respectively [12]. The project lifetime is 15 years and the capital expenditure was \$32.35 million [12]. The storage system was designed to be used in frequency regulation, renewable capacity firming, and renewable energy time-shift services. The declining price, use of advanced materials, and improved safety features will make this a promising future technology [126].

Na-S technology is becoming increasingly attractive for large commercial-scale energy storage because of its high energy density, longer lifetime, and almost zero maintenance [127-129]. This battery can sustain 6-8 hours of continuous discharge [12]. The world's largest Na-S battery storage was deployed by the Abu Dhabi Water and Electricity Authority and has a capacity of 108 MW [130]. The system operates in a time-shift mode, that is, it stores energy when demand is low and discharges electricity to the grid when demand is high [130].

Although Ni-Cd batteries have high energy density and low maintenance, disposing of the toxic metals nickel (Ni) and cadmium (Cd) is a challenge [6]. The life cycle of Ni-Cd batteries could reach up to 50,000 cycles for a 10% depth of discharge [91]. Golden Valley Electric Association's battery energy storage system is the world's biggest Ni-Cd battery system. It was designed to operate at a rated capacity of 27 MW for 15 minutes discharge. It was commissioned on September

19, 2003 and designed for a 25-year lifetime. The expenditure for the project was \$35 million [12]. The services it provides are black start, electric supply reserve capacity, grid-connected commercial (reliability and quality), grid-connected residential (reliability), and voltage support.

The main advantage of flow batteries is that power and energy rating design can be done independently, which makes them suitable for power- and energy-related applications [28]. The operation principle of flow batteries can be found in Appendix A. Flow batteries can discharge electricity for up to 10 hours [126]. According to the DOE database, the largest energy storage with a VRF battery is located in Dalian, China, and has a capacity of 200 MW/800 MWh [12]. The system is used for electric energy time-shift, black start, renewables capacity firming, renewable energy time-shift, and resiliency. The largest Zn-Br flow battery, with a power capacity of 25 MW and an energy capacity of 100 MWh, is situated in Kazakhstan and is used for electric energy time-shift and renewable energy time-shift [12].

2.2.3. Hydrogen and thermal storage

According to the DOE database, the two largest plants in the world (at 6 MW) are located in Germany [12]. Energiepark Mainz was the first multi-MW project to use proton exchange membrane (PEM) electrolysis with a discharge duration of 4 hours and 20 minutes. The capital expenditure for the project was \$19 million [12]. The high capital cost and low conversion efficiency are the two main constraints in implementing this technology for commercial-scale grid applications.

Thermal storage system has the second highest installed capacity of 3.21 GW [12]. Thermal energy storage is a promising technology that can reduce dependence on fossil fuels (coal, natural gas, oil, etc.). Although the growth rate of thermal energy storage is predicted to be 11% from 2017 to

2022, the intermittency of solar insolation constrains growth [131]. Thermal energy storage (TES) stores energy in the form of heat to use when there is high demand [131]. The typical applications of TES include energy shifting, peak shaving, and electric bill management [12, 132]. Although TES systems can be used for centralized or distributed heating/cooling [132], the focus of this chapter is on TES systems for electricity generation. TES systems can be classified into sensible heat TES, latent heat TES, and thermochemical storage [133, 134].

Each energy storage system has unique characteristics in terms of efficiency, specific energy, cycle duration, self-discharge, etc. These properties determine the suitability of a particular storage device for various services (e.g., supply capacity, time-shift, frequency, and voltage regulation, etc.). Detailed information on these applications can be found in earlier studies [8, 100, 106, 135, 136]. The technical features of different ESSs can be found in Table 2.3.

Table 2.3: Technical parameters of different energy storage technologies

Technology	Rated power (MW)	Specific energy (Wh/kg)	Energy efficiency (%)	Discharge at rated capacity (h)	Response time	Lifetime (cycles)	Self-discharge/day (%)
PHS	100-5000 [10], 1000-3000 [137]	0.5-1.5 [10]	65-75 [138], 75-80 [15]	1-24+ [10]	Minutes [139]	>15,000 [115]	No [140], very small [115]
CAES	5-300 [10], 100-3000 [137], 50-350 [141]	30-60 [10]	41-75 [115]	1-24+ [10]	Seconds- minutes [139]	>10,000 [115]	No [140], small [115]
FES	0-0.25 [10], 0-1.65 [139], 0-10 [137]	10-30 [10], 5-80 [142]	85 [92], 80-90 [115]	0.000–0.01 [77]	<1 cycle [139]	104-107 [115]	100 [6, 115]
Pb-A	0-20 [10], 0.05-10 [143], 0-40 [144]	35-50 [145], 30-50 [10]	70-80 [146], 75-80 [138]	1-5 [77]	<1/4 cycle [139]	250-1500 [115], 500-1000 [10]	<0.1 [6], 0.1 [147, 148], 0.2 [149]
Li-ion	0-0.1 [10], 0.015-50 [150]	75-200 [10], 120-200 [151]	65-75 [115], 78 [152], 88 [153]	0.017–2+ [10]	<1/4 cycle [8]	600-1200 [115], <1000 [10]	1 [147], 5 [6]

Technology	Rated power (MW)	Specific energy (Wh/kg)	Energy efficiency (%)	Discharge at rated capacity (h)	Response time	Lifetime (cycles)	Self-discharge/day (%)
Na-S	0.05-8 [10], 0.05-34 [154]	100 [155], 175 [156], 150-240 [10]	70-85 [115], 84-87 [6]	4-8 [77]	<1/4 cycle [8]	2500-4500 [115], 2500 [10]	No [157]
Ni-Cd	0-40 [10]	50-75 [10], 45-80 [145]	75 [77], 60-80 [115]	6-8 [158]	<1/4 cycle [8]	1500-3000 [115], 2000-2500 [10]	0.2 [148], 0.3 [6]
VRFB	0.03-3 [10], 12 [159]	25-35 [159], 10-30 [10]	60-75 [115], 75-85 [160]	2-12 [77]	<1/4 cycle [8]	>10,000 [115], >12,000 [10]	Small [115]
Zn-Br	0.05-2 [10]	70-90 [161], 75-85 [160]	65-75 [162], 75-85 [160]	2-5 [77]	<1/4 cycle [139]	1000-3650 [115], >2000 [10]	Very small [115]
Hydrogen	0-50 [10], 0.1-15 [92]	400-1000 [161]	35-40 [163], 42 [164]	12+ [77]	<1/4 cycle [139]	103-104 [115], >1000 [10]	0 [115]
Thermal	50-250 [131]	80-200 [10]	14-18 [165]	1-24+ [10]	-	5-15* [10]	0.05-1 [10]

* The unit is year.

2.3. Review of the techno-economic assessments of energy storage technologies

Up-to-date peer-reviewed journal articles and reports on techno-economic assessments of energy storage technologies were identified using academic search engines, such as Google Scholar and Science Direct. Studies older than 10 years were eliminated as publications before 2010 are covered in earlier reviews [8, 28, 42, 105]. In addition, the costs of most energy storage technologies have come down significantly in the last few years as a result of the increased use of ESSs [166-168], and this aspect is captured better in the recent research articles. This section provides a detailed review on cost models, techno-economic performance, and future cost projections of different ESSs (PHS, CAES, FES, Pb-A, Li-ion, Na-S, Ni-Cd, VRFB, Zn-Br, H₂, and TES). All the cost numbers are in 2020 USD unless otherwise mentioned. An inflation rate of 2% was used to adjust the costs [60].

2.3.1. Cost models

The power conversion system (PCS), storage unit (SU), and balance of plant (BOP) are the three main components of an energy storage system. The PCS includes several electrical power devices (e.g., inverter, transformer, etc.) that regulate voltage, current, and frequency based on the load pattern. The SU contains the storage medium: battery cells in electro-chemical storage systems, storage tank in CAES, and water reservoirs in PHS. The BOP refers to all the remaining items that are not parts of PCS and SU. These are research and development, transportation and installation, land and access roads, and so on [28, 169]. The cost models developed in the TEA studies are mainly based on the above-mentioned components. Figure 2.3 shows a generalized cost structure for the TEA of ESSs. A few studies estimated only the total capital cost (TCC), while others calculated the life cycle cost (LCC). For example, Mostafa et al. calculated the LCC of various ESSs considering the TCC, replacement cost (RC), operation and maintenance (O&M) cost, and

end-of-life cost [24]. Zakeri and Syri [28] and Schoenung [139] used a similar approach. The LCC is a better indicator than the TCC as it includes all the cost components in the lifetime of an ESS. While a few studies were restricted to the TCC [91, 116, 170], some left out the replacement cost [105, 171, 172]. The replacement cost is vital for electro-chemical ESSs as most of the batteries have a limited lifetime and need replacements after a certain period, i.e., 10-15 years for Li-ion [93]. According to Das et al., a battery's initial cost and replacement cost are similar [173]. In addition to the TCC and LCC, some studies, such as those by Kapila et al. [31, 174], Mostafa et al. [24], Thaker et al. [131], and others [119, 175, 176] estimated the levelized cost of electricity (LCOE). The advantage of estimating the LCOE is that it indicates the price at which the electricity should be sold to cover the cost elements over an ESS's lifetime [174]. This indicator allows the comparison among different ESSs to be compared provided they have the same operational conditions, such as number of cycles per year and discharge duration [23, 177, 178]. A detailed calculation method for the TCC, LCC, and LCOE can be found in section A.2 of Appendix A.

The TEA approaches used in different ESS studies can be categorized as top-down, bottom-up, or a combination. The bottom-up approach uses engineering first principles to characterize the storage system and design the equipment used in each unit operation, and to determine component costs. Cost estimation is transparent, and the results can be reproducible. However, there are assumptions involved when data are not available and need to be validated. A top-down approach, on the other hand, uses aggregated data and so lacks process specificity. The results, therefore, are usually opaque and details are not shared [30]. Recent TEA studies by Thaker et al. [131] and Kapila et al. [31] used a bottom-up approach to design the system components of thermal and mechanical energy storage, respectively, and to estimate the capital cost using scientific principles. For example, technical parameters such as head of water, flow rate, velocity of water, etc., were

used to design the PHS capacity [31]. Design parameters such as heat transfer coefficient, temperature, pressure, flow rate, etc., were used to design the heat exchangers for the thermal storage [131]. Both studies developed cost functions to estimate the system TCC [31, 131]. Studies by Schmidt et al. used a bottom-up approach to estimate the material and production costs of various ESSs [23, 179]. Another example of a bottom-up study Wu et al.'s, in which the LCOE of an integrated liquid air energy storage (LAES) and thermal storage was assessed [180]. Other studies considered the costs of PCS, SU, and BOP to estimate the TCC without developing any cost functions of system components [28, 105, 176, 181, 182]. The studies by Karellas and Tzouganatos [183] and Mostafa et al. [24] used a bottom-up approach in system design and top-down in cost estimation. Table 2.4 shows the cost items for the various ESSs found in our review.

The variation in costs among the studies is due to different assumptions in efficiency, cycle life, discharge duration, commodity price, and so on. The uncertainties in costs of mature technologies, such as PHS and Pb-A battery, are relatively lower than costs of emerging technologies, such as Li-ion, VRFB, FES, and fuel cell. Although the differences in input cost parameters and some technical assumptions are considerable, there have been few uncertainty analyses conducted to address the variabilities to improve the reliability of the estimates. A handful of studies [23, 31, 51, 131] performed uncertainty analyses. The impact of uncertainties in input data and assumptions can be realized from the LCOE ranges published by Thaker et al. [131] and Kapila et al. [31]. Thaker et al. [131] included plant capacity and lifetime, duration of discharge, capacity factor, solar multiple, and discount rate in the uncertainty analysis of LCOE of different thermal ESSs. Similarly, Kapila et al. [31] considered the ranges of various economic and technical parameters and studied their impact in the uncertainty analysis of different mechanical energy storage. The LCOE of TES (latent heat storage with one tank) can range from \$6/MWh to \$43/MWh because

of the commodity price range of phase change materials [131]. The LCOE for PHS can range from \$74/MWh to \$138/MWh as a result of variation in input parameters such as head, velocity and flow rate of water, efficiency, and duration of discharge [31]. Baumann et al. presented a range in the LCC of various electro-chemical batteries [51]. The highest level of uncertainty is found in the VRFB and is a result of the quality of available data. Along with the technical and cost parameters, such as number of cycles and discount rate, future improvement is a source of uncertainty of future LCOE of ESSs [23].

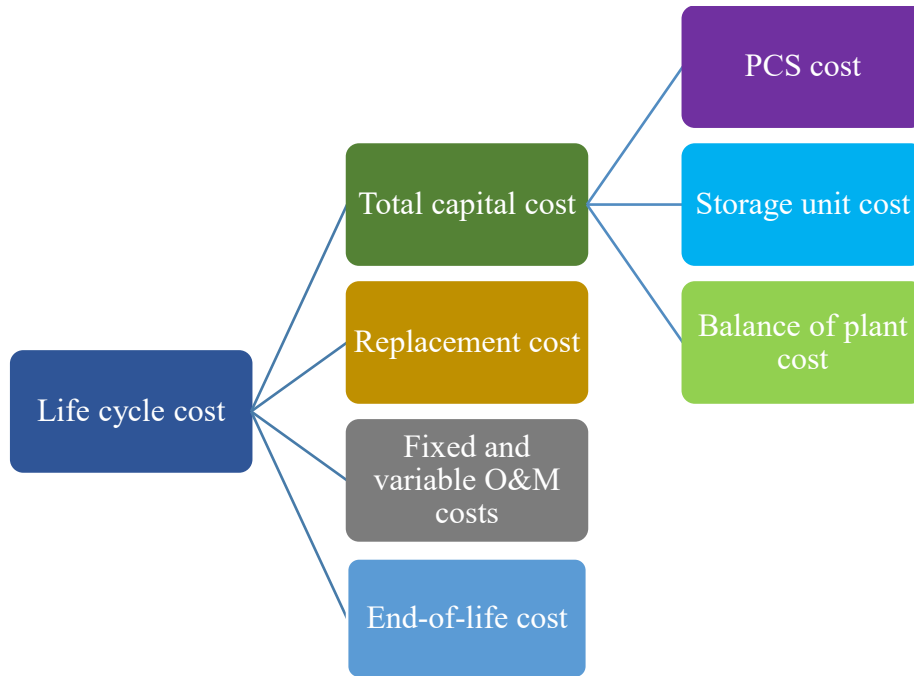


Figure 2.3: ESS's generalized total life cycle cost structure

Table 2.4: Cost items of various energy storage systems [24, 25, 28, 69, 94, 105, 176, 184-194]

ESS	Storage section cost (\$/kWh)	PCS cost (\$/kW)	BOP cost (\$/kW)	O&M cost (\$/kW-year)
PHS	5-136	403-4644	3-30	2-10
CAES (A)	93-141	868-960	3-30	2-4
CAES (U)	2-130	432-1674	3-30	2-5

ESS	Storage section cost (\$/kWh)	PCS cost (\$/kW)	BOP cost (\$/kW)	O&M cost (\$/kW-year)
FES	216-162,000	32-756	54-300	5-6
Pb-A	132-915, 220 ^a	211-648, 211 ^a	46-140, 95 ^a	3-26, 8 ^a
Li-ion	282-4104, 189 ^a	161-4320, 211 ^a	0-130, 95 ^a	2-123, 8 ^a
Na-S	194-1080, 465 ^a	221-3240, 211 ^a	68-130, 95 ^a	2-54, 8 ^a
Ni-Cd	609-1210	281-355	76-130	4-26
VRFB	142-1080, 393 ^a	351-1620, 211 ^a	11-151, 95 ^a	4-51, 8 ^a
Zn-Br	192-783	163-810	11-151	3-7
Hydrogen	2-15	540-4809	11-43	17-48
Supercapacitor	108-101,520	108-864	11-108	1-6

(A) = aboveground and (U)= underground.

^a 2025 cost predictions [189].

2.3.2. Economic performance of various ESSs

Although most of the studies used LCOE as a performance indicator to compare various ESSs for different applications, a few studies used, for example, payback period [43, 180], TCC [22, 189], and benefit/cost ratio [26, 191]. This section reviews the economic performance of different storage technologies. The costs are summarized in Table 2.5 (for mechanical storage), Table 2.6 (for electro-chemical storage), and Table 2.7 (for hydrogen and thermal storage).

2.3.2.1. Mechanical storage

PHS and CAES are bulk energy storage technologies with a lower cost per unit energy than the other ESSs [195]. Long life and storage duration, along with large capacity, are the main advantages of these technologies [24]. Several studies examined the economic performances of PHS and CAES. Studies by Schmidt et al. [23], Mostafa et al. [24], and Jülch [176] show that PHS has the lowest LCOE among the mature ESSs. Mostafa et al. found that the LCOE for PHS is \$0.08 lower than that of underground CAES per kWh electricity [24]. Compared to a conventional

hydro power plant, the construction and installation costs of PHS are twice as much for the same capacity. However, the O&M costs are similar [196]. For the CAES, the compressed air can be stored in underground caverns or aboveground vessels. Although underground storage provides greater cost competitiveness [24, 31], aboveground pressure vessels are easy to construct and implement [28]. The size of underground reservoirs facilitates longer discharge time, typically 8-26 hours, whereas aboveground vessels are usually designed to discharge for only 2-4 hours [28]. Although underground CAES is a cheaper option, finding and verifying airtight storage is a challenge. The techno-economic feasibility of C-CAES and A-CAES was assessed in a few studies. Kapila et al. found a higher LCOE for A-CAES than for C-CAES [31]. Fuel cost is the major contributor to the total LCC of C-CAES, and capital cost in the case of A-CAES. Similar results were obtained by Caralis et al. [197]. The estimated LCOE per kWh for C-CAES is about \$0.05 lower than for A-CAES.

Economies of scale dictate that large-scale plants like PHS or CAES be built for longer discharge duration (more than 8 to 10 hours) [119]. Bulk ESSs (e.g., PHS and CAES) tend to exhibit the lowest cost per unit energy because of economies of scale [195]. Kapila et al. found that the bigger capacity PHS plants show greater cost competitiveness at a scale factor of 0.52 [31]. The scale factors of conventional and adiabatic CAES systems are 0.87 and 0.88, respectively.

FESS has already become feasible for short-duration grid applications [198-200]. FESS was found to be economical when operated for more than 5000 cycles per year with a storage duration of less than 30 minutes [23]. The LCOEs reported by Mostafa et al. [24] and Akhil et al. [119] are within the range of \$0.41-\$0.64/kWh. According to Nikolaidis and Poullikkas, the cost per cycle could go up to \$1.62/kWh [22]. Flywheels can be made of steel or composite materials. The capital cost of a 20 MW frequency regulation plant by Beacon Power is about \$1872/kW (high-speed

composite flywheel). In contrast, the total capital cost of Active Power's 250 kW flywheel is about \$804/kW (low-speed steel flywheel) [201]. The material cost of carbon fiber composite is 20 times the cost of steel [202]. High-speed flywheels use costly magnetic bearings, and low-speed flywheels typically use inexpensive mechanical bearings [203-205].

Table 2.5: A summary of TEAs of mechanical storage systems

ESS	Capital cost (\$/kW)	Capital cost (\$/kWh)	LCOE (\$/kWh)	Applications	Future cost	Sensitivity/uncertainty	Comments	Reference
PHS	850-2126	22-58	0.07-0.14	EA	N	Y/Y	Single reservoir and two-reservoir scenarios were considered. The total investment cost ranges from \$208-\$572 million for capacities of 98-491 MW.	[31]
-	-	-	0.17	LT	N	Y/N	The amortized capital cost is \$54/kW for the long-term application.	[24]
-	-	-	1.09-2.16, 0.06-0.11	LT and ST	Y	Y/N	The LCOE ranges represent the long- and short-term applications, respectively.	[176]
-	1768-3328	110-208	-	16 h discharge	Y	N/N	The capital cost refers to the total project cost.	[189]
-	-	-	-	Long-duration	N	N/N	The present worth of a 10-year operation of PHS with 8 hours duration is \$2868/kW.	[25]
-	1396-2538	-	-	EA	N	N/N	The annualized return on investment was calculated for a range of capital costs.	[206]
-	1827-5237	304-524	-	BES and RI	N	N/N	The energy capacity ranges from 1680-14,000 MWh.	[207]
-	-	15-99	-	Wind power	N	N/N	The costs are taken from several studies.	[91]

ESS	Capital cost (\$/kW)	Capital cost (\$/kWh)	LCOE (\$/kWh)	Applications	Future cost	Sensitivity/uncertainty	Comments	Reference
	2252-3285	167-411	0.18-0.25	BES	N	N/N	Costs vary with capacity from 280-1300 MW. The net present installed cost ranges from \$6402-\$9098/kW.	[119]
	1928	-	-	LB	Y	Y/N	PHS scenarios are more cost-effective because of their long lifetime of 50 years.	[181]
	-	-	0.04	-	N	N/N	There is no information about the capital cost.	[208]
	624	104	-	-	N	N/N	The costs are taken from several studies.	[116]
	2048	256	-	EA	N	Y/N	The PHS is modeled as a 300 MW/2400 MWh system. The benefit to cost ratio is 1.32.	[209]
	636-2120	5-106	-	PQ, BP, and EM	N	N/N	The capital cost per cycle ranges from \$0.0002-\$0.02/kWh.	[22]
	-	-	-	SO, NO, and consumption	Y	Y/Y	12 stationary applications were considered for the analysis. The authors presented the LCOE from 2015-2050.	[23]
	-	-	0.02-0.31	Utility	N	Y/Y	The LCOE was calculated from the real operating plants' capital cost.	[175]

ESS	Capital cost (\$/kW)	Capital cost (\$/kWh)	LCOE (\$/kWh)	Applications	Future cost	Sensitivity/uncertainty	Comments	Reference
	1641	-	0.28	Wind energy curtailment	N	N/N	The costs are for a 100 MW system.	[197]
CAES	-	-	-	Back-up power	N	Y/Y	The LCC of A-CAES ranges from about \$2.18-2.27 million for a MW scale plant.	[29]
	-	-	0.07-0.10	BES	N	Y/N	10 MW advanced A-CAES with 8-hour storage. The TCC is about \$9.5 million.	[210]
	645-750	1-33	0.06-0.07	EA	N	Y/Y	Salt cavern, porous formation, and hard rock cavern storage mediums were considered. The investment cost ranges from \$63-\$286 million for C-CAES depending on the storage medium for capacities of 81-404 MW.	[31]
	1999-2364	1-54	0.10-0.13	EA	N	Y/Y	Salt cavern, porous formation, and hard rock cavern storage mediums were considered. The investment cost ranges from \$149-\$743 million for A-CAES depending on the storage medium for capacities of 60-298 MW.	[31]

ESS	Capital cost (\$/kW)	Capital cost (\$/kWh)	LCOE (\$/kWh)	Applications	Future cost	Sensitivity/uncertainty	Comments	Reference
-	-	-	0.25	LT	N	Y/N	Underground CAES. The amortized capital cost is approximately \$65/kW for long-term application.	[24]
-	-	-	0.26	LT	N	Y/N	Aboveground CAES. The amortized capital cost is approximately \$120/kW for long-term application.	[24]
-	-	-	>2, 0.12-0.14	LT and ST	Y	Y/N	The LCOE ranges represent long- and short-term applications, respectively, for C-CAES.	[176]
-	-	-	2-5, 0.08-0.13	LT and ST	Y	Y/N	The LCOE ranges represent the long- and short-term applications for A-CAES, respectively.	[176]
1090-2646	98-238	-	-	16 h discharge	Y	N/N	The capital cost refers to the total project cost.	[189]
-	-	-	-	Long-duration	N	N/N	The present worth of a 10-year operation of CAES with an 8-hour duration is \$1781/kW.	[25]
952-1269	-	-	-	EA	N	N/N	The annualized return on investment was calculated for a range of capital costs.	[206]

ESS	Capital cost (\$/kW)	Capital cost (\$/kWh)	LCOE (\$/kWh)	Applications	Future cost	Sensitivity/uncertainty	Comments	Reference
	1218-1523	73-152	-	BES and RI	N	N/N	Underground CAES. The energy capacity ranges from 1080-2700 MWh.	[207]
	-	4-99	-	Wind power	N	N/N	The costs are taken from several studies.	[91]
	1101-1421	18-210	0.14-0.24	BES	N	N/N	Costs vary with capacity from 50-103 MW. The net present installed cost ranges from \$4934-\$5452/kW.	[119]
	-	-	0.04	-	N	N/N	Advanced A-CAES. There is no information about the TCC.	[208]
	-	-	0.05	-	N	N/N	C-CAES. There is no information about the TCC.	[208]
	940, 2350	59, 118	-	-	N	N/N	The costs are taken from several studies. The capital costs are for underground and aboveground CAESs, respectively.	[116]
	2128	266	-	EA	N	Y/N	The aboveground CAES is modeled as a 100 MW/800 MWh system. The benefit to cost ratio is 1.27.	[209]
	424-848	2-53	-	PQ, BP, and EM	N	N/N	The capital cost per cycle is \$0.0003-\$0.02/kWh.	[22]

ESS	Capital cost (\$/kW)	Capital cost (\$/kWh)	LCOE (\$/kWh)	Applications	Future cost	Sensitivity/uncertainty	Comments	Reference
	-	-	-	SO, NO, and consumption	Y	Y/Y	12 stationary applications were considered for the analysis. The authors presented the LCOE from 2015-2050.	[23]
	-	-	0.02-0.16	Utility	N	Y/Y	The LCOE was calculated from the real operating plants' capital cost.	[175]
	1607, 2356	-	0.23, 0.28	Wind energy curtailment	N	N/N	The costs are for C-CAES and advanced A-CAES, respectively.	[197]
FESS	-	-	0.64	ST	N	Y/N	The amortized capital cost is \$65/kW for short-term application.	[24]
	1123-2995	4493-11,981	-	0.25 h discharge	Y	N/N	The capital cost represents the total project cost.	[189]
	-	-	-	Short-duration	N	N/N	The present worth of a 10-year operation of FESS with 0.25-hour duration is \$1103-\$1154/kW.	[25]
	2373-2700	9491-10,708	-	FR and RI	N	N/N	The power and energy capacities are 20 MW and 5 MWh, respectively.	[207]
	-	487-973	-	Wind power	N	N/N	The costs are taken from several studies.	[91]
	2627	10,510	0.41	FR	N	N/N	The net present installed cost is \$4784/kW.	[119]
	412	5876	-	-	N	N/N	The costs are taken from several studies.	[116]

ESS	Capital cost (\$/kW)	Capital cost (\$/kWh)	LCOE (\$/kWh)	Applications	Future cost	Sensitivity/uncertainty	Comments	Reference
-	-	437-2860	-	-	N	N/N	The costs are taken from several studies.	[170]
265-371	-	1060-5300	-	PQ, BP, and EM	N	N/N	The capital cost per cycle is \$0.0001-\$0.02/kWh.	[22]
-	-	-	-	SO, NO, and consumption	Y	Y/Y	12 stationary applications were considered for the analysis. The authors presented the LCOE from 2015-2050.	[23]
-	-	-	-	Back-up power	N	Y/Y	The LCC is about \$0.05 million for fast response.	[29]
1872	-	-	-	FR	N	N/N	Beacon power's composite rotor flywheel [211].	[201]
804	-	-	-	UPS	N	N/N	Active Power's 4340 alloy steel rotor flywheel [55].	[201]

Y = yes, N = no.

EA = energy arbitrage, BES = bulk energy storage, RI = renewable integration, FR = frequency regulation, LB = load balancing, PQ = power quality, BP = bridging power, EM = energy management, SO = system operation, NO = network operation, A-CAES = adiabatic compressed air energy storage C-CAES = conventional compressed air energy storage, PS = peak shaving, ISC = increase of self-consumption, UPS = uninterruptible power supply, ST = short-term, LT = long-term.

2.3.2.2. Electro-chemical storage

Electro-chemical batteries can be used for various applications whose characteristics dictate the cost of electricity. The TCC and LCOE in various applications are primarily influenced by the technical parameters of the electro-chemical ESSs, such as discharge duration and cycle life, as well as depth of discharge [23, 212]. Several studies assessed the LCC and LCOE of different stationary applications. Battke et al., for example, estimated the LCOE of Pb-A, Li-ion, Na-S, and VRF batteries and found a wide range of LCOEs, depending on the application [105]. The energy applications (time-shift, T&D investment deferral, energy management, and increase of self-consumption) are cheaper than the power applications (frequency regulation and voltage regulation). In the energy applications, the electricity throughput is higher because of the higher battery use with longer discharge time. The relative ranking of batteries across various applications depends on cycle life and number of cycles, which ultimately dictate investment and replacement costs [105]. For a small-scale application, Pb-A is cost-competitive. Li-ion performs well in applications with a high energy/power ratio and large number of cycles [105]. The LCOEs estimated by Baumann et al. [51] differ from one scenario to the next mainly due to different operational characteristics considered in the applications. The daily number of cycles for electric-time shift, PV self-consumption, primary regulation, and renewable support are 2, 1, 34, and 1.12, respectively, and the discharge durations are 4, 3.2, 1, and 10 hours, respectively. Baumann et al. mentioned that lower capital costs for the PCS and BOP lead to lower LCOEs in energy applications than in the power applications [51]. Li-ion performs economically better in all the applications than the other batteries. Short lifetime and low efficiency are the main challenges of Pb-A. The performance of a VRFB is comparable with Li-ion for energy applications. However, due to increased capital costs for large stacks and membrane area, a VRFB is not suitable for power

applications. According to Jülch, application scenarios are characterized by size, duration of discharge, and number of cycles [176]. Zakeri and Syri changed the duration of discharge from 1 hour to 8 hours and observed a drop in LCOE with increased duration of discharge [28]. According to Staffell and Rustomji, Li-ion achieves a larger profit as a result of its high efficiency [195]. Na-S's lower capital cost leads to a higher rate of return (ROR). Because of its long cycle life and high efficiency, as well as strong capital cost reduction potential, the Li-ion battery is expected to dominate the energy market by 2030 [23]. Nikolaidis and Poullikkas estimated the LCOE for several electro-chemical ESSs [22]. According to the authors, the low investment cost of Pb-A is the reason it is widely used in the energy storage market. Although Ni-Cd has a longer lifetime and higher specific energy than Pb-A, its higher investment cost is a problem. The LCOE of electro-chemical ESSs is expected to decrease with improvements in material and technologies [176]. Schmidt et al. forecasted a decrease in the LCOE of electro-chemical ESSs, which could challenge the growth of PHSs and CAESs [23]. For a discharge duration of less than 4 hours and fewer than 300 cycles per year, Li-ion would be attractive by 2030. For a longer discharge duration and number of cycles, the VRFB would be competitive, according to Schmidt et al. [23]. Moreover, the round-trip efficiency and cycle life will be the most influential parameters in future LCOE calculations [23]. For example, a 16% efficiency improvement for a VRFB from 2015-2030 can make it cheaper than the Li-ion ESS.

Table 2.6: A summary of TEAs of electro-chemical storage systems

ESS	Capital cost (\$/kW)	Capital cost (\$/kWh)	LCOE (\$/kWh)	Applications	Future cost	Sensitivity/uncertainty	Comments	Reference
Pb-A	-	-	0.63	MT	N	Y/N	The amortized capital cost is about \$60/kW for medium-term application.	[24]
	-	-	0.36-1.38	TS, PVSC, PR, and RS	N	Y/Y	The LCOE varies with Li-ion chemistry. The electric time-shift has the lowest LCOE, primary regulation the highest.	[51]
	1487-1622	372-656	-	4 h discharge	Y	N/N	The capital cost refers to the total project cost.	[189]
	-	-	0.18-0.22	LT and ST	Y	Y/N	The LCOE is for short-term application with 100 MW/400 MWh.	[176]
	-	-	-	Long- and short-duration	N	N/N	The costs are for an advanced Pb-A battery. The present worth ranges from \$826-\$3330/kW depending on the duration and frequency of discharge.	[25]
	-	-	-	Long- and short-duration	N	N/N	The costs are for an advanced Pb-A battery with carbon-enhanced electrodes. The present worth varies from \$748 to \$2411/kW depending on the duration and frequency of discharge.	[25]

ESS	Capital cost (\$/kW)	Capital cost (\$/kWh)	LCOE (\$/kWh)	Applications	Future cost	Sensitivity/uncertainty	Comments	Reference
1135-5489	507-4535	-	BES and RI, TS, FR, T&D support, etc.	N	N/N	The energy capacities are 200, 0.25-50, and 3.2-48 MWh for bulk energy storage, frequency regulation, and utility T&D grid support, respectively. The LCOE varies with the application.	[207]	
-	57-372	-	Wind power	N	N/N	The costs are taken from several studies.	[91]	
1404-7013	409-5615	0.15-1.4	BES, FR, RI, utility T&D, etc.	N	N/N	The costs are for an advanced Pb-A battery. The LCOE varies with the application.	[119]	
-	-	0.33-2.9	TS, T&D investment deferral, EM, ISC, FR, and SVR	N	Y/Y	The energy time-shift has the lowest LCOE, frequency regulation the highest.	[105]	
346	461	-	-	N	N/N	The costs are taken from several studies.	[116]	
318-636	212-424	-	PQ, BP, and EM	N	N/N	The capital cost range per cycle is between \$0.15 and \$3.12/kWh.	[22]	

ESS	Capital cost (\$/kW)	Capital cost (\$/kWh)	LCOE (\$/kWh)	Applications	Future cost	Sensitivity/uncertainty	Comments	Reference
-	-	-	-	SO, NO, and consumption	Y	Y/Y	12 stationary applications were considered for the analysis. The authors presented the LCOE from 2015 to 2050.	[23]
-	-	0.04-0.12	0.04-0.12	Utility	N	Y/Y	The LCOE was calculated from the real operating plants' capital cost.	[175]
-	-	-	-	Back-up power	N	Y/Y	The LCC is about \$0.21 million for fast response.	[29]
-	-	0.83-1.70	0.83-1.70	TS, PVSC, PR, and RS	N	Y/Y	The LCOE is for the VRLA battery. Electric time-shift has the lowest LCOE and primary regulation the highest.	[51]
-	-	-	-	EA, FR, T&D upgrade deferral, PS, and ISC	N	Y/Y	The authors provided a range of LCCs for Poland, Germany, and Switzerland.	[213]
-	-	-	-	SD, RPD, and REB	N	Y/N	The system would be feasible if the Pb-A battery cost is reduced to \$0.06/kWh per cycle.	[214]

ESS	Capital cost (\$/kW)	Capital cost (\$/kWh)	LCOE (\$/kWh)	Applications	Future cost	Sensitivity/uncertainty	Comments	Reference
Li-ion	-	-	0.32-1.34	TS, T&D investment deferral, EM, ISC, FR, and SVR	N	Y/Y	Energy management has the lowest LCOE, voltage regulation the highest.	[105]
	-	-	0.27-0.43	LT and ST	Y	Y/N	The LCOE is for short-term application with 100 MW/400 MWh.	[176]
	1632-2414	408-604	-	4 h discharge	Y	N/N	The capital cost refers to the total project cost.	[189]
	-	-	0.66	MT	N	Y/N	The amortized capital cost is about \$124/kW for the medium-term application.	[24]
	-	-	-	Long- and short-duration	N	N/N	The present worth ranges from \$1126-\$3400/kW depending on the duration and frequency of discharge.	[25]
	-	1074-1551	-	Wind power	N	N/N	The costs are taken from several studies.	[91]
	1207-5945	1183-5247	0.11-1.40	FR, RI, utility T&D, etc.	N	N/N	The net present installed costs range from \$2386-\$8951/kW for frequency regulation and from \$2745-\$13,366/kW	[119]

ESS	Capital cost (\$/kW)	Capital cost (\$/kWh)	LCOE (\$/kWh)	Applications	Future cost	Sensitivity/uncertainty	Comments	Reference
							for utility T&D. The LCOE varies with the application.	
	4610	2882	-	-	N	N/N	The costs are taken from several studies.	[116]
	1272-4240	636-2650	-	PQ, BP, and EM	N	N/N	The capital cost per cycle is between \$0.08 and \$1.10/kWh.	[22]
	-	-	-	SO, NO, and consumption	Y	Y/Y	12 stationary applications were considered for the analysis. The authors presented the LCOE from 2015 to 2050.	[23]
	-	-	0.05-0.20	Utility	N	Y/Y	The LCOE was calculated from the real operating plants' capital cost.	[175]
	-	-	-	Back-up power	N	Y/Y	The LCC is about \$0.12 million for fast response.	[29]
	-	-	-	EA, FR, T&D upgrade deferral, PS, and ISC	N	Y/Y	The authors provided a range of LCCs for Poland, Germany, and Switzerland.	[213]
	-	-	-	SD, RPD, and REB	N	Y/N	The system would be feasible if the Li-ion battery cost is reduced to \$0.09/kWh per cycle.	[214]

ESS	Capital cost (\$/kW)	Capital cost (\$/kWh)	LCOE (\$/kWh)	Applications	Future cost	Sensitivity/uncertainty	Comments	Reference
Na-S	-	-	-	Long- and short-duration	N	N/N	The present worth is from \$2861-\$2965/kW depending on the frequency of discharge.	[25]
	-	-	0.31	MT	N	Y/N	The amortized capital cost is about \$54/kW for medium-term application.	[24]
	-	495	-	-	N	N/N	There is no information about the LCOE.	[170]
	-	-	0.29-0.34	-	N	N/N	The net present cost ranges from \$220-\$268 million.	[215]
	3700-4774	531-662	-	BES and RI, TS, FR, T&D support, etc.	N	N/N	The energy capacities are 300 and 7.2 MWh for bulk energy storage and utility T&D grid support, respectively. The LCOE varies with the application.	[207]
	-	292-517	-	Wind power	N	N/N	The costs are taken from several studies.	[91]
	3665-4098	525-611	0.29-0.0.33	BES and utility T&D	N	N/N	The net present installed costs range from \$6885-\$7280/kW for bulk energy storage and from \$7242-\$7885/kW for utility T&D. The LCOE varies with the application.	[119]

ESS	Capital cost (\$/kW)	Capital cost (\$/kWh)	LCOE (\$/kWh)	Applications	Future cost	Sensitivity/uncertainty	Comments	Reference
	-	-	0.23-1.75	TS, T&D investment deferral, EM, ISC, FR, and SVR	N	Y/Y	Energy management has the lowest LCOE, voltage regulation the highest.	[105]
	3458	576	-	-	N	N/N	The costs are taken from several studies.	[116]
	>1060	318-530	-	PQ, BP, and EM	N	N/N	The capital cost per cycle is between \$0.07 and \$0.40/kWh.	[22]
	-	-	-	SO, NO, and consumption	Y	Y/Y	12 stationary applications were considered for the analysis. The authors presented the LCOE from 2015 to 2050.	[23]
	2783	-	0.62	Wind energy curtailment	N	N/N	The costs are for 85 MW Na-S ESS.	[197]
Ni-Cd	-	-	0.67-1.1	-	N	N/N	The net present cost is from \$498-\$585 million.	[215]
	-	-	0.69	MT	N	Y/N	The amortized capital cost is about \$113/kW for medium-term application.	[24]
	-	477-2864	-	Wind power	N	N/N	The costs are taken from several studies.	[91]
	1729	1729	-	-	N	N/N	The costs are taken from several studies.	[116]

ESS	Capital cost (\$/kW)	Capital cost (\$/kWh)	LCOE (\$/kWh)	Applications	Future cost	Sensitivity/uncertainty	Comments	Reference
	530-1590	848-1590	-	PQ, BP, and EM	N	N/N	The capital cost per cycle is \$0.30-\$1.76/kWh.	[22]
VRFB	-	-	-	Long- and short-duration	N	N/N	The present worth is from \$1173-\$3846/kW depending on the duration and frequency of discharge.	[25]
	-	-	0.50-3.60	TS, PVSC, PR, and RS	N	Y/Y	Electric time-shift has the lowest LCOE, primary regulation the highest.	[51]
	2852-5435	713-1359	-	4 h discharge	Y	N/N	The capital cost refers to the total project cost.	[189]
	-	-	0.37-0.42	LT and ST	Y	Y/N	The LCOE is for short-term application with 100 MW/400 MWh.	[176]
	-	-	0.48	MT	N	Y/N	The amortized capital cost is about \$76/kW for medium-term application.	[24]
	3585-4416	740-990	-	BES and RI, TS, FR, T&D support, etc.	N	N/N	The energy capacities are 250 and 4-40 MWh for bulk energy storage and utility T&D grid support, respectively. The LCOE varies with the application.	[207]
	-	716	-	Wind power	N	N/N	The costs are taken from several studies.	[91]

ESS	Capital cost (\$/kW)	Capital cost (\$/kWh)	LCOE (\$/kWh)	Applications	Future cost	Sensitivity/uncertainty	Comments	Reference
	1912-4405	880-978	0.52-0.56	BES, utility T&D, etc.	N	N/N	The net present installed cost is from \$7273-8445/kW. The LCOE varies with the application.	[119]
	-	-	0.24-1.61	TS, T&D investment deferral, EM, ISC, FR, and SVR	N	Y/Y	Energy management has the lowest LCOE, voltage regulation the highest.	[105]
	636-1590	159-1060	-	PQ, BP, and EM	N	N/N	The capital cost per cycle is between \$0.12 and \$0.78/kWh.	[22]
	-	-	-	SO, NO, and consumption	Y	Y/Y	12 stationary applications were considered for the analysis. The authors presented the LCOE from 2015 to 2050.	[23]
	-	-	0.32-0.37	Utility	N	Y/Y	The LCOE was calculated from the real operating plants' capital cost.	[175]
	-	-	-	EA, FR, T&D upgrade deferral, PS, and ISC	N	Y/Y	The authors provide a range of LCCs for Poland, Germany, and Switzerland.	[213]

ESS	Capital cost (\$/kW)	Capital cost (\$/kWh)	LCOE (\$/kWh)	Applications	Future cost	Sensitivity/uncertainty	Comments	Reference
	-	-	-	BES	N	N/N	The ratios of benefit/cost are 5-6% and 43%, respectively, for day-ahead market and reserve market.	[191]
Zn-Br	-	-	-	Long- and short-duration	N	N/N	The present worth is from \$819-\$2953/kW depending on the duration and frequency of discharge.	[25]
	-	-	0.50	MT	N	Y/N	The amortized capital cost is about \$54/kW for the medium-term application.	[24]
	1731-2405	346-1612	-	BES and RI, TS, FR, T&D support, etc.	N	N/N	The energy capacities are 250 and 5-50 MWh for bulk energy storage and utility T&D grid support, respectively. The LCOE varies with the application.	[207]
	-	597	-	Wind power	N	N/N	The costs are taken from several studies.	[91]
	1925-3468	385-1734	0.23-1.03	BES, utility T&D, FR, RI, etc.	N	N/N	The net present installed cost is from \$4047-\$6681/kW. The LCOE varies with the application.	[119]
	742-2650	159-1060	-	PQ, BP, and EM	N	N/N	The capital cost per cycle is between \$0.06 and \$0.71/kWh.	[22]

ESS	Capital cost (\$/kW)	Capital cost (\$/kWh)	LCOE (\$/kWh)	Applications	Future cost	Sensitivity/uncertainty	Comments	Reference
-	-	-	-	SO, NO, and consumption	Y	Y/Y	12 stationary applications were considered for the analysis. The authors presented the LCOE from 2015 to 2050.	[23]
-	-	0.15-0.19	Utility	N	Y/Y	The LCOE was calculated from the real operating plants' capital cost.	[175]	
-	-	-	BES	N	N/N	The ratios of benefit/cost are 5-6% and 43%, respectively, for day-ahead market and reserve market.	[191]	

Y = yes, N = no.

EA = energy arbitrage, BES = bulk energy storage, RI = renewable integration, FR = frequency regulation, LB = load balancing, PQ = power quality, BP = bridging power, EM = energy management, SO = system operation, NO = network operation, PS = peak shaving, ISC = increase of self-consumption, SD = smooth demand, RPD = reducing peak demand, REB = reducing electricity bill, TS = time-shift, SVR = support of voltage regulation, PVSC = PV self-consumption, PR = primary regulation, RS = renewables support, VRLA = valve-regulated lead-acid, ST = short-term, MT = medium-term, LT = long-term.

2.3.2.3. Hydrogen storage

Several studies considered the integration of renewable sources like solar and wind with hydrogen storage from a technical perspective [216-220]. However, the concept of integrating hydrogen storage into the electrical network depends on the system's economy [183]. Parra and Patel report the capital cost and LCOEs for hydrogen production using electricity from the Swiss grid [221]. On the kW scale, the LCOE for PEM electrolyzers is about 15% higher than alkaline's due to the higher capital cost for stacks [221]. However, the difference in LCOE for these two technologies is less than 5% on the MW scale due to economies of scale [221]. A similar power-to-gas pathway was used by Preuster et al. [222] and Jülch [176]. Jülch assumed that the H₂ will be stored underground [176]. These studies did not consider fuel cells for electricity generation. Depending on the storage medium, storage costs range from \$17/kWh for aboveground storage to \$0.002-\$55/kWh for underground storage [28]. Using underground storage rather than aboveground lowers the cost of electricity by 6-18% [215]. A power-to-power pathway was used by Mostafa et al. [24] and Ferrero et al. [223]. Ferrero et al. reported the lowest LCOE for the combination of alkaline electrolysis with a PEM fuel cell among the various electrolyzer and fuel cell combinations because of the alkaline electrolyzer's low capital cost and high efficiency [223]. Mostafa et al. estimated the LCOE for hydrogen storage to be \$0.48/kWh for medium-term stationary applications such as time-shift, transmission congestion relief, and substation on-site power [24]. Marocco et al. found a similar LCOE in a micro-grid application of hydrogen storage on a wind farm [224]. A recent study by Nguyen et al. assessed a grid-connected hydrogen production system through alkaline and PEM electrolyzers and found similar costs for both technologies [225]. The study is limited to hydrogen production only. Table 2.7 shows the summary of the review.

2.3.2.4. Thermal storage

Integrating TES with the electrical grid could help stabilize the grid. There has been research on the economic feasibility of integrating TES (sensible heat, latent heat, and thermochemical) to the power network [226-228]. Thaker et al. estimated the investment cost and LCOE for sensible heat, latent heat, and thermochemical storage systems [131]. The LCOE for indirect sensible heat storage using two tanks is higher than for direct sensible heat storage using two tanks because the former has a higher investment cost due to the use of an extra heat exchanger, which includes extra piping, pumps, and valves. With an increase in capacity, the LCOE decreases, and there is a strong relationship between discharge time and LCOE [229-231]. Flueckiger et al. varied the solar multiple and storage hour to find the best combination [190]. The authors observed a decrease in LCOE with storage hours for solar multiple values of 2-4. However, the LCOE was found to increase with a solar multiple of 1. This is because without sufficient solar radiation the storage system adds capital cost but cannot provide enough power. The LCOE decreases from \$0.80/kWh to \$0.69/kWh when the discharge time increases from 1 hour to 8 hours [229]. Similarly, Seitz et al. found that the LCOE decreases with increased capacity for latent heat thermal energy storage [230]. Boudaoud et al. determined 8 hours to be the optimum discharge time with a solar multiple of 1.6 [229]. Wu et al. examined a thermochemical ESS integrated with liquid air [180]. The round-trip efficiency is about 13% higher than the only thermochemical ESS's efficiency. The energy density is 3.4 times higher [180].

Table 2.7: A summary of TEAs of hydrogen and thermal storage systems

ESS	Capital cost (\$/kW)	Capital cost (\$/kWh)	LCOE (\$/kWh)	Applications	Future cost	Sensitivity/uncertainty	Comments	Reference
Hydrogen	-	-	0.48	MT	N	Y/N	The amortized capital cost is \$108/kW for medium-term application.	[24]
	-	0.22	-	IP and mobility	N	N/N	Power-to-gas pathway.	[222]
	-	-	0.30-0.50, 0.13-0.21	LT and ST	Y	Y/N	Power-to-gas pathway. The values represent the future cost in 2030. The LCOE ranges represent long-term and short-term applications, respectively.	[176]
	1183-1361	-	-	LL, DG, and POCWP	N	Y/N	The target capital costs for aboveground and underground storage are \$730 and \$616/kW, respectively.	[232]
	11,717	-	-	-	N	N/N	The number represents the capital cost of the fuel cell. No information was provided for other cost components.	[116]
	1238-2920	2-16	-	-	N	N/N	The values are based on costs found in the literature.	[233]
-	-	-	0.12	-	N	N/N	The cost of electrolyzers is about \$1313/kW.	[208]

ESS	Capital cost (\$/kW)	Capital cost (\$/kWh)	LCOE (\$/kWh)	Applications	Future cost	Sensitivity/uncertainty	Comments	Reference
-		3-19	-	-	N	N/N	The values are based on costs found in the literature.	[91]
1402-3507	-		0.44	EG	Y	N/N	Power-to-power pathway. The capital cost represents the cost of an alkaline fuel cell.	[223]
2712	-		0.54	EG	Y	N/N	Power-to-power pathway. The capital cost represents the cost of a PEM fuel cell.	[223]
510, 1086	-		-	NGN and mobility	N	Y/N	Power-to-gas pathway. The capital costs are for alkaline and PEM electrolyzers, respectively.	[221]
6423-9231	-		0.45-0.59	Micro-grid	N	N/N	Power-to-power pathway. The capital cost includes the costs of the electrolyzer and the fuel cell.	[224]
11,794	-		-	Off-grid	N	Y/N	Power-to-power pathway. The electricity source is solar. The capital cost includes the costs of the electrolyzer and the fuel cell.	[234]
465-859	-		-	GB	N	Y/N	Power-to-gas pathway. The range in the capital cost is for different system configurations, such as electrolysis-based balancing and gas turbine-based balancing.	[235]

ESS	Capital cost (\$/kW)	Capital cost (\$/kWh)	LCOE (\$/kWh)	Applications	Future cost	Sensitivity/uncertainty	Comments	Reference
	-	-	-	SO, NO, and consumption	Y	Y/Y	12 stationary applications were considered for the analysis. The authors presented the LCOE from 2015-2050.	[23]
	-	-	0.29	Stand-alone operation	N	N/N	A fuel cell system integrated with solar photovoltaic thermal (PVT).	[236]
TES	-	-	0.08-0.61	PG	N	Y/Y	The TCC is from \$100 to \$739 million depending on the configuration of the TES. The highest and lowest cost options are thermochemical and direct sensible using one tank, respectively.	[131]
	-	-	0.61-0.65	PG	N	N/N	A 15 MWh TES system for a concentrated solar power plant. A single-tank TES system was proposed. The TCC ranges from \$3-\$6 million.	[237]
	-	-	-	PG	N	N/N	The TCCs are \$1.91-\$2.01 million for two-tank and \$1.12-\$1.50 million for thermocline TES systems.	[238]
	-	-	0.05-0.07	PG	N	Y/N	A TES system with concentrated solar power. The TCCs are from \$732-\$795 million.	[239]

ESS	Capital cost (\$/kW)	Capital cost (\$/kWh)	LCOE (\$/kWh)	Applications	Future cost	Sensitivity/uncertainty	Comments	Reference
-	-	<96	-	PG	N	Y/N	Thermochemical ESSs for a solar thermal power plant. 8 thermochemical ESSs were identified as feasible in the near term.	[240]
-	-	-	0.18-0.19	PG	N	N/N	The payback period is 10 years for a new thermochemical ESS integrated with liquid air ESS.	[180]
-	-	-	0.13-0.19	PG	N	N/N	100 MW solar power plant with thermocline storage. The LCOE varies with the various solar multiple values for a 6-hour storage capacity.	[190]
-	-	-	0.14-0.23	PG	N	Y/N	A thermocline energy storage for a combined cycle solar power plant. The cost data were obtained from the SOLGATE project report [241].	[242]
571	-	-	0.11	PG	N	N/N	A 60 MW sensible heat TES with 6 hours of charging.	[231]
392-426	-	-	0.10	PG	N	N/N	A 60 MW latent heat TES with 6-8 hours charging using different materials.	[231]

ESS	Capital cost (\$/kW)	Capital cost (\$/kWh)	LCOE (\$/kWh)	Applications	Future cost	Sensitivity/uncertainty	Comments	Reference
-		59-117	0.16-0.18	PG	N	Y/N	Latent heat thermal storage. The LCOE varies with capacity up to 1200 MWh.	[230]
-	-	-	0.69-0.80	PG	N	Y/N	The effect of storage capacity factor, solar field size, solar insolation intensity, and plant capacity on the LCOE was assessed. The LCOE varies with storage duration.	[229]
-	-	-	0.65-1.4	PG	N	Y/N	The effect of storage capacity factor, solar field size, solar insolation intensity, and plant capacity on the LCOE was assessed. The LCOE varies with solar multiples.	[229]
-		34-38	-	PG	N	N/N	A 2165 MWh utility-scale packed bed TES system.	[243]
-	-	-	<0.07	PG	N	Y/N	A latent TES system integrated with a 200 MW concentrated solar power plant.	[244]
-	-	-	0.08-0.14	PG	Y	N/N	Latent heat TES with CSP tower.	[228]

Y = yes and N = no.

LL = load-leveling, DG = distributed generation, POCWP = purchase of off-peak curtailed wind power, ST = short-term, MT = medium-term, LT = long-term, EG = electricity generation, NGN = natural gas network, IP = industrial production, GB = grid balancing, PG = power generation, CSP = concentrated solar power, SO = system operation, NO = network operation.

2.3.3. Future cost estimates

Several recent studies presented the future costs of ESSs, which are vital for investment decisions [23, 166, 176, 179, 188, 189, 245-247]. Mongird et al. projected the future cost of electro-chemical ESSs for 2025 [189]. A 25% cost reduction is possible for the Li-ion PCS cost from the 2018 cost due to increased production capacity. The projection assumes that the PCS for all the batteries would exhibit uniform cost reduction. For the BOP, a 5% reduction was assumed from 2018. This reduction would be possible because of lower permitting costs and planning with an increased number of installations. Multiples ranging from 0.65 for Li-ion to 0.85 for Pb-A were used to forecast 2025 costs from 2018 costs [189]. These multiples were obtained from the cost information for various ESSs in the years 2018 and 2025 as reported in Kleinberg [188]. Mongird et al. also calculated the TCC using the predicted cost inputs [189]. Lazard forecasted the TCC of Li-ion, VRF, Zn-Br, Pb-A, and advanced Pb-A batteries [246]. The reduction in the TCC ranges from 6% for advanced Pb-A to 36% for Li-ion battery. The main drivers behind the huge reduction for the Li-ion are market competition and the benefit from electric vehicle manufacturing [246]. The study by Schmidt et al. projected the future prices of several energy storage technologies based on the experience curves [179]. The capital costs for stationary systems and battery packs are $\$340 \pm 60/\text{kWh}$ and $\$175 \pm 25/\text{kWh}$, respectively, regardless of storage technology in the years 2015-2040 [179]. The reduction of LCOE will be one-third by 2030 and one-half by 2050. Among the technologies, Li-ion seems to become the most cost-competitive for stationary uses from 2030. The battery storage systems are predicted to have the lowest LCOE in most application scenarios after 2025. Hayward and Graham projected battery storage costs to 2050 for the Australian energy market [245]. IREA projected the installed energy cost for different ESSs to 2030 [166]. The reduction potential is 50% for a Pb-A to 66% for a VRF battery. The installed cost reduction for

Li-ion is 54-61% from 2016-2030. Among the mechanical ESSs, FESS has a great cost reduction potential of 35% by 2030. It is expected that the lifetime will extend with improvement in materials and efficiency [166]. Ferrero et al. found an LCOE drop of 67% in 2030 from 2013 for alkaline-based hydrogen storage [223]. Although these costs are helpful for investment decisions, they are subject to some uncertainties due to technology changes, raw material price change, breakthroughs, etc. [179, 248, 249].

2.4. Review of the life cycle assessments of energy storage technologies

A number of studies review the life cycle environmental impacts of energy storage for transportation applications [30, 113, 250-252]. To the best of the author's knowledge, there is not a single paper that reviews ESSs for stationary applications. The recent study by Pellow et al. reviewed only a handful of LCA studies related to the Li-ion battery for stationary applications [113]. We conducted a literature search to include different ESSs, such as mechanical, electrochemical, hydrogen, and thermal. We found 33 relevant LCA studies on ESSs for stationary applications. This section provides a literature review of the LCAs of several ESSs.

2.4.1. Goal and scope definition

The goal defines the main purpose of conducting an LCA and its intended application, the type of analysis, the method used, and how and to whom the results are communicated; the scope includes the product system, the functional unit, the system boundary, allocation procedure, system inclusion, and exclusion criteria. Figure 2.4 shows a generalized system boundary of an LCA of ESSs. The system boundary includes material production and transportation, construction, operation, and decommissioning. System boundaries are set in accordance with the stated goal and scope of the study and the availability of inventory data. For example, Oliveira et al. assessed the environmental performance of ESSs for grid applications in Belgium [52]. Raw material extraction

and processing, assembly of equipment, transportation of equipment to Belgium, and its use and disposal were included in the system boundary; the electricity distribution network was left out as it was beyond the scope of the study. While a few studies assessed the impacts from cradle-to-grave [52, 253, 254], some considered cradle-to-gate without including the electricity for charging in the use phase [15, 255, 256] because the GHG emissions in this phase are location-specific and depend on the electricity mix. The end-of-life phase was excluded in some of the studies reviewed [255, 257-259]. The lack of information [260] and cradle-to-gate scope definition [261] are the main reasons for omitting the end-of-life phase. Because transportation makes up less than 1% of life cycle GHG emissions [256], many studies do not include transportation in their analysis. Longo et al., for instance, while building the life cycle inventory, did not include the energy consumption in transportation [108]. Table 2.8 shows the system boundaries used in different studies.

Of the 33 studies, only 2 conducted a consequential LCA [262, 263]. The attributional approach is used where the inputs and outputs are attributed to the selected functional unit. The consequential LCA, on the other hand, evaluates how the inputs and outputs flow within a system to respond to a change in decision [264-266]. Vandepaer et al. assessed the cradle-to-grave environmental impacts of grid-connected 6 MWh Li-ion and lithium metal polymer (LMP) batteries [262]. The analysis was conducted for the Swiss grid for a 2020 scenario with high renewable penetration. There is a lack of information on the operational characteristics of the batteries; however, the authors considered the marginal electricity mix as well as fractions of virgin and recycled materials for battery production in the analysis. They found that GHG emissions could be reduced significantly using these batteries to integrate renewable energy, for example, 439 g-CO₂eq/kWh for the Li-ion battery. Elzein et al. performed a cradle-to-grave consequential LCA of the Li-ion

battery integrated into the French grid for the year 2017 using the ecoinvent database [263]. The research highlights that the integration of an ESS in the grid could offer a significant environmental benefit in the operation phase.

Another important aspect of the goal and scope phase is the definition of the functional unit, used as a reference unit in quantifying energy use and resulting emissions. The functional unit should be based on the primary service of a system. For an energy storage system, the primary service is delivering the stored electricity. GJ, kWh, and MWh of electricity are common functional units used in earlier studies [52, 256, 258, 267]. A common unit allows us to compare different ESSs. However, some studies did not use a functional unit, which makes it difficult to compare the results for various storage types [54, 55, 268]. While most of the studies selected the functional unit based on the energy delivery (i.e., 1 MWh), the work by Ryan et al. used the power capacity (i.e., 1 MW of reserve capacity for 1 year), as bids are placed based on the power over a certain period [49]. As the frequency level changes with the change in output power of generators, presenting GHG emissions per MW basis could be appropriate in this scenario.

The modeling approach is also one of the critical aspects in current LCA literature for ESSs. In most process-based LCA, commercial software and database are used. For example, Oliveira et al. [52] and Wang et al. [255] used SimaPro, Peters et al. [269] used OpenLCA, and Sternberg and Bardow [270] used GaBi for modeling purposes. Some studies developed bottom-up process models using scientific principles. For example, Kapila et al. [256] and Thaker et al. [271] developed bottom-up LCA models to quantify the GHG and energy performances of mechanical and thermal storage systems, respectively. Such models maintain the process specificity of a product system and offer flexibility to modify the system based on any user's needs. However, the

main challenge with these models is in dealing with complex systems and multiple environmental impacts.

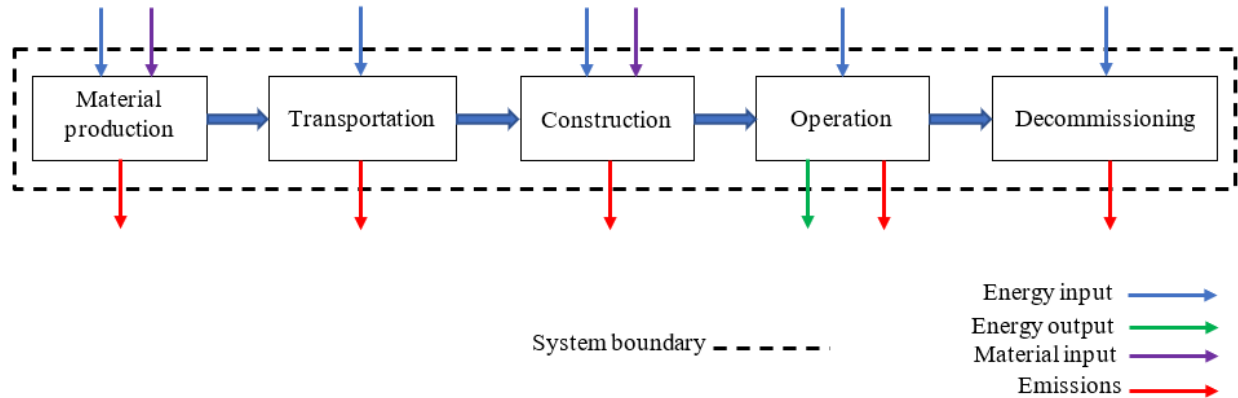


Figure 2.4: General LCA system boundary considered for energy storage systems

2.4.2. Inventory analysis

Life cycle inventory (LCI) analysis involves collecting data and establishing material and energy balances for each unit process considered in the system boundary. The amount of material and energy required depends on the system size. Once the material requirement is quantified, the energy requirement is estimated based on the material’s specific energy demand.

For inventory analysis, some studies rely on databases, such as ecoinvent [44, 253, 272], GREET [256, 271], NEEDS [52], and EIO [15, 268], and others use literature inventories [258] and data provided by manufacturers [146, 255]. Engineering equations are used to quantify material requirements for some components. For example, the reservoir volumes for PHS can be calculated from the volume of water required to operate a complete cycle [256]. For batteries, the individual material requirement is quantified from the percentage contribution of each material and the total weight of the battery [52, 108, 146]. The material inventories from Majeau-Bettez et al. [273], Sullivan and Gaines [109], Zackrisson et al. [274], Troy et al. [275], and Rydh and Sandén [146]

are widely used for different electro-chemical batteries. The NEEDS LCI database is one of the inventories for the fuel cell stack and electrolyzers for hydrogen storage systems [52]. It is important to mention that the quality of data used in the inventories should be checked as it dictates the environmental performance. The technology (energy and material requirements) and energy sources have a regionalized context. For example, a battery manufactured in China will have different impacts than one produced in Canada, depending on the manufacturing technology and electricity mix. The inventories should be adjusted accordingly to reflect such variabilities.

During the operation phase, energy is stored and discharged based on demand. The overall efficiency, depth of discharge and self-discharge rate, and lifetime are considered to calculate the lifetime electricity output from an energy storage system [276]. Increasing ESS efficiency or service life improves its environmental performance [276]. When the electricity source for the ESS is taken into account, the results will differ based on the source of electricity considered because GHG emissions from solar, wind, and fossil fuel power plants are different [52]. Hiremath et al. [258] and Kapila et al. [256] considered grid electricity for charging. Oliveira et al.'s inventory includes electricity from grid, solar, and wind [113]. Round-trip efficiency and upstream emissions for electricity generation together dominate the operation phase [113]. The energy and material requirements for system maintenance are considered if data are available [15, 256].

The biggest challenge in the end-of-life phase is the lack of data, as mentioned in a number of studies [44, 108, 213]. Longo et al. used average data for the European recycling process [108]; Weber et al. adapted existingecoinvent data sets [44]. Among the electro-chemical batteries, Pb-A is highly recyclable. Hiremath et al. modeled a scenario for 70% recycled lead [258] and Van den Bossche [110] considered 98.3% recyclability, assuming secondary lead quality is as good as virgin. Although some studies include the recycling of Li-ion batteries, it is difficult to get reliable

process parameters and robust results. Swain estimated that less than 3% of the world's Li-ion batteries are recycled [277]. According to Weber et al., only a little electricity is required to balance the vanadium electrolyte when used again [44]. The authors assumed a 95% recovery of vanadium electrolyte. With the increasing use of electro-chemical batteries, it is expected that recycling processes will be established, and recycling rates may improve in the future.

2.4.3. Impact assessment

The life cycle impact assessment (LCIA) translates the inventory results to defined impact categories (e.g., acidification, cumulative energy demand [CED], eutrophication, fossil fuel depletion, human toxicity, global warming potential [GWP], etc.). CED and GWP are the most common impact categories in ESS studies [30] because of their wide acceptance in decision-making. Human toxicity, particulate matter formation, and fossil resource depletion are also used. In addition to emissions, the net energy ratio (NER) is a performance indicator used in LCA studies on ESSs. NER is defined as a ratio of energy output to the total energy input of the product system throughout its lifetime [278].

Oró et al.'s [259] LCA of thermal energy storage is based on the Eco-indicator 99 (EI99) method [279]. The reasons for selecting the EI99 are its wide acceptance and the availability of extensive data, as mentioned by Oró et al. Three different damage categories are grouped into a single indicator. For example, the overall score considering the ecosystem quality, human health, and resources is 5.67/kWh for molten salt thermal storage under normal conditions [259]. Stougie et al. used ReCiPe 2016 to assess the environmental sustainability of different ESSs [280]. A total normalized score is given to each energy storage type. The total scores for Li-ion and PHS are 2346 and 100, respectively. The lower the ESS score, the higher its environmental performance is. Oliveira et al. [52] and Hiremath et al. [258] used ReCiPe 2008 [281] for impact assessment. The

difference between ReCiPe 2008 and ReCiPe 2016 is that weighting and normalization factors to calculate the endpoint indicator are unavailable in ReCiPe 2016 [280].

The environmental impacts of different ESSs found in various studies are listed in Table 2.8. Each life cycle stage makes different contributions to the environmental impacts depending on the system boundary and assumptions. Kapila et al. found that in PHS and CAES systems, the construction phase is the most material and energy intensive of the life cycle phases [256]. The authors amortized the energy consumption and resulting emissions from the life cycle stages over the lifetime of the storage system and estimated that about 95% of the emissions is resulted from the material and energy use in the construction phase [256]. With respect to life cycle emissions, conventional CAES is the most GHG intensive among mechanical storage technologies because it requires additional fuel, e.g., natural gas, during operation. Denholm and Kulcinski report that dam construction makes up 28% of the life cycle energy use of PHS when the electricity generation source is not considered [15]. Around 49% of the life cycle energy use is from natural gas consumption and the rest is from electricity use in different equipment. Storing electricity from renewable rather than non-renewable sources can reduce overall emissions significantly, as mentioned by Oliveira et al. [52].

The construction phase is one of the biggest sources of energy consumption for electro-chemical batteries. The disposal of the lead smelter is the main source of environmental impacts for Pb-A batteries. Oliviera et al. found that for Li-ion batteries, the mining activities of copper and lithium have the largest impact [52], and Rydh found that the largest impact for the VRFB is in the production of polypropylene tanks, flow frames, and steel stacks [146]. According to Denholm and Kulcinski, power stack materials and manufacturing make up 42-44% of the life cycle GHG emissions [15]. The BOP contributes 19-24% of the emissions. The anode and cathode materials

contribute considerably to the manufacturing energy use and GHG emissions. In Li-ion batteries, for example, anode and cathode materials make up 46% of the manufacturing emissions [253]. The use of recycled materials can significantly reduce energy consumption in material production. Rydh found that the use of 99% secondary lead, for instance, can reduce CO₂ emissions by 13% compared to the use of 50% secondary lead in Pb-A batteries [146].

Oliveira et al. conducted an LCA of proton exchange membrane fuel cell technology, which is scalable in a module of 500 kW [52]. This technology uses hydrogen from electrolyzers at high pressure. The authors compared mechanical and electro-chemical storage systems with hydrogen storage and found hydrogen storage to have the worst environmental performance. This is due to poor efficiency in hydrogen production and fuel cell conversion. However, GHG emissions from infrastructure requirement for fuel cell technology are marginal, less than 10 g-CO₂eq/kWh. The overall environmental footprint of fuel cells can be reduced considerably if electricity is stored from a low GHG-intensive source, and hydrogen storage could potentially compete with PHS and CAES [253].

The environmental performance of thermal ESSs has been assessed in a number of studies [254, 259, 267, 268, 271]. Among the manufacturing, construction, operation, dismantling, and disposal phases, the manufacturing phase makes up 46% of the life cycle GHG emissions. The solar collector assembly and heat transfer fluid are the largest sources of emissions in this phase [254]. According to Heath et al., life cycle GHG emissions can be reduced if the salt inventory for the thermocline storage system is reduced [268]. Oró et al. compared sensible heat storage in high temperature concrete and molten salts media with latent heat storage using phase change materials [259]. Although the storage capacity of the solid media is lower than in the salt system, its environmental impacts are lower than in systems using molten salt and phase change materials

because of the low material requirement in solid media [259]. Because the molten salt system requires special equipment to withstand high temperatures, it has a higher footprint than the phase change material system.

In most ESSs, the operation phase is one of the largest contributors to the life cycle emissions and is dictated by the emission intensity of the electricity used for charging [258]. The transition from fossil fuel-based electricity to renewables reduces the overall GHG emissions dramatically [52, 258]. The life cycle GHG emissions of utility-scale solar and wind power plants are 26-183 g-CO₂eq/kWh [282] and 3-45 g-CO₂eq/kWh [283], respectively, while coal and natural gas plants emit 66-1300 g-CO₂eq/kWh and 380-1000 g-CO₂eq/kWh, respectively [284].

Life cycle environmental impacts vary widely with the application scenario because of the discharge duration and number of cycles. PHS, CAES, and solar thermal are used for energy applications where discharge duration is high. For example, Kapila et al. [256] and Thaker et al. [271] designed mechanical and thermal energy storages for 12 hours and 8 hours, respectively, while Heath et al. [268] assumed 6 hours discharge duration for thermal storage. Electro-chemical storage systems can be used for different power and energy applications. A few studies assessed the environmental sustainability of ESSs for different applications. Discharge duration and number of cycles appear to be among the important characteristics of the applications. Hiremath et al. considered seven application scenarios, each having specific power and energy capacities [258]. Under-use of the batteries is the main reason for differences in the environmental footprints of the system. Baumann et al. considered four stationary cases [51]. Primary regulation and electric time-shift have higher carbon footprints because grid mix electricity is used, rather than renewable support and PV self-consumption, which uses renewables. The key parameter in all cases is the duration of discharge. The discharge durations for electric time-shift, PV self-consumption,

primary regulation, and renewable support are 4, 3.2, 1, and 10 hours, respectively. The corresponding number of cycles are 2, 1, 34, and 1.12, respectively. The number of cycles is crucial for battery life because higher frequency in charge/discharge cycles leads to high replacement rates. The performance of the Li-ion is better than the Pb-A because of Li-ion's longer lifetime [51].

The impact assessment results in most of the studies were limited to point estimates and do not provide the most likely ranges. Life cycle impact assessment results are subject to a certain degree of uncertainty. This could be due to uncertainties in input and output parameters, modeling choice, temporal and spatial variabilities, and so on. Therefore, in order to have a better understating and interpretation of LCA results, it is important to perform sensitivity and uncertainty analyses. However, few published LCA studies on ESSs do this. Some incorporate uncertainty analysis. Kapila et al. [256], for example, used a Regression, Uncertainty, and Sensitivity Tool (RUST) [285] to identify the influential variables and provide a range of results. Thaker et al. [271] and Baumann et al. [51] also generated a wide range of GHG emissions results by using a range of input parameters in order to have a better comparative assessment of the alternative energy storage technologies.

A direct comparison of the environmental impacts of different ESSs is difficult because of the difference in system boundaries and assumptions adopted in various studies. C-CAES has higher emissions than PHS and A-CAES because of the use of natural gas. The problems of electro-chemical ESSs have been with replacing batteries due to their short lifetime and with the disposal of chemicals. The ranking of various electro-chemical ESSs differs among studies because of the variations in key technical parameters, i.e., round-trip efficiency, depth of discharge, and cycle life. The source of electricity used for charging can also influence the results. For thermal ESSs,

life cycle GHG emissions depend largely on the configuration. For example, the total emissions of a latent heat thermal storage system are higher than from sensible heat. This is mainly due to the use of phase change material, which requires additional energy. However, in order to have a reasonable comparison of the environmental performance of different ESSs and avoid any misleading conclusions, it is important to establish a consistent system boundary and set of assumptions.

Table 2.8: A summary of LCAs of energy storage technologies

ESS	Functional unit	System boundary	Data sources and models	Impact categories considered	Sensitivity/uncertainty	Emissions	Comments	Reference
PHS	1 kWh	Cradle-to-gate, transportation, and decommissioning	Existing studies and ecoinvent database	NER and GWP	Y/Y	7.79 g-CO ₂ eq/kWh	The net energy ratio (NER) and emissions are calculated for a PHS with a capacity of 118 MW. The NER is 0.778. 52% of the total construction emissions are from dam construction.	[174]
	1 GWh	Cradle-to-gate, operation, and decommissioning	Economic Input/Output (EIO) database	ER and GWP	N/N	5.6 g-CO ₂ eq/kWh	The total energy requirement is 0.066 MJ _{thermal} /kWh (without stored electricity). The calculations are based on a 20% capacity factor and 60-year project lifetime.	[15]
	1 kWh	Cradle-to-grave	Ecoinvent and NEEDS Life Cycle Inventory Database	CC, HT, PMF, and FFD	N/N	23.5-650 g-CO ₂ eq/kWh, 15.70-418 g-1,4 DBeq/kWh, 0.05-0.85 g-	Emissions from electricity production were also included in the analysis. The emissions are from different energy sources including wind, photovoltaic, the Belgium grid, and the Union for	[52]

ESS	Functional unit	System boundary	Data sources and models	Impact categories considered	Sensitivity/uncertainty	Emissions	Comments	Reference
						PM10eq/kWh, 5.61-189 g-oileq/kWh	the Coordination of the Transmission of Electricity (UCTE).	
	1 kWh	Cradle-to-grave	Existing studies and ecoinvent database	GWP	Y/N	145-179 g-CO ₂ eq/kWh	The range results from the variation of efficiency and lifetime of a 100 MW system.	[253]
	1 MJ*day	Cradle-to-grave	Ecoinvent database	GWP, HT, PMF, FFD, OD, POF, TA, etc.	N/N	5.43-324 g-CO ₂ eq/kWh, 1.64-129 g-oileq/kWh, 3.34-17.6 g-DCBeq/kWh, 0.002-0.44 g-SO ₂ eq/kWh	The range represents the various sources for electricity, i.e., wind, natural gas, and the local grid.	[272]

ESS	Functional unit	System boundary	Data sources and models	Impact categories considered	Sensitivity/uncertainty	Emissions	Comments	Reference
	1 kWh	Cradle-to-gate, transportation, maintenance, operation, and decommissioning	Existing studies and ecoinvent database	NER and GWP	Y/Y	269.75-276.04 g-CO ₂ eq/kWh	The NER and emissions are calculated for a PHS with a capacity of 118 MW. The NER ranges from 0.77-0.79.	[256]
	10 kWh	Cradle-to-gate, transportation, operation, and decommissioning	SimaPro	ReCiPe 2016 indicators	Y/N	100	The value represents the normalized environmental impact considering human health (40%), ecosystems (40%), and resources (20%).	[280]
CAES	1 kWh	Cradle-to-gate, transportation, and decommissioning	Existing studies and ecoinvent database	NER and GWP	Y/Y	264.36 g-CO ₂ eq/kWh	The NER and emissions are calculated for a conventional CAES with a capacity of 81 MW. The NER is 0.542. The combustion of natural gas is included. The transportation of natural gas and the compressors are the main contributors to	[174]

ESS	Functional unit	System boundary	Data sources and models	Impact categories considered	Sensitivity/uncertainty	Emissions	Comments	Reference
							construction emissions at 28% and 26%, respectively.	
						4.96 g-CO ₂ eq/kWh	The NER and emissions are calculated for an adiabatic CAES with a capacity of 60 MW. The NER is 0.702. Compressors and underground cavern development are the main contributors to construction emissions at 44% and 26 %, respectively.	
	1 GWh	Cradle-to-gate, operation, and decommissioning	Economic Input/Output (EIO) database	ER and GWP	N/N	292 g-CO ₂ eq/kWh	The energy requirement is 5.27 MJ _{thermal} /kWh plus 0.735 kWh _{electricity} /kWh (without stored electricity). The calculations are based on a system of 2700 MW with a 20% capacity factor and a 40-year project lifetime.	[15]

ESS	Functional unit	System boundary	Data sources and models	Impact categories considered	Sensitivity/uncertainty	Emissions	Comments	Reference
	1 kWh	Cradle-to-grave	Ecoinvent and NEEDS Life Cycle Inventory Database	CC, HT, PMF, and FFD	N/N	27.1-740 g-CO ₂ eq/kWh, 24.90-475 g-1,4 DBeq/kWh, 0.08-1.0 g-PM10eq/kWh, 7.48-217 g-oileq/kWh	Emissions from electricity production were also included in the analysis. The emissions are from different energy sources including wind, photovoltaic, the Belgium grid, and UCTE.	[52]
	1 kWh	Cradle-to-grave	Existing studies and ecoinvent database	GWP	Y/N	161-272 g-CO ₂ eq/kWh	The range results from the variation of efficiency and lifetime of a 100 MW system.	[253]
	1 kWh	Cradle-to-gate and operation	Existing studies and ecoinvent database	CC, FWET, FWE, HT, MRD, PMF, POF, TA, and AULO	N/N	380 g-CO ₂ eq/kWh, 0.24 g-1,4 DCBeq/kWh, 0.31 g-SO ₂ eq/kWh	An LCA was conducted for a 200 MW conventional CAES for a 400 MW offshore wind farm.	[257]

ESS	Functional unit	System boundary	Data sources and models	Impact categories considered	Sensitivity/uncertainty	Emissions	Comments	Reference
						19 g-CO ₂ eq/kWh, 0.47 g-1,4 DCBeq/kWh, 0.13 g-SO ₂ eq/kWh	An LCA was conducted for a 150 MW adiabatic CAES for a 400 MW offshore wind farm.	
	1 kWh	Cradle-to-gate, transportation, maintenance, operation, and decommissioning	Existing studies and ecoinvent database	NER and GWP	Y/Y	97.23-403.1 g-CO ₂ eq/kWh	The NER and emissions are calculated for a conventional CAES with a capacity of 81 MW. The NER ranges from 0.53-0.54.	[256]
						296.12-308.85 g-CO ₂ eq/kWh	The NER and emissions are calculated for an adiabatic CAES with a capacity of 60 MW. The NER ranges from 0.70-0.72.	
	10 kWh	Cradle-to-gate, transportation, operation, and decommissioning	SimaPro	ReCiPe 2016 indicators	Y/N	3970	The value represents the normalized environmental impact considering human health (40%), ecosystems (40%), and resources (20%).	[280]

ESS	Functional unit	System boundary	Data sources and models	Impact categories considered	Sensitivity/uncertainty	Emissions	Comments	Reference
FESS	Not specified	Cradle-to-gate and operation	Existing studies	CC	N/N	838,315 kg-CO ₂	Total GHG emissions in the material production and operation phases over the 20-year lifetime.	[54]
	Not specified	Cradle-to-gate	Existing studies	CC	N/N	6785 kg-CO ₂	Total GHG emissions in the material production over the 15-year lifetime.	[55]
Pb-A	150 kW h/day	Cradle-to-grave	Existing studies and manufacturers	GWP, POF, acidification, eutrophication, and RD	N/N	25.22 g-CO ₂ eq/kWh, 0.20 g-SO ₂ /kWh, 0.05 g-CO/kWh, 0.22 g-NO _x /kWh	The emissions calculation assumes a 50 kW system that can generate an average of 150 kWh electricity per day for 20 years. The system uses 50% secondary lead for battery manufacturing. We converted the CO ₂ , CH ₄ , and N ₂ O emissions to CO ₂ equivalents with GWPs of 1, 25, and 298 for CO ₂ , CH ₄ , and N ₂ O, respectively.	[146]

ESS	Functional unit	System boundary	Data sources and models	Impact categories considered	Sensitivity/uncertainty	Emissions	Comments	Reference
						21.91 g-CO ₂ eq/kWh, 0.13 g-SO ₂ /kWh, 0.04 g-CO/kWh, 0.16 g-NO _x /kWh	The emissions calculation assumes a 50 kW system that can generate an average of 150 kWh electricity per day for 20 years. The system uses 99% secondary lead for battery manufacturing. We converted the CO ₂ , CH ₄ , and N ₂ O emissions to CO ₂ equivalents with GWPs of 1, 25, and 298 for CO ₂ , CH ₄ , and N ₂ O, respectively.	
	1 kWh	Cradle-to-grave	Ecoinvent and NEEDS Life Cycle Inventory Database	CC, HT, PMF, and FFD	N/N	104-770 g-CO ₂ eq/kWh, 189-610 g-1,4 DBeq/kWh, 0.28-1.13 g-PM10eq/kWh	Emissions from electricity production were also included in the analysis. The emissions are from different energy sources including wind, photovoltaic, the Belgium grid, and UCTE.	[52]

ESS	Functional unit	System boundary	Data sources and models	Impact categories considered	Sensitivity/uncertainty	Emissions	Comments	Reference
						h, 29.90-226 g-oileq/kWh		
	1 MWh	Cradle-to-gate and operation	Existing studies and ecoinvent database	CED and GWP	Y/N	215-1157 g-CO ₂ eq/kWh	The energy requirement is from 7.67-18.5 MJ/kWh. The energy requirement and emissions ranges are based on base case scenarios for various battery uses including frequency regulation, energy time-shift, etc.	[258]
	1 kWh	Cradle-to-gate and recycling	Existing studies and ecoinvent database	GWP	N/N	65-92 g-CO ₂ eq/kWh	The GHG emissions are calculated for a Pb-A battery integrated with solar PV based on the technology in 2013 and 2020+.	[286]
	1 kWh	Cradle-to-gate and operation	Industry and ecoinvent database	GWP	Y/Y	170-740 g-CO ₂ eq/kWh	The emissions are for a valve-regulated lead-acid battery used for various services including time-shift and renewable integration.	[51]

ESS	Functional unit	System boundary	Data sources and models	Impact categories considered	Sensitivity/uncertainty	Emissions	Comments	Reference
	1 MWh	Cradle-to-gate	Manufacturer and SimaPro	CC, OD, TA, FWE, HT, POF, FFD, etc.	Y/N	102.76 g-CO ₂ eq/kWh, 0.51 g-SO ₂ eq/kWh, 59.82 g-1,4 DBeq/kWh, 0.21 g-PM10eq/kWh	We have calculated the emissions for a lead-acid battery based on the functional unit.	[255]
	1 MJ	Cradle-to-gate	Existing studies, SimaPro, and ecoinvent	CED, GWP, HT, OD, POF, IR, etc.	N/N	0.017-0.025 g-CO ₂ eq/kWh, 0.02-0.03 g-1,4 DBeq/kWh	Only the environmental impact due to battery production was considered as the operation phase varies considerably by application.	[261]
	10 kWh	Cradle-to-gate, transportation, operation, and decommissioning	SimaPro	ReCiPe 2016 indicators	Y/N	7310	The value represents the normalized environmental impact considering human health	[280]

ESS	Functional unit	System boundary	Data sources and models	Impact categories considered	Sensitivity/uncertainty	Emissions	Comments	Reference
							(40%), ecosystems (40%), and resources (20%).	
	1 kWh	Cradle-to-gate and transportation	Existing studies and ecoinvent	GWP	Y/Y	190-730 g-CO ₂ eq/kWh	Loss of electricity in charging and discharging is considered. The range of GHG emissions represents various applications and jurisdictions.	[213]
Li-ion	1 kWh	Cradle-to-grave	Ecoinvent and NEEDS Life Cycle Inventory Database	CC, HT, PMF, and FFD	N/N	72.30-600 g-CO ₂ eq/kWh, 86.40-417 g-1,4 DBeq/kWh, 0.13-0.81 g-PM10eq/kWh, 30.50-186 g-oileq/kWh	Emissions from electricity production were also included in the analysis. The emissions are from different energy sources including wind, photovoltaic, the Belgium grid, and UCTE.	[52]
	1 MWh	Cradle-to-gate and operation	Existing studies and	CED and GWP	Y/N	177-810 g-CO ₂ eq/kWh	The energy requirement is from 6.25-12.9 MJ/kWh. The energy requirement and emissions	[258]

ESS	Functional unit	System boundary	Data sources and models	Impact categories considered	Sensitivity/uncertainty	Emissions	Comments	Reference
			ecoinvent database				ranges are based on base case scenarios for various battery uses including frequency regulation, energy time-shift, etc.	
	1 kWh	Cradle-to-grave	Existing studies and ecoinvent database	GWP	Y/N	259-335 g-CO ₂ eq/kWh	The range results from the variation of efficiency and lifetime of a 100 MW system.	[253]
	1 kWh	Cradle-to-gate and recycling	Existing studies and ecoinvent database	GWP	N/N	60-72 g-CO ₂ eq/kWh	The GHG emissions are calculated for a lithium-ferrophosphate (LFP) battery integrated with solar PV based on the technology in 2013 and 2020+.	[286]
	1 kWh	Cradle-to-gate and operation	Industry and ecoinvent database	GWP	Y/Y	100-500 g-CO ₂ eq/kWh	The emissions are for a lithium-iron-phosphate battery with graphite anode used for various services including time-shift and renewable integration.	[51]

ESS	Functional unit	System boundary	Data sources and models	Impact categories considered	Sensitivity/uncertainty	Emissions	Comments	Reference
						70-490 g-CO ₂ eq/kWh	The emissions are for a lithium-iron-phosphate battery with lithium-titanate anode used for various services including time-shift and renewable integration.	
						150-600 g-CO ₂ eq/kWh	The emissions are for a lithium-manganese-oxide battery with graphite anode used for various services including time-shift and renewable integration.	
	1 MWh	Cradle-to-gate	Manufacturer and SimaPro	CC, OD, TA, FWE, HT, POF, FFD, etc.	Y/N	27.80 g-CO ₂ eq/kWh, 0.18 g-SO ₂ eq/kWh, 16.80 g-1,4 DBeq/kWh	We calculated the emissions for a lithium-manganese battery per kWh based on the functional unit.	[255]
						16.10 g-CO ₂ eq/kWh, 0.12 g-	We calculated the emissions for a lithium-iron-phosphate battery	

ESS	Functional unit	System boundary	Data sources and models	Impact categories considered	Sensitivity/uncertainty	Emissions	Comments	Reference
						SO ₂ eq/kWh, 10.73 g-1,4 DBeq/kWh	per kWh based on the functional unit.	
	1 MW-year	Cradle-to-grave	Existing studies, BatPaC, and GREET	GWP, CED, and acidification	N/N	45-180 and 5-15 GWP annual person impact equivalent	The values represent the average changes in GWP emissions for the coal and natural gas cases, respectively, due to the addition of a 1 MW-year capacity of Li-ion battery.	[49]
	1 MWh	Cradle-to-grave	Ecoinvent and CLCA model	CC, OD, FWE, POF, Acidification, etc.	Y/N	-439 g-CO ₂ eq/kWh	A consequential LCA for integrating the surplus electricity from renewables in the Swiss grid for 2030 using a Li-ion battery with a capacity of 6 MWh. The negative sign for the GHG emissions represents the reduction in GHG emissions for using the battery with renewables in the grid.	[262]

ESS	Functional unit	System boundary	Data sources and models	Impact categories considered	Sensitivity/uncertainty	Emissions	Comments	Reference
	1 MJ	Cradle-to-gate	Existing studies, SimaPro, and ecoinvent	CED, GWP, HT, OD, POF, IR, etc.	N/N	0.06-0.1 g-CO ₂ eq/kWh, 0.01-0.02 g-1,4 DBeq/kWh	Only the environmental impact associated with battery production was considered as the operation phase varies considerably by application.	[261]
	10 kWh	Cradle-to-gate, transportation, operation, and decommissioning	SimaPro	ReCiPe 2016 indicators	Y/N	2346	The value represents the normalized environmental impact considering human health (40%), ecosystems (40%), and resources (20%).	[280]
	1 MWh	Cradle-to-grave	Ecoinvent	CC, HH, EQ, etc.	Y/N	-2 kg-CO ₂ eq/year/kg battery pack	A consequential LCA of the Li-ion battery. The negative value represents the amount by which GHG emissions reduce if the battery is used.	[263]
	1 kWh	Cradle-to-gate and transportation	Existing studies and ecoinvent	GWP	Y/Y	80-390 g-CO ₂ eq/kWh	Loss of electricity in charging and discharging was considered. The range of GHG emissions	[213]

ESS	Functional unit	System boundary	Data sources and models	Impact categories considered	Sensitivity/uncertainty	Emissions	Comments	Reference
							represents various applications and jurisdictions.	
Na-S	1 kWh	Cradle-to-grave	Ecoinvent and NEEDS Life Cycle Inventory Database	CC, HT, PMF, and FFD	N/N	37.90-640 g-CO ₂ eq/kWh, 15.30-417 g-1,4 DBeq/kWh, 0.08-0.85 g-PM10eq/kWh, 9.97-187 g-oileq/kWh	Emissions from electricity production were also included in the analysis. The emissions are from different energy sources including wind, photovoltaic, the Belgium grid, and UCTE.	[52]
	1 MWh	Cradle-to-gate and operation	Existing literature and ecoinvent database	CED and GWP	Y/N	201-937 g-CO ₂ eq/kWh	The energy requirement is from 7.3-15 MJ/kWh. The energy requirement and emissions ranges are based on base case scenarios for battery uses including frequency regulation, energy, time-shift, etc.	[258]

ESS	Functional unit	System boundary	Data sources and models	Impact categories considered	Sensitivity/uncertainty	Emissions	Comments	Reference
	1 MJ	Cradle-to-gate	Existing studies, SimaPro, and ecoinvent	CED, GWP, HT, OD, POF, IR, etc.	N/N	0.007 g-CO ₂ eq/kWh, 0.002 g-1,4 DBeq/kWh	Only the environmental impact due to battery production was considered as the operation phase varies considerably by application.	[261]
VRFB	1 GWh	Cradle-to-gate, operation, and decommissioning	Economic Input/Output (EIO) database	ER and GWP	N/N	40.20 g-CO ₂ eq/kWh	The energy requirement is 0.56 MJ _{thermal} /kWh (without stored electricity). The calculations are based on a system of 15 MW with a 20% capacity factor and a 20-year project lifetime.	[15]
	150 kWh/day	Cradle-to-grave	Existing studies and manufacturers	GWP, POF, acidification, eutrophication, and RD	N/N	7.26 g-CO ₂ eq/kWh, 0.03 g-SO ₂ /kWh, 0.004 g-CO/kWh, 0.04 g-NO _x /kWh	The emissions calculation assumes 50 kW system that can generate an average of 150 kWh electricity per day for 20 years. The system uses 99% secondary vanadium for battery manufacturing. We converted the CO ₂ , CH ₄ , and N ₂ O emissions to	[146]

ESS	Functional unit	System boundary	Data sources and models	Impact categories considered	Sensitivity/uncertainty	Emissions	Comments	Reference
							CO ₂ equivalents with GWPs of 1, 25, and 298 for CO ₂ , CH ₄ , and N ₂ O, respectively	
	1 MWh	Cradle-to-gate and operation	Existing studies and ecoinvent database	CED and GWP	Y/N	208-1022 g-CO ₂ eq/kWh	The energy requirement is from 7.87-16.6 MJ/kWh. The energy requirement and emissions ranges are based on base case scenarios for various services provided by the batteries including frequency regulation, energy time-shift, etc.	[258]
	1 MWh	Cradle-to-grave	Ecoinvent database	GWP, HT, acidification, and abiotic depletion	N/N	52-279 g-CO ₂ eq/kWh, 91-150 g-1,4 DCBeq/kWh, 0.7-1.01 g-SO ₂ eq/kWh, 0.013-0.025 g-Sbeq/kWh	Emissions from electricity production were also included in the analysis. The emissions are from different energy sources including wind, photovoltaic, and the grid. The battery materials are not recycled in this case.	[44]

ESS	Functional unit	System boundary	Data sources and models	Impact categories considered	Sensitivity/uncertainty	Emissions	Comments	Reference
						21-247 g-CO ₂ eq/kWh, 44-113 g-1,4 DCBeq/kWh, 0.13-0.44 g-SO ₂ eq/kWh, 0.003-0.014 g-Sbeq/kWh	Emissions from electricity production were also included in the analysis. The emissions are from different energy sources including wind, photovoltaic, and the grid. The battery materials are recycled in this case.	
	1 kWh	Cradle-to-gate and operation	Industry and ecoinvent database	GWP	Y/Y	190-580 g-CO ₂ eq/kWh	The emissions are for a VRFB battery used for various services including time-shift and renewable integration.	[51]
	1 kWh	Cradle-to-gate and transportation	Existing studies, SimaPro, and ecoinvent	CC, HT, acidification, POF, OD, etc.	Y/Y	136.5 kg-CO ₂ eq/kWh, 225 kg-1,4 DBeq/kWh, 1.67 kg-SO ₂ eq/kWh	The environmental impact of the vanadium battery is lower than the Li-ion battery. The biggest advantage is the reusability of vanadium electrolyte.	[287]

ESS	Functional unit	System boundary	Data sources and models	Impact categories considered	Sensitivity/uncertainty	Emissions	Comments	Reference
	1 kWh	Cradle-to-gate and transportation	Existing studies and ecoinvent	GWP	Y/Y	120-840 g-CO ₂ eq/kWh	Loss of electricity in charging and discharging was considered. The range of GHG emissions represents various applications and jurisdictions.	[213]
Polysulphide Battery	1 GWh	Cradle-to-gate, operation, and decommissioning	Economic Input/Output (EIO) database	ER and GWP	N/N	32.6 g-CO ₂ eq/kWh	The energy requirement is 0.45 MJ _{thermal} /kWh (without stored electricity). The calculations are based on a system of 15 MW with a 20% capacity factor and a 20-year project lifetime.	[15]
Blue battery system	10 kWh	Cradle-to-grave	SimaPro	ReCiPe 2016 indicators	Y/N	586	The value represents the normalized environmental impacts considering human health (40%), ecosystems (40%), and resources (20%).	[280]
NaNiCl	1 kWh	Cradle-to-grave	Ecoinvent and NEEDS Life Cycle	CC, HT, PMF, and FFD	N/N	32.50-607 g-CO ₂ eq/kWh, 86.40-450 g-	Emissions from electricity production were also included in the analysis. The emissions are	[52]

ESS	Functional unit	System boundary	Data sources and models	Impact categories considered	Sensitivity/uncertainty	Emissions	Comments	Reference
	1 kWh	Cradle-to-gate and operation	Inventory Database Industry andecoinvent database	GWP	Y/Y	1,4 DBeq/kWh, 0.33-1.08 g- PM10eq/kWh, 8.10-178 g-oileq/kWh 130-630 g- CO2eq/kWh	from different energy sources including wind, photovoltaic, the Belgium grid, and UCTE. The emissions are for a NaNiCl battery used for various services including time-shift and renewable integration.	[51]
Ni-Cd	1 MJ	Cradle-to-gate	Existing studies, SimaPro, andecoinvent	CED, GWP, HT, OD, POF, IR, etc.	N/N	0.04-0.05 g- CO2eq/kWh, 0.014-0.02 g- 1,4 DBeq/kWh	Only the environmental impact from battery production was considered as the operation phase varies considerably by application.	[261]
Hydrogen	1 kWh	Cradle-to-grave	Ecoinvent and NEEDS Life Cycle	CC, HT, PMF, and FFD	N/N	50.60-1620 g- CO2eq/kWh, 35.30-1030	Emissions from electricity production were also included in the analysis. The emissions are from different energy sources	[52]

ESS	Functional unit	System boundary	Data sources and models	Impact categories considered	Sensitivity/uncertainty	Emissions	Comments	Reference
			Inventory Database			g-1,4 DBeq/kWh, 0.16-2.18 g- PM10eq/kWh, 17.40-475 g-oileq/kWh	including wind, photovoltaic, the Belgium grid, and UCTE.	
	1 kWh	Cradle-to-grave	Existing studies and ecoinvent database	GWP	Y/N	386-700 g-CO ₂ eq/kWh	The range results from the variation of efficiency and lifetime of a 100 MW system.	[253]
TES	1 kWh	Cradle-to-gate, operation, and dismantling	Ecoinvent database	Environmental impact calculated in points based on Eco-indicator 99 considering eco systems	N/N	0.3-0.7/kWh 5.7-29/kWh	Sensible heat is stored in high-temperature concrete. The range of numbers is due to the changes in the temperature gradient of the storage material in different scenarios. The sensible heat is stored in liquid media, molten salt. The range in numbers is a result of the	[259]

ESS	Functional unit	System boundary	Data sources and models	Impact categories considered	Sensitivity/uncertainty	Emissions	Comments	Reference
				quality, HT, and resources			changes in the temperature gradient of the storage material in different scenarios.	
						4.7-13.8/kWh	Latent heat and sensible heat are stored using the phase change material. The range in numbers is a result of the changes in the temperature gradient of the storage material in different scenarios.	
	Not specified	Cradle-to-gate, operation, and decommissioning	Ecoinvent and Economic Input/Output LCA databases	GWP	N/N	17,100 MTCO ₂ eq	The emissions are calculated for a two-tank indirect thermal energy storage system designed to supply 6 hours of storage for a 50 MW CSP plant.	[268]
						7890 MTCO ₂ eq	The emissions are calculated for a thermocline indirect molten salt thermal energy storage system	

ESS	Functional unit	System boundary	Data sources and models	Impact categories considered	Sensitivity/uncertainty	Emissions	Comments	Reference
							designed to supply 6 hours of storage for a 50 MW CSP plant.	
	1 kWh	Cradle-to-grave	Manufacturer, contractor, andecoinvent database	GWP, water use, and ER	Y/N	26 g-CO ₂ eq/kWh, 4.7 L water/kWh	The cumulative energy demand is 0.43 MJ/kWh. The environmental impacts are calculated for a 103 MW CSP plant with thermal storage.	[254]
	1 GJ	Cradle-to-grave	Not specified	GWP, acidification, eutrophication, and POF	N/N	22.68-36 g-CO ₂ /kWh, 0.17-0.25 36 g-SO ₂ /kWh, 0.0075-0.01 g-phosphate/kWh	We converted the numbers to get the emissions per kWh from GJ.	[267]
	1 kWh	Cradle-to-grave	Existing studies and GREET database	NER, GWP	Y/Y	13-47 g-CO ₂ eq/kWh 7-28 g-CO ₂ eq/kWh	Two-tank indirect sensible heat storage. Two-tank direct sensible heat storage.	[271]

ESS	Functional unit	System boundary	Data sources and models	Impact categories considered	Sensitivity/uncertainty	Emissions	Comments	Reference
						5-21 g-CO ₂ eq/kWh	One-tank direct sensible heat storage.	
						9-34 g-CO ₂ eq/kWh	Latent heat storage.	
						9-27 g-CO ₂ eq/kWh	Thermochemical storage.	

Net energy ratio (NER) = Energy output/(construction energy+maintenance energy+operational energy).

1,4 DBeq is 1,4 dichlorobenzene equivalents, PM10eq is particulate matter (<10 μm) emission equivalents.

Y = yes and N = no.

GWP = global warming potential, ER = energy requirements, CED = cumulative energy demand, CC = climate change, HT = human toxicity, PMF = particulate matter formation, FFD = fossil fuel depletion, FWET = freshwater ecotoxicity, FWE = freshwater eutrophication, MRD = mineral resource depletion, POF = photochemical oxidant formation, TA = terrestrial acidification, AULO = agricultural and urban land occupation, RD = resources depletion, OD = ozone depletion.

2.5. Land footprint of energy storage systems

Table 2.9 shows the land area requirement for several energy storage technologies. For electro-chemical energy storage systems, data from Mastro's study [288] was used to calculate the area required per kWh of battery capacity. The land footprint for PHS was calculated from the direct use of land and the storage capacity. For conventional and adiabatic CAESs, the values were taken from Bouman et al. [257]. The advantage of conventional electro-chemical batteries (Li-ion, Na-S, and Pb-A) is that they are highly modular, so they can be divided into racks and cabinets and built vertically. A VRF's land footprint is much higher than other batteries' as it requires different equipment to operate, i.e., storage tanks, heat exchangers, pumps, and stacks, that are not required for Li-ion, Na-S, or Pb-A batteries. The main advantages of a Li-ion battery are that it is very compact and lightweight. However, the compact nature makes its weight per square meter high, which could be challenging for some building floors [288]. C-CAES and A-CAES systems have a large footprint because they require several components such as a compressor, turbine, heat exchanger, storage medium, etc. The A-CAES's land footprint is higher than a C-CAES's because it needs storage for the thermal fluid that extracts heat during air compression and rejects heat to increase air temperature before the air enters the turbine, in addition to the other components [31]. For PHS, the land footprint ranges from 0.10 m² [289] to 0.14 m²/kWh [256].

Table 2.9: Land footprint of different energy storage technologies

Technology	Land footprint (m²/kWh)	Source	Comment
C-CAES	0.43	[257]	
A-CAES	0.61	[257]	
PHS	0.10	[289]	Calculated from the direct use of land (m ²) and storage capacity (kWh).
	0.14	[256]	Calculated from the area of vegetation removal (m ²) and storage capacity (kWh).
Li-ion	0.02	[288]	Calculated from the total footprint (m ²) and battery size (kWh).
Na-S	0.03	[288]	Calculated from the total footprint (m ²) and battery size (kWh).
Pb-A	0.09	[288]	Calculated from the total footprint (m ²) and battery size (kWh).
VRFB	0.24	[288]	Calculated from the total footprint (m ²) and battery size (kWh).

2.6. Identified gaps and recommendations

The following section discusses the gaps identified from the review of techno-economic and life cycle assessments of ESSs.

2.6.1. Economy of scale

Although there are few studies that developed economies of scale and scale factors for pumped hydro, compressed air, and thermal ESSs, electro-chemical batteries and flywheel for commercial-scale operations require extensive study to understand their economic feasibility. The relation between the capacity and the investment cost needs to be investigated by developing scale factors

and economies of scale for different technologies, such as VRFB, Na-S, Ni-Cd, hydrogen storage, FESS, and other emerging storage technologies for utility applications.

In addition, the relation between the depth of discharge and cycle life of ESSs should be included in the techno-economic assessment. Increasing the depth of discharge can reduce the cycle life of electro-chemical batteries considerably. Including this aspect in the analysis could change our understanding of cost performance.

2.6.2. Consistency in cost estimation

Our review of the techno-economic assessments of ESSs found that the calculations of the TCC and LCOE are inconsistent. For example, many studies underestimate the LCOE by not considering the BOP and fixed O&M costs of the system. All the cost components in the analysis need to be included to generate results robust enough to compare various storage technologies.

The cost of charging is reflected in the levelized cost of electricity. The LCOE will change if the source of electricity changes, because electricity production cost differs by source. Therefore, the levelized cost of storage (excluding the cost of charging) could be a better performance indicator than the levelized cost of electricity for comparing the ESSs. Although a handful of studies estimated the LCOS for pumped hydro, compressed air storage, and thermal storage, very few estimated the LCOS for electro-chemical, flywheel, and hydrogen storage systems. Future studies should estimate the LCOS for a better economic comparison.

2.6.3. LCA system boundary and data sources

Like economic assessment, environmental performance is an important aspect in the selection of energy storage technologies. However, there is little information on environmental performance,

especially for electro-chemical batteries, liquid air ESSs, and flywheels. Most of the earlier studies considered the material manufacturing, transportation, and operation of the storage section only and did not account for PCS and BOP. The PCS and BOP are also important components of the storage system. The environmental impacts of these components should be included in the analysis.

An important limitation found in the review of LCAs of ESSs is inconsistencies in the system boundary, which could generate misleading results. Including all the life cycle stages from cradle-to-grave is required to quantify NERs and environmental footprints of ESSs. To understand the end-of-life impact, recycling should be included. Recycling of materials can reduce the overall burden by displacing virgin materials. This topic is not sufficiently addressed in the earlier studies. There may be an opportunity to increase the burden if the recycling process is more energy-intensive compared to virgin material production.

Most studies use generic databases for inventory analysis. Product-specific data inventory should be built to accurately conduct LCA. Specific energy consumption and emissions differ with the technology used and the jurisdiction. Future LCA studies should also use appropriate values for specific energy consumption and emission factors.

2.6.4. Need for uncertainty analysis

LCA and TEA are subject to uncertainties that arise from the parameters used, modeling choice, and scenario development. It is important to incorporate those uncertainties into the LCA and TEA if they are used as decision support tools. However, uncertainty analysis has been overlooked in most LCA and TEA studies on ESSs. Comparative assessment of different technologies using only

point estimating could be misleading. Only a handful of studies provide possible cost ranges and environmental footprints considering the variabilities in input parameters, modeling choice, and other sources of uncertainty in their analyses. Techno-economic and life cycle assessment results with uncertainty ranges have more credibility and reliability. Hence, sensitivity and uncertainty analysis practices should be encouraged in future research in the ESS domain.

2.6.5. LCA of emerging energy storage technologies

Most of the reviewed LCA studies focus on PHS and CAES from mechanical energy storage, Li-ion and Pb-A batteries from electro-chemical batteries, and thermal ESSs with various configurations. Those technologies are already widely implemented or at a high maturity level. The availability of technical and environmental data are the main motivations behind these studies. LCA studies on emerging storage technologies, such as lithium-sulfur and solid-state batteries, liquid air energy storage, etc., are limited. However, understanding the environmental performance of technologies in their early stages of development offers opportunities to make design adjustments to minimize environmental burdens.

In summary, developing an integrated bottom-up techno-economic and life cycle assessment model incorporating all the technical parameters and components to estimate the levelized cost of electricity and environmental footprints associated with storage systems is crucial to fill knowledge gaps in the research. Incorporating uncertainty analysis in the model would help us understand the influence of each parameter on the overall results.

2.7. Conclusion

Energy storage systems (ESSs) help mitigate the uncertainty associated with the electrical load in the power network. To incorporate ESSs in the grid, it is essential to understand their technical parameters as well as their economic and environmental performances. This chapter provided a review of the current status of energy storage technologies along with their technical characteristics and operating principles. Further, decision-making indicators, i.e., total capital costs, levelized cost of electricity, and environmental footprints, were reviewed. The pumped hydro storage system dominates the market and will continue to dominate it in the near future. The shares of electro-chemical storage systems are increasing. Lithium-ion battery use is growing the fastest, followed by sodium-based batteries.

Following the review, we conclude that the most influential technical parameters affecting cost and environmental performances are lifetime, round-trip efficiency, and cycle length. Among the bulk ESSs, PHS outperforms other technologies because of its very long lifetime, usually 60 years. However, due to their operational flexibility, electro-chemical batteries are growing faster. The economic and environmental performances of electro-chemical ESSs depend on the stationary applications they provide. It is expected that the Li-ion battery will dominate the electricity market for all stationary applications because its costs will decrease sharply. While improving efficiency and cycle life can reduce environmental footprints, storing electricity from green sources can drastically reduce GHG emissions.

ESSs are used for various utility-scale stationary applications and the choice depends on technical characteristics, cost, and environmental emissions. Considering these criteria, pumped hydro, compressed air, hydrogen, and thermal energy storage appear to be suitable for the energy

applications, such as bulk energy storage and T&D investment deferral. Although flywheels are not suitable for energy applications because of their high energy loss, they can be used for frequency regulation. The advantages of electro-chemical ESSs are quick response time and modularity, which make them favorable for most energy and power applications, such as bulk energy storage, T&D investment deferral, frequency regulation, and support of voltage regulation. They are also suitable for power quality and power reliability applications.

This study provides a database for future research on techno-economic and life cycle assessments of ESSs. However, to handle the range in datasets for each ESS, an uncertainty analysis needs to be carried out to better understand the results.

Chapter 3: The development of techno-economic models for the assessment of utility-scale electro-chemical battery storage systems³

3.1. Introduction

Concerns about climate change impacts associated with fossil fuel use and energy independence have contributed to the growing share of renewables in the global electricity production. Among the renewables, the cumulative growth of wind and solar has been significant, from 223 GW in 2010 to 1049 GW in 2018 [290]. According to the International Renewable Energy Agency (IRENA), the share of renewable sources in the electricity sector is expected to increase from 25% in 2017 to 85% in 2050, mostly through wind and solar capacity additions [291]. This transformation in the global electricity sector would create challenges to power system planning and operations [291]. Energy storage systems (ESSs) can encourage the integration of renewable energy sources such as wind and solar into electricity systems [9, 292] by mitigating the uncertainty associated with planning and with electrical grid network operations. While ESSs are a flexible option to the intermittency of wind and solar energy sources (both of which provide a high level of grid penetration), the economics of each storage technology is highly dependent on each stationary application [11, 293] and thus each requires in-depth analysis.

Stationary applications include time-shifting, ancillary services, power quality, etc. [23, 51, 115].

Mechanical storage systems, particularly pumped hydro storage (PHS) and compressed air energy

³ A version of this chapter has been published as Rahman MM, Oni AO, Gemechu E, Kumar A. The development of techno-economic models for the assessment of utility-scale electro-chemical battery storage systems. *Applied Energy*. 2021;283:116343.

storage (CAES), are mature technologies used primarily for time-shift and supply capacity [12, 24, 119] and hence their technical and economic characteristics are well known. Electro-chemical battery technologies, such as valve-regulated lead-acid (VRLA), lithium-ion (Li-ion), sodium-sulfur (Na-S), nickel-cadmium (Ni-Cd), and flow batteries, are more versatile; they are used for any service an ESS can provide [12, 28, 105]. Although the technical aspects are well developed, the economic aspects of these systems for stationary applications are not and thus require thorough investigation. Moreover, the contributions of different components (e.g., the storage section, power conversion system, and balance of plant) to the capital cost need to be understood, along with the system's life cycle costs and the cost of electricity delivery. For decision making and policy formulation toward the deployment of ESSs in the power network, it is important to incorporate technical characteristics, such as depth of discharge, round-trip efficiency, and other similar characteristics into economic models to predict the levelized cost of storage (LCOS) and economies of scale for various application capacities. Therefore, it is necessary to develop bottom-up techno-economic models to provide more insight into the economics of electro-chemical ESSs.

There are many studies in the literature to help us understand technical characteristics, for example, the round-trip efficiency, depth of discharge, energy and power densities, and sizing of ESSs [6, 92, 95], as well as the challenges associated with their application [8, 100, 101]. There are a few studies on the techno-economic performance of ESSs, specifically of mechanical storage technologies [31, 294, 295], thermal energy storage [131, 238], and electro-chemical storage systems [27, 105, 296, 297].

With respect to electro-chemical storage systems, most of the existing techno-economic assessments use a top-down approach. The top-down approach uses aggregated data and provides

opaque results without sharing the details. Due to the lack of process specificness, this approach cannot capture the full interaction between the technical parameters and economic outputs. For example, the aggregated capital cost of an ESS can be used to calculate the LCOS, but it is impossible to determine the effects of efficiency, depth of discharge, battery pack cost, and other technical parameters on the outputs. The bottom-up approach, on the other hand, uses engineering principles to calculate the installed ESS capacity, design the components, and estimate the costs of components. The bottom-up approach is transparent, and the results are easily reproducible. The studies by Schoenung [25] and Schoenung and Eyer [26] used data collected from various sources to estimate and compare the costs and benefits of different types of electro-chemical storage technologies. The impacts of depth of discharge and cycle life on capital and life cycle costs were not addressed. Abrams et al. developed a framework to evaluate the cost effectiveness of the Pb-A and Li-ion using data from manufacturers [27].

Other important aspects to consider while estimating the capital cost and levelized cost of storage of electro-chemical storage are replacement cost, and fixed and variable operation and maintenance (O&M) costs. Some studies overlooked these factors [10, 91, 116, 170]. For electro-chemical batteries, replacement cost is vital as these batteries need to be replaced after a certain period depending on the operating conditions. Furthermore, some batteries, such as Pb-A, need frequent maintenance. All of these cost components need to be considered in order to accurately estimate the real cost of electricity delivery from electro-chemical storage technologies.

Although electro-chemical ESSs can be used for various stationary applications, early studies focussed on their use in bulk energy storage applications (electric time-shift and supply capacity) [215, 298, 299]. A few studies considered the cost performance of other stationary applications.

Schmidt et al. conducted a techno-economic assessment of different Li-ion battery types for a number of applications [213]. Jülch compared the cost performance of Pb-A, Li-ion, and vanadium redox flow (VRF) for long-term and short-term applications [176]. Because they respond rapidly to need, electro-chemical ESSs are suitable for various stationary applications, and these are worth investigating.

A scale factor shows how the total investment cost of a plant changes with a change in plant capacity. Developing a scale factor is also a key element in performing a techno-economic assessment of a technology, and this was not done in earlier studies. Although a few studies show how the LCOS varies with increasing ESS capacity [28, 105, 297], none of these studies have developed scale factors to show how the storage system performs at higher energy capacities.

Cost estimates of a technology in the literature inherently differ given the differences in input parameters, modeling approach, and assumptions, among others. These variabilities should be reflected in the output results following sensitivity analysis and quantifying the uncertainty. However, most existing studies are limited to point estimates, hence these do not provide a cost range that considers multiple assumptions and input parameters.

There is a significant lack of information on electro-chemical ESSs that include all the cost parameters to evaluate their techno-economic feasibility for various stationary applications. In this chapter, the aim is to fill this research gap by developing comprehensive techno-economic assessment models to evaluate the cost-effectiveness of large-scale electro-chemical storage systems. Five electro-chemical batteries – Na-S, Li-ion, VRLA, Ni-Cd, and VRF – were studied to compare their techno-economic feasibility in four stationary application scenarios – bulk energy

storage, transmission and distribution investment deferral, frequency regulation, and support of voltage regulation. The specific objectives of this study are to:

- Develop bottom-up data-intensive techno-economic models for five electro-chemical battery storage technologies;
- Estimate total investment cost, annual life cycle cost, and levelized cost of storage of these technologies;
- Develop scale factors and study the impact of economies of scale for bulk energy storage;
- Compare the economic feasibility in four stationary application scenarios – bulk energy storage, transmission and distribution investment deferral, frequency regulation, and support of voltage regulation; and
- Conduct sensitivity and uncertainty analyses to determine the effect of variability in input parameters on output results.

3.2. Model development

3.2.1. Modeling approach

In this study, bottom-up data-intensive spread-sheet-based techno-economic models were developed for large-scale electro-chemical battery storage systems. First, scenarios were developed based on the operational characteristics of batteries, such as rated power, duration of discharge, and number of cycles. Second, systems were sized using the engineering principles for the power conversion system (PCS) and storage section. Once the system components were identified and sized, the technical model was integrated with the economic model. The economic model consists of cost metrics including capital costs for the power conversion system (PCS),

storage section (battery and foundation) and balance of plant (BOP), fixed and variable O&M costs for the battery, fixed cost for the PCS, charging cost, replacement cost, and contingency cost. The developed techno-economic models estimate technical parameters such as installed battery capacity, number of PCSs required, delivered electricity, and cost metrics, such as total investment cost (TIC), replacement cost (RC), and levelized cost of storage. Sensitivity and uncertainty analyses were conducted using the Regression, Uncertainty, and Sensitivity Tool (RUST) developed by Di Lullo et al. [285] to identify the technical and cost inputs that have the greatest influence on the outputs and to improve the reliability of the model results. Figure 3.1 shows the overview of the modeling methodology used in this research.

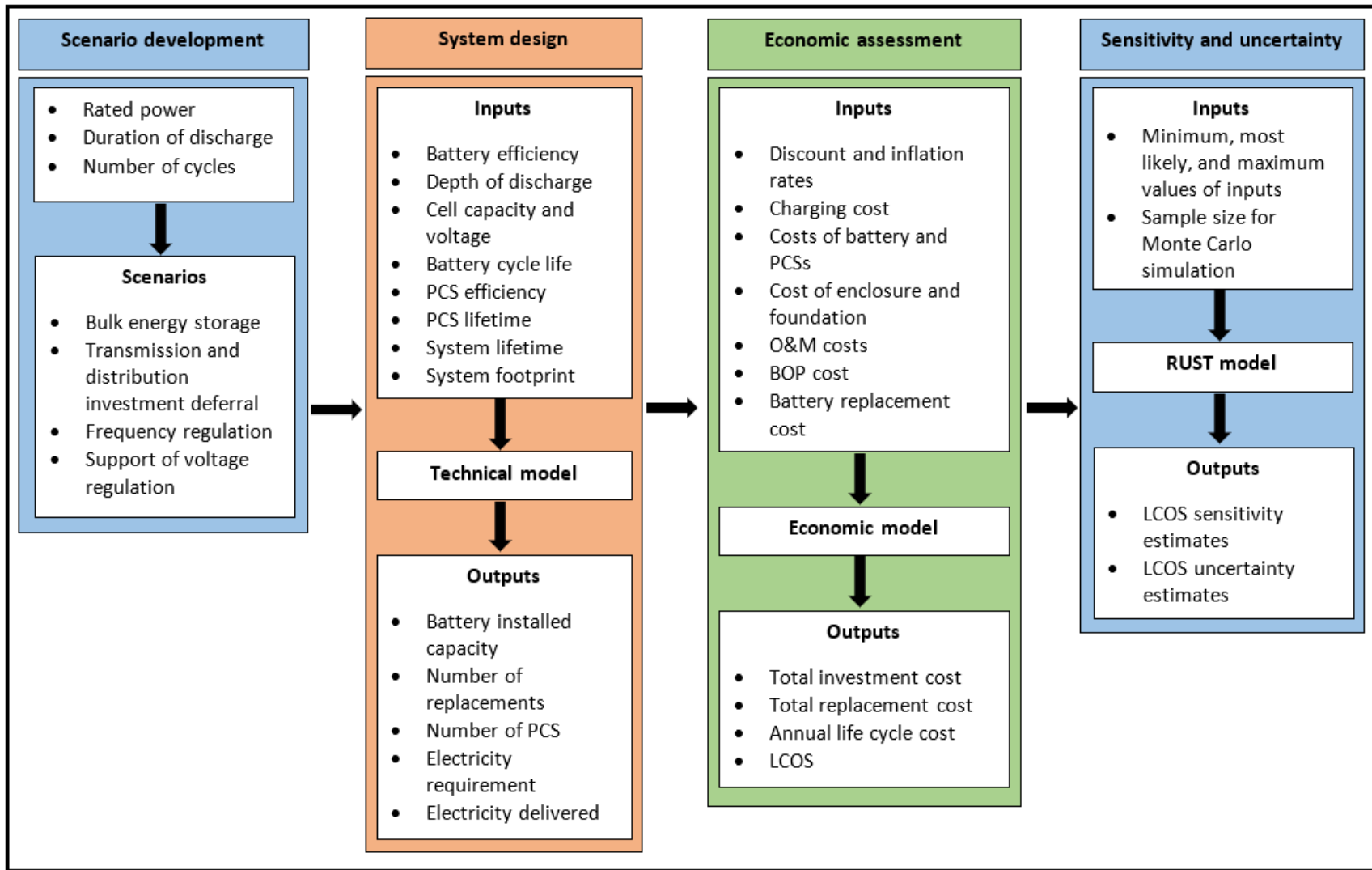


Figure 3.1: Developed techno-economic modeling methodology used in this study

3.2.1.1. Stationary application scenario development

The following four stationary application scenarios were developed to determine their economic feasibility when utility-scale electro-chemical batteries are integrated with electrical grid networks: bulk energy storage (S1), T&D investment deferral (S2), frequency regulation (S3), and support of voltage regulation (S4). A description of these applications can be found in section B.1 of Appendix B. The bulk energy storage application is already in use. T&D investment deferral, frequency regulation, and support of voltage regulation have become more important as the share of renewables in electricity generation increases [105]. ESSs have the potential to cut down the cost of grid operation and can generate revenue by providing T&D investment deferral, frequency regulation, and support of voltage regulation [300]. Usually, the applications supported by ESSs are classified as energy and power. Scenarios S1 and S2 are energy applications with discharge durations of more than 30 minutes, and S3 and S4 are power applications with discharge durations of 30 minutes or less [301]. The scenarios were developed based on rated power, duration of discharge, and number of cycles per year. The rated power and discharge duration determine the rated energy capacity of a particular ESS. The amount of electricity delivered in a year can be calculated from the rated energy capacity and number of cycles in a year.

Different capacity ranges were considered for each scenario based on current operational electro-chemical storage systems capacities. A capacity range of 5-100 MW was assumed for S1 and S3, while 5-25 MW and 5-30 MW for S2 and S4, respectively, were considered to capture most of the operational large utility-scale electro-chemical ESSs [12]. The base case capacities are 50 MW, 10 MW, 50 MW, and 15 MW for S1, S2, S3, and S4, respectively. Table 3.1 shows the assumptions used to develop the scenarios. The discharge duration for bulk energy storage varies widely [119].

Therefore, in this research, we varied the discharge duration from 1 hour to 8 hours and discerned the impact on cost.

Table 3.1: Scenario assumptions

Scenario	S1	S2	S3	S4
Base case rated power (MW)	50	10	50	15
Power range (MW)	5-100	5-25	5-100	5-30
Duration of discharge (h)	5	5	0.25	0.25
Rated energy capacity ^a (MWh)	250	50	12.5	3.75
Number of cycles per year	365 [119]	248 [105]	12,410 ^b	248 [105]

^a The values represent the amount of energy discharged during each cycle except for frequency regulation.

^b For frequency regulation, the number of cycles per year assumes 34 small cycles per day with 5% depth of discharge, equivalent to 1.7 full cycles [258].

3.2.1.2. System boundary and sizing

This study considers the components of an energy storage system (the PCS, storage section, and BOP). The PCS converts the alternating current to direct current and vice versa, and the storage section stores the electricity. The BOP items are the supporting components that help the ESS run effectively. A detailed description of these components can be found in section B.2 of Appendix B. Figure 3.2 shows the system boundary adopted in this study for techno-economic modeling. The source of electricity generation (e.g., solar and wind) and the electrical grid network were not included in the system boundary.

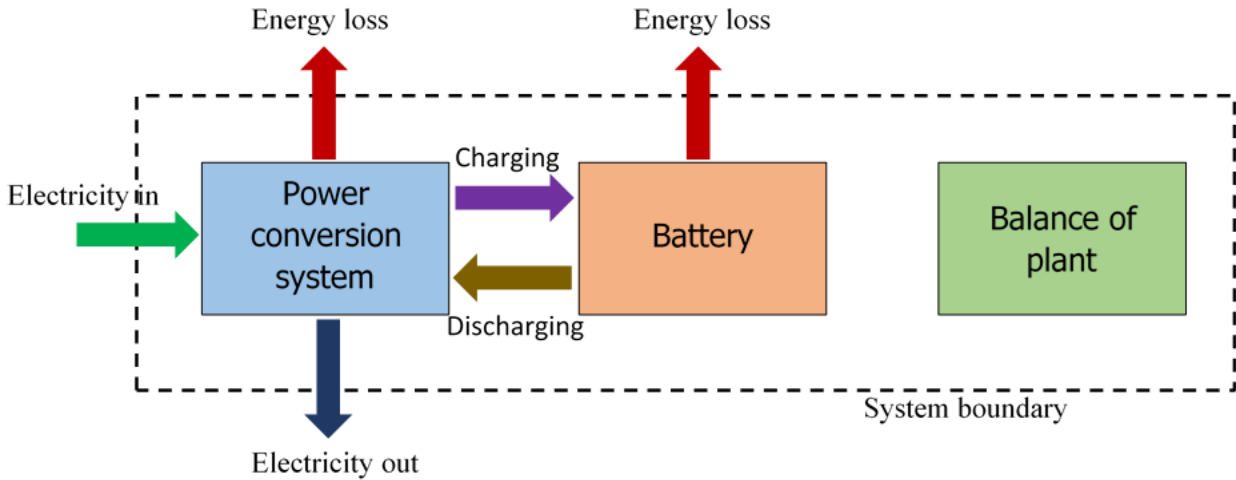


Figure 3.2: Main components of an electro-chemical energy storage system with energy flows

The sizing of a PCS is based on the rated power in MW of the storage system, as presented in Table 3.1. The capacity of each PCS is considered to be 5 MW (containerized⁴) [302]. The number of parallel connected PCSs was calculated from the system's rated power capacity and the capacity of each PCS. The PCS efficiency of 95% and 20-year lifetime were taken from Eckroad and Gyuk [169] and Rodrigues et al. [299], respectively.

The installed capacity of the storage system was calculated using Equation 3.1, adapted from Akinyele et al. [303] and Kaldellis et al. [304]:

$$E_{ESS} = \frac{E_R}{\eta_b} * \frac{1}{DOD} \quad (3.1)$$

⁴ The power conversion systems can be built in standard shipping containers to make installation easy.

where E_{ESS} is the installed capacity of the storage system (MWh), E_R is the rated energy storage capacity (MWh), η_b is the battery round-trip efficiency⁵ (%), and DOD⁶ is the depth of discharge (%).

The technical parameters used in model development are given in Table 3.2. Different approaches were used to design the storage sections of conventional batteries (Na-S, VRLA, Li-ion, and Ni-Cd) and the flow battery (VRF). For the conventional batteries, a battery cell, containing electrodes and electrolyte, provides the power and energy. The installed capacity was calculated to satisfy the rated power and energy based on the round-trip efficiency and depth of discharge. Because of their modular design, electro-chemical batteries can be scaled to any capacity to serve utility-scale applications [305]. It was assumed that the battery cells are stacked to form a module, modules are attached to form a rack, racks are connected to form a section, and several sections are required to satisfy the installed capacity. The connections can be made in parallel, in a series, or in parallel and a series combination, depending on the requirements. For VRFs, the power and energy capacities are determined by the size of the active area of the cell stack and the volume of electrolyte solutions in the electrolyte tanks, respectively. There are some accessories, such as heat exchangers and pumps. The lifetime of conventional batteries is limited by the DOD. The deeper the battery is discharged, the faster its lifetime reduces. However, for the VRF battery, the DOD does not affect the cycle life [306] because the electrolyte does not degrade [307]. The equations given in Table 3.2 were used to find the cycle life for the specified DOD. After the number of cycles in a lifetime were determined, the battery replacement period and the number of replacements required were calculated for the ESS over a 20-year life [258].

⁵ The ratio of the energy delivered to the energy required for charging.

⁶ It is a measure of how deeply a battery is discharged.

Table 3.2: Technical parameters used to design the storage systems

Technology	Efficiency	Depth of discharge	Average cell voltage (V)	Number of cycles in lifetime	Footprint (m ² /kWh)
Na-S	78% [308]	80% [119]	2 [309]	$1.978 \cdot 10^6 (\text{DOD})^{-1.73+3101}$ [299]	0.030 ^a [288]
Li-ion	90% [258]	80% [310]	3.7 [305]	$2731.7 (\text{DOD})^{-0.679} \cdot \exp [1.614(1-\text{DOD})]$ [311]	0.017 ^a [288]
VRLA	82% [258]	60% [119]	2 [312]	$1248.6 (\text{DOD})^{-0.889}$ ^b	0.062 ^c [313]
Ni-Cd	80% [314]	80% [119]	1.2 [315]	$2016.1 (\text{DOD})^{-1.301}$ ^d	0.057 ^a [288]
VRF	75% [105]	90% ^e [316]	1.19 [316]	13,000 ^f [317]	0.243 ^a [288]

^a Calculated from the total footprint (m²) and battery size (kWh).

^b The equation was developed using data from Discover Battery [318]. Details can be found in Appendix B in section B.3.

^c Calculated from the total footprint (m²) and battery size (kWh) of a CUB EC 40 container [313].

^d The equation was developed using data from Eckroad and Gyuk [169]. Details can be found in Appendix B in section B.3.

^e Calculated from the minimum (5%) and maximum (95%) states of charge [316].

^f The DOD does not affect the cycle life [306].

A VRF battery is designed quite differently from a conventional battery because it stores the energy in the electrolyte instead of the electrodes, as is the case for conventional batteries. As a result, the design of power and energy ratings should be done independently. While power capacity is determined by the number of cells and the size of the electrodes, an energy capacity is calculated based on the volume of the electrolytes stored in the storage tanks. The technical parameters to design both power and energy ratings for a VRF battery are listed in Table 3.3. The number of cells required to satisfy the power requirement was calculated from the average cell voltage, current density, and cell area, as shown in Equation 3.2, found in an earlier study [316]:

$$N_{cells} = \frac{P}{I * V} \quad (3.2)$$

where N_{cells} is the number of cells required, P is the rated power (W), V is the average cell voltage (V), and I is the current (A). The current can be calculated from the current density and active cell area (see Table 3.3).

When many cells are connected, these form a stack. The stack is comprised of individual cells made up of electrodes, membranes, a current collector, bipolar plates, and stack frames [296]. In this study, the power subsystem was assumed to be modular, with a 1 MW capacity consisting of four 250 kW stacks that can be fitted into 40-foot containers if needed [319]. The number of stacks required was calculated from the number of cells required for the system (see Equation 3.2) and the number of cells required for a 250 kW stack (the same equation applies). It was assumed that the stacks will be replaced after 10 years [320] because of corrosion and degradation of gaskets and membranes [44].

To design the energy capacity, the main components of the energy subsystem were identified. The main components are vanadium electrolyte and electrolyte tanks. After the system components were identified, the volumes of positive and negative electrolytes and electrolyte tanks, along with pump flow rate, were calculated. The flow rate of the vanadium in the system was estimated using Equation 3.3, adapted from Minke et al. [296]:

$$Q_V = \frac{P}{V * F} \quad (3.3)$$

where Q_V is the flow rate of vanadium (mol/s), P is the rated power (W), V is average cell voltage (V), and F is Faraday's constant (96,485 C/mol).

The amount of vanadium pentoxide (V_2O_5) determines the energy potential of a VRF battery. The amount of vanadium required for the positive and negative electrolytes can be calculated using Equation 3.4, adapted from Minke et al. [296]:

$$N_{V(PE)} = N_{V(NE)} = N_V = \frac{Q_V * t * 3600}{DOD * \eta_b} \quad (3.4)$$

where N_V is the amount of vanadium (mol), t is the discharge duration (h), DOD is depth of discharge (%), and η_b is the efficiency of the battery (%).

Once the required amount of vanadium (N_V) is determined, the volume of positive and negative electrolytes was calculated using the concentration of vanadium as indicated in Equation 3.5:

$$V_{PE} = V_{NE} = \frac{N_V}{C_V} \quad (3.5)$$

where V_{PE} and V_{NE} are the volume of positive and negative electrolytes (L), respectively, and C_V is the vanadium concentration (mol/L).

The tank volume should be more than the electrolyte volume to allow some void space. Therefore, the tank volume for each electrolyte was assumed to be 1.5 times the electrolyte volume [296]. Each 1 MW power subsystem will be connected to two electrolyte tanks. The size of each tank was calculated using the power capacity (1 MW) and specified duration of discharge (see Table 3.1). As the system was designed to be modular, the number of tanks was calculated from the volume of electrolyte required for the rated energy of the system and the volume of electrolyte for a 1 MW subsystem to be discharged for the considered discharge duration.

Pumps and heat exchangers (HXs) are the accessories, along with some piping and fittings (for electrolyte circulation), required for the VRF battery systems. The details of the pump and HX design can be found in Appendix B in section B.4.

Table 3.3: Technical and cost inputs used for the VRF battery system

Parameter	Value	Reference	Comment
Current density (A/m ²)	3000	[316]	
Active cell area (m ²)	1	[316]	
Capacity of each stack (kW)	250	[296]	
Stack lifetime (year)	10	[320]	
Vanadium concentration (mol/L)	1.6	[44]	
Molecular mass of vanadium (g/mol)	181.90	[316]	V ₂ O ₅ in this case.
Electrolyte density (kg/m ³)	1200	[316]	
HX thermal resistance (m ² K/W)	0.006	[296]	
HX log-mean temperature difference (K)	14	[296]	
Lifetime of pump (year)	10	[321]	
Length of pipeline per module (m)	70		Assumed for both electrolyte tanks.
Pump cost (\$/m ³ h ⁻¹)	47.41	[296]	Average of the cost range reported in the study by Minke et al. [296]. The cost of the pump is a function of flow rate.
HX cost (\$/m ²)	353.04	[296]	Average of the range reported in the study by Minke et al. [296].
Stack capital cost (\$/kW)	1065.20	[296]	Calculated from the capital cost and the capacity of each stack made of

Parameter	Value	Reference	Comment
			standard Nafion™ membranes.
Stack replacement cost (\$/kW)	1065.20		Assumed to be the same as capital cost because of the unavailability of future cost estimates.
Tank cost (\$/m ³)	365.21	[296]	Steel tank is considered.
V ₂ O ₅ cost (\$/kg)	24.35	[296]	
H ₂ SO ₄ cost (\$/kg)	0.06	[296]	
Specific cost of pipeline and fittings (\$/m)	21.2		\$10.6/m was assumed for pipeline only [320]. Due to the lack of data, a factor of 100% was assumed for the costs of fittings [296].
Labour cost for assembly (\$/kWh)	1.13	[320]	

All the cost numbers are in 2019 US dollars.

3.2.1.3. Techno-economic model

Once the system components were identified and designed, the technical parameters were integrated into the cost models. The cost models were developed based on the assumptions listed in Table 3.4. All the cost numbers are in 2019 US dollars unless otherwise mentioned.

Table 3.4: Input data for investment cost estimation and LCOS calculation

Parameter	Value	Reference	Comment
Project lifetime (year)	20	[258, 322]	
Off-peak electricity pool price (\$/MWh)	15.81	[323]	Average calculated for years 2013-17 for Alberta, Canada.
On-peak electricity pool price (\$/MWh)	37.98	[323]	Average calculated for years 2013-17 for Alberta, Canada.

Parameter	Value	Reference	Comment
Nominal discount rate	10%	[131, 174]	Based on the values reported for similar projects.
Average inflation rate	1.72%	[324]	Average inflation rate in Canada from 2010 to 2018.

Table 3.5 summarizes the battery cost data used for model development. The total investment cost comprises the storage section (battery and foundation with enclosure), PCS, BOP, and contingency costs. In this study, contingency cost was considered as a fixed percentage of capital cost (5-10%, depending on the technology), and decommissioning cost was not included as there is insufficient cost data for the end-of-life phase. The capital cost for conventional batteries is based on the battery's unit price (\$/kWh). Table 3.5 shows several cost parameters for energy storage technologies. For a VRF battery, once the system components were designed, the capital cost of all components was calculated using the cost parameters listed in Table 3.3. The stacks and pumps of the VRF battery need to be replaced after 10 years of operation [320, 321]. The replacement costs (if any) of batteries (stacks and pumps in case of the VRF) were considered to be equal to the capital cost to avoid complexity [299]. The costs for the exterior enclosure and foundation required for the battery systems are based on the energy storage footprint (m²/kWh) (see Table 3.2). The enclosure and foundation cost was assumed to be \$282.96/m² [169].

Table 3.5: Battery cost data used for model development

Technology	Na-S	Li-ion	VRLA	Ni-Cd	VRF
Battery capital cost (\$/kWh)	217.73 ^a	216.27 [325]	231.08 ^b	788.64 [215]	-
Fixed O&M cost (\$/kW-year)	3.5 [172]	10.35 ^c [326]	6.14 [297]	14.34 [28]	5 [327]

Technology	Na-S	Li-ion	VRLA	Ni-Cd	VRF
Variable O&M cost (\$/MWh)	2.35 [28]	2.74 [28]	0.48 [28]	8.81 ^d [169]	1.17 [28]
BOP cost (\$/kW)	97.46 ^e	106.75 ^f	103.91 ^g	131.44 [328]	65.84 ^g
Contingency cost (% of capital cost of the system)	5% [207]	10% [207]	10% [207]	10% [119]	7% [119]

^a The cost was estimated from the cost of a G50 module (\$84,913.45) and its capacity (390 kWh). The details can be found in section B.5 in Appendix B.

^b The cost function was developed for capital cost based on battery size. The details can be found in section B.5 in Appendix B.

^c Average of the fixed O&M cost range reported in Aquino et al. [326].

^d The unit is in \$/kW-year.

^e Average of the BOP costs reported in earlier studies (Kintner-Meyer et al. [172], Zakeri and Syri [28], and Battke et al. [105]).

^f Average of the BOP costs reported in earlier studies (Kintner-Meyer et al. [172], Zakeri and Syri [28], Aquino et al. [326], and Kintner-Meyer et al. [329]).

^g Average of the BOP costs reported in studies by Zakeri and Syri [28] and Battke et al. [105].

The PCS was assumed to be containerized and thus includes transformers, a power converter, controller(s), and grid disconnect and breaker protection [169]. Characteristics and cost data for PCSs are given in Table 3.6. Like batteries, PCSs are considered to be modular. It was assumed that the smallest unit of the PCS is 5 MW. The capital cost of the first unit of the PCS was calculated using Equations 3.6 and 3.7, found in Eckroad and Gyuk's work [169]:

$$C_{PCS} = 255 * P^{-0.3} \quad (3.6)$$

$$C_{PCS} = 300 * P^{-0.3} \quad (3.7)$$

where P is power (MW) and C_{PCS} is the cost of the PCS (\$/kW). The cost numbers in the above equations were adjusted to 2019 US dollars. To calculate the costs of multiple parallel PCS units, a 95% learning rate was applied for the economy of multiplicity [169]. PCS selection depends on

the applications for which the energy storage systems are used. Equation 3.6 was used for scenarios S1, S2, and S3; Equation 3.7 was used for S4, based on Eckroad and Gyuk’s guidelines for PCS selection and cost estimation [169].

Table 3.6: PCS characteristics and cost data

Parameter	Value	Reference
Capacity of each PCS (MW)	5	[302]
Lifetime (year)	20	[299]
Efficiency	95%	[169]
Capital cost (\$/kW)	206.81 ^a , 243.31 ^b	[169]
Fixed O&M cost (\$/kW-year)	2.63	[172]

^a This value is used for all the applications considered in the study except for the support of voltage regulation.

^b This value is used for the support of voltage regulation.

Once the TIC and RC for the system were evaluated, these costs were amortized over the lifetime of the project. The annual life cycle cost (ALCC) is expressed in \$/kW-year and includes TIC, O&M cost, RC, and charging cost. The yearly charging cost was estimated from the yearly electricity requirements and the charging price of electricity. In this study, the off-peak price of electricity in Alberta, Canada was taken as the charging cost of electricity. In Alberta, each day is separated into on-peak (7 am-11 pm) and off-peak (remaining hours) periods [323].

The ALCC and yearly electricity production determine the LCOS, the price at which the electricity should be sold to cover the expenditures associated with the system over its entire life. The number of cycles per year and length of the discharge cycle are required to calculate the amount of yearly electricity discharge. Equation B.4 in Appendix B is an expression for the LCOS using a discounted cash flow that mathematically correlates several parameters used in the models. Another important aspect, the levelized cost added by storage (LCAS), can be determined by

subtracting the charging cost from the LCOS using Equation B.5 (see Appendix B). Except for the charging cost, the LCAS accounts for all other cost components, such as capital, replacement, and O&M costs. As the charging cost is dependent on the market and operator, the LCAS could be a useful indicator to compare the economic performance of the energy storage technologies.

3.2.1.4. Sensitivity and uncertainty analyses

The Morris method was used for the sensitivity analysis to examine the effects of input parameters on the total investment cost (TIC) and LCOS. The values of technical and economic parameters, such as battery cost, depth of discharge, discount rate, inflation rate were taken from the literature. Uncertainty analysis was conducted to assess the effect of a simultaneous change in multiple inputs on the TIC and LCOS. The uncertain inputs were identified with their lowest and highest ranges. To obtain output distribution, a random sample was chosen from the range of input variables and iterated 100,000 times.

3.3. Results and discussion

3.3.1. Technical analysis

With respect to efficiency and DOD, the systems were designed in such a way that these can satisfy the rated power and energy requirements. For instance, for S1, 401.16 MWh of Na-S ESS should be installed to deliver 250 MWh of energy at a rate of 50 MW. For all four scenarios, the installed battery capacity for all five electro-chemical batteries is listed in Table 3.7. For the same rated energy capacity, the installed capacity of a VRLA is higher than a Na-S's because the product of round-trip efficiency and DOD is lower for a VRLA battery. The Li-ion has the smallest installed capacity in every scenario because of its high efficiency. Except for the VRF, all the batteries must be replaced after a period of time that ultimately depends on the cycle life and number of cycles per year. The VRLA battery requires the most frequent replacement because of its comparatively

lower cycle life (1966 cycles at 60% DOD and 17,908 cycles at 5% DOD). The round-trip efficiency, DOD, PCS efficiency, and number of cycles per year determine the yearly electricity requirements for charging. The electricity requirement, along with system footprint and overall efficiency, are listed in Table 3.7. The amount of electricity required for charging is highest for the VRF because of its low efficiency (68% overall efficiency), a result of the pumps operating to circulate the electrolytes. The Na-S needs the second highest amount of electricity (because of the heat requirement for the cells to operate). It has the second lowest overall efficiency of 70% (see Table 3.7). The Li-ion needs the least amount of electricity as it is the most efficient of the technologies considered. The rated power, duration of discharge, and number of cycles determine the amount of electricity delivered from the ESSs. The amount of electricity delivered from the ESSs is 86.69, 11.78, 7.37, and 0.88 GWh/year for S1, S2, S3, and S4, respectively, for the base cases described in Table 3.1.

The total footprint of the system was calculated based on the installed capacity and specific area requirement (m^2/kWh). The total footprint of the VRF battery is much higher than the other battery technologies as it requires equipment such as tanks, pumps, heat exchangers, and stacks that are not required for conventional batteries. The Li-ion uses the least amount of space of the ESSs to deliver 1 kWh of electricity as it needs only $0.017 \text{ m}^2/\text{kWh}$. Among the battery technologies, S1 and S4 have the highest and lowest land requirements, respectively, because they have the highest and lowest energy capacities, respectively (see Table 3.1).

The components of the VRF battery were individually designed to satisfy power and energy capacities, as discussed in section 3.2.1.2. 200, 40, 200, and 60 250 kW stacks are required for S1, S2, S3, and S4, respectively. The amount of vanadium and the volume of positive and negative electrolytes for a 50 MW/250 MWh system for S1 were estimated to be 23,225,574.26 mols and

7258 m³ each. The resulting volume of each electrolyte tank is 10,887 m³. The system was assumed to be modular (1 MW/5 MWh each); fifty 218 m³ tanks are required to satisfy S1's energy capacity for each electrolyte circuit. For S2, ten 218 m³ tanks are required for each electrolyte circuit; this scenario needs less vanadium (4,645,114.85 mols) because it has a lower energy capacity than S1. S3 requires 1,161,278.71 mols of vanadium and S4 needs only 348,383.61 mols for energy capacities of 12.5 MWh and 3.75 MWh, respectively. The electrolyte flow rate for each pump was estimated using Equation B.1 (see Appendix B) to be 19.60 m³/h; therefore, S1 and S3 require 100 pumps for 50 MW. On the other hand, S2 and S4 require 20 and 30 pumps to satisfy the base cases of 10 and 15 MW, respectively. A plate type HX is installed in each electrolyte circuit to dissipate the heat flow. As for the pumps, 100 HXs are required for S1 and S3, and S2 and S4 require 20 and 30 HXs, respectively. Each HX can dissipate 88 kW (half the heat flow, 176 kW/MW). The resulting HX area in each apparatus requires 38 m². The results for all the scenarios are presented in Table 3.8.

Table 3.7: List of technical outputs from the models

ESS type	Installed system size (MWh)	Number of replacements required	Electricity requirements for charging (GWh/year)	Total footprint (m²)	Number of PCS required	System overall efficiency
Scenario: S1						
Na-S	401.16	1	123.31	11,963.20	10	70%
Li-ion	347.22	1	106.73	5919.34	10	81%
VRLA	508.13	3	117.18	31,471.21	10	74%
Ni-Cd	390.63	2	120.08	22,191.48	10	72%
VRF	370.37	0*	128.07	60,874.69	10	68%
Scenario: S2						
Na-S	80.23	1	16.76	2392.64	2	70%

ESS type	Installed system size (MWh)	Number of replacements required	Electricity requirements for charging (GWh/year)	Total footprint (m ²)	Number of PCS required	System overall efficiency
Li-ion	69.44	1	14.50	1183.87	2	81%
VRLA	101.63	2	15.92	6294.24	2	74%
Ni-Cd	78.13	1	16.32	4438.30	2	72%
VRF	74.07	0*	17.40	12,174.94	2	68%
Scenario: S3						
Na-S	20.06	1	10.48	598.16	10	70%
Li-ion	17.36	2	9.07	296.97	10	81%
VRLA	25.41	9	9.96	1573.56	10	74%
Ni-Cd	19.53	2	10.21	1109.57	10	72%
VRF	18.52	0*	10.89	3043.73	10	68%
Scenario: S4						
Na-S	6.02	1	1.26	179.45	3	70%
Li-ion	5.21	1	1.09	88.79	3	81%
VRLA	7.62	2	1.19	472.07	3	74%
Ni-Cd	5.86	1	1.22	332.87	3	72%
VRF	5.56	0*	1.31	913.12	3	68%

* Only the stacks and pumps need to be replaced after 10 years.

Table 3.8: List of technical outputs from the VRF ESS model

Parameter	Unit	S1	S2	S3	S4
Amount of vanadium required for the system	Mols	23,225,574.26	4,645,114.85	1,161,278.71	348,383.61
Volume of positive and negative electrolytes ($V_{PE} = V_{NE}$)	m ³	7257.99	1451.60	362.90	108.87

Parameter	Unit	S1	S2	S3	S4
The volume of electrolyte for each module ($V_{PE} = V_{NE}$)	m ³	145.16	145.16	7.26	7.26
The volume of each tank for the module	m ³	218	218	11	11
Number of tanks required	Nos.	100	20	100	30
Number of pumps required	Nos.	100	20	100	30
Number of HXs required	Nos.	100	20	100	30

3.3.2. Economic analysis

Table 3.9 lists the base case cost estimates of the five ESSs for each stationary application scenario (with capacities of 50, 10, 50, and 15 MW for S1, S2, S3, and S4, respectively). Additional results for various power capacities can be found in section B.6 of Appendix B. The Ni-Cd has the highest TIC among the conventional batteries in all the scenarios because of the high cost of the battery (\$788.64/kWh) (see Table 3.5). The Ni-Cd appears to have the highest RC among the conventional batteries in every scenario except S3 because of its high unit replacement cost. In S3, the VRLA has the highest RC, followed by the Ni-Cd. The Ni-Cd requires only 2 replacements (at 8 and 16 years), and the VRLA needs nine replacements (one every 2 years); this is because the Ni-Cd can operate for 99,346 cycles and the VRLA for only 17,908 cycles in a lifetime at a 5% DOD.

The VRF battery has the highest TIC of all the technologies in S3 and S4. The VRF operates differently than the other conventional batteries, whose power and energy come from the same battery cell. In a VRF battery, the power comes from the stacks and the energy comes from the

electrolyte. This makes the VRF battery more component-intensive. In S1 and S2, the TIC of the VRF is the second highest, after the Ni-Cd. On the other hand, in S3 and S4, the VRF has the highest TIC among the ESSs. The conventional batteries' cost advantage for smaller energy capacities is because the battery cost is per kWh, but the VRF battery's cost is based on the cost of the energy and power components, along with the accessories. While the capital cost of the battery alone is \$15.4 million for the Ni-Cd storage system, the VRF's capital cost is \$53.3 million for the stacks and \$5.4 million for the electrolytes, tanks, pumps, and HXs in S3. Similar costs were found in S4.

The capital costs of the storage section and PCS, the BOP, and the contingency cost have key contributions to the TIC depending on the stationary application. For example, in S1 and S2, the storage section accounts for 76-87% and the PCS contributes 3-9% to the TIC. On the other hand, in S3 and S4, the PCS contributes greatly to the TIC at 41-52%, followed by the storage section at 17-28% for the Na-S, Li-ion, and VRLA. However, for the Ni-Cd and VRF, the largest contributor to the TIC is the storage section (42-45% for the Ni-Cd and 74-77% for the VRF) followed by the PCS (27-31% for the Ni-Cd and 12-15% for the VRF) in S3 and S4 because of the higher capital cost of the storage section compared to the other technologies, where the capital cost of the PCS is higher.

Table 3.9: Comparison of cost outputs for different electro-chemical ESSs

Scenario	Na-S	Li-ion	VRLA	Ni-Cd	VRF
TIC (million \$)					
S1	110.01	100.50	154.86	363.19	175.99
S2	22.17	20.28	31.15	72.82	35.37
S3	19.60	20.28	22.85	34.70	77.19
S4	6.63	6.87	7.64	11.20	23.93

Scenario	Na-S	Li-ion	VRLA	Ni-Cd	VRF
RC (million \$)					
S1	87.25	75.09	352.26	616.13	53.35
S2	17.45	15.02	46.97	61.61	10.67
S3	4.36	7.51	52.84	30.81	53.35
S4	1.31	1.12	3.52	4.62	16.01

A discounted cash flow analysis was performed to calculate the ALCC. Figure 3.3 shows the components that make up the ALCC. The ALCC of the Ni-Cd storage system is highest in S1 and S2 because of the storage system's high capital and replacement costs. Capital cost appears to be the key contributor of the ALCC in all the batteries in S1 and S2. Replacement cost is also significant in the Ni-Cd and VRLA, either from the more frequent replacement of batteries or higher battery cost (in S1 and S2). The ALCC values are comparably lower in S3 and S4, below \$200/kW-year in most batteries, because of the lower energy capacity than in S1 and S2. The major portion of the ALCC comes from the capital cost except for the VRLA in S3, where the ALCC is dominated by the replacement cost. The amortized replacement cost (\$53.89/kW-year) is higher than the amortized capital cost (\$47.02/kW-year) due to the VRLA's large number of replacements (nine).

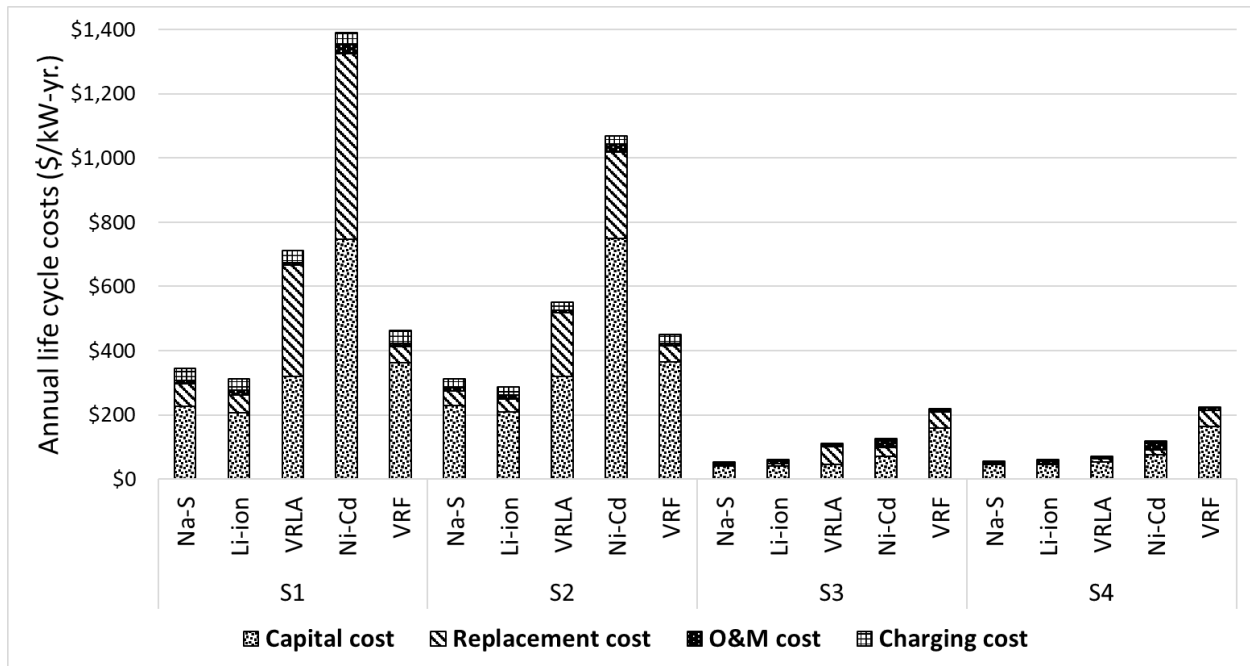


Figure 3.3: Annual life cycle cost for electro-chemical ESSs

The LCOS point estimates for the base cases, based on the default inputs (see Tables 3.1-3.6), are shown in Figure 3.4. The LCOS values vary considerably across the applications and technologies. For the applications, technical parameters, such as discharge duration and number of cycles per year, determine the LCOS. For instance, the LCOS for all the battery technologies is lowest in S1 and highest in S4 even though S1 has a much higher TIC than S4, mainly because S4 has a lower discharge duration and fewer cycles than S1. On the other hand, for the technologies, differences in cost parameters and lifetime are the main drivers. For example, for Scenario 1, the LCOS for the Ni-Cd (\$801.61/MWh) is much higher than the LCOS for the Li-ion (\$179.69/MWh) due to higher capital cost and number of replacements in the case of the Ni-Cd. When the point estimates are considered, the ranking of electro-chemical ESSs varies across applications. As shown in Figure 3.4, the Li-ion has the lowest LCOS in S1 and S2, while the Na-S leads in S3 and S4 (power application scenarios). While the VRF battery performs well in energy applications (S1 and S2) because of economies of scale, its performance in power application scenarios (S3 and S4) is poor.

The Ni-Cd is an expensive option in every scenario due to the high capital cost of battery cells. The Li-ion and Na-S showed greater cost competitiveness because of their longer lifetime, which ultimately reduces the replacement cost.

The LCAS is the cost added to the wholesale and retail price of electricity from the use of a storage system. The LCAS could be calculated from the LCOS using the charging cost and system efficiency. The LCAS could be calculated from the LCOS using the charging cost and system efficiency. The charging cost is influenced by the battery efficiency. The greater the battery efficiency, the less electricity is required for charging. The LCAS follows a similar trend as the LCOS for the applications and technologies. The LCAS ranges from \$160.22/MWh for the Li-ion to \$779.71/MWh for the Ni-Cd in S1, \$223.33/MWh for the Li-ion to \$885.51/MWh for the Ni-Cd in S2, \$343.34/MWh for the Na-S to \$1471.47/MWh for the VRF in S3, and \$918.93/MWh for the Na-S to \$3770.55/MWh for the VRF in S4. The difference between the LCOS and LCAS is only \$19.47 for the Li-ion and \$23.36 for the VRF per MWh electricity discharged.

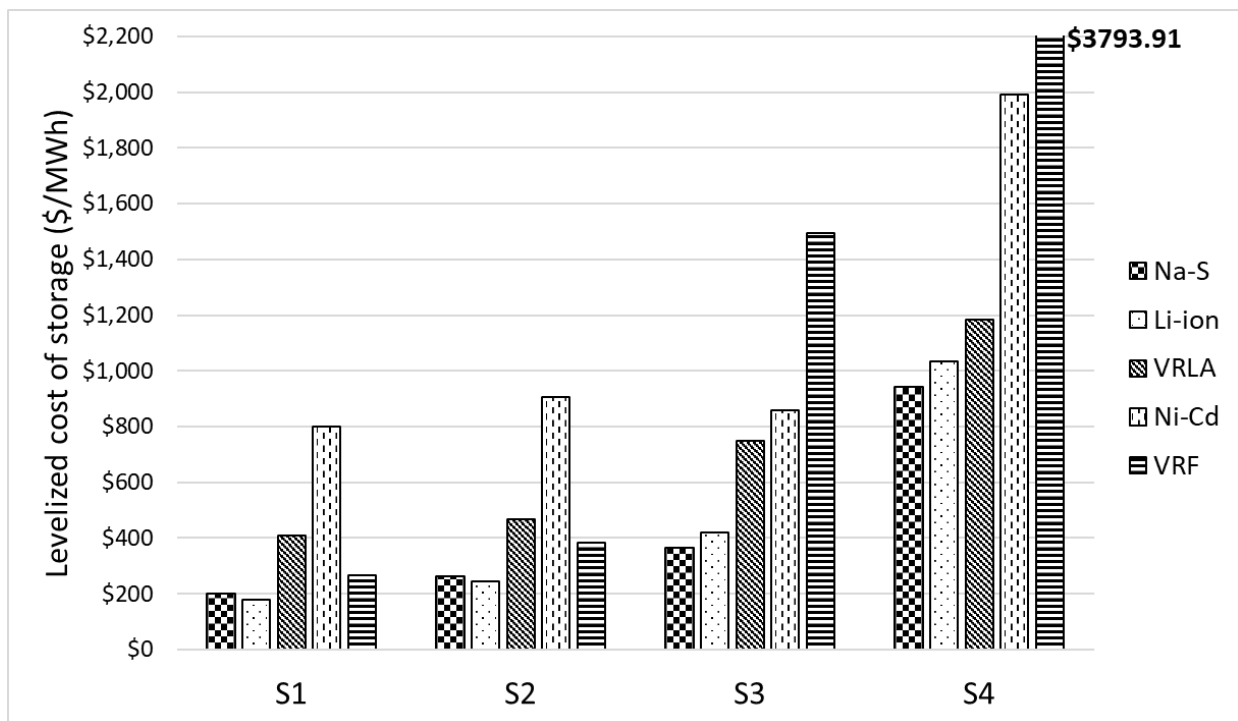


Figure 3.4: The levelized cost of storage developed in this study in the four scenarios

3.3.3. The effect of discharge duration on the TIC and LCOS

For the bulk energy storage scenario (S1), discharge time varies from project to project depending on the energy requirements. The base case was designed as 5 hours of discharge for a 50 MW ESS. However, the discharge duration was varied from 1 hour to 8 hours to observe the impact on the TIC and LCOS. If the TIC is plotted with respect to the energy capacity of the ESS, the plot gives the scale factor. The developed scale factors for all the ESSs studied are shown in Table 3.10. The TIC increases at a much lower rate than the ESS's energy capacity. An increase in energy capacity decreases the unit capital cost which establishes economies of scale. A scale factor less than 1 indicates a cost advantage, as capacity increases due to economies of scale. Figure 3.5 shows the range in the LCOS from changes in discharge duration. For all the ESSs, the LCOS decreases with an increase in discharge duration because of economies of scale. At a discharge duration of 2 hours, the VRF battery is cheaper than the VRLA ESS. If it is discharged for 8 hours or more, the VRF battery shows excellent cost competitiveness and can deliver electricity at a cost near to the electricity cost for the Na-S and Li-ion. When the duration of discharge is increased (keeping the power the same), the VRF system only needs to increase the size of the electrolyte tanks without changing the number of stacks, which makes it economically favourable at a longer duration of discharge. These results suggest that the VRF ESS is more suitable for energy applications than the power applications. For any length of discharge, the Ni-Cd is the most expensive ESS option, and the Li-ion is the cheapest among the ESSs considered in S1.

Table 3.10: Total investment cost (TIC) model for 1-8 hours of discharge in S1 (50 MW)

ESS type	TIC (million \$)
Na-S	$y = 32.052x^{0.77}$
Li-ion	$y = 31.006x^{0.74}$

ESS type	TIC (million \$)
VRLA	$y = 41.702x^{0.82}$
Ni-Cd	$y = 84.333x^{0.91}$
VRF	$y = 86.099x^{0.46}$

x is in MWh.

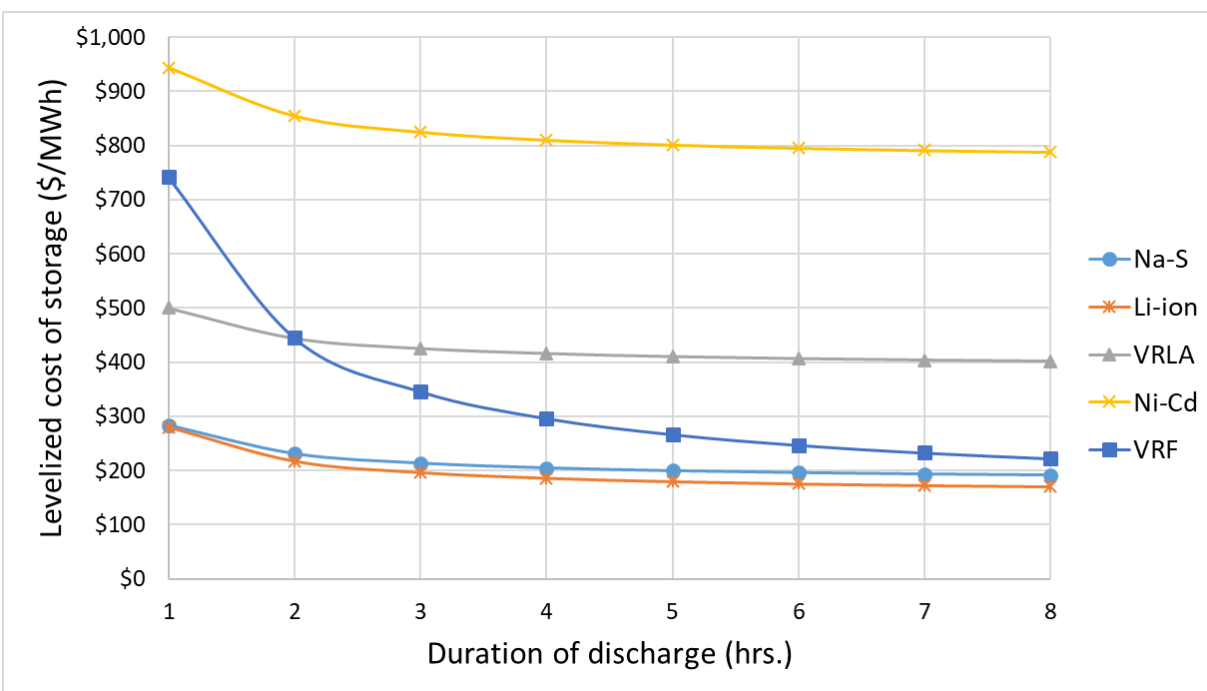


Figure 3.5: The levelized cost of storage with variations in discharge duration, Scenario 1

3.3.4. Sensitivity and uncertainty analyses

Results based on point estimates provide limited useful information. To improve the reliability and accuracy of our techno-economic models, sensitivity and uncertainty analyses were performed. A sensitivity analysis was performed using the Morris method to identify key technical and cost inputs that have impacts on the TIC and LCOS. Figures 3.6 and 3.7 present the results for the Na-S ESS for bulk energy storage. The higher the values of the Morris mean and standard deviation, the higher the sensitivity in the output result. The TIC and LCOS are most sensitive to battery

capital cost, depth of discharge, round-trip efficiency, nominal discount rate, and inflation rate. As the round-trip efficiency increases, the installed capacity and amount of electricity required decrease, ultimately lowering the TIC and LCOS. On the other hand, increasing the depth of discharge reduces the life of the battery, meaning more replacement of batteries will be required, thus increasing the RC. However, increasing the depth of discharge decreases the TIC because of the lower installed capacity. Figures 3.6 and 3.7 show the sensitivity results for the Na-S battery for S1. Similar results were found for the Li-ion, VRLA, and Ni-Cd in the other scenarios.

Battery efficiency, V_2O_5 cost, nominal discount rate, inflation rate, and the cost of enclosure and foundation are the parameters that have the most impact on the TIC and LCOS for the VRF system. The sensitivity results for the VRF system for bulk energy storage are presented in Figures B.4 and B.5 in Appendix B. Similar results were found for the other scenarios.

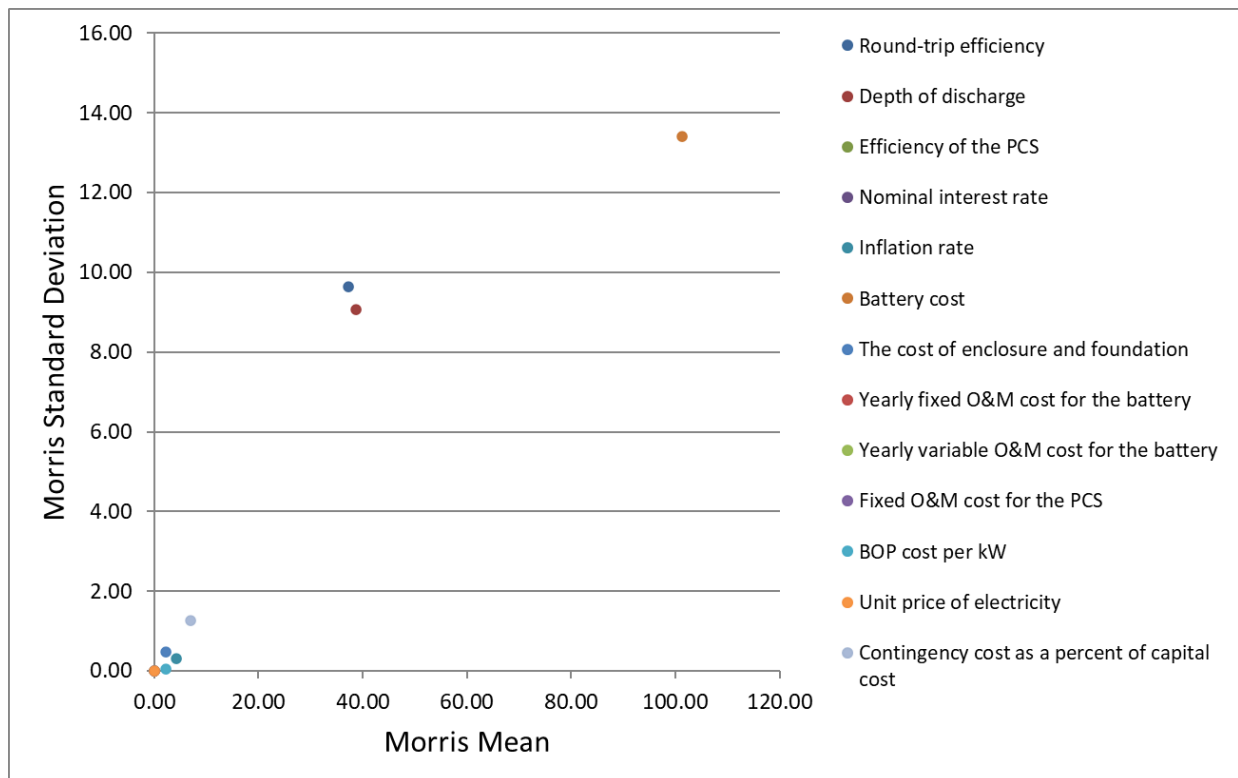


Figure 3.6: Sensitivity analysis for the TIC in the Na-S ESS for bulk energy storage

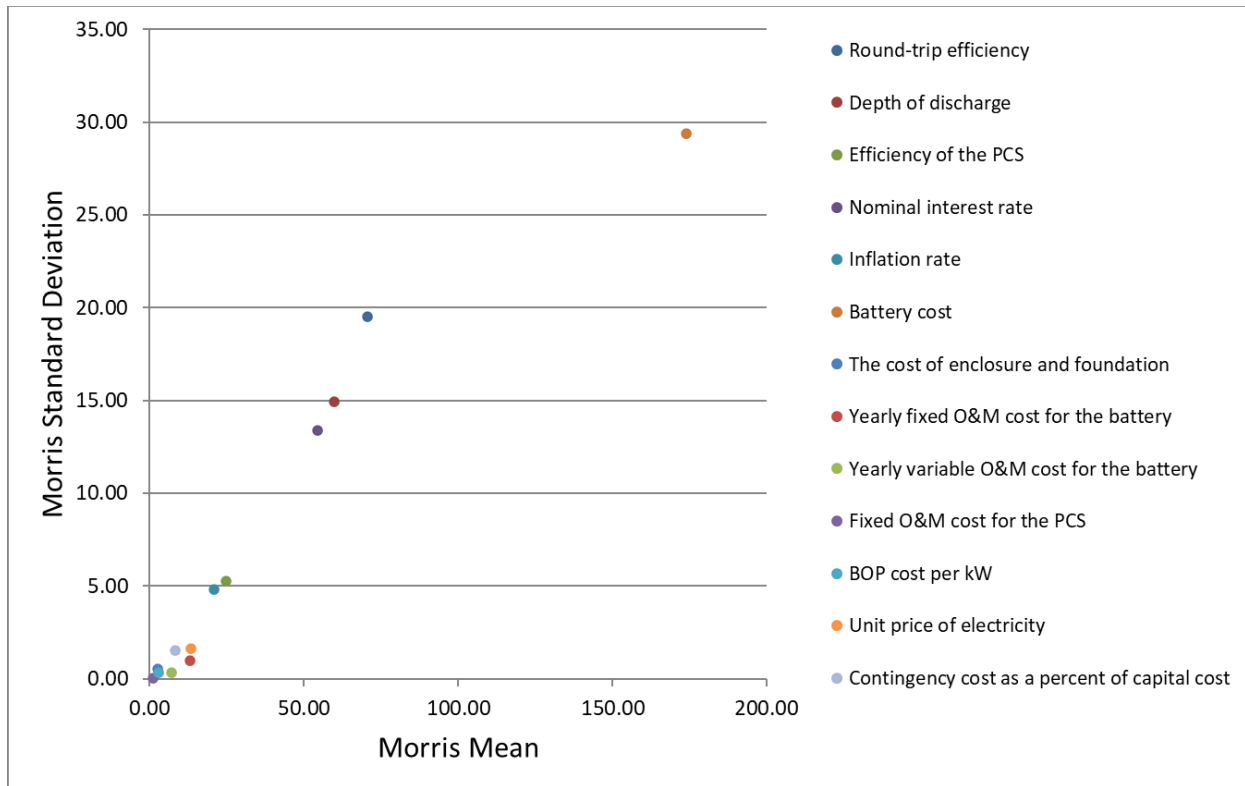


Figure 3.7: Sensitivity analysis for the LCOS in the Na-S ESS for bulk energy storage

Uncertainty analysis was also conducted to assess the effect of a simultaneous change in several inputs on the TIC and LCOS. Several input parameters were varied by a range found in the literature. The most likely values are the default values used in the techno-economic models and are given in Tables 3.1-3.6. The minimum and maximum values for each ESS can be found in section B.7 in Appendix B along with the details of the uncertainty analysis. Different statistical distributions (i.e., triangular, PERT, and uniform) of the input variables were used to perform the simulations. To obtain output distribution, a random sample was chosen from the range of input variables and iterated 100,000 times. Equation B.6 in Appendix B shows the formula used to estimate the sampling error.

Figures 3.8-3.11 show the uncertainties in the LCOS for all four scenarios; uncertainty in the TIC is provided in section B.7.2 of Appendix B. The bottom and top of the rectangular boxes in the figures represent the 25th and 75th percentiles, respectively, and the bottom and top of the error bars represent the 5th and 95th percentiles, respectively. The dots in the rectangular boxes represent the means. In S1 and S2, the scenarios in which the energy output is much higher than the power output, the ranking of batteries was found to be similar. A wider LCOS range is found in the Ni-Cd, mainly from the uncertainties in battery cost, round-trip efficiency, depth of discharge, and discount and inflation rates. While the mean LCOSs are \$233.46/MWh for the Na-S, \$212.44/MWh for the Li-ion, \$406.57/MWh for the VRLA, \$846.23/MWh for the Ni-Cd, and \$295.89/MWh for the VRF in S1, in S2 the mean LCOSs are \$308.38, \$284.24, \$475.47, \$973.58, and \$424.32/MWh for the Na-S, Li-ion, VRLA, Ni-Cd, and VRF, respectively. The mean LCOS is from \$449.98-\$1153.19/MWh for the Na-S, \$444.19-\$1086.95/MWh for the Li-ion, \$793.47-\$1297.33/MWh for the VRLA, \$925.82-\$2148.24/MWh for the Ni-Cd, and \$1549.54-\$3935.67/MWh for the VRF in S3 and S4, respectively. Figures 3.8-3.11 show overlaps in technologies; this is due to the range of input parameters (see Table B.3 in Appendix B). Even taking the LCOS range into account, the Ni-Cd is the most expensive option for both energy application scenarios (S1 and S2) due to the high capital cost of the Ni-Cd battery. In the power scenarios, the VRF is the most expensive option, ranging from \$1425.37/MWh to \$1678.94/MWh in S3 and \$3626.96/MWh to \$4260.18/MWh in S4. S4 is the most costly scenario; this is because its batteries are used the least (for only 15 minutes and 248 cycles per year).

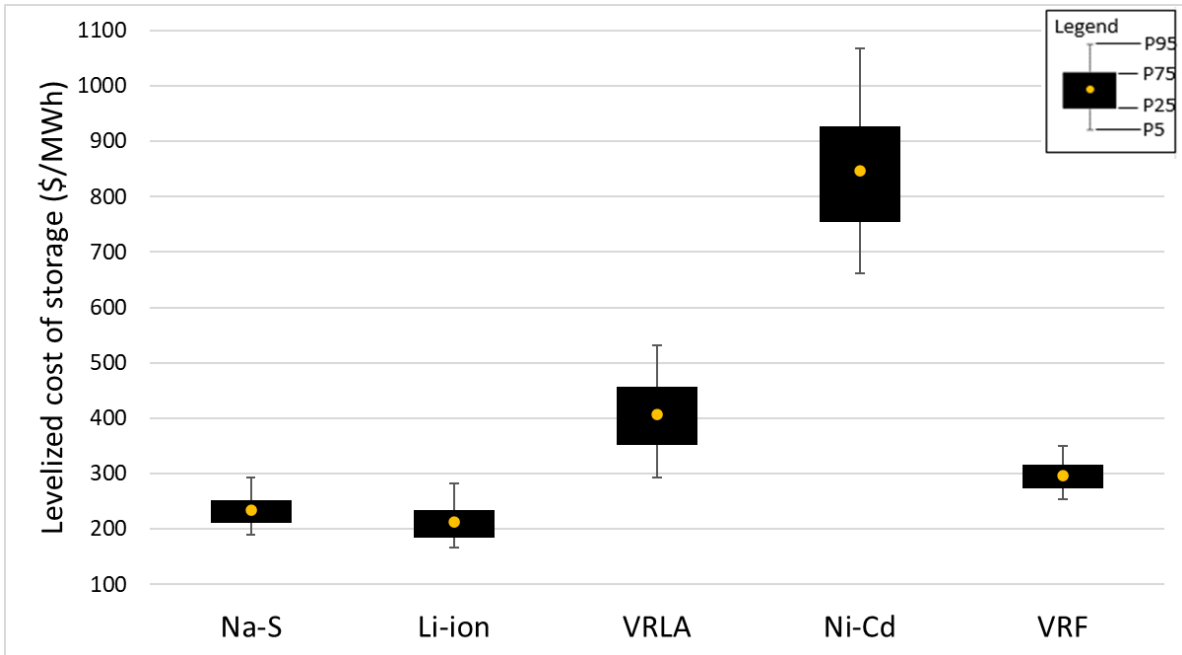


Figure 3.8: Uncertainty analysis for the LCOS for bulk energy storage (S1)

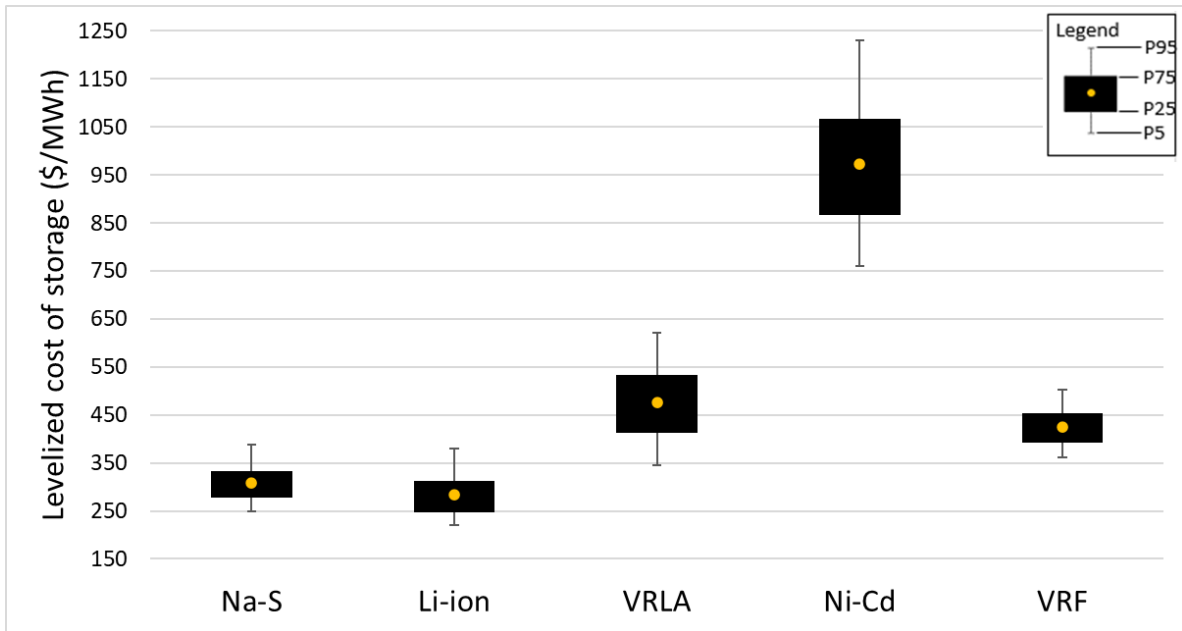


Figure 3.9: Uncertainty analysis for the LCOS for T&D investment deferral (S2)

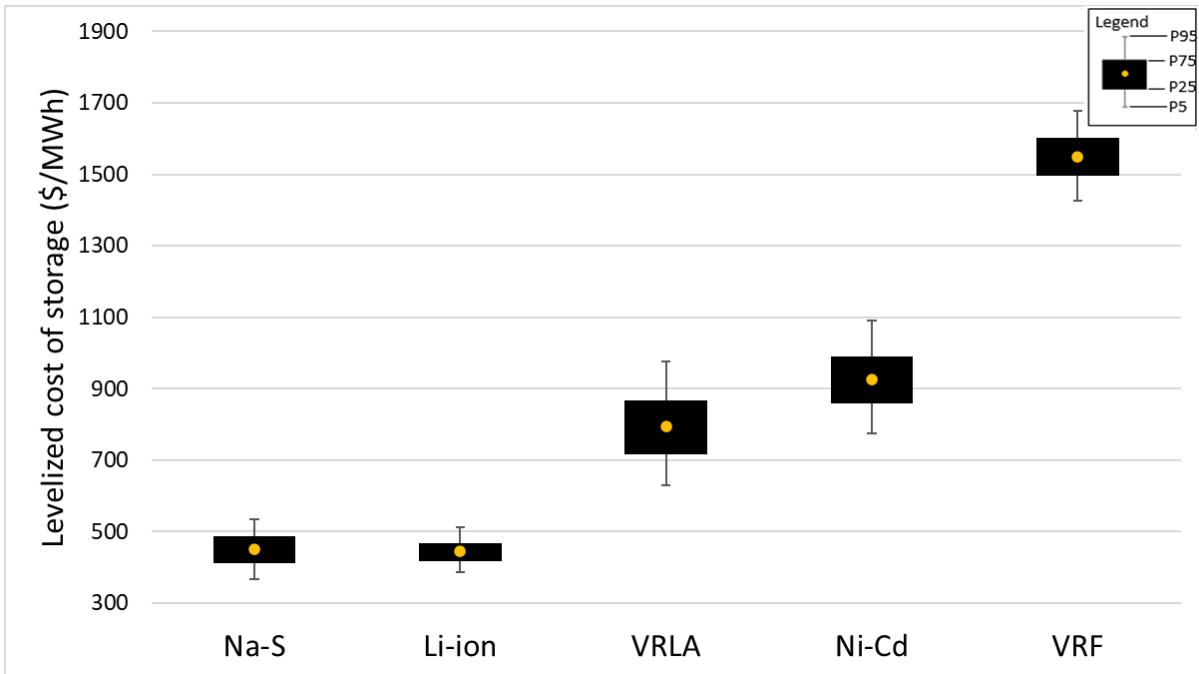


Figure 3.10: Uncertainty analysis for the LCOS for frequency regulation (S3)

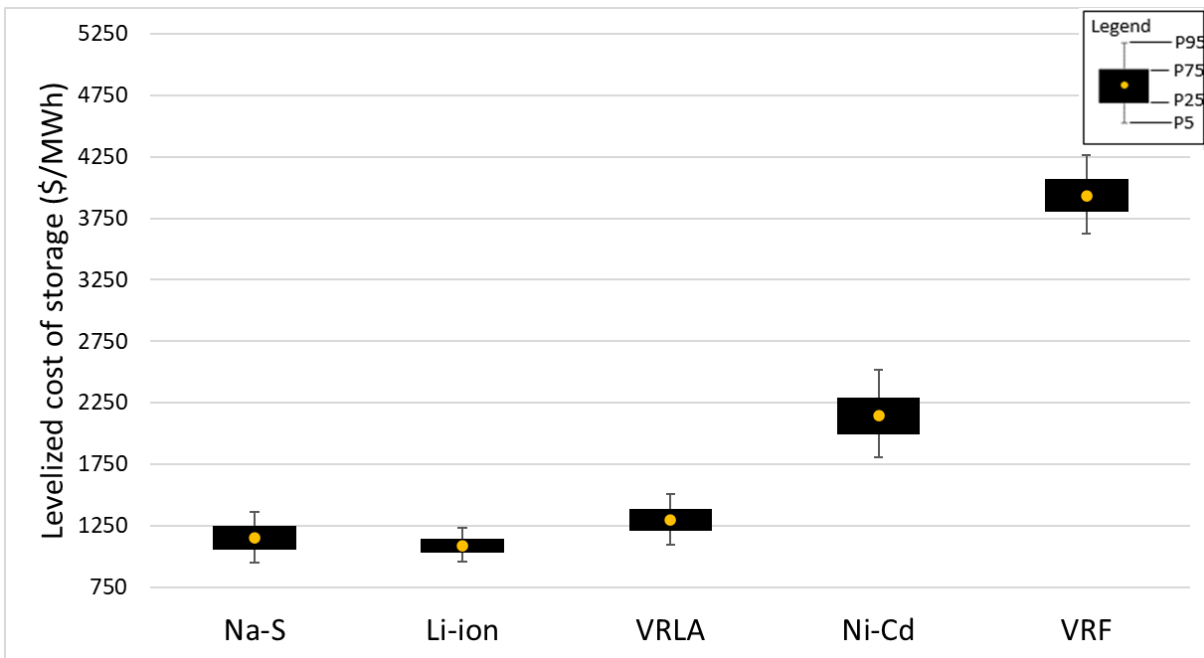


Figure 3.11: Uncertainty analysis for the LCOS for support for voltage regulation (S4)

3.3.5. Comparison with other energy storage technologies

The results of this study were compared with values reported in the literature. Very few studies have assessed the LCOS of stationary applications. The results of this study were compared with values reported by Battke et al. [105] and Steward et al. [215]. Battke et al. considered the Na-S, Li-ion, and VRF battery systems. The LCOS they reported for the Na-S is \$196/MWh for the energy time-shift mode, \$294/MWh for T&D investment deferral, \$883/MWh for frequency regulation, and \$1395/MWh for support of voltage regulation. The LCOSs reported for the Li-ion and VRF are \$501 and \$283/MWh for energy time-shift, \$730 and \$425/MWh for T&D investment deferral, \$872 and \$1210/MWh for frequency regulation, and \$1068 and \$1657/MWh for support of voltage regulation. The LCOS Battke et al. reported for the Li-ion is higher than that calculated in this study because their study's Li-ion battery pack had a higher capital cost; in recent years, the price of a Li-ion battery has dropped [330]. The difference in the VRF's LCOS reported in this study and Battke et al.'s is due to differences in methods. While this research used a bottom-up approach to design the components and estimated costs based on the design, Battke et al. used a top-down approach and took the battery's capital cost from the literature. The authors did not assess the VRLA or the Ni-Cd. Steward et al. reported the LCOSs to be \$240-\$280/MWh for the Na-S and \$540-\$890/MWh for the Ni-Cd [215]. The LCOSs for the VRF are \$270-\$390/MWh for the energy arbitrage mode, which is comparable to this study's Scenario 1. The numbers obtained in this research are in good agreement with those reported by Steward et al. [215].

In addition to comparing the electro-chemical energy storage technologies, an "apples-to-apples" comparison of the LCOS for different energy storage technologies was made, keeping the system boundary the same. The LCOSs for electro-chemical ESSs were compared with the LCOSs for mechanical energy storage systems reported by Kapila et al. [174] and thermal energy storage

systems reported by Thaker et al. [131]. Figure 3.12 shows that mechanical ESSs can deliver electricity at a lower cost than the electro-chemical ESSs. Although the capital cost of mechanical ESSs is higher than that of most electro-chemical ESSs, the mechanical ESS's long cycle life will lower the LCOS. Unlike mechanical ESSs, batteries in the electro-chemical ESS need to be replaced after a certain period. Thermal energy storage systems show a wide LCOS range depending on the technology used. While direct sensible heat using one tank (scenario T3 in Thaker et al.'s study) is the cheapest option, indirect sensible heat using two tanks (scenario T1) is the most expensive option for thermal energy storage. This is obvious because, as the study shows, T1 requires extra equipment (e.g., pump, heat exchanger, valves, etc.), which increases capital cost. The LCOS for a latent heat thermal energy storage system (scenario T4) is in the range of the LCOS for the Na-S and VRF battery ESSs. The main advantage of the electro-chemical ESSs is that these are more flexible in terms of application. While mechanical and thermal ESSs are mostly used for bulk energy storage, electro-chemical ESSs could be used for shorter or longer discharge durations.

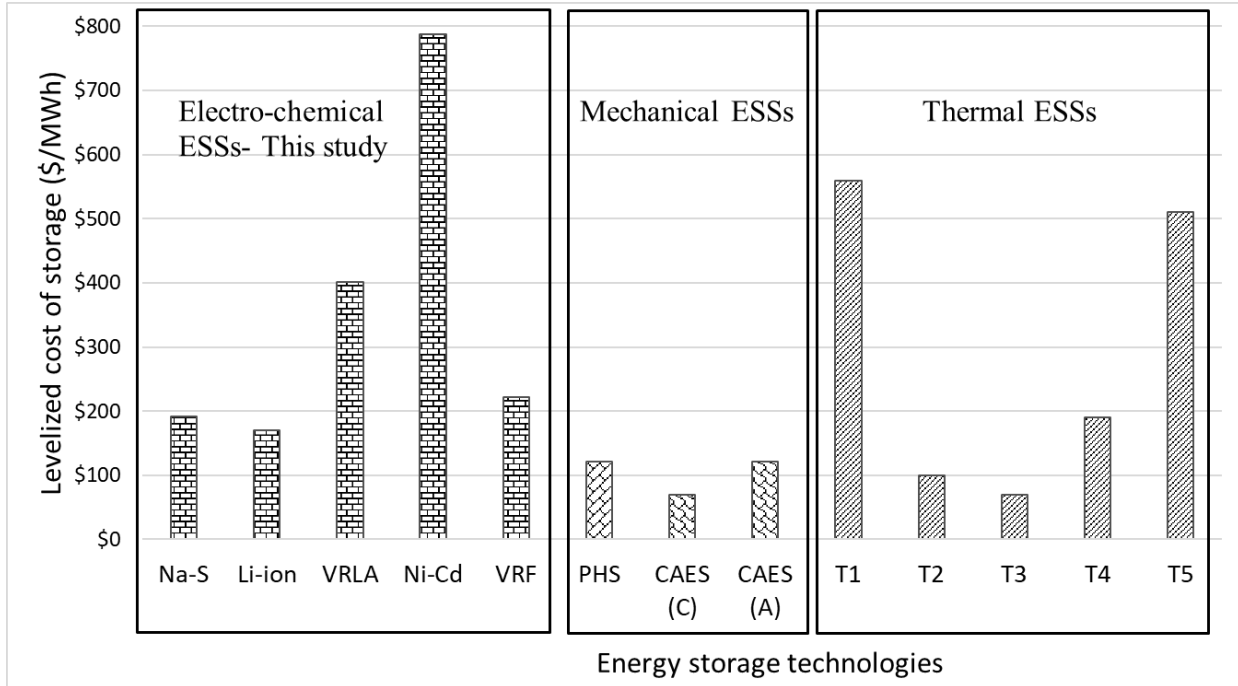


Figure 3.12: LCOSs for different ESSs for a discharge duration of 8 hours

(Note: PHS- pumped hydro storage, CAES (C)- conventional compressed air energy storage, CAES (A)- adiabatic compressed air energy storage, T1- indirect sensible heat using two tanks, T2- direct sensible heat using two tanks, T3- direct sensible heat using one tank, T4- latent heat using one tank, and T5- thermochemical storage).

3.4. Conclusion

In this study, bottom-up techno-economic models were developed to assess the economic feasibility of five electro-chemical ESSs in four stationary application scenarios. The life cycle costs were estimated for capacities of 5-100 MW for bulk energy storage, 5-25 MW for transmission and distribution investment deferral, 5-100 MW for frequency regulation, and 5-30 MW for support of voltage regulation. The economic performance indicators – total investment cost and levelized cost of storage – were evaluated for economic feasibility. In addition, scale factors were developed for the ESSs with discharge durations of 1-8 h. The developed scale factors are 0.77, 0.74, 0.82, 0.91, and 0.46 for the sodium-sulfur, lithium-ion, valve-regulated lead-acid,

nickel-cadmium, and vanadium redox flow, respectively. The results show that unit capital cost falls sharply with an increase in discharge duration for the vanadium redox flow; thus, this technology has a cost advantage for higher energy capacities due to stronger economies of scale.

The sensitivity analysis showed that battery cost, depth of discharge, round-trip efficiency, discount rate, and inflation rate are the most sensitive parameters for the electro-chemical batteries.

To provide more robust results and mitigate risks, an uncertainty analysis was performed and yielded a range of total investment cost and levelized cost of storage for the application scenarios.

Bulk energy storage is the least costly scenario; sodium-sulfur and lithium-ion energy storage systems perform better in terms of the levelized cost of storage. On the other hand, support of voltage regulation is the most expensive scenario; an overlap in levelized cost of storage was observed among sodium-sulfur, lithium-ion, and valve-regulated lead-acid energy storage systems.

The cycle life and battery capital cost mainly determine the relative ranking of storage technologies based on the levelized cost of storage. In bulk energy storage and transmission and distribution investment deferral, nickel-cadmium energy storage system is the most expensive option even with uncertainty taken into account because of the high capital cost of nickel-cadmium battery cells.

Although the vanadium redox flow energy storage system performs better in bulk energy storage and transmission and distribution investment deferral, this technology is the most expensive option for the power applications, frequency regulation, and support of voltage regulation, because of the very short discharge duration. The levelized cost of storage values for the sodium-sulfur and lithium-ion are lowest in every scenario because of these batteries' relatively low capital cost and long cycle life.

The findings of this research are expected to provide a better understanding of the cost competitiveness of different electro-chemical energy storage technologies for stationary applications, which should ultimately help stakeholders in decision-making.

Chapter 4: The greenhouse gas emissions' footprint and net energy ratio of utility-scale electro-chemical energy storage systems⁷

4.1. Introduction

The need to use energy storage systems (ESSs) in electricity grids has become obvious because of the challenges associated with the rapid increase in renewables [331]. ESSs can decouple the demand and supply of electricity and can be used for various stationary applications [213]. Among the ESSs, electro-chemical storage systems will play a vital role in the future. The advantages of electro-chemical ESSs are two-fold – fast response time and modularity, which make them suitable for a wide range of stationary applications [84] and give them the flexibility to be deployed when and where required [332]. Electro-chemical ESSs have received increased attention from the energy industry, government, and academia. However, before ESSs can be implemented, it is important to understand their environmental performance in terms of the net energy ratio (NER) and the life cycle GHG emissions in various stationary applications. Life cycle assessment (LCA) is the most widely used tool to evaluate the environmental performances of a product system throughout its life cycle [333]. LCA has become increasingly important in making informed decisions regarding the deployment of ESSs. An ESS with lower life cycle GHG emissions and higher NER is preferred.

Earlier LCA studies on electro-chemical batteries have focussed on the comparison of lithium-ion (Li-ion) and other batteries for electric vehicle applications, for example, Li-ion with nickel-metal-

⁷ A version of this chapter has been published as Rahman MM, Gemechu E, Oni AO, Kumar A. The greenhouse gas emissions' footprint and net energy ratio of utility-scale electro-chemical energy storage systems. *Energy Conversion and Management*. 2021;244:114497.

hydride [334] and Li-ion with sodium-nickel-chloride (NaNiCl) [335]. These studies provide useful information on the batteries' technical parameters and material and energy inventories, but the findings cannot be directly applied to stationary applications because of differences in system requirements and characteristics. There are a few published papers on the LCA of different ESSs for stationary applications; most of them focus on leading technologies for utility-scale applications, such as pumped hydro storage [256], compressed air energy storage [336], and thermal storage [271, 337]. These studies facilitate the comparison of environmental performances of large-scale mechanical and thermal ESSs. LCAs of electro-chemical ESSs focus on comparative assessments, for example, vanadium redox flow (VRF) with Li-ion [44], aluminium ion (Al-ion) with Li-ion [45], and VRF with lead-acid (Pb-A) and sodium-sulfur (Na-S) [46]. Two studies [47, 48] compared the environmental footprints of different Li-ion batteries. However, none of these studies provides a relative ranking of battery technologies in different applications, considering the impacts of operational characteristics in the use phase. Only a limited number of studies investigates the environmental performances of electro-chemical ESSs in different stationary applications. Ryan et al. [49] conducted an LCA of three types of Li-ion batteries to estimate the cumulative energy demand (CED), global warming potential (GWP), and acidification for frequency regulation. Jones et al. [50] evaluated the GWP of Li-ion and VRF storage systems for black start, renewables support, reserve, and balancing. Baumann et al. [51] assessed the GWP of Li-ion, valve-regulated lead-acid (VRLA), VRF, and NaNiCl for renewables support, primary regulation, time-shift, and increase of self-consumption. In addition to the GWP, a few studies [52, 53] estimated a wide range of environmental impacts, such as human toxicity, particulate matter formation, freshwater ecotoxicity, etc. These studies considered several battery chemistries and found that sodium- and lithium-based batteries have lower environmental footprints than the other

batteries. These studies provide useful information on the environmental performances of electro-chemical ESSs. However, life cycle inventory analysis and impact assessment in these studies relied on generic databases, which might not be applicable for a specific project or application, as material and energy inventories can vary by application and jurisdiction [11]. While one cannot avoid using generic inventory data, especially for background systems, primary data can be accurately estimated by applying fundamental engineering principles to size the storage systems and develop the material and energy inventories for different applications. In addition, these studies overlooked the environmental impacts arising from the use of the power conversion system (PCS). To the best of the author's knowledge, none of the earlier LCA studies included the PCS in the system boundary to evaluate the energy use and resulting GHG emissions for the material production and manufacturing of the PCS. Moreover, some studies omitted one or more life cycle stages, for example, dismantling and transportation of dismantled components. Excluding any of these aspects when comparing different energy storage technologies can generate misleading information. Finally, there is a lack of detailed sensitivity and uncertainty analyses in the previous studies. For example, the impacts of important design parameters, such as depth of discharge, battery manufacturing energy requirements, cell voltage, and efficiency of the PCS on the environmental performances were not evaluated. According to ISO 14040, an LCA should have sensitivity and uncertainty analyses to improve the reliability of models and results by identifying the most influential parameters and providing a probable range of results [57].

To address the gaps in the literature, data-intensive bottom-up LCA models were developed to quantify the NER and life cycle GHG emissions of five promising electro-chemical ESSs – lithium-ion (Li-ion), sodium-sulfur (Na-S), valve-regulated lead-acid (VRLA), nickel-cadmium (Ni-Cd), and vanadium redox flow (VRF) battery to provide useful insights into their stationary

applications in Alberta's (a Canadian province) electricity network. The focus of this study is on four stationary application scenarios – bulk energy storage, transmission and distribution (T&D) investment deferral, frequency regulation, and support of voltage regulation. Fundamental engineering principles were used to size the storage systems and calculate the material and energy requirements. The specific objectives are to:

- Conduct a life cycle assessment of five electro-chemical ESSs – lithium-ion, sodium-sulfur, valve-regulated lead-acid, nickel-cadmium, and vanadium redox flow storage systems;
- Develop material and energy inventories for all the life cycle stages from material production to end-of-life using fundamental engineering first principles;
- Evaluate the NER and life cycle GHG emissions considering all the life cycle stages from material production to end-of-life; and
- Assess four stationary application scenarios – bulk energy storage, transmission and distribution investment deferral, frequency regulation, and support of voltage regulation.

The remainder of the chapter is divided into three sections. Section 4.2 describes the method used for this study that includes the selection of application scenarios, system design, and life cycle assessment. Section 4.3 discusses the results including the NER and life cycle GHG emissions. Conclusions are outlined in section 4.4.

4.2. Method

The details on application scenarios, system design, and LCA are discussed in this section. The data and assumptions used to build material and energy inventories are also described.

Figure 4.1 shows an overview of the modeling approach used in this study. First, application scenarios and their technical characteristics were defined followed by the estimation of the energy capacity of each scenario. Second, different system components were identified, their technical parameters were defined, and components were sized to satisfy the rated power and energy for the applications. The last segment of the framework describes the LCA procedure followed to evaluate the NER and life cycle GHG emissions. This involves goal and scope definition (setting the system boundary and functional unit), inventory analysis, and translation of the inventory data to NER and GHG emissions. The system design and LCA handle a large number of input parameters that can influence the model outputs. To handle the variability in inputs, sensitivity and uncertainty analyses were conducted through the Regression, Uncertainty, and Sensitivity Tool (RUST) [285].

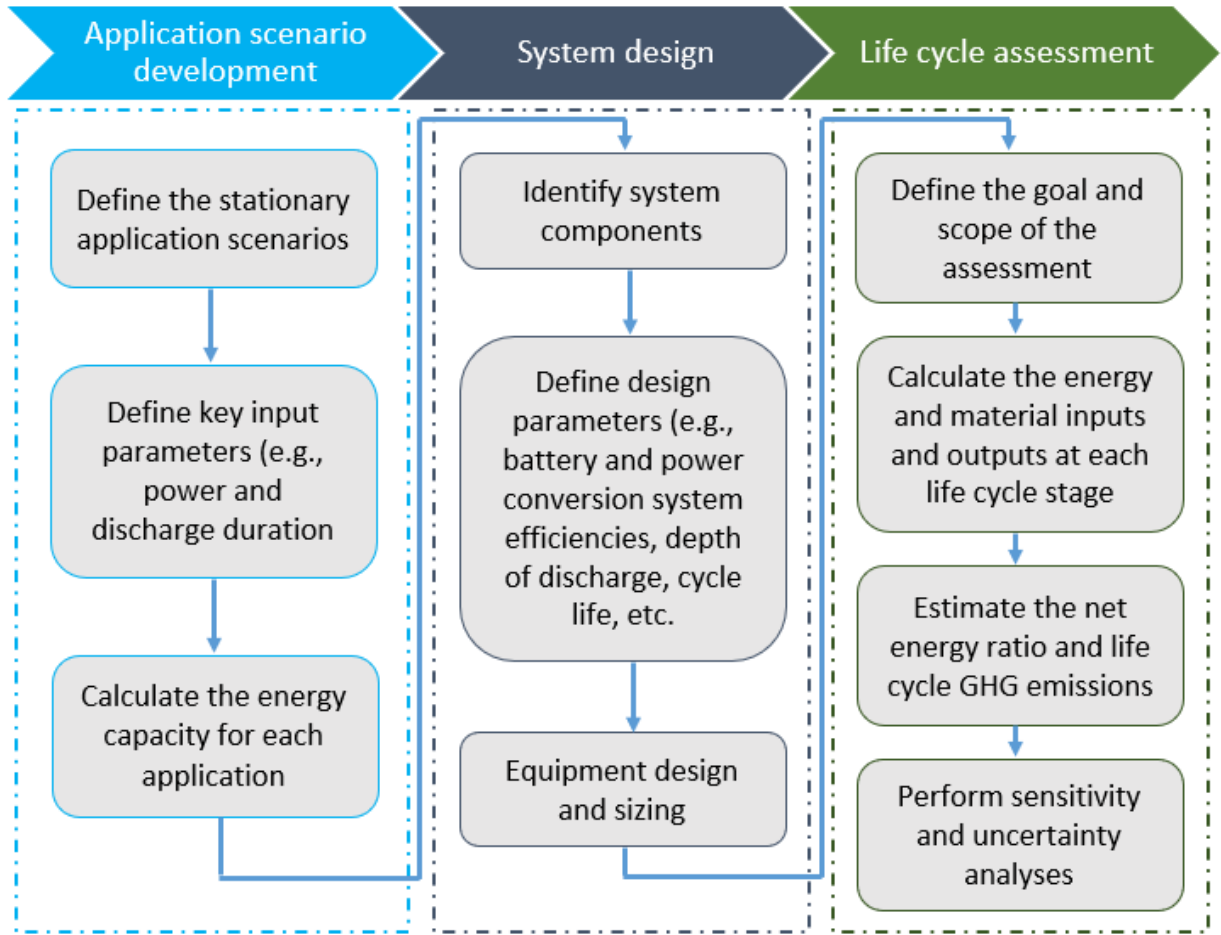


Figure 4.1: Methodological framework

4.2.1. Application scenario development

Because of flexibility in operation, electro-chemical ESSs can be used for both short-term and long-term storage applications. To evaluate the environmental footprints of electro-chemical ESSs, two short-term and two long-term application scenarios were developed based on cycle duration. Typically, short-term applications have a discharge duration of less than 2 hours, while long-term applications have 2-8 hours of discharge duration [139]. Bulk energy storage and T&D investment deferral are the long-term application scenarios and named Scenario 1 (S1) and Scenario 2 (S2), respectively. Bulk energy storage involves charging an ESS when the electricity price is low during

off-peak hours and discharging during peak hours at a high price. T&D investment deferral helps to defer or avoid additional investments related to the transmission and distribution infrastructure. Although compressed air, pumped hydro, and power-to-chemical storage systems are widely used for long-term applications, because of rapid cost decline and modularity, electro-chemical ESSs are increasingly being considered [84]. Furthermore, the availability of suitable geographic sites is an issue for compressed air and pumped hydro storage systems. Frequency regulation and support of voltage regulation are the short-term application scenarios, Scenario 3 (S3) and Scenario 4 (S4), respectively. Frequency regulation maintains grid frequency within the permissible bounds by balancing short-term fluctuations of electricity generation and consumption. An ESS used for support of voltage regulation maintains the voltage within a pre-defined level by managing the reactance in the distribution grid. These applications are increasingly important for stabilizing electrical grids with high shares of renewables [105]. Table 4.1 presents the operational characteristics of these applications.

Table 4.1: Assumptions used in the stationary application scenarios

Scenario	Bulk energy storage (S1)	T&D investment deferral (S2)	Frequency regulation (S3)	Support of voltage regulation (S4)
Rated power (MW)	50 [338]	10 [338]	50 [338]	15 [338]
Discharge duration (h)	5 [119]	5 [339]	0.25 [119]	0.25 [340]
Energy rating (MWh)	250	50	12.5	3.75
Cycles/year	365 [119]	248 [105]	12,410 ^a [257]	248 [105]

^aFor frequency regulation, each cycle will be equivalent to a 5% depth of discharge of the corresponding battery size.

4.2.2. System design

The PCS and storage section are the main components of an electro-chemical ESS. The PCS includes an inverter and a transformer. The storage section has batteries connected in various combinations (series, parallel, or both) to meet voltage and capacity requirements [6]. The number of PCSs required was calculated based on the application scenario's rated power and the rated power of each PCS. It was assumed that each PCS would have 5 MW rated power. 5 MW is one of the largest containerized PCSs in the market [302]; they have significant cost advantages because of their large capacity [169]. The installed capacity of the storage section was calculated using the rated power, discharge duration, battery round-trip efficiency, and depth of discharge (DOD). Equation 4.1, adapted from Akinyele et al. [303], was used to calculate the battery installed capacity.

$$E_I = \frac{P_R}{\eta_b} * \frac{H}{DOD} \quad (4.1)$$

Here, E_I is the installed energy storage capacity (MWh), P_R is the rated power (MW), H is the discharge duration (h), η_b is the round-trip efficiency of the battery (%), and DOD is the depth of discharge (%).

Table 4.2 summarizes the technical parameters used to design the storage systems. The design of conventional batteries (Na-S, VRLA, Li-ion, and Ni-Cd) is different from that of flow batteries (VRFBs). For conventional batteries, power and energy come from the same battery cell, which contains electrodes and the electrolyte. The installed capacity was calculated to satisfy the rated power and energy capacities. The advantages of these batteries are that they can be designed in modules and can be scaled up. Battery cells form a module; many modules can be connected to form a rack. Racks can be attached in a section and several sections need to be connected to meet

the installed capacity requirement. For VRFs, the size of the active area of the cell stack determines the power capacity and the volume of electrolyte solutions in the electrolyte tanks determines the energy capacity [10]. There are some accessories, such as heat exchangers (HXs), which dissipate the electrolyte’s heat, and pumps, which circulate the electrolyte to the cell stacks. The technical parameters used to design the power and energy components of the VRF battery are listed in Table C.1 in Appendix C.

The cycle life determines the number of battery replacements, which ultimately depends on the DOD and the number of cycles a battery operates. For conventional batteries, cycle life decreases with increasing DOD, but the cycle life of VRFs is not affected by the DOD [306]. VRF batteries are good for about 13,000 cycles [258] because the electrolyte does not degrade over time [307]. The details of a VRF system sizing can be found in section C.1 in Appendix C.

Table 4.2: Technical inputs used to design the energy storage systems

ESS	Depth of discharge (%)	Battery efficiency (%)	Cycle life (number of cycles)	Footprint (m ² /kWh)
Na-S	80 [119]	78 [308]	$1.978 \cdot 10^6 (\text{DOD})^{-1.73} + 3101$ [299]	0.030 [338]
Li-ion	80 [310]	90 [258]	$2731.7 (\text{DOD})^{-0.679} \cdot \exp$ [1.614(1-DOD)] [311]	0.017 [338]
VRLA	60 [119]	85 [258]	$1248.6 (\text{DOD})^{-0.889}$ [338]	0.062 [338]
Ni-Cd	80 [119]	80 [314]	$2016.1 (\text{DOD})^{-1.301}$ [338]	0.057 [338]
VRF	90 [316]	75 [105]	13,000 [258]	0.243 [338]

4.2.3. Life cycle assessment

4.2.3.1. Goal and scope definition

The most promising large-scale electro-chemical ESSs for future energy storage applications are Li-ion, Na-S, Pb-A, Ni-Cd, and VRF. This study aims to understand the relative rankings of these electro-chemical ESSs in utility-scale applications based on their NER and life cycle GHG performances. We developed spreadsheet-based models to build material and energy inventories and to translate inventories to environmental impacts. The material and energy inventories were developed based on engineering principles. Publicly available data were used where relevant. Data sources are discussed in section 4.2.3.2. The NER and life cycle GHG emissions are the environmental metrics used. The NER is the ratio of total energy output to the total energy expended in material production, manufacturing, transportation, and end-of-life (EOL) over the lifetime. Intergovernmental Panel on Climate Change (IPCC) 100-year global warming potential values were used to translate the inventory to GHG emissions (CO₂ equivalent). The functional unit was considered to be 1 MWh electricity delivered from the ESSs. The project lifetime of the ESSs was taken to be 20 years [258].

Figure 4.2 shows the common system boundary used to compare the environmental performance of electro-chemical ESSs. In the operational phase, electricity from the Alberta grid was considered. Landfilling and incineration in the EOL were not included in the analysis due to the lack of data. The recycling of battery materials at the EOL was not modeled in the base case due to the lack of data; however, an additional case study was conducted with the limited data available to understand the impact of battery recycling.

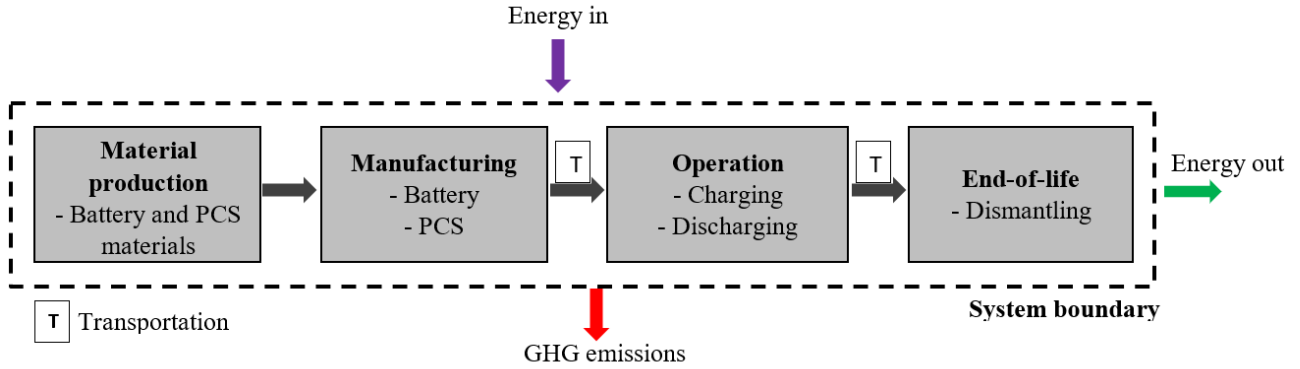


Figure 4.2: System boundary for electro-chemical energy storage systems

4.2.3.2. Inventory analysis

The inventory analysis involves the calculation of material and energy inputs and outputs at all the life cycle stages in the system boundary for the storage section and PCS. The details on how inventories were built for all the life cycle stages of an ESS with relevant data sources are provided below.

4.2.3.2.1. Material production

To build the material inventory list, we first estimated the mass of the battery and the PCS separately. For conventional batteries (Na-S, Li-ion, VRLA, and Ni-Cd), the total mass was calculated from the installed capacity and energy density using Equation 4.2, adapted from Spanos et al. [341]:

$$m = \frac{E_I}{E_d} \quad (4.2)$$

where m is the total mass of the battery (kg), E_I is the installed battery capacity (Wh), and E_d is the energy density (Wh/kg).

The energy densities of Li-ion, Na-S, VRLA, and Ni-Cd ESSs are presented in Table 4.3. In this study, three Li-ion battery types, lithium manganese oxide (LMO), lithium nickel manganese

cobalt (NMC), and lithium iron phosphate (LFP), were considered as they are the types used frequently.

Table 4.3: Energy densities considered for various electro-chemical batteries

ESS	Default energy density (Wh/kg)	Source/comment
Li-ion	110 (LMO), 135 (NMC), and 102.5 (LFP) [342]	Average of the ranges reported by Stan et al. [342]. Sensitivity and uncertainty analyses were conducted using the range reported in the literature.
Na-S	116 [258]	Hiremath et al. reported 116 Wh/kg for grid applications. The range of energy density considered for the uncertainty analysis is from 100 [343] to 206 Wh/kg [344].
VRLA	35 [345]	The energy density calculated for the VRLA ranges from 30-40 Wh/kg, according to Discover Battery's brochure [346].
Ni-Cd	55 [347]	Average of the range reported by Omar et al. [347]. However, the range of energy density considered for the uncertainty analysis is from 50-75 Wh/kg, as reported by Fan et al. [348].

Once the total mass of the batteries was determined, the mass of each material was calculated from the mass fraction of battery materials. The mass fraction of different materials for the batteries can be found in Table C.2 of Appendix C. The Na-S battery inventory is best described in Sullivan and Gaines [349]; that inventory was used in this study. The material fraction for VRLAs was taken from Spanos et al., who provide the inventory with information from the manufacturer [341]. The material composition for Li-ion batteries was taken from Greenhouse Gases, Regulated Emissions, and Energy Use in Transportation (GREET) model [350]. The material inventory for the Ni-Cd

battery was taken from Rydh and Karlström [351]. The inventory was validated with Saft Batteries' material safety data sheet [352]. The power subsystem inventory for the VRF battery was taken from an earlier study [44], while the inventory for the energy subsystem was estimated using the scientific principles described in Appendix C in section C.1.

Different methods were used to estimate the material inventory for the VRF battery, as its energy and power components are independent. The energy subsystem components are an electrolyte (a mixture of V_2O_5 , H_2SO_4 , and water) and the tanks that hold the electrolyte. The amount of electrolyte needed and the volume of positive and negative electrolyte tanks were calculated using the energy rating; the calculation details can be found in Appendix C in section C.1. For the electrolyte tanks, it was assumed that the tank material is glass fiber [44].

The power subsystem consists of the stacks. The mass of the different stack components for the rated power was estimated based on the mass fraction of components and the mass of a 1 MW power subsystem [44]. The total mass of the components of a 1 MW power subsystem is 10.02 tonnes [44]. A similar approach was used to find the mass of accessories, pumps, pipes, cables, and heat exchangers (HXs). The details can be found in Appendix C in section C.2.

The PCS consists of inverters and transformers [302]. The mass of the inverter and transformer varies with capacity. The higher the capacity, the lower the mass per unit capacity. The mass of various capacity inverters and transformers were taken from industrial datasheets [353, 354]. From the plots of mass vs. capacity, best-fit equations were obtained and used to calculate the mass of the inverter and the transformer (see Figures C.1 and C.2 in Appendix C). The details of mass calculations along with the material composition for the inverter and transformer can be found in Appendix C in section C.2.

A concrete foundation is required for the storage section as it carries a huge load. The PCS is assumed to be containerized [302]. The amount of concrete needed was calculated from the total area required for each battery, the thickness of the concrete floor, and the density of the concrete. The area requirements were estimated from the battery's footprint (m^2/kWh) and installed capacity.

Once the material requirements for the batteries and PCS were estimated, the energy consumption for the materials' production and the resulting GHG emissions were calculated using specific energy consumption (MJ/tonne) and emission factors ($\text{kg-CO}_2\text{eq}/\text{tonne}$), respectively. Table C.3 in Appendix C shows the developed material inventory for the five ESSs.

4.2.3.2.2. Manufacturing

The total primary energy (PE) required for the manufacturing of batteries is based on the specific PE (MJ/Wh) and the capacity of each battery. Table 4.4 shows the specific PE to manufacture various batteries. The replacement of batteries, if required, was also considered. Once the primary energy was estimated, the sources of energy were identified to calculate the GHG emissions. Electricity and heat are the sources of energy in the manufacturing of batteries [273]. The shares of PE attributable to electricity for the batteries are presented in Table 4.4. The rest is attributable to heat generation from natural gas [355]. A 40% conversion efficiency was used to convert primary fuel to electricity [146]. Once the amount of electricity and natural gas was known, the GHG emissions were calculated from the amount of energy and the emission factors (EFs). It was assumed that Na-S and Ni-Cd batteries are manufactured in Japan. NGK, a Japanese company, is the only producer of Na-S [356] and Japan is the largest manufacturer of Ni-Cd batteries in the world [351]. As China is the global leader in VRF battery manufacturing and use, it was assumed that the VRF battery is manufactured in China. Li-ion and VRLA are widely used battery

technologies and are considered to be manufactured in the USA. The electricity emission factors for Japan, the USA, and China are presented in Table 4.4. Although the electricity EFs can vary depending on the location and the share of different energy sources over time, the method considered in this research would be valid for other jurisdictions with a slight adjustment in the emission factors.

Table 4.4: Energy requirements for manufacturing electro-chemical batteries

Battery	Manufacturing energy requirement (MJ_{PE}/Wh)	Share of PE used to produce electricity (%)	Manufacturing country	Electricity EFs (kg-CO₂eq/MWh)
Na-S	0.60 [357]	70 [357]	Japan [358]	0.49 [359]
Li-ion	1.20 [357]	75 [357]	USA [360]	0.46 ^b [361]
VRLA ^a	0.42 [357]	65 [357]	USA [362]	0.46 ^b [361]
Ni-Cd	2.10 [357]	68 [357]	Japan [363]	0.49 [359]
VRF	0.74 [357]	41 [357]	China [364]	0.62 [359]

^a It was assumed that the manufacturing energy and shares of primary energy used to generate electricity are the same for lead-acid and valve-regulated lead-acid batteries.

^b USA average electricity mix.

The energy requirements in manufacturing the inverter and transformer were also considered in this study. The energy requirement data for 2.5-20 kW inverters were used to calculate the energy requirements for a 5 MW inverter [365]. A scale factor was developed from the plots of energy required vs. rated power to calculate the amount of energy used for a 5 MW inverter. The data to generate the inventory for the transformer were taken from Burger Mansilha et al.'s study [366], which provides energy requirements for a 75 kVA transformer. Due to the lack of data, the same scale factor developed for the inverter was used for the transformer. Table C.6 in Appendix C

shows the inventory list for the manufacturing phase of the PCSs used in the stationary application scenarios.

After estimating the energy requirements for the inverter and transformer, with the EFs of different energy sources, GHG emissions were calculated. Although there are many PCS manufacturers in Asia and Europe, several American companies manufacture PCSs, and it was assumed that the PCS was manufactured in the USA. For electricity, US average EFs were used (see Table 4.4).

4.2.3.2.3. Operation

The operation phase includes charging and discharging the batteries. The amount of electricity discharged from the system was calculated based on the rated power, duration of discharge, number of cycles per year, and PCS efficiency. The amount of electricity required for charging depends on the rated power, duration of discharge, number of cycles per year, battery round-trip efficiency, and depth of discharge. The input in this phase is the electricity used during charging. For the base case, electricity from the Alberta grid (35% coal, 30% cogeneration, 16% natural gas, 9% wind, 6% hydro, and 4% others) was considered for charging [367]. However, additional scenarios were developed for other provinces where the grid mixes are different than Alberta. The GHG emissions in the operation phase were calculated based on the amount of electricity required and the EF of Alberta grid electricity (471 kg-CO₂eq/MWh) [367].

4.2.3.2.4. End-of-life (EOL)

The EOL phase includes dismantling and the transportation of dismantled components. Given the limited data and lack of confidence in their quality, recycling was not included in the base case. However, to understand the importance of recycling battery materials, a case study was done for recycling using the data available and some assumptions. It was assumed that battery parts and the

PCS are dismantled mechanically; the electricity and diesel requirements for these are 0.01 kWh/kg and 0.10 MJ/kg, respectively [44].

For recycling, a literature review was conducted to find which battery materials could be recycled with existing recycling processes. The amount of recycled materials was determined using the recovery rate of various materials. It was assumed that the remaining material would come from virgin materials. Only those materials were considered for recycling for which information on recovery rate and specific energy required for recycling was available. The materials recycled with their recovery rate and the specific energy consumption in recycling can be found in Table C.7 in Appendix C.

4.2.3.2.5. Transportation

The amount of energy required in transportation depends on the mode and the distance. Figure 4.3 provides an overview of the supply chain routes for the PCSs and batteries. PCSs, as well as Li-ion and VRLA batteries, are manufactured in the USA and exported from California. The transportation distance by ship was calculated from the Port of San Francisco (California) to the Port of Kitimat (British Columbia, Canada) using the Portworld Distance Calculator [368]. Because British Columbia (BC) is Alberta's nearest province with seaports, it was assumed that all the ESS components would go to the Port of Kitimat in BC. Na-S and Ni-Cd batteries are transported from Japan and VRFs from China. Since Alberta ESSs are the focus of this research, the distance from the Port of Kitimat to Edmonton, Alberta (1370 km) was considered. Another 300 km was assumed for the transportation of the components from the manufacturers to the seaports in the manufacturing countries. For the EOL phase, it was assumed that after dismantling, the components are transported 300 km to a recycling plant or landfilling zone in Alberta. The recyclable materials were assumed to be used in remanufacturing in the recycling case. For inland

transportation, heavy-duty trucks were assumed. As distances can vary, an uncertainty analysis was performed for different transportation distances. The energy consumption was then calculated using the distance, mass transported, and specific energy consumption for ships and trucks. After the energy requirement for transportation was calculated, the GHGs were estimated from the EFs for diesel (truck transportation) and bunker fuel (marine transportation).

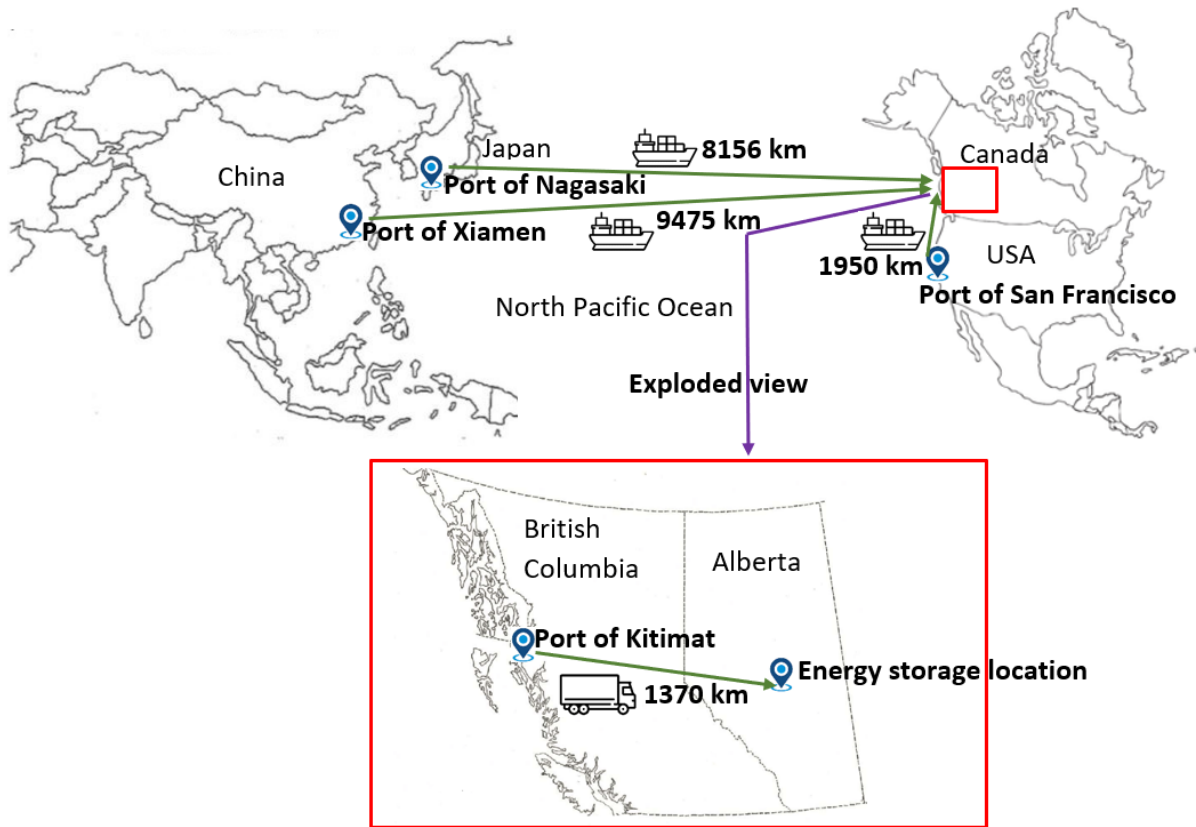


Figure 4.3: Overview map of the supply chain routes for the batteries and power conversion system

4.2.3.4. Sensitivity and uncertainty analyses

The LCA models developed in this study handle a large amount and range of input data. To understand the effects of variations in input data, sensitivity and uncertainty analyses were

performed using RUST, an Excel-based tool [285]. The Morris method [369] was used for the sensitivity analysis to investigate the impacts of inputs on the NER and GHG emissions. The advantage of the Morris method is that it helps us understand the interactions among input parameters and their non-linear effects [285]. The most influential parameters identified in the Morris analysis were included in the uncertainty analysis, which was performed using a Monte Carlo simulation. Parameters with negligible effect were excluded in the uncertainty analysis. Distributions for the input parameters were obtained from the literature. A random sample was selected from the range of input variables to obtain output distributions, and 100,000 iterations were performed to achieve a sampling error of less than 1% of the mean. The lowest and highest values for each uncertain parameter were identified and used in the sensitivity and uncertainty analyses (they can be found in Table C.8 in Appendix C).

4.3. Results and discussion

The net energy ratio and life cycle GHG emissions are presented and discussed in this section. Sensitivity and uncertainty analyses results are also presented and discussed.

4.3.1. Net energy ratio (NER)

The electricity outputs in bulk energy storage (S1), T&D investment deferral (S2), frequency regulation (S3), and support of voltage regulation (S4) are 1733.75, 235.60, 147.37, 17.67 GWh, respectively. The total energy consumption is the sum of the energy required for material production, manufacturing, operation, transportation, and dismantling. Figure 4.4 shows the NERs for the electro-chemical ESSs. The NERs range from 0.50 for the Ni-Cd to 0.69 for the Li-ion for S1, 0.47 for the VRF to 0.65 for the Li-ion for S2, 0.50 for the VRLA to 0.70 for the Li-ion for S3, and 0.38 for the VRF to 0.63 for the Li-ion for S4. The NERs are different in the application scenarios and are dictated by the duration of discharge and the number of cycles the ESSs operate.

In all the scenarios, the Na-S and Li-ion have higher NERs than the other storage systems because of their higher energy density and longer lifetime.

In bulk energy storage (S1), Na-S has lower NER than Li-ion mainly because of its higher energy requirement in material production. Among the Li-ion batteries, LMO has the highest NER and NMC the lowest because the production of cathode material for NMC requires 3.45 times more energy than for LMO. Na-S and Li-ion perform better than other batteries because of their comparatively higher energy density, meaning comparatively lower material requirements and longer cycle lives. The cycle lives of Na-S and Li-ion are 1.5 and 1.6 times longer than that of the Ni-Cd battery. Although the VRLA has the lowest manufacturing energy requirement (see Table 4.4), it has the lowest energy density (35 Wh/kg), hence high energy requirements in material production. The VRLA is the third-best performer in S1. Although the cycle life of the VRF is very high (13,000 cycles), it can not compete with Na-S or Li-ion. This is mainly due to the large number of components required for the VRF system. This is a unique battery that requires positive and negative electrolyte tanks, pumps, and heat exchangers. In addition, stacks and pumps need to be replaced after 10 years of operation. The additional components make the battery system more energy-intensive. The NER of a VRF is 0.52, slightly lower than a VRLA's (0.56). The Ni-Cd ESS has the lowest NER in S1 because of the higher energy consumption in material production and manufacturing due to the replacements (2 replacements). A similar trend can be seen in S2 except for the Ni-Cd and VRF ESSs. The Ni-Cd performs better than the VRF; it is the reverse in S1. In S2, the Ni-Cd requires only 1 replacement versus 2 replacements in S1 due to the higher number of cycles in S1. In S3, although the Li-ion needs 2 replacements (1 more than the Na-S), the Li-ion has a higher NER. This is mainly because the energy required for material production is much higher in the Na-S due to energy-intensive β -alumina production and Na-S's lower round-

trip efficiency meaning it needs more electricity for charging than the Li-ion. The NER of the VRLA is the lowest because, in S3, the VRLA battery needs 9 replacements because of its short cycle life. The relative rankings of ESSs in S4 are similar to those of S2. The NER of the VRF ESS is only 0.38. For the same amount of electricity delivery, the energy required for material production is very high for the VRF ESS because of its material-intensive design.

Among the life cycle stages, the operation stage has the highest share of the total life cycle energy use followed by the material production and manufacturing stages. For example, for the Na-S ESS in Scenario 1, the contribution of energy use in the operation phase (charging) is 87%, while material production and manufacturing contribute 8% and 5%, respectively, to the total energy requirement. The electricity required for charging varies among the batteries because of the difference in their efficiencies. Li-ion requires the least electricity in charging because it has the highest efficiency among the batteries considered. Although the contributions of operation, material production, and manufacturing may vary among ESSs, these are the most energy-intensive stages. The contribution of energy consumption in transportation and dismantling is insignificant.

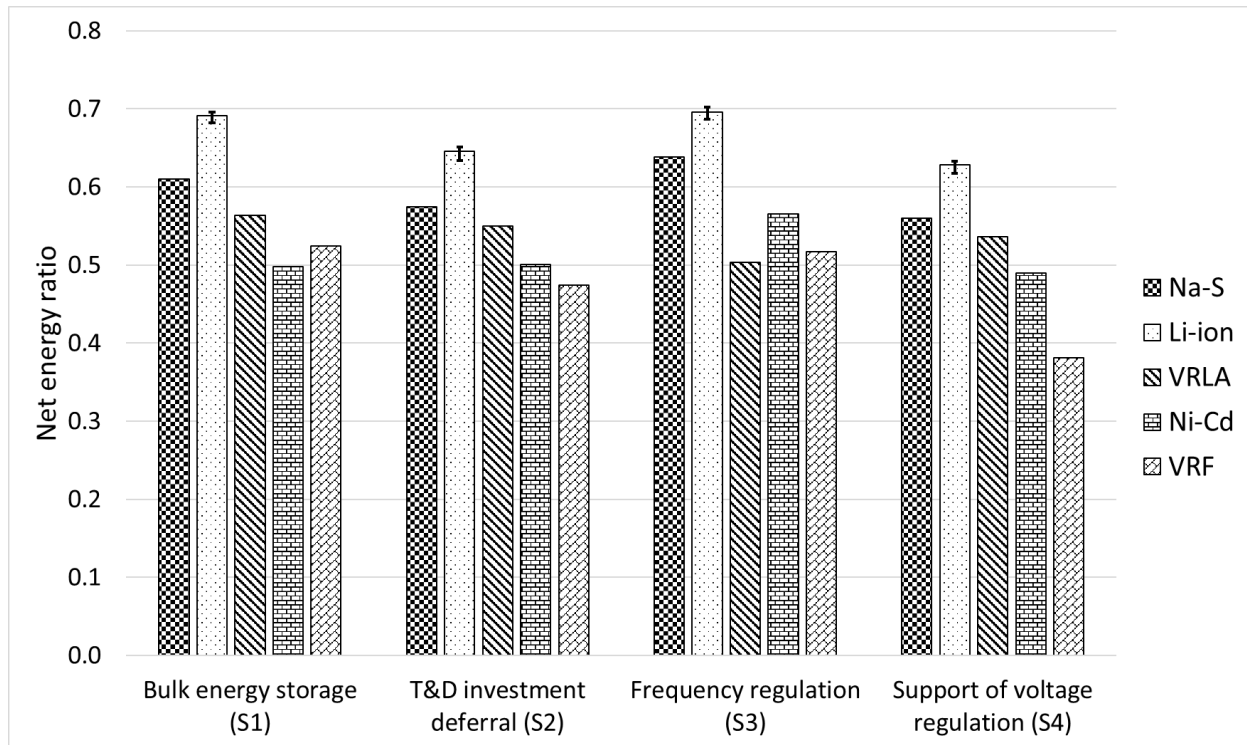


Figure 4.4: Net energy ratio (NER) for electro-chemical energy storage technologies

[Note: The negative error bars represent the NERs for lithium nickel manganese cobalt (NMC), the positive error bars represent the NERs for lithium manganese oxide (LMO), and the base case values represent the NERs for lithium iron phosphate (LFP)].

4.3.2. Life cycle GHG emissions

The results of all the life cycle phases were aggregated to calculate the total life cycle GHG emissions. The life cycle GHG emissions range from 624.96 kg-CO₂eq/MWh for the Li-ion to 800.19 kg-CO₂eq/MWh for the VRF in S1, from 646.23 kg-CO₂eq/MWh for the Li-ion to 849.42 kg-CO₂eq/MWh for the VRF in S2, from 624.43 kg-CO₂eq/MWh for the Li-ion to 802.81 kg-CO₂eq/MWh for the VRLA in S3, and from 658.77 kg-CO₂eq/MWh for the Li-ion to 963.37 kg-CO₂eq/MWh for the VRF in S4.

Figure 4.5 shows that among the life cycle stages, the total GHG emissions are highly dominated by the operation phase. The contributions of material production and manufacturing are 3-25% and 1-10%, respectively, depending on the technology and application. Transportation contributes less than 1%, and EOL (dismantling) emissions are negligible. The storage section and PCS are the components of an ESS. The GHG emissions' contribution to the life cycle GHG emissions from the material production and manufacturing of a PCS is small: 0.43, 0.63, 5.02, and 12.56 kg-CO₂eq/MWh in S1, S2, S3, and S4, respectively.

The emission factor of the electricity grid mix along with the electricity requirement for charging determines the operational GHG emissions. The operational emissions differ among battery technologies depending on the round-trip efficiency. For instance, the operational GHGs of a Ni-Cd ESS are higher than those of a Li-ion ESS because Ni-Cd has a lower efficiency (80%) than Li-ion (90%). The operational emissions vary with electricity mixes; a slight modification of EFs in the models is required if the source changes. Since the electricity EF has a significant influence on the total GHGs, the implications of different electricity mixes were explored. Figure C.4 in Appendix C shows the operational GHG emissions for different Canadian provinces. Operational GHGs differ significantly among provinces. For example, the British Columbia grid mix, a hydro-dominated mix, has 93% fewer GHGs in the operational phase than the Alberta grid mix. Because operational emissions depend on battery efficiency and the electricity EF only, GHGs per MWh do not change among application scenarios for a particular ESS. Therefore, the relative rankings of the ESSs in the scenarios are mainly dictated by the material production and manufacturing stages. In S1, the Li-ion ESS performs best, with relatively low GHG emissions. Although Figure 4.5 shows the GHG emissions for an LFP-type Li-ion battery, the environmental performances of LMO and NMC are the best and worst, respectively. The difference in total GHG emissions

between NMC and LFP is 4.69-7.82 kg-CO₂eq/MWh and between LFP and LMO is 0.56-0.93 kg-CO₂eq/MWh, depending on the application. This is mainly because there are fewer GHG emissions in cathode material production for LMO. GHG emissions in the production of cathode material for NMC are 3.8 times higher than those of LMO cathode material production. Although the Na-S battery needs less energy in manufacturing, the GHG emissions from its material production are higher than the Li-ion's because of the GHG-intensive β -alumina production. The production of β -alumina is a GHG-intensive process, and about 98% of the process energy comes from electricity. The production of β -alumina contributes to 70% of material production emissions. The VRLA ranks third in S1, and its material production emissions are higher than those of the Na-S or Li-ion because it is replaced every five years. The GHG emissions of Ni-Cd and VRF ESSs are much higher than Na-S and Li-ion ESSs. For the Ni-Cd ESS, manufacturing accounts for about 11% of the total GHG emissions, while the production of Ni alone contributes 41% of the total material production emissions. For the VRF, the energy supply comes from the electrolyte solution, which contains V₂O₅. To produce 1 kg of V₂O₅, 33.1 kg of GHGs are emitted [370]. The system requires two electrolyte tanks that contain positive and negative electrolytes. The production of V₂O₅ accounts for 94% of the material production emissions. The Na-S and Li-ion perform well in the other scenarios as well because of their high energy densities and longer cycle lives. VRLA emissions are highest in S3 as the VRLA battery requires 9 replacements because of its short lifetime. The relative rankings of the ESSs in S4 are similar to those in S2. The life cycle GHG emissions of the VRF in S4 are very high due to the large amount of energy required for material production.

For the recycling case, a mix of virgin and recycled materials was used for material requirements for each battery technology to assess the impact of recycling. Figure C.3 in Appendix C shows the

change in overall GHG emissions when recycling is included in the analysis. There was a significant reduction in GHG emissions for VRLA and VRF because of the high recovery rates of lead and vanadium electrolyte, respectively. The impact of recycling on the life cycle GHG emissions is discussed in section C.4 in Appendix C.

Some of the results of this research were compared with numbers found in the literature. A few studies assessed life cycle GHG emissions for stationary application scenarios. Most of the earlier studies conducted LCA for bulk energy applications. The GHGs calculated in this study were compared to the results reported by Hiremath et al. [258] and Oliveira et al. [52] as they are most relevant for comparison, even though they make different assumptions for the electricity mix. Excluding the operation phase, the GHGs in the other stages were compared. Hiremath et al. [258] reported 13-43, 34-76, and 13-23 kg-CO₂eq/MWh for the Li-ion, Na-S, and VRF, respectively. The VRLA and Ni-Cd ESSs were not considered. There is good agreement between the results of this study and Hiremath et al.'s study except for the VRF, largely because of differences in modeling for the VRF battery. While Hiremath et al. designed the VRF ESS based on energy density, in this research the power and energy components were designed through a bottom-up method. Oliveira et al. reported 63 and 23 kg-CO₂eq/MWh for the Li-ion and the Na-S, respectively [52]. Although the results for the Li-ion obtained from this study and Oliveira et al.'s work are in good agreement, there is a difference of 45 kg-CO₂eq/MWh for the Na-S. This is due to differences in assumptions for the cycle life, storage lifetime, and round-trip efficiency. No detailed information about the emission factors of materials was found; the EFs might have an impact on the results. A VRLA is a maintenance-free lead-acid battery with an energy density similar to a Pb-A [345]. Hiremath et al. reported 87-139 kg-CO₂eq/MWh for a Pb-A, whereas Oliveira et al. reported 102 kg-CO₂eq/MWh for a VRLA battery excluding the operation stage.

The corresponding value in this study is 111.85 kg-CO₂eq/MWh, which is in good agreement with the values reported by Hiremath et al. [258] and Oliveira et al. [52].

In addition to the NER and GHG emissions, an economic indicator is necessary to evaluate the comparative performance of electro-chemical ESSs. The levelized cost of storage is the cost at which the electricity should be sold to overcome all the expenses related to an ESS during its lifetime. Rahman et al. [338] evaluated the techno-economic performance of similar electro-chemical ESSs for stationary applications. The levelized cost of storage ranges from \$199–\$941 for the Na-S, from \$180–\$1032 for the Li-ion, from \$410–\$1184 for the VRLA, from \$802–\$1991 for the Ni-Cd, and from \$267–\$3794 for the VRF per MWh, depending on the application scenario [338]. Schmidt et al. [213] found Li-ion batteries show greater cost competitiveness compared to Pb-A and VRF batteries. The Li-ion and Na-S have the lowest GHG footprints as well as the lowest levelized cost of storage for both short-term and long-term applications. The advantages of these batteries are a longer lifetime, high energy density, and lower capital cost. The environmental and economic footprints of a VRF are high because of its component-intensive design. Although the capital cost of a VRLA is low, its cycle life is not impressive. A Ni-Cd, on the other hand, is an expensive option with a high capital cost.

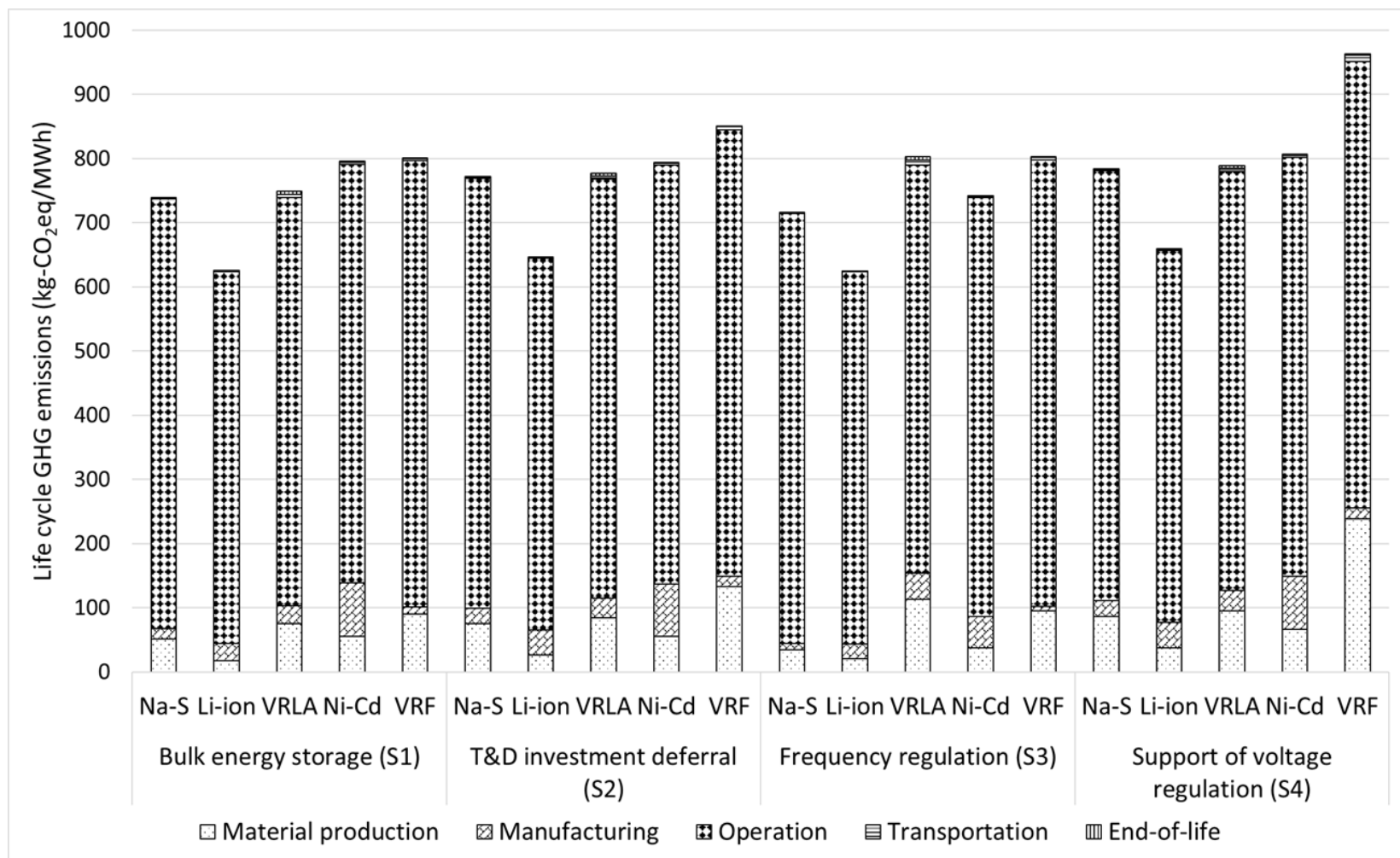


Figure 4.5: Comparative life cycle GHG emissions of five electro-chemical ESSs

[Note: Na-S: sodium-sulfur, Li-ion: lithium-ion, VRLA: valve-regulated lead-acid, Ni-Cd: nickel-cadmium, and VRF: vanadium redox flow].

4.3.3. Sensitivity and uncertainty analyses

The Morris method was used for sensitivity analysis to understand the interactions of inputs and their effects on net energy ratio and life cycle GHG emissions. An example of sensitivity analysis for the life cycle GHG emissions of the Li-ion for bulk energy storage (S1) is presented in Figure 4.6. The high Morris mean and standard deviation values of an input parameter indicate that the input has a large influence on the results. As shown in Figure 4.6, because of the high mean and standard deviation values, the PCS efficiency, electricity emission factor, and battery round-trip efficiency have the most influence on the GHG emissions. The moderate influential parameters are discharge duration, the number of cycles, battery manufacturing energy, energy density, and depth of discharge. These parameters also have an influence on the life cycle GHG emissions of Na-S, VRLA, and Ni-Cd ESSs in all the application scenarios. For the VRF ESS, however, given its design, the parameters with the most influence on the GHG emissions are cell voltage, battery and PCS efficiencies, electricity emission factor, discharge duration, and the number of cycles. Figure C.5 in Appendix C shows the sensitivity analysis for the GHG emissions of the VRF ESS for bulk energy storage. The same trend was observed in the other scenarios as well. The parameters with the lowest Morris mean and standard deviation values, such as transportation distances and the fuel mix for manufacturing the PCS, have the least impact on the results and can therefore be excluded in the uncertainty analysis.

An uncertainty analysis using a Monte Carlo simulation was conducted to provide a range of NER and life cycle GHG emission results. The simulations were based on minimum, most likely, and maximum values of input parameters found in the literature. The most likely values are the default values used in the models. The uncertainty analysis NER results are presented in Figure 4.7, and the uncertainty analysis life cycle GHG emissions results are presented in Figure 4.8. There are

overlaps among the ESS technologies due to differences in input data. Na-S and Li-ion ESSs have higher NERs than Ni-Cd and VRF ESSs because they consume comparatively less energy in the material production phase due to higher energy densities. There are some overlaps between the Ni-Cd and the VRF in S1, S2, and S3, and between the Li-ion and the VRLA in S2 and S4. The results of uncertainty analysis show that the batteries with high efficiency and energy density as well as long cycle life have high NERs.

As with the NERs, there are overlaps in life cycle GHG emissions. The contribution of operational GHGs is more than 80% to the life cycle GHG emissions for all the ESSs. Therefore, the wide range of the life cycle GHG emissions in Figure 4.8 is mainly due to the operational GHGs. The maximum and minimum Alberta electricity emission factors considered are 559 kg-CO₂eq/MWh (2021 value) and 252 kg-CO₂eq/MWh (projected value for 2041), respectively, considering the 20-year change in the Alberta electricity grid mix [367]. Because of this wide range of emission factors, the life cycle GHGs of Li-ion ranges from 374 kg-CO₂eq/MWh to 737 kg-CO₂eq/MWh in S1, for example. If the mean values (the yellow dots in Figure 4.8) based on the most likely input data are considered for comparison purposes, the life cycle GHG emissions' footprints of the Li-ion ESS are the lowest in all the scenarios.

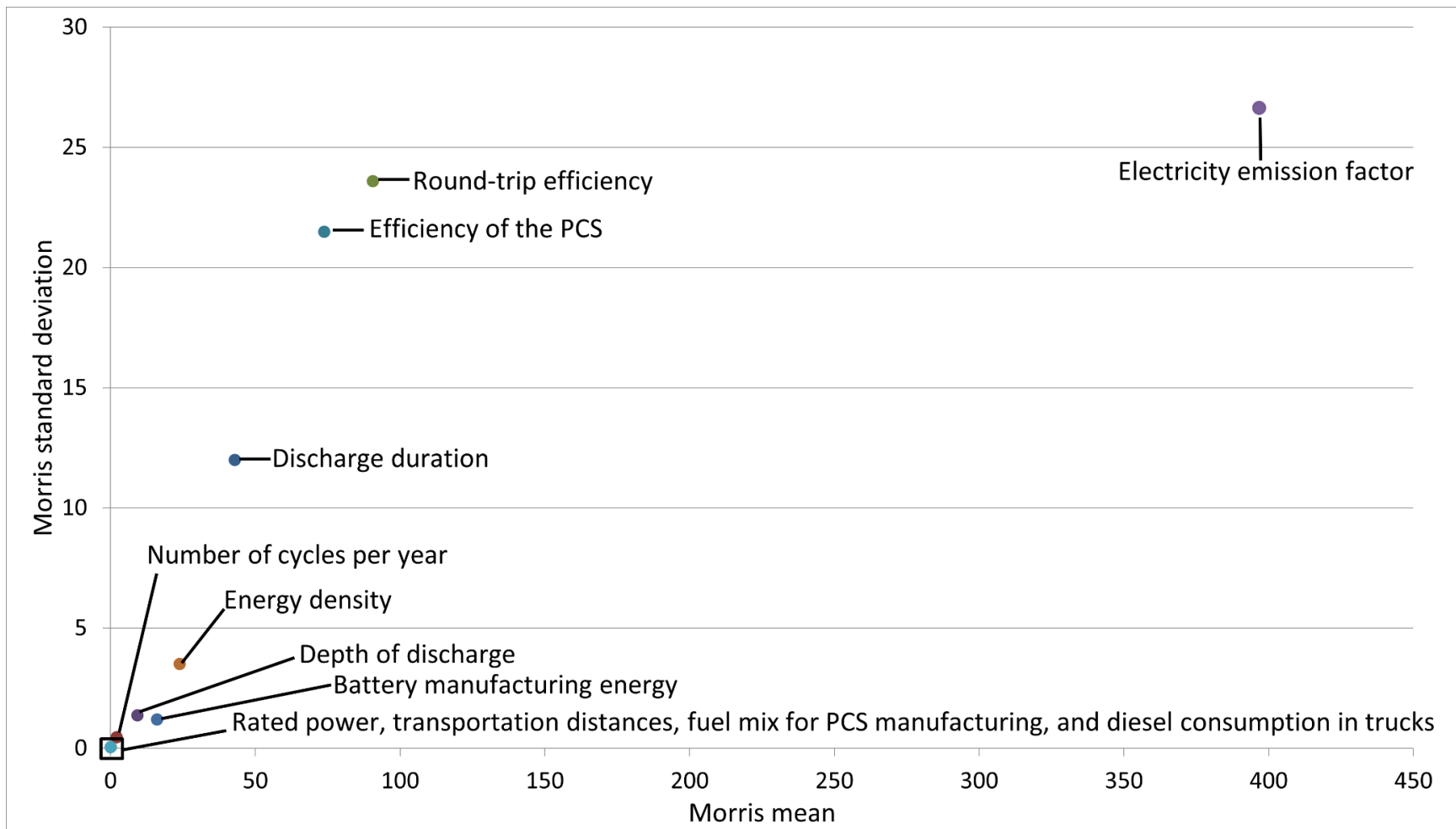


Figure 4.6: Sensitivity analysis for the GHG emissions of the Li-ion ESS for bulk energy storage (S1)

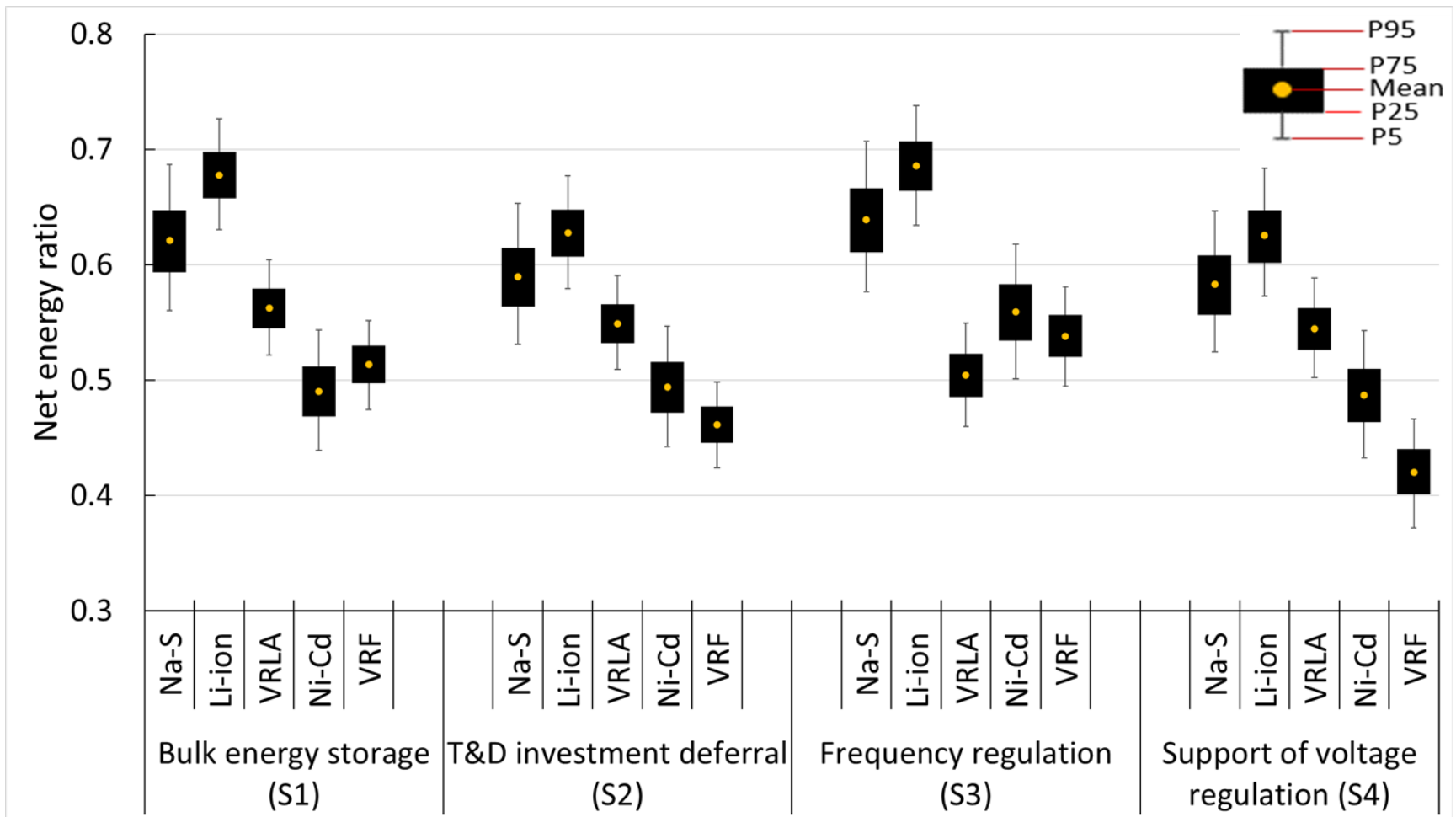


Figure 4.7: Uncertainty analysis for the net energy ratio

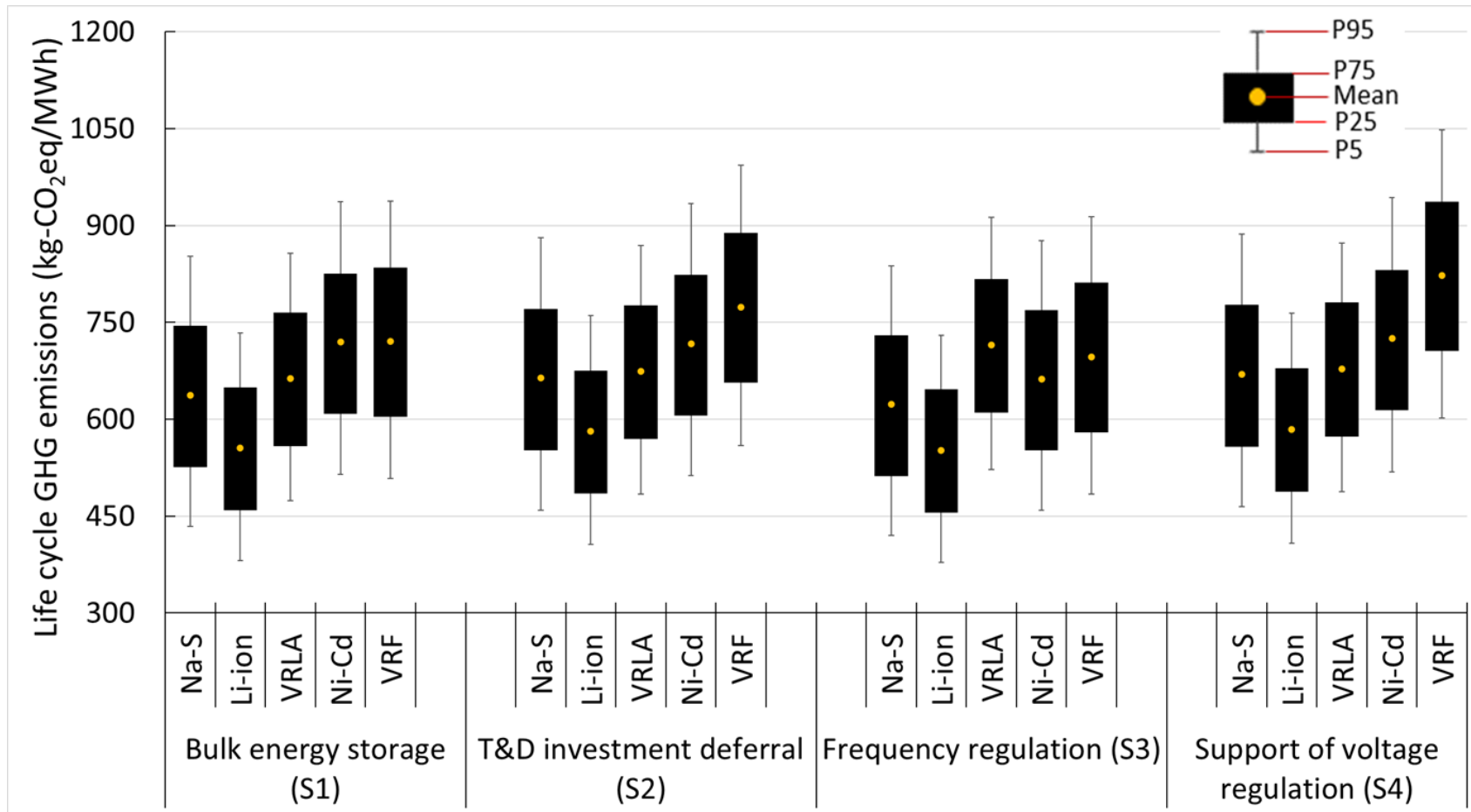


Figure 4.8: Uncertainty analysis for the life cycle GHG emissions

4.4. Conclusion

The main objective of this research was to evaluate the environmental performance of Na-S, Li-ion, VRLA, Ni-Cd, and VRF energy storage systems by developing data-intensive, process-based LCA models. The NER and life cycle GHG emissions were used to compare these electrochemical ESSs for four different stationary application scenarios: bulk energy storage, T&D investment deferral, frequency regulation, and support of voltage regulation. In the life cycle stages considered, the emissions are dominated by the operation phase, while material production and manufacturing phases have moderate contributions. Transportation and dismantling have negligible contributions. The environmental performance of the ESSs varies among bulk energy storage, T&D investment deferral, frequency regulation, and support of voltage regulation because of the number of cycles and discharge duration. The GHG emissions are mostly influenced by the electricity emission factor, the efficiency of the PCS, and battery round-trip efficiency. Due to the variability in inputs, uncertainty analysis results overlap. However, when the mean values were used for comparison purposes, it was found that the Li-ion appears to offer better environmental performance in all application scenarios. The VRF in bulk energy storage (S1), T&D investment deferral (S2) and support of voltage regulation (S4), and the VRLA in frequency regulation (S3) show the highest GHG emissions mean values. The ESSs with high efficiency, long cycle life, and high energy density are preferable, as they need less electricity for charging and less energy in material production. Thus, the Li-ion and Na-S ESSs outperform other technologies based on NER and life cycle GHG emissions.

Chapter 5: The development of a techno-economic model for the assessment of the cost of flywheel energy storage systems for utility-scale stationary applications⁸

5.1. Introduction

The global energy transition from fossil fuels to renewables along with energy efficiency improvement could significantly mitigate the impacts of anthropogenic greenhouse gas (GHG) emissions [72, 371]. It has been predicted that about 67% of the total global energy demand will be fulfilled by renewables by 2050 [372]. The use of energy storage systems (ESSs) is necessary because of the challenges in increasing the share of renewables (i.e., solar and wind) in electricity grids given the intermittency of renewables [213, 373]. ESSs can be used for short- or long-duration applications in the transmission and distribution (T&D) grid to improve reliability [105, 374]. Pumped hydro storage (PHS), compressed air energy storage (CAES), thermal energy storage, and different electro-chemical batteries have already been proven to be feasible for long-duration applications including energy arbitrage and T&D investment deferral [11]. Short-duration applications, such as frequency regulation and voltage leveling, are crucial for the safety and reliability of electricity networks [198, 199]. Electro-chemical ESSs can be used in short-duration services [84, 375], but they suffer from a short lifetime and the need to dispose of toxic materials [11, 258]. Flywheel energy storage systems (FESSs) are a promising alternative to electro-chemical batteries for short-duration support to the grid [11]. Frequency regulation is the most

⁸ A version of this chapter has been published as Rahman MM, Gemechu E, Oni AO, Kumar A. The development of a techno-economic model for the assessment of the cost of flywheel energy storage systems for utility-scale stationary applications. *Sustainable Energy Technologies and Assessments*. 2021;47:101382.

common service a FESS can provide in the electricity network [119, 376]. FESSs can play a vital role in the grid to maintain its frequency by matching electricity demand and supply for a short-duration [105]. A FESS is a mechanical storage system that converts electricity into kinetic energy, which is converted to electricity when needed [377, 378]. FESSs have a long lifetime, typically 15-20 years, and high efficiency and power density [106, 115]. A FESS mainly consists of a rotor, a motor-generator set, an enclosure, a set of mechanical or magnetic bearings, a vacuum pump, and a power conversion system (PCS). A bi-directional converter is used as a PCS to convert alternating current to direct current or vice versa. A flywheel rotor is usually made of steel or composite materials. Typically, composite rotors have a high rotational speed of up to 100,000 RPM [379], and steel rotors can rotate up to 6000 RPM [380].

With the current cumulative global capacity of 931 MW [11], it is projected that the FESS market will increase by about 77% from 2019 to 2027 [20, 21]. Given their rapid market growth, FESSs are receiving increased attention in industry and academia, which has led to research related to rotor design and optimization. There are several studies on FESSs with different focuses: the optimization of flywheel rotors made of different materials [198, 381], and the design of bearings [382, 383] and motor-generators [384, 385]. These studies provide useful insight into technical parameters and their effects on flywheels' performances. However, a techno-economic assessment is needed to make investment decisions regarding the deployment of FESSs. A techno-economic assessment is a decision-making tool used to assess the economic feasibility of a system [386, 387].

Large-scale flywheels could be an attractive option for short-duration utility applications given their fast response time, longer cycle life, and large power discharge [168, 388]. Before a FESS can be integrated into the grid, a techno-economic evaluation is required to answer three key

research questions: How do the composite and steel rotor flywheels perform in stationary applications in terms of cost? How much does each component contribute to the total investment cost? How do the systems perform at different capacities? Efforts have been made to understand the techno-economic implications of FESSs. Most studies performed comparative assessments, for example, flywheel with PHS, CAES, and several electro-chemical batteries [22, 23] or with supercapacitor and superconducting magnetic energy storage [24]. Nikolaidis and Poullikkas [22] found that based on the power capital cost, a FESS performs better than PHS and CAES, and, according to Mostafa et al. [24], a FESS has a higher levelized cost of electricity (LCOE) than supercapacitor energy storage and superconducting magnetic energy storage systems. Schmidt et al. [23] projected the LCOE to 2050 and found that FESSs are more competitive when the discharge duration is less than 30 minutes and the number of cycles is more than 5000 per year. Zakeri and Syri [28] and Li et al. [29] also found that a FESS is economically more attractive than lithium-ion and lead-acid for frequency regulation and uninterruptible power supply, respectively. Although these studies provide useful information on the economic performance of various energy storage technologies in stationary applications, there are limitations. The studies used aggregated capital cost data without considering equipment design and sizing. They did not specify the rotor type used. The rotor material could significantly influence the investment cost since the composite material costs more than steel (\$20/kg for composite and \$1/kg for steel, for example) [389]. Rupp et al., on the other hand, designed a FESS system and estimated its cost for non-stationary use [204]. Although they evaluated equipment design and cost, their model cannot be applied to a stationary utility application because of differences in system characteristics and requirements. There are also some techno-economic studies specific to steel [205, 390] and composite rotors [189, 391]. These studies provided high-level cost estimates but did not evaluate the cost of

electricity delivery for utility-scale stationary applications. Some studies provided total capital cost ranges without conducting a detailed assessment of economic performance [91, 116, 170].

Another important aspect that has not been well addressed in the literature is how economies of scale change the techno-economic performance of a FESS or how to find the optimal point at which the cost per unit output is lowest. A few studies developed scale factors for large-scale PHS, CAES, and electro-chemical storage systems and showed there is a cost advantage for large-capacity plants due to economies of scale. For example, Kapila et al. [31] found scale factors of 0.53, 0.87, and 0.88, respectively, for PHS, conventional CAES, and adiabatic CAES. Rahman et al. [338] also developed scale factors for 5 electro-chemical ESSs, from 0.46 for vanadium redox ESS to 0.91 for nickel-cadmium ESS. The scale factors help to understand the impacts of the increase in capacity on the overall cost of the system. However, to the best of the author's knowledge, in the existing literature no scale factors have been developed for FESSs.

A wide range of capital costs is reported in the literature; for example, according to Akinyele and Rayudu [42], the capital cost of a FESS can be from \$1000-\$5000/kW and \$250-\$350/kWh. There are uncertainties not only in cost inputs but also in technical parameters and assumptions. For instance, flywheel efficiency reported in two studies is 85% [392] and 95% [43]. Another source of uncertainty is the standby power loss, 0.5-2% for composite rotor FESSs with magnetic bearings [393, 394] versus 1-5% for steel rotor FESSs with mechanical bearings [205, 395]. Despite the range in input technical and cost parameters, most studies provide point estimates. Studies that attempt to understand the techno-economic performance of storage systems should be supported with detailed sensitivity and uncertainty analyses. This allows us to make a reasonable comparison among the storage alternatives. This is another key gap in the literature.

While existing studies help us understand some economic parameters of FESSs, their use of aggregated cost data makes it difficult to predict and compare the economic performances of different projects. The results from such high-level analysis are limited in application. Also, there are no cost functions or scale factors, which are needed to evaluate the system performance at different capacities. To the best of the author's knowledge, there is no comparative assessment of steel rotor and composite rotor FESSs that uses the same system boundary. To fill the abovementioned knowledge and literature gaps, a comprehensive techno-economic assessment of utility-scale flywheel storage systems for short-duration applications was conducted by developing a bottom-up model that considers the interactions among the technical and cost parameters. Two configurations – composite rotor and steel rotor FESSs – were analyzed. The novel contributions of this research are to:

- Apply engineering principles to design various components of flywheel energy storage systems;
- Develop cost functions for the components of flywheel energy storage systems;
- Develop a scale factor for flywheel energy storage systems;
- Evaluate the total investment cost, annual life cycle cost, and levelized cost of storage;
- Compare the economic feasibility of composite rotor and steel rotor flywheel storage systems for frequency regulation; and
- Conduct comprehensive sensitivity and uncertainty analyses to assess the impact of various parameters on the cost.

Insights from the study will help the flywheel industry and electric utilities understand the economic performance of the flywheel storage systems and ultimately help make informed decisions on policies and investments.

5.2. Modeling method

Figure 5.1 shows an overview of the modeling framework developed to assess the feasibility of utility-scale flywheel storage systems for frequency regulation. Data for application parameters as well as technical and cost parameters were gathered from published sources and used in various stages of model development. In the system design, the storage plant capacity was determined, and flywheel components were sized. The number of flywheels required was calculated from the plant capacity and the capacity of each flywheel. After determining the size and capacities of different components, we developed the cost functions for individual pieces of equipment to determine techno-economic performance using various cost indicators (total investment cost, annual life cycle cost, and levelized cost of storage). Finally, sensitivity and uncertainty analyses were performed to identify the most sensitive parameters and provide a probable range of total investment cost and levelized cost of storage. Each stage of model development is described in detail in the following sections.

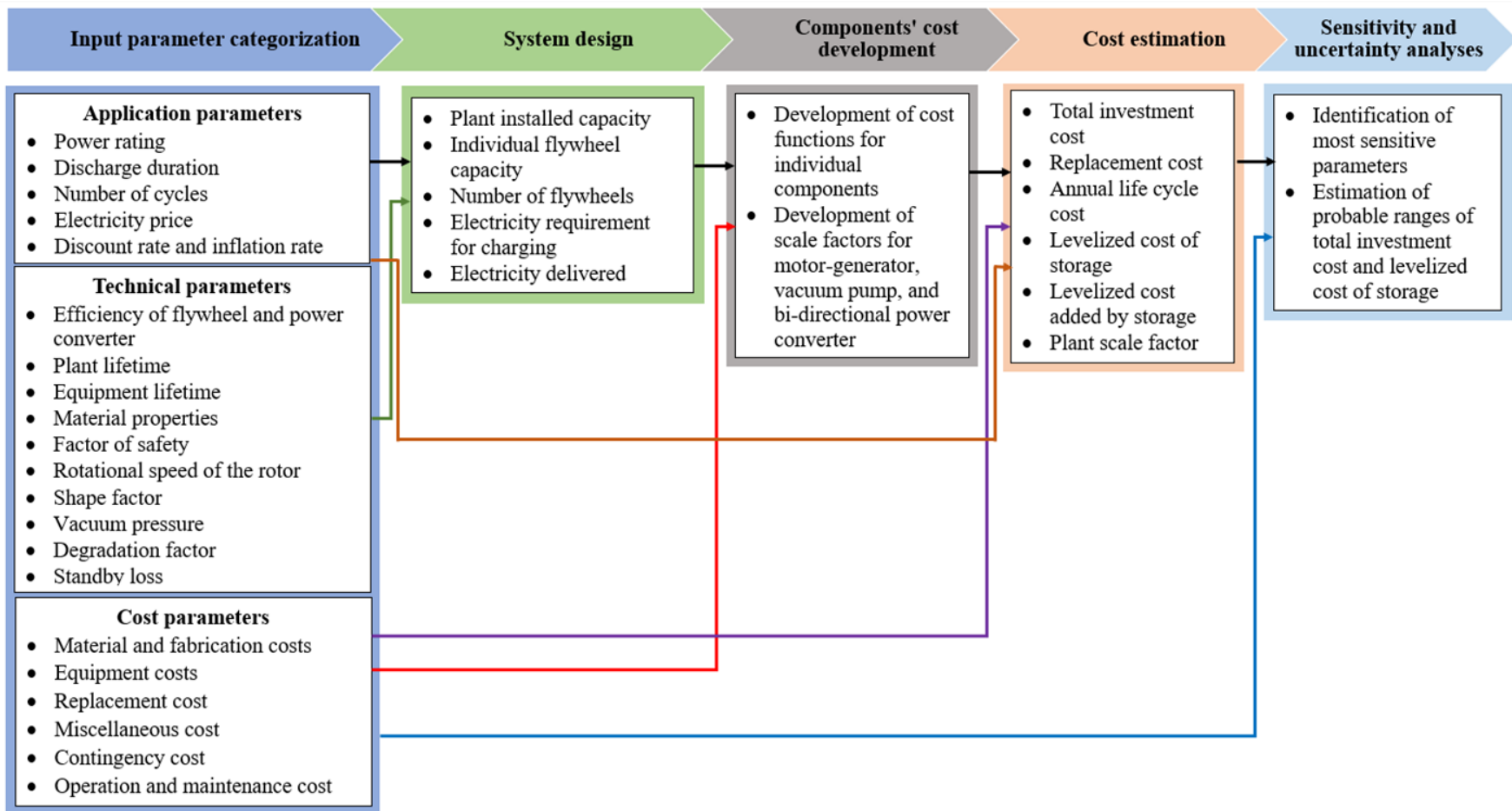


Figure 5.1: Overview of the modeling framework

5.2.1. Input parameter categorization

The first step in techno-economic modeling is data gathering and categorization. A detailed literature search was conducted to collect the data relevant to the storage application as well as technical and cost aspects. A particular stationary application is characterized by the rated power, duration of discharge, and the number of cycles. Other application-specific inputs are the discount rate, inflation rate, and electricity price for charging. These parameters could vary considerably depending on the project and its location. The default inputs for the nominal discount rate and inflation rate were taken as 10% [31, 131] and 2% [131, 396], which are standard values for Canada; these values can be adjusted in the model.

A flywheel consists of several components including the rotor, shaft, motor-generator, and bearings. Technical inputs were used to design and size these components. For example, rotor material tensile strength, shape factor, angular speed, etc., were used as technical inputs to calculate the kinetic energy delivered from a flywheel. Other technical parameters are the degradation factor, standby loss, etc.

The cost parameters include the material and manufacturing costs of various components, such as the rotor, shaft, and enclosure. For the motor-generator, vacuum pump, and bi-directional power converter, cost functions were developed using their capacities and individual component costs. Operation and maintenance (O&M) costs, along with miscellaneous and contingency costs, were also considered as cost parameters.

5.2.2. System design and sizing

Utility-scale energy storage systems for stationary applications typically have power ratings of 1 MW or more [397]. The largest flywheel energy storage is in New York, USA by Beacon Power

with a power rating of 20 MW and 15 minutes discharge duration [398]. Utility-scale flywheel storage is typically used for frequency regulation to maintain grid frequency by matching electricity supply and demand for a short period, usually 15 minutes [105, 293]. In this study for the base case scenario, both the composite rotor and steel rotor flywheels were modeled for a 20 MW nameplate capacity with 15 minutes discharge duration and 4000 cycles per year. However, a range in rated power of 1-40 MW was considered to develop the scale factor. The number of cycles differs depending on the requirement of electric utilities, hence a range of 3000-5000 per year was considered to determine the effect on the economic performance of the systems [119, 399].

Flywheel rotors can be made of steel or composites. Usually, a steel rotor can rotate up to 6000 RPM [28] and the rotational speed of a composite rotor is up to 100,000 RPM [379]. It was assumed that magnetic and mechanical bearings will be used for the composite rotor and steel rotor flywheels, respectively, because to support the high-speed composite rotor, contactless magnetic bearings are needed [400], while simple mechanical bearings can be used for a low-speed steel rotor [203]. In this study, hollow and solid cylindrical shapes were considered for composite and steel rotors, respectively, because of their typical use in rotor design [379, 401]. To satisfy the rated capacity (20 MW/5 MWh) of the composite rotor and steel rotor FESSs, the number of flywheels required was calculated from the capacity of each flywheel. The kinetic energy stored in a flywheel can be calculated from the height and shape factor of the rotor, density of rotor material, minimum and maximum angular velocities, and radius of the rotor. Equation 5.1, adapted from Amiryar and Pullen [203], was used to calculate the useful energy stored in the flywheel:

$$E = \frac{1}{2} k \pi \rho h (\omega_{max}^2 - \omega_{min}^2) (r_o^4 - r_i^4) \quad (5.1)$$

where E is the kinetic energy (J), k is the shape factor, ρ is the rotor material density (kg/m^3), h is the height of the rotor (m), ω is the angular speed (rad/s), and r_i and r_o are the inner and outer radii (m), respectively.

The outer radius of a rotor depends on the flywheel speed and strength of the rotor material. Equations D.1 and D.2 (in Appendix D) were used to calculate the outer radii of the cylindrical hollow composite rotor and solid steel rotor, respectively. The composite rotor's inner radius was calculated from its outer radius and the inner-to-outer diameter ratio of 0.60. An inner-to-outer diameter ratio of 0.50-0.75 is typically used by flywheel manufacturers [201]. The rotor height was calculated from the rotor's outer diameter and a length-to-rotor outer diameter ratio of 0.95 to avoid bending [391, 402]. Table 5.1 shows the design parameters used to calculate the capacity of the flywheels.

Table 5.1: Design parameters used in the techno-economic model

Parameter	Composite rotor flywheel	Steel rotor flywheel	Source/comment
Flywheel efficiency (%)	90	90	[6]
Rotor material tensile strength (GPa)	4	1.24	[389, 403]
Rotor material density (kg/m^3)	1700	7780	[201, 389]
Shape factor	0.5	0.5	[404, 405]
Factor of safety	4	4	[406]
Poisson's ratio of steel	-	0.3	[401]
Maximum rotational speed (RPM)	16,000	6000	[198, 407]

Parameter	Composite rotor flywheel	Steel rotor flywheel	Source/comment
Minimum rotational speed (RPM)	8000	3000	The minimum speed is 40% to 60% of the maximum speed [404]; 50% was considered in this analysis.
Shaft diameter-to-rotor outer diameter ratio	0.15	0.15	[408]
Inner-to-outer diameter ratio	0.6	-	0.50 to 0.75 is a good design typically used in the flywheel industry [201].
Rotor length-to-outer diameter ratio	0.95	0.95	A value less than 1 is considered to avoid mechanical issues, such as bending and vibration [391, 402]; 0.95 was assumed in this study.
Thickness of the housing (m)	0.05	0.05	[409]
Bi-directional power converter efficiency (%)	95	95	[169]
Standby loss (%)	1	2.5	Standby losses range from 0.5-2% for a composite rotor flywheel with magnetic bearings [393, 394] and 1-5% for a steel rotor flywheel with mechanical bearings [205, 395]. The upper and lower bounds were considered in the uncertainty analysis.
Yearly degradation rate (%)	0.14	0.14	[189]

Parameter	Composite rotor flywheel	Steel rotor flywheel	Source/comment
Vacuum pump capacity (kW)	0.55	0.55	Assumed based on the studies by Amber Kinetics [389] and Caprio et al. [410].
Outer diameter of the rotor (m)	0.46	0.49	Calculated.
Mass of each rotor (kg)	623	5627	Calculated.
Density of shaft and enclosure material (kg/m ³)	7700	7700	Assumed to be made of steel [391].
Mass of shaft (kg)	198	251	Calculated.
Mass of enclosure (kg)	2951	3416	Calculated.
Kinetic energy stored in each flywheel (kWh)	26	28	Calculated using Equation 5.1.
Electrical energy delivered from each flywheel (kWh)	25	27	Calculated from the kinetic energy stored in the flywheel assuming a 95% generator efficiency [411].
Rated power of each flywheel (kW)	100	108	Calculated from the kinetic energy stored in the flywheel and the discharge duration.
Number of flywheels required	200	186	Calculated from the capacity of each flywheel and the rated capacity of the plant, 20 MW/5MWh.

5.2.3. Components' cost development

The total cost of the rotors, shafts, and enclosures is made up of the material and manufacturing costs. Material costs for the steel rotor and shaft are \$1.2/kg [201] and \$1.4/kg [405], respectively. For the composite, \$49.6/kg was considered, an average of the range reported by Wang et al. [412]. Manufacturing costs are \$2.3/kg for the steel rotor [201], \$4.1/kg for the shaft [391], and \$9.5/kg for the composite rotor [391]. For the enclosure, the material cost is \$1.2/kg [201] and the manufacturing cost is \$0.6/kg [391]. The capital costs for the permanent magnet motor-generator, vacuum pump, and bi-directional power converter were plotted against various capacities of these components to obtain their cost functions (see Figures 5.2-5.4). The equations in Figures 5.2-5.4 show the cost functions developed for the motor-generator, vacuum pump, and power converter, respectively. x refers to the capacity in kW and y represents the capital cost of each piece of equipment, i.e., the motor-generator, vacuum pump, and power converter. A permanent magnet motor-generator set is typically used for energy conversion [413], and a cost equation was developed for a wide range of capacities (30-315 kW) using cost estimates for brushless permanent magnet motors [414]. A scale factor of 0.66 was found; this shows the cost advantage at large capacities due to economies of scale. For the vacuum pump, the cost function was developed using the market price from Atlas Corpo [415], and it shows a scale factor of 0.74 for a capacity range of 0.55-2.98 kW. Data from various studies were compiled to develop the cost function for the bi-directional power converter [416-420]. The cost per kW decreases with an increase in capacity due to economies of scale. Mechanical bearings are used for the steel rotor flywheel for \$80.8/kWh, as estimated from the study by Brown and Chvala [205]. There is limited information on the cost of magnetic bearings for a composite rotor flywheel. The cost of magnetic bearings is usually 30-

70% of the composite rotor material cost [204]; 60% was assumed in this study as the default. The range (30-70%) was used in the uncertainty analysis to see its impact on the results.

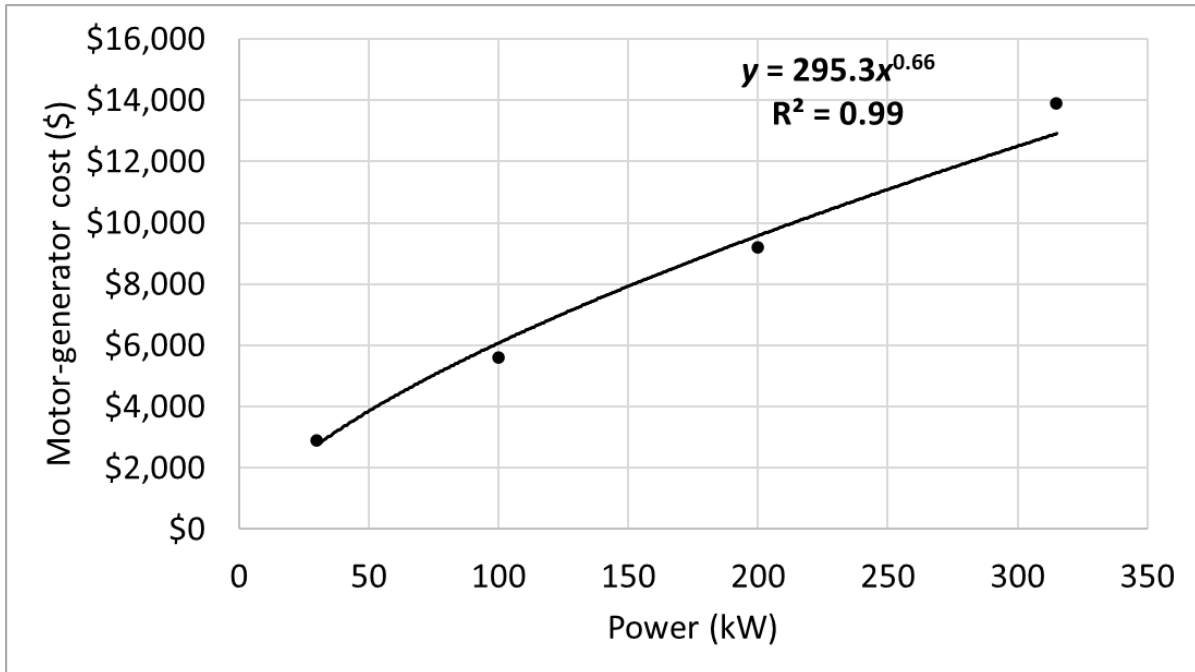


Figure 5.2: Capital cost curve for a motor-generator

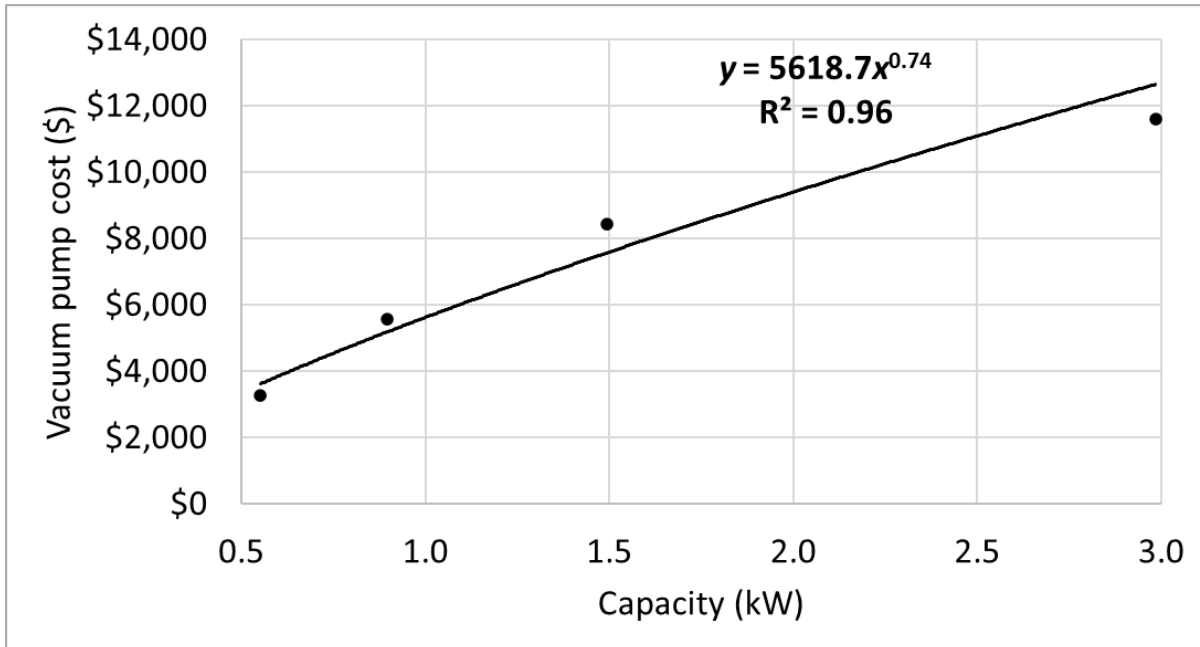


Figure 5.3: Capital cost curve for a vacuum pump

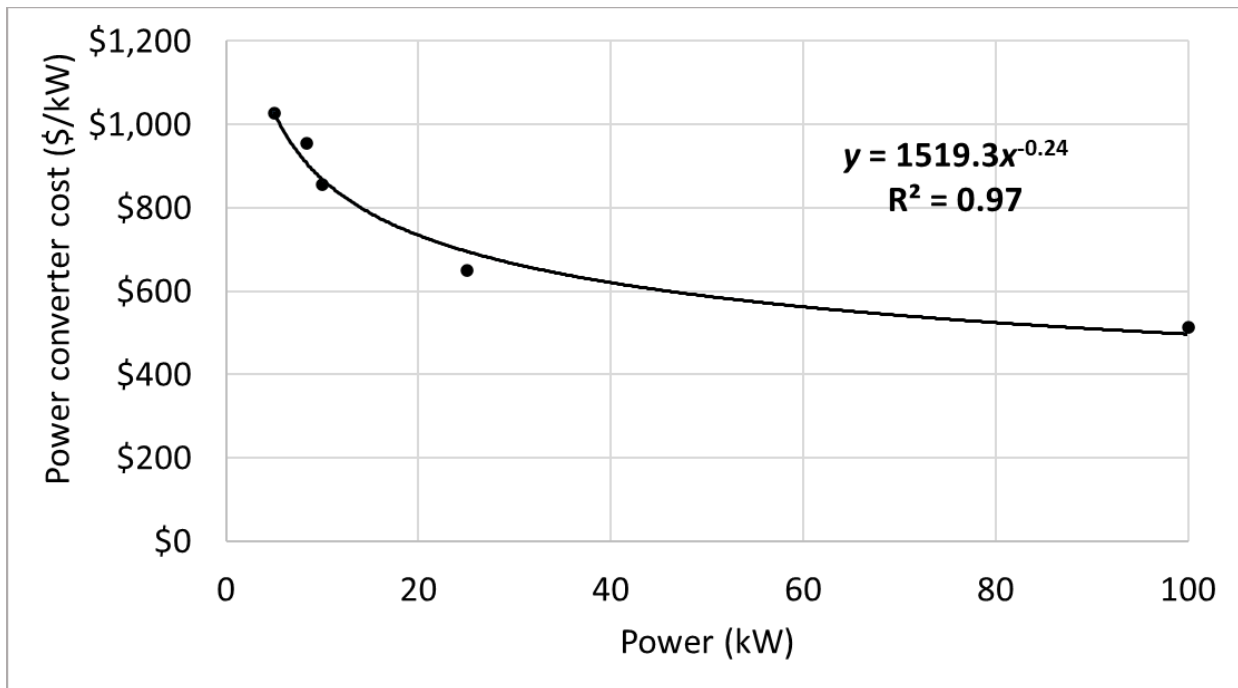


Figure 5.4: Capital cost curve for a power converter

5.2.4. Cost estimation

The first cost component is the total investment cost (TIC), which is the sum of the total direct cost (TDC) and the contingency cost (CoC). The TDC is the function of the total equipment cost (TEC), miscellaneous items cost (MIC), and construction and commissioning cost (CC). The total equipment cost (TEC) is the combined cost of the individual components listed in section 5.2.3. The cost of any unaccounted item (miscellaneous cost) is assumed to be 10% of the TEC. The construction and commissioning cost includes the costs related to procurement, transportation, installation, etc., and was considered to be 20% in the base case (usually it is from 5-25%) [189]. To handle any uncertainties in TIC estimates, 10% of the TDC was assumed to be the contingency cost (CoC).

Although a FESS can operate for more than 20 years, some components, such as the vacuum pump and mechanical bearings, need to be replaced (see Table 5.2 for the lifetimes). Because the future costs of these components are unknown, the replacement cost (RC) of a component was assumed to be equal to its equipment cost. Once the TIC and RC were calculated, a discounted cash flow (DCF) analysis was performed. The cost parameters used in the DCF analysis are the TIC, total RC, total operation and maintenance (O&M) cost, and charging cost. The total O&M cost includes the fixed O&M cost and the cost of standby energy consumption. The TIC and the RC were amortized over the lifetime of the system, 20 years [201, 392]. The amortized values of the TIC, total RC, charging cost, and O&M cost were summed to calculate the annual life cycle cost (ALCC), expressed in \$/kW-year.

Along with the ALCC, the amount of yearly electricity delivery was used to calculate the levelized cost of storage (LCOS). The LCOS is the minimum selling price of electricity to cover all the costs over the life of an ESS and can be calculated using Equation 5.2, adapted from Rahman et al. [338]. In this study, the average pool price of electricity in Alberta, Canada was used for the charging cost. However, a small adjustment to the charging cost can be made in the model to estimate the LCOS for other locations. The charging cost depends on electricity price, which differs by jurisdiction. Therefore, to facilitate an appropriate comparison of various ESSs, an indicator (in this case the levelized cost added by storage [LCAS]) can be used that does not include the cost of charging. Equation 5.3, from Rahman et al.'s work [338], shows that the LCAS can be calculated from the LCOS, charging cost, and overall efficiency of the FESS.

$$LCOS = \frac{TIC * \frac{i(1+i)^n}{(1+i)^n - 1} + O\&M + El_{in} * C_c * N + \left[\frac{RC}{(1+i)^n}, RC * \frac{i(1+i)^n}{(1+i)^n - 1} \right]}{El_{out} * N} \quad (5.2)$$

$$LCAS = LCOS - \frac{C_c}{\eta_{ov}} \quad (5.3)$$

In Equations 5.2 and 5.3, i is the real discount rate ($i = \left[\frac{1+d}{1+f}\right] - 1$), f is the inflation rate, d is the nominal discount rate, n is the lifetime of the project (year), C_c is the charging cost (\$/MWh), N is the number of cycles/year, RC is the replacement cost (\$), n, RC is the replacement period (year), El_{in} and El_{out} are electricity input and output in one cycle (MWh), respectively, and η_{ov} is the overall efficiency of the system (%).

Table 5.2: Economic parameters used to calculate the levelized cost of storage

Parameter	Value	Source/comment
Base year	2020	
Discount rate	10%	Based on the values reported for similar projects [31, 131].
Inflation rate	2%	[60, 131]
Project lifetime (year)	20	Based on the lifetime of a flywheel energy storage system [201, 392].
Total equipment cost (TEC)	Sum of the cost of each piece of equipment	Calculated using cost functions.
Miscellaneous items cost (MIC)	10%*TEC	[131]
Learning rate (LR)	95%	After the first flywheel, a 95% LR was assumed for repetitive manufacturing.
Construction and commissioning cost (CC)	20%*(TEC+MIC)	[189]
Total direct cost (TDC)	(TEC+MIC+CC)	
Contingency cost (CoC)	10% TDC	[119]
Total investment cost (TIC)	TDC+CoC	

Parameter	Value	Source/comment
Total replacement cost	Sum of the cost of replaced equipment	
Charging cost (\$/MWh)	27.6	Average Alberta electricity pool price from 2015-2019 [421].
Fixed O&M cost for steel rotor FESS (\$/kW-year)	6.9	Average of the range reported by Kailasan for Active Power's FESS [201].
Fixed O&M cost for composite rotor FESS (\$/kW-year)	13.3	Reported for Beacon Power's FESS by Kailasan [201].
Lifetime of a mechanical bearing (year)	5	[205]
Lifetime of a magnetic bearing (year)	20	[422]
Lifetime of a vacuum pump (year)	10	[423]
Lifetime of a bi-directional power converter (year)	20	[424]

5.2.5. Sensitivity and uncertainty analyses

To check the effects of model inputs and to provide a probable range of results, sensitivity and uncertainty analyses were conducted. To do that, the model developed in this study was integrated with the Excel-based Regression, Uncertainty, and Sensitivity Tool (RUST) developed by Di Lullo et al. [285]. The Morris method was used for the sensitivity analysis to show the impact of different interacting input parameters on the TIC and LCOS. Unlike the usual one-at-a-time approach, the Morris method accounts for interactions among the inputs. A Monte Carlo simulation was conducted for the uncertainty analysis to provide a distribution of the TIC and LCOS. The range

of values for the sensitivity and uncertainty analyses is presented in Table 5.3. The most likely values of the input parameters are the default inputs presented in Tables 5.1 and 5.2. To make sure that the sampling error is <1% of the mean, 100,000 samples were used in the Monte Carlo simulation.

Table 5.3: Input parameters for sensitivity and uncertainty analyses

Parameter	Minimum value	Maximum value
Efficiency of the flywheel	85% [392]	95% [43]
Efficiency of the bi-directional converter	90% [425]	98% [426]
Number of cycles per year	3000 [399]	5000 [119, 399]
Safety factor	3 [201]	5 [201]
Tensile strength of carbon composite (GPa)	2 [201]	6 [427]
Tensile strength of steel (GPa)	0.80 [428]	1.4 [389]
Inside-outside diameter ratio for composite rotor	0.50 [201]	0.75 [201]
Composite rotor FESS standby loss	0.50% [393]	2% [394]
Steel rotor FESS standby loss	1% [205]	5% [395]
Nominal discount rate	8% [338]	12% [338, 429]
Inflation rate	0.9% [338]	2.9% [338]
Fixed O&M cost for composite rotor FESS (\$/kW-year)	11.5 [201]	23 [201]
Fixed O&M cost for steel rotor FESS (\$/kW-year)	5.7 [201]	8.0 [201]
Composite material cost (\$/kg)	20.3 [430]	86.1 [430]
Cost of steel (\$/kg)	1.2 [390]	5.7 [390]
Cost of magnetic bearings as a percent of rotor material cost	30% [204]	70% [204]
Construction and commissioning cost	5% [189]	25% [189]
Lifetime of mechanical bearings (year)	3 [205]	10 [205]
Lifetime of a vacuum pump (year)	5 [205]	10 [205]
Charging cost (\$/MWh)	18.5 [421]	32.1 [421]
Mechanical bearing cost (\$/kWh)	40.4 [205]	121.1 [205]

5.3. Results and discussion

This section discusses the results for composite and steel rotor FESSs for frequency regulation. All the results in this study were adjusted to 2020 USD.

5.3.1. Total investment cost (TIC)

The total investment costs are \$25.88 and \$18.28 million, respectively, for composite and steel rotor FESSs. The corresponding number of flywheels required was calculated to be 200 and 186 (see Table 5.1). The TIC comprises total equipment cost, miscellaneous items cost, construction and commissioning cost, and contingency cost. The TEC, which comprises the costs of different components of the system, alone contributes about 68% to the TIC. The distribution of the individual equipment cost to the TEC is presented in Figure 5.5. The costs of the rotor, magnetic bearings, and bi-directional power converter have large contributions to the TEC for the composite rotor FESS. For the steel rotor FESS, on the other hand, the rotor and bi-directional power converter contribute significantly to the TEC. There is a significant difference in the costs of bearings in the two systems. The sophisticated magnetic bearings for the composite rotor are more expensive than the simple mechanical bearings for the steel rotor. However, mechanical bearings have a shorter lifetime than magnetic bearings. The shaft, enclosure, vacuum pump, and motor-generator set have similar contributions in both systems. The rotor cost is a key contributor to the TEC. Although the mass of a composite rotor is much lower than that of a steel rotor because of the difference in material density, the composite rotor costs more because of the higher material (\$49.6/kg) and manufacturing (\$9.5/kg) costs; the material and manufacturing costs of a composite rotor are \$36,786 and \$19,392 are for a steel rotor. Composite materials are still in the research and development stage and therefore cost more than steel. The manufacturing cost is also higher

for the composite rotor because of the complex composite fiber manufacturing process. The cost of composite rotors is expected to drop because of increased production capacity and market competition, as is the TEC. Because of its high unit capital cost (\$496.18/kW), the power converter has a significant contribution to the overall TEC. The costs of a power converter for composite and steel flywheels are \$49,618 and \$52,595, respectively. The cost difference is due to the difference in rated power, 100 kW for the composite flywheel, and 108 kW for the steel flywheel.

FESSs are used for short-duration power applications. Therefore, power capital cost (\$/kW) could be a useful parameter to compare the economic feasibility of energy storage systems for similar power applications. The power capital costs of the composite and steel rotor FESSs are \$1294 and \$914/kW, respectively. Although both FESSs have the same power capacity, the power capital cost for the composite rotor FESS is higher because of its higher total investment cost due to the use of an expensive composite rotor and magnetic bearings. The energy capital costs of the composite and steel rotor FESSs were found to be \$5176/kWh and \$3656/kWh, respectively. The energy capital cost is significantly higher than the power capital cost because of the short discharge duration in frequency regulation.

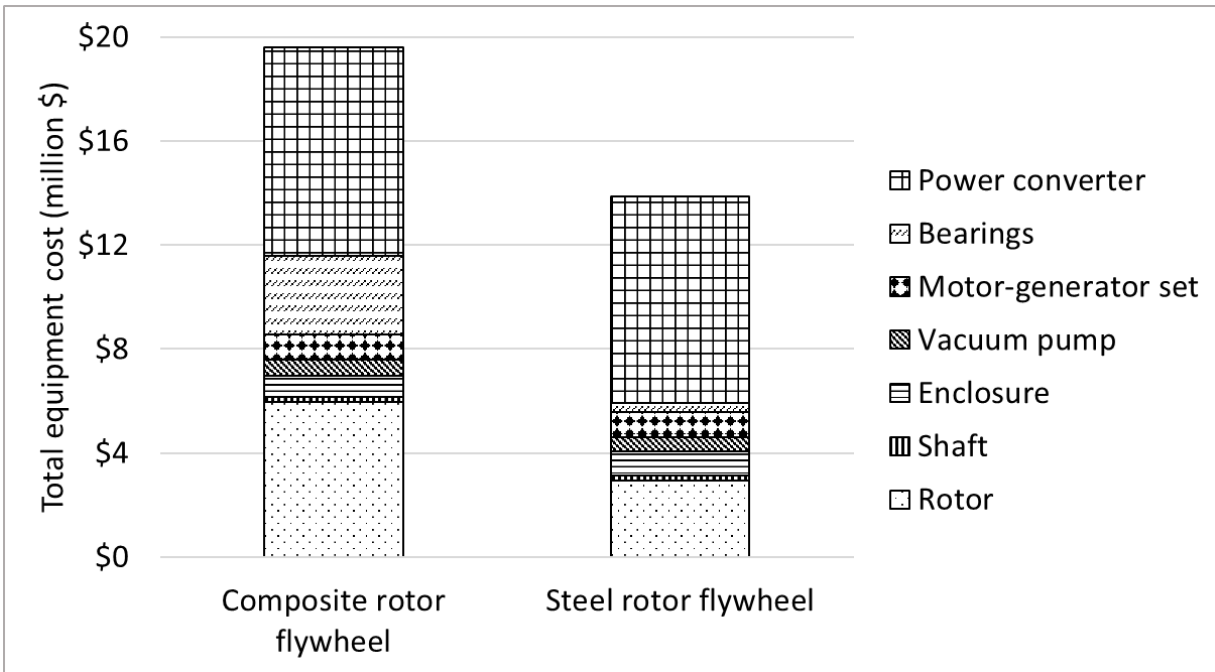


Figure 5.5: Equipment cost distribution for the flywheel energy storage systems

5.3.2. Annual life cycle cost (ALCC)

The ALCC refers to the minimum annual payment to cover upfront capital costs and any loan repayment [28]. The ALCCs are \$178.07 and \$137.36/kW-year for the composite and steel rotor FESSs, respectively. To calculate the total annual life cycle cost, we performed a discounted cash flow analysis (DCF) using the nominal discount rate and inflation rate. A DCF includes all the cost components, that is, the TIC, O&M cost, and charging and replacement costs, as shown in Figure 5.6. The amortized TIC makes the largest contribution to the ALCC, followed by the charging cost and the O&M cost. The composite rotor FESS has a higher amortized TIC (\$130.26//kW-year) than the steel rotor FESS (\$92.01/kW-year) because of the high material and manufacturing costs of the rotor as well as the magnetic bearing cost. Magnetic bearings are more expensive as they require a more sophisticated design than simple mechanical bearings. The O&M cost includes the fixed O&M cost and the cost of energy consumed to compensate for the loss of power in the systems. The total O&M cost is higher for the composite rotor FESS than the steel rotor FESS

because of the higher cost per unit power for the composite rotor. The costs of energy consumption to compensate for the power loss are \$11,018 and \$27,546/year, respectively, for the composite rotor and steel rotor FESSs. These costs were calculated from the standby losses. A higher standby loss (2.5%) for the steel rotor makes the cost higher than the composite rotor's (with only a 1% loss). This is because a mechanical bearing suffers from high frictional loss due to the close contact between the shaft and the bearing, while magnetic bearings support the shaft without physical contact. The charging cost for both systems is \$644,354/year with an electricity cost of \$27.6/MWh. The amortized replacement costs for the composite rotor and steel rotor FESSs are \$34,211/year and \$95,123/year, respectively. The DCF analysis considers the lifetime of components and the replacement costs to calculate the amortized replacement cost. The problem with a steel rotor FESS is that its bearings need to be replaced frequently (typically every 5 years). Magnetic bearings, on the other hand, provide service for 20 years or more. Both systems need a vacuum pump replacement after 10 years of operation.

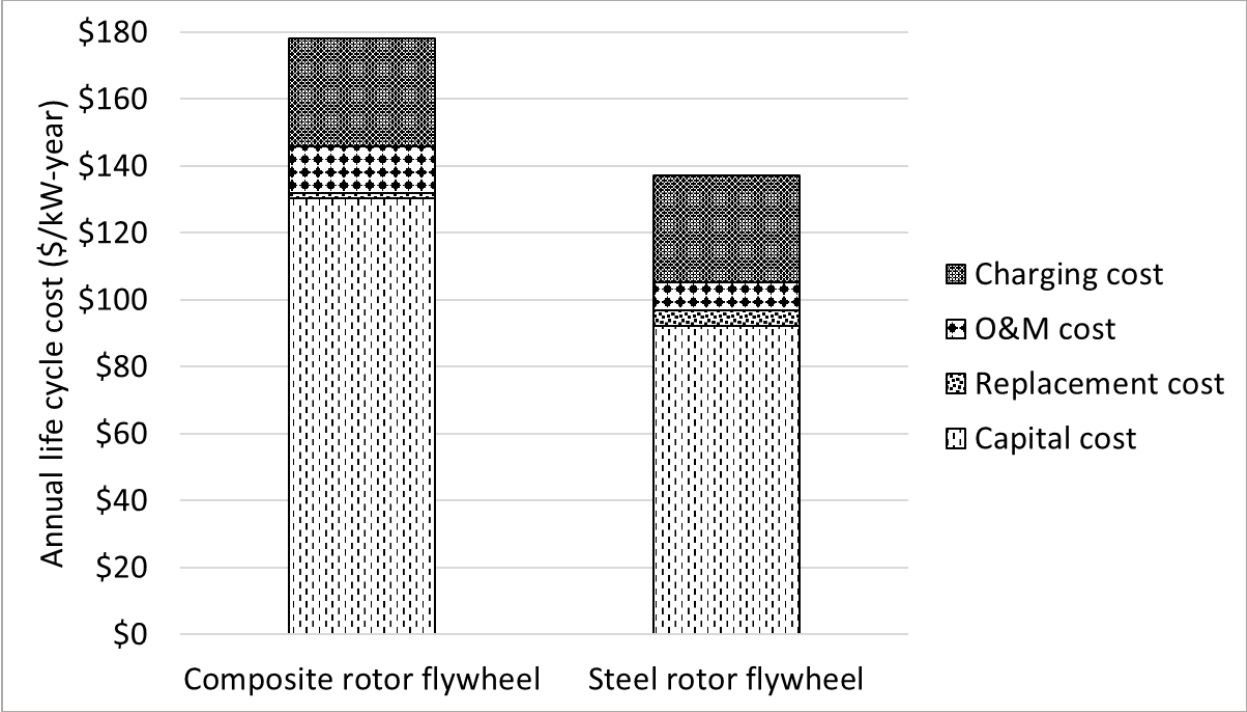


Figure 5.6: Annual life cycle cost for flywheel energy storage systems

5.3.3. Levelized cost of storage (LCOS)

The key economic performance indicators for composite rotor and steel rotor FESSs with 20 MW/5 MWh rated capacity for frequency regulation are summarized in Table 5.4. Results were also generated for wider capacity ranges (1-40 MW) and are provided in section D.2 in Appendix D. The LCOSs are based on the annual life cycle cost, amount of electricity delivery from the FESSs, and number of cycles per year. The LCOS largely depends on the number of cycles and discharge duration. For the base case, we considered 4000 cycles, although we varied this in the sensitivity and uncertainty analyses to examine its impact on the overall cost. For the same number of cycles, the LCOS of the steel rotor flywheel is cheaper than the composite rotor, which is mainly due to the steel rotor flywheel’s lower capital cost. The amortized capital costs are \$130.26 and \$92.01/kW-year for composite and steel rotor FESSs, respectively. The corresponding LCOSs are \$189.94 and \$146.41/MWh, respectively.

The levelized cost added by storage does not account for the charging cost. The LCAS is a useful indicator that can be used to compare different storage technologies for a specific application. The LCAS is the added cost to the price of electricity when a storage system is in place. The LCASs for composite and steel rotor FESSs are \$155.58 and \$112.05/MWh, respectively.

A scale factor (SF) was developed in this study using the TICs at different capacities. The value of the SF was calculated to be 0.93. This means that the rate at which the TIC increases is lower than the rate of increase in the rated power of the storage plant. Therefore, higher capacity plants have higher returns on investment. Figure 5.7 shows the cost advantage at larger capacities. The LCOS decreases with an increase in the rated power of the storage plant because of economies of scale benefits, indicated by a scale factor of less than 1. Because the LCOSs presented for the base case are specific to a particular plant capacity (20 MW), these results are not applicable for a plant of a different capacity. We used the data generated from the model to plot LCOSs vs. plant capacities to develop equations that can be used to estimate the LCOSs for different plant capacities. The LCOS decreases from \$217.76/MWh to \$183.11/MWh for the composite rotor FESS and from \$175.07/MWh to \$141.55/MWh for the steel rotor FESS, for a range of capacities from 1-40 MW (see Figure 5.7). Equation 5.4 [431] can be used to calculate the TIC of a plant with a different capacity for the selected technology with an SF of 0.93:

$$\frac{TIC_B}{TIC_A} = \left(\frac{RP_B}{RP_A} \right)^{SF} \quad (5.4)$$

where TIC_A is the total investment cost of the base case storage system (\$25.88 million for the composite rotor FESS and \$18.28 million for the steel rotor FESS), TIC_B is the total investment cost of the required storage system, RP_A is the rated power of the base case storage system (20 MW), and RP_B is the rated power of the required storage system.

To demonstrate the validity of the model, the results were compared with those found in existing studies. The power capital cost is the indicator widely used; this is because flywheels are used in power applications rather than in energy applications. The power capital costs found in this study are \$1294/kW for the composite rotor and \$914/kW steel rotor FESSs. The corresponding energy capital costs are \$5176/kWh and \$3656/kWh. In the thirteen studies we reviewed, the power and energy capital costs range from \$250/kW [22] to \$2880/kW [189] and from \$1053/kWh [22] to \$10,510/kWh [119], respectively. These studies did not conduct detailed cost assessments for the components of FESSs. Moreover, the material used for the rotors was not specified. Kailasan [201] reported the power capital cost provided by specific manufacturers. The results of this study are in good agreement with the values reported by Kailasan. The power capital costs of the FESSs by Beacon Power and Powerthru (manufacturers of flywheels with composite rotors) are \$1630/kW and \$1200/kW, respectively. \$700/kW [201] and \$950/kW [432] are the power capital costs of the FESSs manufactured by Active Power and Amber Kinetics (manufacturers of flywheels with steel rotors), respectively. Different assumptions, system boundary selections, and input parameters might be the reasons for the small differences in the power capital costs between this and other studies. In addition, the LCOSs obtained in this study were compared with the values reported in a recent study by Schmidt et al. [23]. The LCOS for a primary response reported by Schmidt et al. [23] is in the range of \$135-\$400/MWh for 2020. We estimated \$189.94/MWh and \$146.41/MWh for the composite rotor and steel rotor FESSs, respectively. Although Schmidt et al. [23] did not specify the rotor type, the LCOS values found in this research are within the range reported by Schmidt et al. for 5000 discharge cycles per year. Mostafa et al. [24] reported about \$705.30/MWh for the LCOS of FESS, which is higher than the LCOS found in the study, mainly because of the differences in discharge duration. While we considered 15 minutes of discharge, which is in

agreement with the assumptions used in the earlier studies for frequency regulation [23, 293], Mostafa et al. [24] assumed a very short-duration of 36 seconds. The results obtained in various studies differ mainly because of data sources, modeling approaches, and assumptions related to the input parameters. Therefore, detailed sensitivity and uncertainty analyses are important to check the reliability of the results. Instead of providing point estimates, we presented a probable range of the results (5th percentile to 95th percentile) considering the uncertainties in assumptions, modeling, and input data. Moreover, unlike most of the published studies, we designed each component of the FESS using fundamental engineering principles and estimated their cost functions, then developed the most useful performance indicators, such as TIC, ALCC, and LCOS.

The flywheel has become competitive with electro-chemical batteries for frequency regulation. Flywheels have several advantages: they have comparatively longer lifetime regardless of operating temperature and depth of discharge, and high power density. In some earlier studies, flywheels were found to have a lower environmental footprint than electro-chemical storage systems [203, 388]. Schmidt et al. [23] showed that flywheels show better cost competitiveness than batteries because they have a longer cycle life. The main challenge of FESSs is the energy loss due to friction. However, research is being conducted to increase the discharge duration of flywheels. Amber Kinetics designed a system made of a steel rotor that can discharge for 4 hours [433]. This will allow FESSs to be used for energy-related applications replacing electro-chemical batteries.

The results of the research can help stakeholders, such as electric utilities and manufacturers, to understand the economic performance of FESSs and will also be useful for making investment decisions and policies regarding their deployment in electricity networks. Because this study considers the design and economic aspects with a detailed sensitivity analysis of design

parameters, it will help flywheel manufacturers to identify the areas where cost could be reduced by improving the design. In addition, this study will facilitate a cost comparison of FESSs and electro-chemical ESSs.

Table 5.4: Cost summary for 20 MW/5MWh flywheel energy storage systems

Cost parameter	Composite rotor FESS	Steel rotor FESS
Total investment cost (million \$)	\$25.88	\$18.28
Total replacement cost (million \$)	\$0.72	\$1.95
Power capital cost (\$/kW)	\$1294.01	\$914.05
Levelized cost of storage (\$/MWh)	\$189.94	\$146.41
Levelized cost added by storage (\$/MWh)	\$155.58	\$112.05

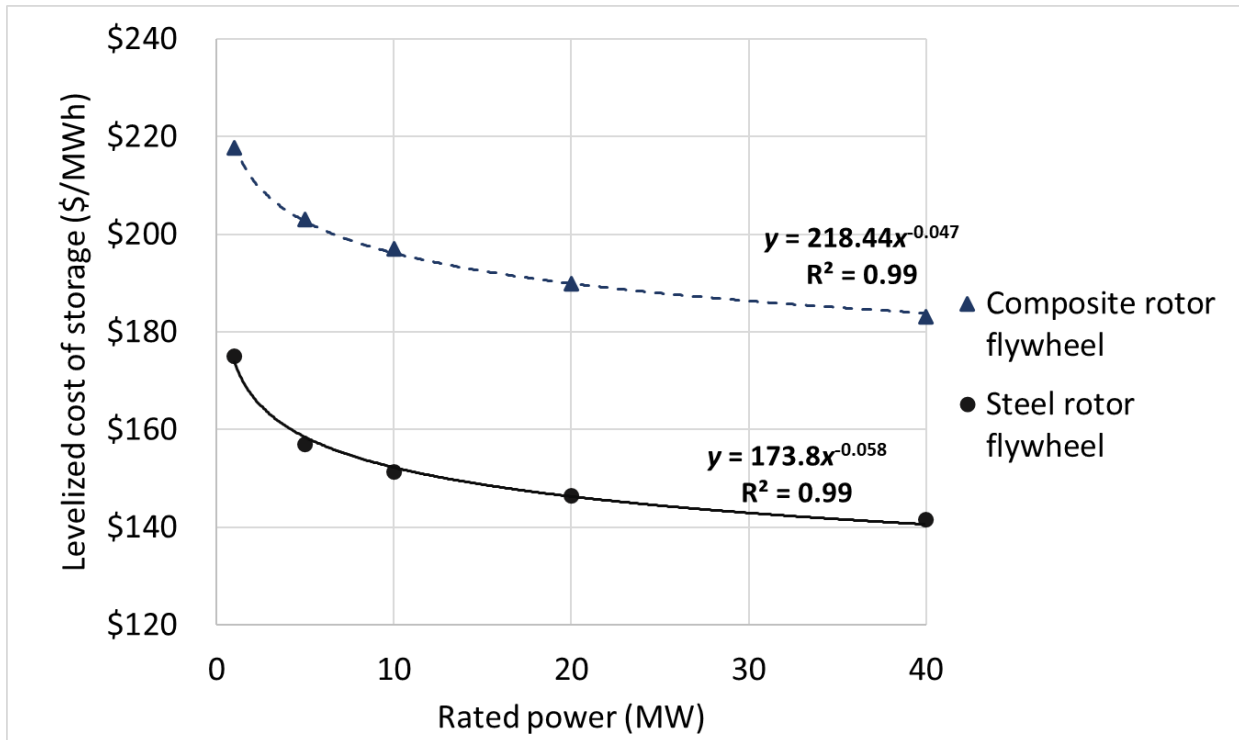


Figure 5.7: Change of the levelized cost of storage (LCOS) with rated capacity of the storage plant. y and x in the equations represent the LCOS (\$/MWh) and the rated capacity (MW), respectively

5.3.4. Sensitivity and uncertainty analyses

Figure 5.8 shows the sensitivity analysis for the LCOS for the composite rotor FESS. The Morris sensitivity analysis was used to identify the most influential parameters. The sensitivity plot was divided into three zones, A, B, and C. In the Morris plot, mean and standard deviation dictate whether a parameter is sensitive or not. The higher the mean, the more sensitive the parameter is. A large standard deviation, on the other hand, indicates that either the parameter has interactions with other variables or the parameter has a non-linear effect. The parameters in zone A have low mean and standard deviations, hence they have insignificant impacts on the LCOS. These parameters are round-trip efficiency, vacuum pump lifetime, and standby loss. Zone C indicates the parameters with high Morris mean and standard deviation. These parameters are critical and

have significant impacts on the LCOS. The sensitive parameters include the factor of safety, tensile strength of the rotor material, number of cycles per year, discount rate, and rotor material cost. The parameters in zone B with moderate impacts are the charging cost, O&M cost, cost of bearings, efficiency of the power converter, etc. A similar trend was observed for the steel rotor FESS, as seen in Figure 5.9.

The Monte Carlo simulations for the uncertainty analysis were conducted using minimum, most likely (defaults in the model), and maximum values of inputs. Figures 5.10 and 5.11 show the uncertainty analysis for the TIC and LCOS, respectively. The TIC ranges from \$16.11 million to \$31.82 million for the composite rotor FESS and \$15.51 million to \$24.77 million for the steel rotor FESS. The LCOSs are from \$122.08/MWh to \$253.52/MWh and from \$108.63/MWh to \$187.64/MWh for the composite rotor and steel rotor FESSs, respectively. It is difficult to choose between the two because of the overlaps in TIC and LCOS. These overlaps result from using a wide range of input data. If the mean values are considered, the steel rotor FESS performs better than the composite rotor FESS in terms of TIC and LCOS. The number of cycles has the most influence on the LCOS for both FESSs. The LCOS ranges from \$152.4/MWh to \$227.6/MWh with 3000-5000 cycles for the composite rotor FESS. If the number of cycles increases, the amount of electricity delivered also increases; hence, the LCOS decreases. The factor of safety, cost of rotor material, rotor material tensile strength, and nominal discount rate are also key parameters that have a significant influence on LCOS distribution.

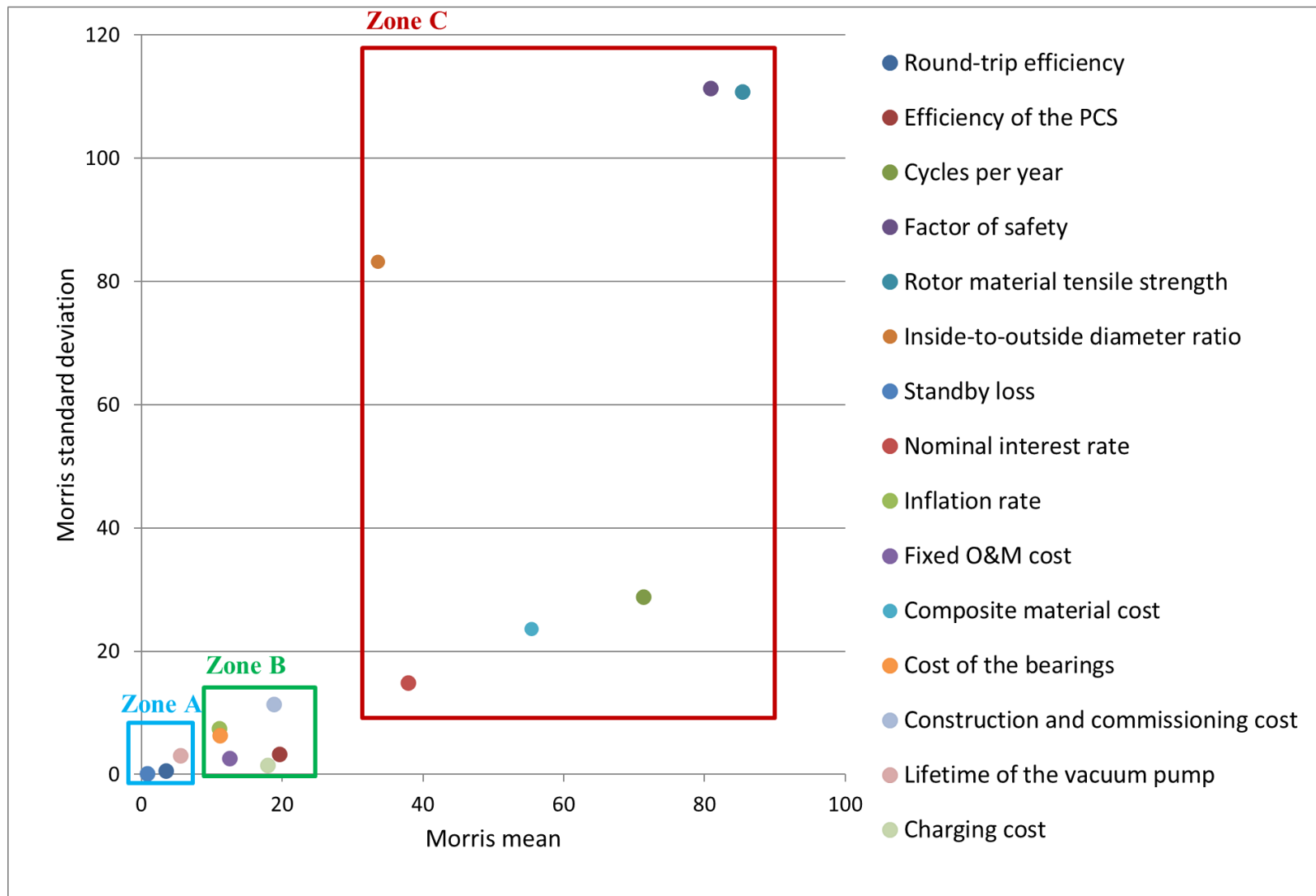


Figure 5.8: Morris sensitivity analysis for the levelized cost of storage for composite rotor flywheel storage

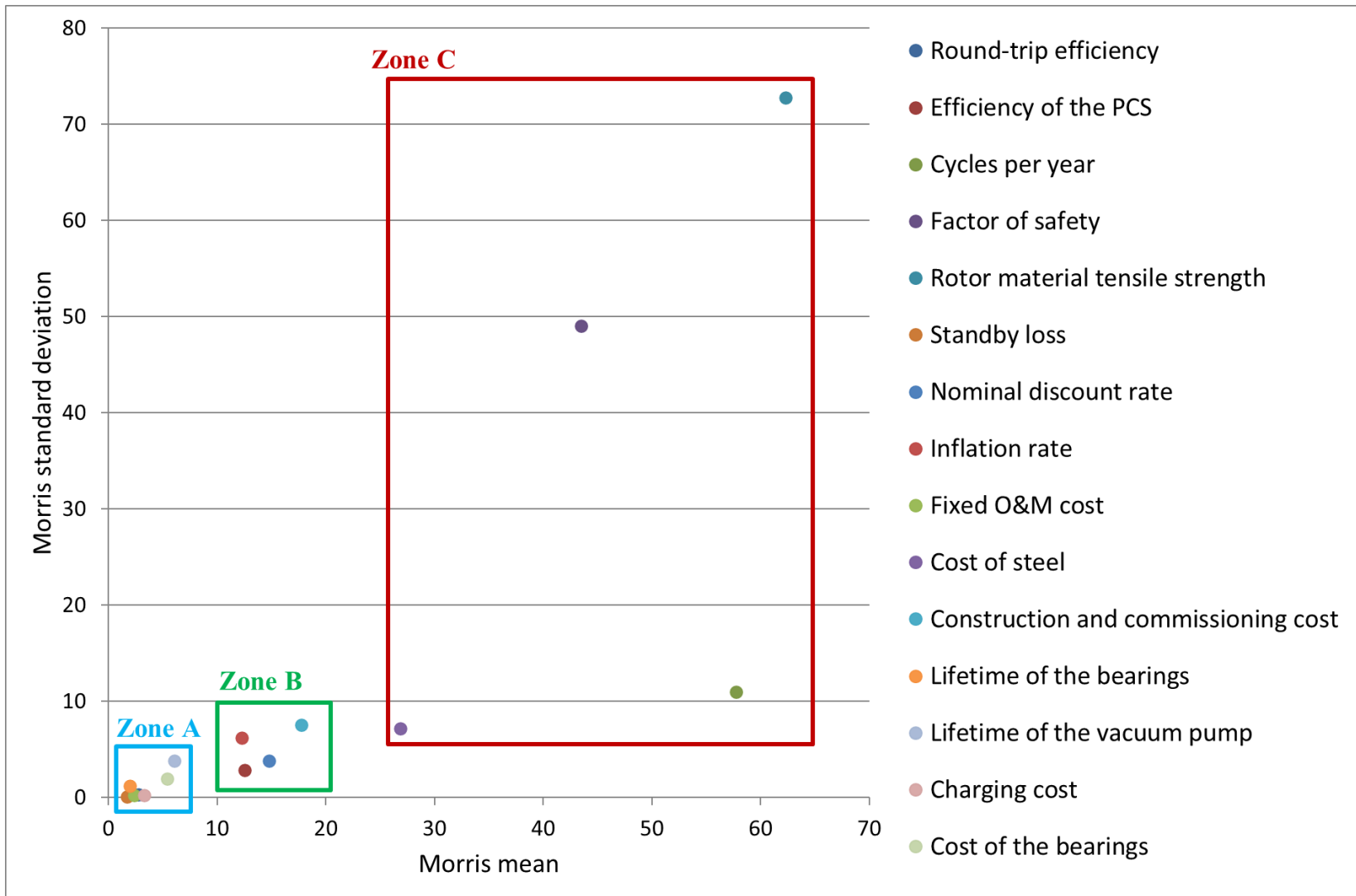


Figure 5.9: Morris sensitivity analysis for the levelized cost of storage for steel rotor flywheel storage

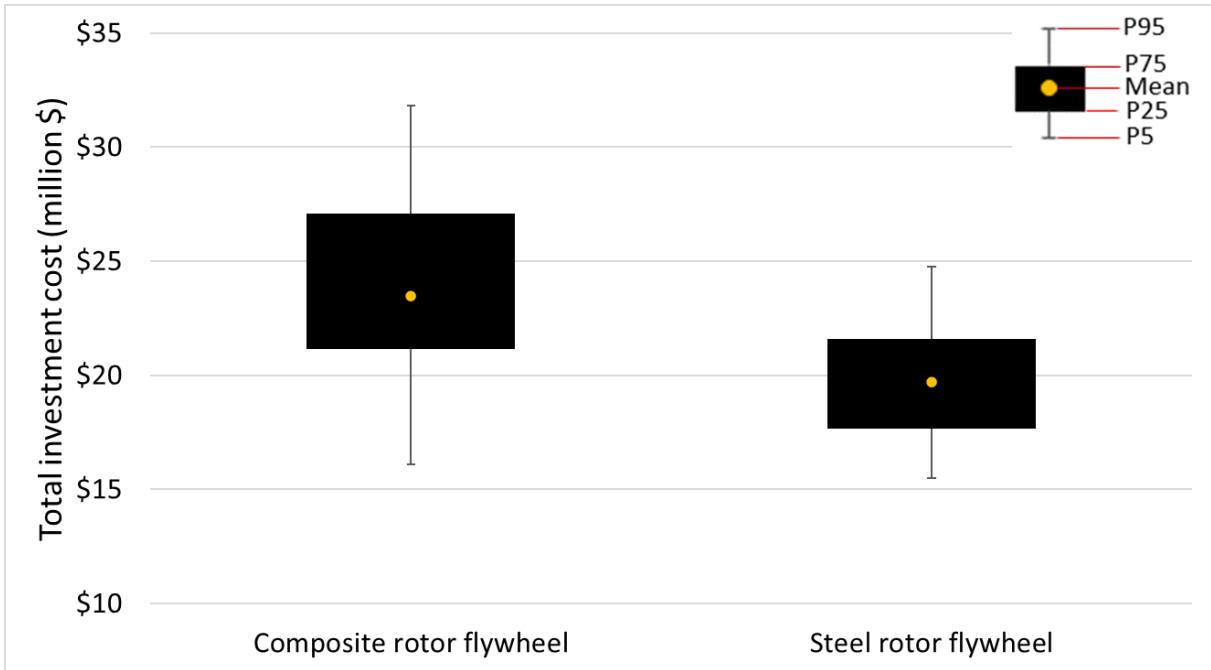


Figure 5.10: Total investment cost uncertainty analysis

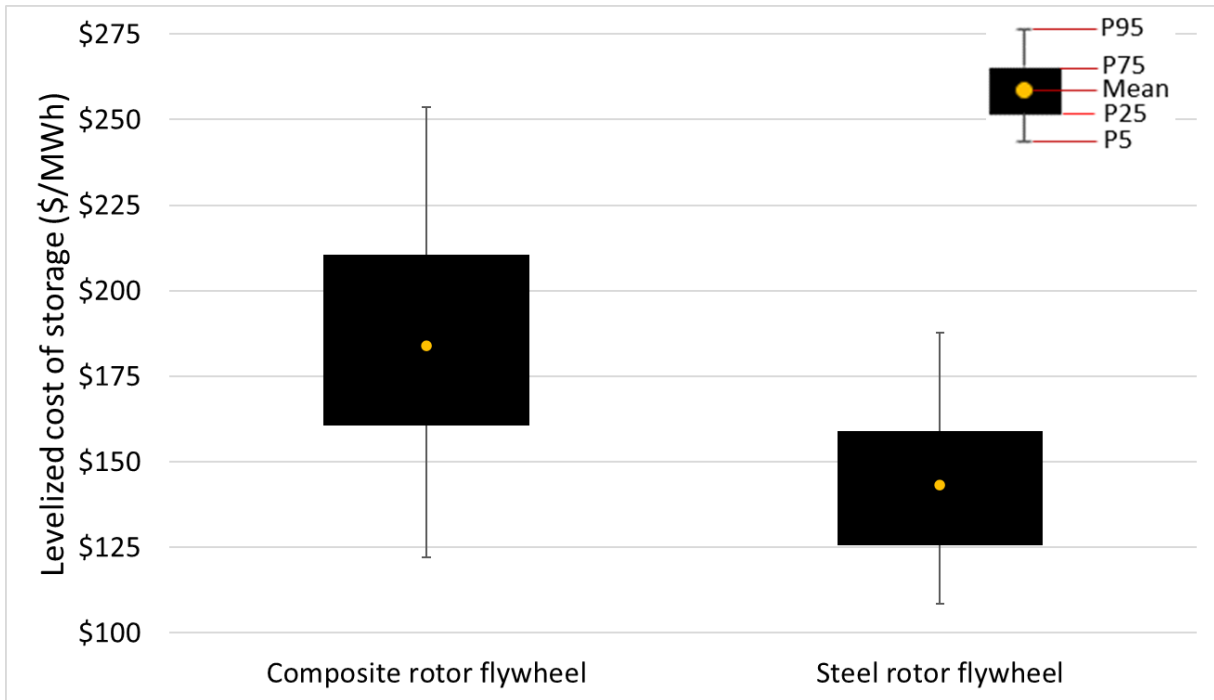


Figure 5.11: Levelized cost of storage uncertainty analysis

5.4. Conclusion

The use of a flywheel storage system for short-duration applications is increasing because of its high power density, long cycle life regardless of the depth of discharge, operating temperature, and low environmental impact. To make investment decisions for the integration of flywheels into electricity grids, their techno-economic feasibility needs to be assessed. However, almost no bottom-up research has been done, i.e., research that considers the technical parameters to size the components of a flywheel storage system, estimate cost parameters based on the design, and provide a probable distribution of the total investment cost and levelized cost of storage. To address the gaps in the literature, we conducted a techno-economic assessment of composite rotor and steel rotor flywheel energy storage systems for a capacity of 20 MW with 15 minutes discharge duration through the development of a bottom-up techno-economic model. We designed the system components, then developed the cost function and conducted a discounted cash flow analysis to estimate the total capital cost and levelized cost of storage. To improve model reliability, we conducted sensitivity and uncertainty analyses to identify the parameters that affect the results and to provide a provable distribution of the results.

The total investment costs of the composite rotor and steel rotor flywheel storage systems are \$25.88 million and \$18.28 million, respectively. The corresponding levelized cost of storage values are \$189.94/MWh and \$146.41/MWh. The differences in the TIC of the two systems are due to differences in rotor and bearing costs. The composite rotor flywheel energy storage system costs more than the steel rotor flywheel energy storage system because composite materials are still in the research and development stage and material and manufacturing costs are high. If a plant's rated capacity increases, the levelized cost of storage decreases because of economies of scale, with a scale factor of 0.93. The factor of safety, tensile strength of the rotor material, the

number of cycles per year, discount rate, and cost of rotor material were identified as the parameters that affect the results the most. The ranges obtained in the uncertainty analysis for the levelized cost of storage are \$122.08-\$253.52/MWh and \$108.63-\$187.64/MWh for the composite rotor and steel rotor FESSs, respectively. The results of the research can help understand the economic performance of flywheel energy storage systems and will be useful for making decisions regarding their deployment in electricity networks.

Chapter 6: Energy and environmental footprints of flywheels for utility-scale energy storage applications⁹

6.1. Introduction

Fossil fuel depletion and the environmental effects of global warming are the main drivers behind the rapid penetration of renewables, such as wind and solar, in the electricity mixes worldwide. The share of renewables in electricity production is projected to be 86% by 2050, up from 26% in 2018. By 2050, solar and wind could generate 67% of global electricity [434]. One of the key challenges of operating an electrical grid with larger fractions of solar and wind is the intermittency of renewables in matching demand and supply [435], and thus energy storage systems (ESSs) are needed [31, 271, 436]. Short-duration ESSs usually operate for less than an hour and are crucial in improving the robustness and reliability of electrical grid systems [11]. Although electro-chemical batteries can be used for short-duration applications, they have a short lifetime, and their chemicals need to be disposed of. Flywheel energy storage systems (FESSs) have proven to be feasible for stationary applications with short duration, i.e., voltage leveling [437], frequency regulation [331], and uninterruptible power supply [24], because they have a long lifespan, are highly efficient, and have high power density [438].

A flywheel is a mechanical storage system that converts electricity to kinetic energy during charging and the kinetic energy back to electricity during discharge. Steel rotor FESSs are the most widely used FESSs, but recent developments in composite materials have encouraged manufacturers to produce composite rotor FESSs. Beacon Power has a 20 MW plant, the largest in North America that uses composite rotor flywheels [439]. The total installed capacity of FESSs

⁹ A version of this chapter has been published as Rahman MM, Gemechu E, Oni AO, Kumar A. Energy and environmental footprints of flywheels for utility-scale energy storage applications. e-Prime, 2021;1:100020.

worldwide is 931 MW for stationary applications [331]. The global market for FESS is projected to be \$479 million in 2025, up from \$264 million in 2018 [440, 441]. The increased use of FESSs in utility applications has encouraged research, especially in flywheel design and optimization [198, 381] and techno-economic assessment [189, 331]. However, the environmental performance assessment of FESSs has received little attention from academia mainly because of the lack of data on energy and material use in each life cycle stage of a FESS. Evaluating the environmental footprints of FESSs over the life cycle helps to identify the hotspots and thus make informed decisions to improve its sustainability performance; to make a reasonable comparison with other storage technologies, such as pumped hydro, compressed air, electro-chemical batteries, and thermal; and to formulate environmental policy in the energy sector. Each unit operation in the supply chain of a FESS, i.e., material production, manufacturing, operation, transportation, and end-of-life (EOL), requires energy input and hence releases greenhouse gases (GHGs). Moreover, the contribution of different components and unit operations to the total energy consumption and life cycle GHG emissions needs to be quantified. In addition, identifying the key input variables that affect the environmental performance of a FESS requires a detailed investigation.

While there are a few LCA studies on FESSs, none include all the components and the full supply chain from material production to EOL. Torell [54] performed an LCA of lead-acid (PbA) batteries and FESSs focusing on the material production, transportation, and operation phases. The author assumed the same footprints for the PbA battery and flywheel in the manufacturing and EOL phases. Although the study provides some information on the carbon footprint, details of assumptions, data sources, and model development are missing. A similar study by Active Power estimated the carbon footprint of a FESS for an uninterruptible power supply application [55]. The study focuses on material production for a steel rotor flywheel. A study by the Beacon Power

Corporation compares the GHG emissions of a 20 MW FES plant with natural gas, coal, and pumped hydro storage [56]. The authors estimated only the GHG emissions from the use of some electricity to compensate for the energy loss in the operation phase without considering the other life cycle stages. While those studies are helpful to understand the inventory for the material production and operation phases, many important aspects are not covered.

First, there are no LCA studies that assess the environmental performances of composite rotor FESSs. Research on composite rotor FESSs mainly evaluates cost performance. As composite rotor flywheels have become popular for their low weight and low space requirement, it is worth investigating the energy and GHG emission characteristics of the system and comparing them with those of conventional steel rotor FESSs.

Second, most LCA studies on FESSs estimate the carbon footprints of the flywheel rotor, which is the heart of the FESS. Other key components such as the bearings, vacuum system, motor/generator, and power conversion system (PCS) are not fully studied. Leaving out the energy required to produce these components may lead to a misleading conclusion.

Third, important LCA phases, such as charging/discharging and EOL, are usually omitted. These stages, in some cases, could make significant contributions. For example, 48 kg-CO₂eq are emitted to generate 1 MWh of electricity (from solar) used for charging [442]. Neglecting the operation (charging/discharging) and manufacturing phases could result in low estimates. Omitting these aspects in the system boundary while conducting an LCA of a FESS can also produce misleading information.

Fourth, none of the studies in the literature calculated the net energy ratio (NER) of FESSs. NER is a ratio of energy generated to the non-renewable energy used over the life cycle of a system. A

storage system with a higher NER is preferred because of its higher energy output per unit energy consumption. It is a useful indicator to compare the effectiveness of different ESSs based on their energy performances.

Finally, earlier studies did not include sensitivity and uncertainty analyses, an important part of the assessment. LCA involves data collection and assumptions in building inventories (material and energy inputs) for all the life cycle phases, and determining the environmental impacts associated with each input. For the same input, different sources may have different values. It is important to identify the variables that most impact the results. Furthermore, to understand the probable range of results from the interactions of the input variables with a range, uncertainty analysis is required. Sensitivity and uncertainty analyses can handle variations in assumptions and data; however, they were not included in the existing LCA studies of FESSs.

This study aims to fill the above-mentioned gaps by developing a data-intensive model using a bottom-up approach to assess the NER and the life cycle GHG emissions of steel rotor and composite rotor FESSs. The components were sized, and material and energy inventories were built using fundamental principles for utility-scale short-duration applications. The specific objectives are to:

- Apply engineering principles to define and design the product system;
- Build inventories for material and energy requirements in the life cycle stages from material production to end-of-life;
- Evaluate the environmental performances of steel rotor and composite rotor FESSs for short-duration stationary applications;

- Assess the life cycle NER and GHG emissions when FESSs use electricity from wind and solar; and
- Perform sensitivity and uncertainty analyses to identify the variables that affect the results most and to provide probable ranges of life cycle NER and GHG emissions.

6.2. Modeling method

Figure 6.1 shows the methodological framework of this study. The first stage is the goal and scope definition, which involves stating the purpose of the study, developing a consistent system boundary that includes all the life cycle stages for the selected systems, and defining the functional unit for a base of comparison. In the system design phase, we used the rated power and discharge duration to estimate the installed energy capacity of the storage plant and size all the components of a FESS to characterize the energy and material requirements in each process unit and piece of equipment. The inventory analysis involves compiling and calculating energy and material inputs and outputs and the associated GHG emissions at each life cycle stage of the product system. The NER was evaluated from the total energy produced and the total primary energy consumed during the lifetime of the FESSs. Finally, sensitivity analysis was carried out followed by an uncertainty analysis to understand the impacts of the design parameters, data variability, and assumptions used in the model on the results. The following sections describe each component of the framework in detail.

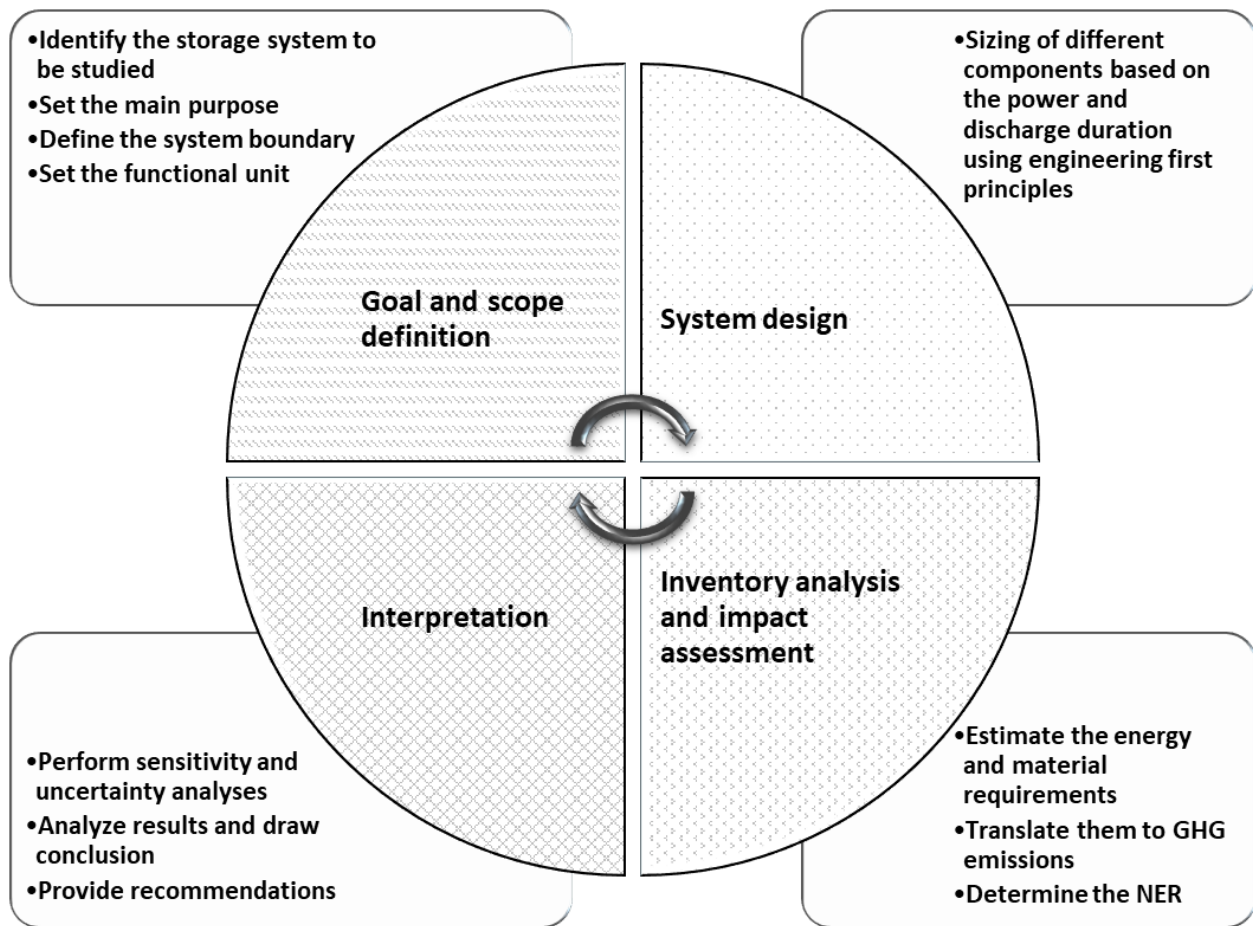


Figure 6.1: Life cycle assessment framework for a flywheel energy storage system

6.2.1. Goal and scope

This research aims to conduct a comparative life cycle assessment of steel rotor and carbon fiber composite rotor FESSs through the development of a scientific principles-based model. The NER and life cycle GHG emissions were used as environmental performance indicators. As the function of an ESS is to deliver electricity, the functional unit is defined as 1 MWh electricity delivered. A 20-year project lifetime, the lifetime of a FESS, was assumed. The replacement of some components, such as mechanical bearings and vacuum pumps, was also considered in this study.

Figure 6.2 shows the system boundary developed to reasonably compare the two FESSs, composite and steel rotor. All the life cycle phases were considered, i.e., material production, manufacturing, operation, transportation, and EOL. The material production phase includes the energy and materials required to extract and process the resources used to build different FESS components, and the manufacturing phase considers the production of the components.

The operation phase includes charging, discharging, and standby modes. In the standby mode, the FESS rotates at a constant speed; this mode requires a small amount of energy for the flywheel to maintain its speed. The amount of electricity required in charging and discharging depends on the flywheel efficiency, power conversion system (PCS) efficiency, rated power of the plant, discharge duration, and the number of cycles in a year. The energy input in this phase is the electricity required for charging and standby modes, and the output is the amount of electricity delivered by the system. Because the motivation behind this study is increased penetration of renewables in the electricity mix, we assumed that electricity from solar and wind would be used for charging.

In the EOL phase, the components are dismantled and transported to a recycling facility and a landfill. As the components are mostly built from metal, it was assumed that metal would be recycled, and the residues disposed of at a landfill. Although the steel rotors are 100% recyclable [443], recycling the composite rotor is not a common practice given the lack of established methods for recycling it [444]. Therefore, the composite material was assumed to be disposed of in a landfill.

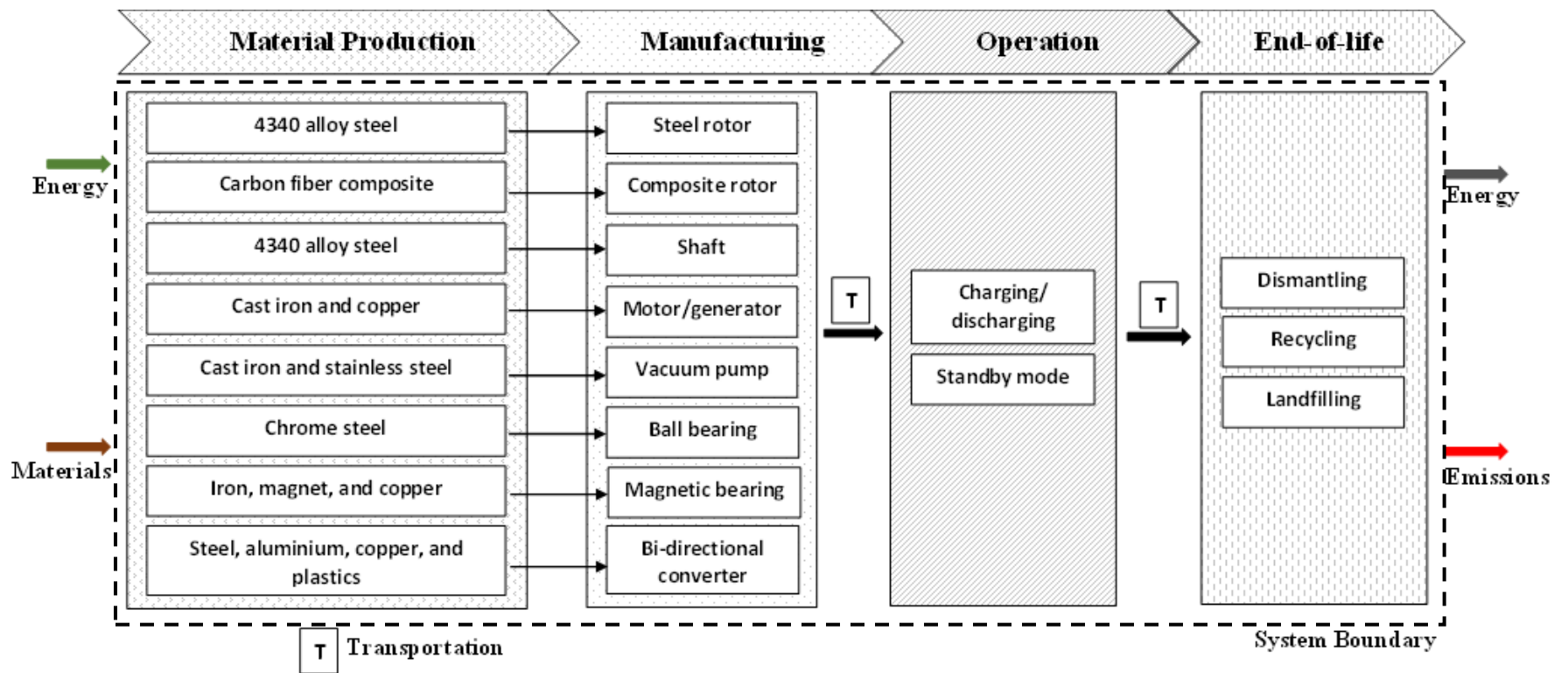


Figure 6.2: System boundary for FESSs

6.2.1.1. FES system description

The main components of a flywheel energy storage system are a rotor, an electrical motor/generator, bearings, a PCS (bi-directional converter), a vacuum pump, and a vacuum chamber [69]. During charging, the rotor is accelerated to a high speed using the electrical motor. The energy is then stored in the FESS in the form of kinetic energy by keeping the rotor at a constant speed. During discharge, the generator converts mechanical energy to electricity. The amount of energy stored in the flywheel rotor is proportional to the moment of inertia and the square of the angular velocity of the rotor. Equation 6.1, adapted from Olabi et al. [438] shows the energy stored in the flywheel rotor:

$$E = \frac{1}{2}I\omega^2 \quad (6.1)$$

where E is the stored energy (J), I is the moment of inertia ($\text{kg}\cdot\text{m}^2$), which depends on the material and shape of the rotor, and ω is the angular velocity (rad/s).

Based on rotational speed, FESSs are categorized as low-speed and high-speed. Low-speed FESSs typically have a speed up to 6000 RPM [28] and are usually made of steel [205]. High-speed FESSs are characterized by higher speed (up to 100,000 RPM [379]) and are typically made of carbon fiber and fiberglass [445]. Magnetic or mechanical bearings are used to support low-speed flywheels [203]; high-speed flywheels require magnetic bearings [203]. The motor/generator is an electrical machine that converts electricity to kinetic energy during the charging process and converts mechanical energy to electricity during discharge [69]. A housing holds the FESS in a vacuum environment using a vacuum pump to reduce drag. The housing is also used to contain the rotor during system failure [203]. A PCS is used to convert AC-DC, DC-AC, or a combination [203].

6.2.2. System design

FESSs are a common choice for power applications and have a discharge duration of a few seconds to less than an hour [446]. Frequency regulation is one of the most common stationary applications for a FESS [331]. A 20 MW system for frequency regulation is the largest North American FESS and is situated in Stephentown, New York, USA [447]. There is a grid-connected FESS in Ontario, Canada with a capacity of 2 MW [448]. Both operate for 15 min at their rated capacities. In this study, the systems were modeled for a rated capacity of 20 MW/5 MWh (0.25 h discharge duration) for frequency regulation. The FESSs were assumed to operate for 4000 cycles per year based on commercial-scale development [449]. However, we varied the number of cycles to determine the impact on the NER and GHG emissions. A FESS of any MW capacity requires hundreds of flywheels, depending on the capacity of each flywheel. The useful energy of a FESS was estimated based on its operational parameters (presented in Table 6.1). Once the power and energy capacities of each flywheel are known, the number of flywheels required for the 20 MW/5MWh plant was quantified. The amount of kinetic energy stored in the flywheel was calculated based on the mass of the rotor, maximum and minimum angular speeds, and radius of the rotors (see Equation E.1 of Appendix E). The maximum surface speed is limited by the tensile strength [401]. The radius of the flywheel rotor for a given rotational speed can be calculated using the tensile strength, the density of the rotor material, and the safety factor. The detailed calculation of the rotor outer radius and energy stored in the flywheel can be found in Appendix E in section E.1. In this study, the shapes of the composite and steel rotors were assumed to be hollow and solid cylinders, respectively, as these are the typical shapes used in the flywheel industry [450]. The outer radii of the steel and carbon fiber rotor were calculated as 0.49 m and 0.46 m, respectively. The inner radius of the composite rotor was calculated based on the outer radius and the ratio of the inner to

the outer diameter (ID/OD) of 0.60. According to Kailasan, an ID/OD of 0.50 to 0.75 is a good compromise typically used in the flywheel industry [451]. In this study, we assumed the length to rotor outer diameter (L/OD) ratio to be 0.95. Usually, this ratio is taken as less than 1 for rotodynamic reasons to avoid bending [452]. Using the above-mentioned geometric characteristics, we found that the kinetic energy stored in a steel rotor FESS and a composite rotor FESS is 28 kWh and 26 kWh, respectively. The corresponding values of electrical energy are 27 kWh and 25 kWh. The rated power capacities of a steel rotor FESS and a composite rotor FESS are 108 kW and 100 kW, respectively, for 15 min discharge duration. Therefore, 186 steel rotor flywheels and 200 composite rotor flywheels are needed for a 20 MW/5 MWh steel rotor FESS and composite rotor FESS, respectively.

The FESS should operate in a vacuum chamber with a pressure of 100 to 0.10 Pa to reduce friction and overcome the heating problem [453]. A 0.14 Pa vacuum chamber requirement is assumed in this study. Similar assumptions were found in the studies in the literature for steel rotor FESSs [454] and composite rotor FESSs [455]. A 0.55 kW vacuum pump can achieve this low pressure [454].

Although a FESS can operate for more than 20 years, some components such as the vacuum pump and mechanical bearing for a steel rotor FESS will need to be replaced sooner (see Table 6.1). However, the magnetic bearing can last for 20-30 years with proper maintenance [456].

Table 6.1: Technical assumptions used for the FESSs

Parameter	Steel rotor FESS	Composite rotor FESS
Shape factor	0.5 [405]	0.5 [404]
Rotor material density (kg/m ³)	7780 [454]	1700 [451]
Rotor material tensile strength (GPa)	1.24 [403]	4 [454]

Parameter	Steel rotor FESS	Composite rotor FESS
Factor of safety	4 [406]	4 [406]
Poisson's ratio for steel	0.3 [401]	-
Maximum rotational speed (RPM)	6000 [407]	16,000 [198]
Minimum rotational speed (RPM)	3000 (assumed)	8000 [198]
Thickness of the housing (m)	0.05 [457]	0.05 [457]
Ratio of shaft diameter to rotor outer diameter	0.15 [458]	0.15 [458]
Flywheel efficiency (%)	90 [6]	90 [6]
PCS efficiency (%)	95 [169]	95 [169]
Generator efficiency (%)	95 [459]	95 [459]
Storage plant lifetime (years)	20 [460]	20 [460]
Vacuum pump lifetime (years)	10 [461]	10 [461]
Magnetic bearing lifetime (years)	-	20 [456]
Mechanical bearing lifetime (years)	5 [205]	-
PCS lifetime (years)	20 [462]	20 [462]

6.2.3. Inventory analysis

In the inventory analysis, all the energy and material input requirements and the corresponding outputs at each stage of the FESSs life cycle are calculated for the 20 MW/5 MWh FESSs. A slight adjustment to the inventory can be made to estimate the environmental footprints of FESSs with any capacity. The following section discusses the detailed considerations in developing material and energy inventories.

6.2.3.1. Material production

To quantify the energy required for material production, the construction materials for each component of the FESS were identified, and then the total mass of each material was calculated.

Once the material quantities are known, with the specific energy consumption (MJ/kg) and emission factors (kg-CO₂eq/kg) to produce these materials, the total energy consumption and resulting GHG emissions in material production can be estimated. Table 6.2 shows the materials estimates for the 20 MW/5 MWh FESSs. The replacement of mechanical bearings for the steel rotor FESS and vacuum pumps for both the steel rotor and composite rotor FESSs was also considered.

Table 6.2: The material inventory for steel rotor and composite rotor FESSs

Component	Material	Steel rotor FESS mass (tonne)	Composite rotor FESS mass (tonne)	Comment
Rotor	4340 alloy steel [55] for steel rotor and carbon fiber composite for composite rotor [439]	1047	124	The mass of the rotor was calculated from the material density and its radius and length, as mentioned in section 6.2.2. See Table E.1 in Appendix E for the composition of 4340 alloy steel.
Rotor shaft	4340 alloy steel [463]	46	40	Similar to the rotor, the mass of the shaft was calculated from the density of the shaft material and its radius and length.
Housing	Steel [203]	636	590	The thickness of the housing was taken to be 0.05 m [457] and the density of the steel was 7700 kg/m ³ [464].
Motor/generator	Cast iron (70%) and copper (30%) [256]	15	15	The mass of each motor/generator was calculated from its capacity (kW) and specific power (kW/kg). The capacities of the motors for the steel rotor and composite rotor FESSs are 108 kW and 100 kW, respectively. The specific power was assumed to be 1.30 kW/kg; it can range from 1.2 to 1.6 kW/kg [465].
Mechanical bearing	Chrome steel [466]	34	-	The mass of each mechanical bearing is 23 kg [467]. See Table E.1 in Appendix E for the composition of chrome steel.

Component	Material	Steel rotor FESS mass (tonne)	Composite rotor FESS mass (tonne)	Comment
Magnetic bearing	Iron, neodymium iron boron (NdFeB) magnet, and non-magnetic material [468]	-	16	Due to data unavailability for the mass, the mass of each magnetic bearing was extracted from a ratio of the rotor mass to the bearing mass (21.82) based on the information provided by Werfel et al. [469]. The estimated mass of a magnetic bearing is 41 kg. For the non-magnetic material, copper was considered based on the information provided by Tantau [470]. Because no information was found, we assumed that every material has the same mass fraction.
Vacuum pump	Cast iron (50%) and stainless steel (50%) [471, 472]	9	10	A 0.55 kW vacuum pump is sufficient to maintain the vacuum requirement, as mentioned in section 6.2.2. The mass of each 0.55 kW vacuum pump is 25 kg [473]. The material composition for the pump is based on the assumption by Nimana et al. [474].
PCS	Steel (60%), aluminium (18%), copper (12%), and plastics (polyamide injection molded) (10%) [475]	273	272	The mass of the PCS was estimated assuming a linear relation between the mass and capacity of the PCS. This approach is common practice in LCA when there is little or no data [256]. The mass of the PCS for this study was calculated from a 100 kW PCS with 1361 kg mass [476].

6.2.3.2. Manufacturing

We estimated the manufacturing energy requirement for each component and identified the energy sources. With appropriate emission factors for the energy sources and energy requirements, we calculated the total GHG emissions in the manufacturing phases. Table 6.3 shows the energy inventory for the manufacturing phase along with the sources of energy used for the 20 MW/5 MWh FESSs.

As shown in Table 6.3, electricity is one of the largest sources of energy supply and the emission factor of electricity depends on the grid mix, which varies by jurisdiction. As the plant location is in Alberta, a western province in Canada, we assumed that the FESSs are manufactured there. For the base case, Alberta's grid emission factor was used for electricity consumption. However, we varied the emission factor in the model for other provinces in Canada to see the impact of changes on GHG emissions. This framework can be used for other jurisdictions around the world by adjusting some input parameters.

Table 6.3: Developed energy inventory for the manufacturing phase

Component	Energy source (unit)	Steel rotor FESS	Composite rotor FESS	Comment
Steel rotor	Electricity (MWh)	11,232	-	Energy consumption in steel rotor manufacturing was estimated from the specific energy (MJ/kg) and the mass of the rotor. The specific manufacturing energy for the steel rotor is 39 MJ/kg, which was estimated from Yu et al.'s work [477].
Composite rotor	Electricity (MWh)	-	504	The specific energy for composite rotor production was quantified using information from various sources. First, the manufacturing steps were identified followed by the estimation of energy requirements in each step. The manufacturing steps for the composite rotor are filament winding, curing at high temperatures, and machining [381]. The specific energy requirements for filament winding and curing were considered to be 4 MJ/kg [478] and 7.5 MJ/kg [479], respectively. A little machining may be required to give the rotor a final shape. The specific energy consumption in machining with a lathe was assumed to be 75,182 MJ/m ³ of material removed [480].
Rotor shaft	Electricity (MWh)	346	294	The manufacturing energy consumption for the rotor shaft was estimated from the specific energy (MJ/kg) and the mass of the shaft. The specific manufacturing energy for 4340 steel alloy shaft is 27 MJ/kg, estimated from Yu et al.'s work [477].

Component	Energy source (unit)	Steel rotor FESS	Composite rotor FESS	Comment
Motor/generator	Electricity (MWh)	19	19	The energy requirements for the motor/generator were taken from the publicly available free version of the ecoinvent 3.6 database [481]. A linear relation between energy requirements and the capacities of the motor/generator was assumed. A 200 kW motor/generator requires 185 kWh electricity, 8626 MJ natural gas, and 8626 MJ diesel for its manufacturing [481]. These values were linearly scaled for the motor/generator of 108 kW and 100 kW for a steel rotor FESS and a composite rotor FESS, respectively.
	Natural gas (GJ)	866	863	
	Diesel (GJ)	866	863	
Mechanical bearing	Electricity (MWh)	249	-	The specific energy requirements for mechanical bearing manufacturing were based on the study by Ekdahl [482]. The specific energy requirements for mechanical bearing production can be found in Table E.2 of Appendix E.
	Natural gas (GJ)	453	-	
	LPG (GJ)	105	-	
	Fuel oil (GJ)	72	-	
	Diesel (GJ)	0.28	-	
	Coal (GJ)	0.06	-	
Magnetic bearing	Electricity (MWh)	-	8	There is no information on magnetic bearing manufacturing. According to Koehler et al., a magnetic bearing stator largely resembles an electric motor's stator [483]. The authors mentioned that it is possible to use identical manufacturing tools, standards, and processes. Therefore, we assumed the same energy for magnetic bearing production as for the
	Natural gas (GJ)	-	7	
	Diesel (GJ)	-	7	

Component	Energy source (unit)	Steel rotor FESS	Composite rotor FESS	Comment
				production of an electric motor, and this was taken from the ecoinvent 3.6 database [481]. The manufacturing energy requirements for a 53 kg electric motor are 26.53 kWh electricity, 22.35 MJ natural gas, and 21.69 MJ diesel [481]. These values were then linearly scaled up for each magnetic bearing of 41 kg.
Vacuum pump	Electricity (MWh)	1	1	A linear relation between energy requirement and capacity of the vacuum pump was assumed. The manufacturing energy requirements for a 22 kW pump are 140 kWh electricity and 1330 MJ natural gas [481]. The values were then scaled down for the 0.55 kW vacuum pump used in this study.
	Natural gas (GJ)	12	13	
PCS	Electricity (MWh)	25	26	The specific energy requirements for the PCS were based on the study by Tschümperlin et al. [484]. The amount of energy in manufacturing a PCS per unit power decreases with increasing rated power [484]. Details of energy requirements for PCS manufacturing can be found in section E.3 of Appendix E.
	Fuel oil (GJ)	0.54	0.55	
	Natural gas (GJ)	9	9	
	Heat from MSW (GJ)	22	23	
Transportation	Diesel (GJ)	490	254	See section 6.2.3.5 for details.

6.2.3.3. Operation

We estimated the electricity requirement for a FESS to be 23.39 GWh/year and the average electricity delivered from the system 18.75 GWh/year, with a 0.14% yearly degradation (from Mongird et al. [189]). The electricity requirement for standby mode is different for the steel rotor FESS and the composite rotor FESS. The standby power consumption was calculated from standby losses. The standby losses range from 1 to 5% [205, 395] and 0.5-2% [485, 486] of the rated capacity for mechanical and magnetic bearings, respectively. In this study, standby losses for the steel rotor FESS and composite rotor FESS were assumed to be 2.5% [485] and 1% [56], respectively. The steel rotor FESS experiences more loss than the composite rotor FESS because of higher frictional losses in the mechanical bearings. The composite rotor FESS's magnetic bearings use magnetic force to support the rotor without friction.

6.2.3.4. End-of-life

We assumed that the flywheel components are dismantled mechanically, based on the assumptions in a study by Weber et al. [44]. The diesel and electricity requirements for dismantling are 0.10 MJ/kg and 0.01 kWh/kg, respectively [44]. The amount of recycled material was calculated from the recovery rate of different metals. If the recovery rate is not 100%, virgin materials would be used to fulfill material requirements. We used a recovery rate of 90% for the metals [44]. Table 6.4 shows the recovery rate along with the specific energy and emission factors for various metals. The energy requirements in landfilling are based on diesel consumption in the compactors and soil excavation and moving, and electricity requirements for the electric machines. The specific diesel and electricity requirements are 2 L and 7 kWh, respectively, for 1 tonne of material landfilled

[487]. With these values and emission factors for diesel and electricity, we estimated the GHG emissions in landfilling.

Table 6.4: Recovery rate, specific energy, and emission factors for different metals

Metal	Recovery rate (%)	Specific energy consumption (MJ/tonne)	Emission factor (kg-CO₂eq/tonne)
Steel	90 [44]	21,032 [488]	1407 [488]
Aluminium	90 [44]	30,703 [488]	1852 [488]
Copper	90 [44]	14,303 [489]	1071 [489]

6.2.3.5. Transportation

As we assumed that flywheels would be manufactured in Alberta, Canada, a distance of 200 km was assumed from the manufacturing location to the storage plant. However, we varied this distance to see the impact of changes on the overall results if the flywheels are transported from other provinces in Canada. We also assumed an additional 200 km transportation for the EOL to transport the dismantled parts to the recycling plant or landfill. The mode of transportation is heavy-duty trucks. The specific energy consumption of diesel in trucks is 0.61 MJ/tonne-km, calculated from the specific diesel consumption of 0.017 L/tonne-km [490] and lower heating value of diesel of 35.94 MJ/L [491]. Once the energy requirements in transportation are quantified, with diesel’s emission factors (Table E.4 of Appendix E), total GHG emissions were calculated. The total energy requirement in the form of diesel for transportation can be found in Table 6.3.

The NER is the ratio of the electricity delivered to the total energy consumption in the life cycle stages from material production to EOL. The amount of electrical energy required during the charging process was not included in the total life cycle energy use because the electricity in this study is assumed to be produced from renewables, either solar or wind. However, the energy

required to produce different components of solar and wind farms is included. The total GHG emissions were calculated by converting and aggregating CO₂, CH₄, and N₂O emissions from each life cycle stage to CO₂ equivalents using global warming potential values of 1, 28, and 265, respectively, for a 100-year time horizon [492].

6.2.4. Sensitivity and uncertainty analyses

Sensitivity and uncertainty analyses were carried out using the Regression, Uncertainty, and Sensitivity Tool (RUST) developed by Di Lullo et al. [285]. Sensitivity analysis was conducted using the Morris method to examine the effects of input parameters on the NER and life cycle GHG emissions. The Morris method can capture the interactions among the input variables; hence it was used in this analysis.

Uncertainty analysis was conducted to determine the possible ranges in the results from the simultaneous change in multiple input factors. Monte Carlo simulations were carried out using the RUST based on the minimum, most likely (the default values used in the model), and maximum values of input parameters found in the literature. To get the final output distribution, a random sample was selected from the input variables' range and iterated 100,000 times. Table E.5 in Appendix E lists the input parameters and values used for uncertainty analysis.

6.3. Results and discussion

This section presents and discusses the results of NER and life cycle GHG emissions based on the default inputs used in the model. To capture the uncertainties in the data and assumptions in the model, the results of sensitivity and uncertainty analyses are also presented and discussed.

6.3.1. Net energy ratio

The rated power, number of cycles, and discharge duration determine the amount of electricity delivered over the life cycle. The lifetime electricity delivered from the system was calculated to be 375 GWh with 0.25 h discharge duration and 4000 cycles per year. The NERs of the steel rotor FESSs are 2.5 and 3.5 for solar and wind, respectively. The corresponding values for composite rotor FESSs are 2.7 and 3.8. The NERs of composite rotor FESSs are higher because they consume less energy during their life cycle to deliver 1 MWh of electricity. Figure 6.3 presents the energy consumption in the life cycle stages of the FESSs. For steel rotor FESSs, operation contributes the most to life cycle energy use at 71-79%, followed by material production at 9-13%, manufacturing at 8-12%, and EOL at 3-4%, depending on the electricity source. For composite rotor FESSs, operation is again the most energy-intensive phase at 65-76%, followed by material production and EOL at 20-29% and 3-5%, respectively. The contribution of manufacturing is about 1% for composite rotor FESSs. Transportation makes an insignificant contribution of less than 0.1% in both systems.

The energy consumption in the material production stage is much lower in a steel rotor FESS (see Figure 6.3). The energy required to produce 4340 alloy steel for the steel rotor contributes 48% to the total energy requirement in material production. For the composite rotor, on the other hand, 68% of the energy requirement in material production is from carbon fiber composite production. Although the weight of the steel rotor is about 8 times the weight of the composite rotor, the production energy of the composite material is much higher (735 MJ/kg) than the 4340 alloy steel's (38 MJ/kg). The energy requirement for material production for the PCSs contributes 21% and 13% to the total energy consumption in material production for the steel rotor FESS and the composite rotor FESS, respectively. The difference in manufacturing energy requirement is mainly

due to rotor production. The energy consumption in steel rotor manufacturing is about 39 MJ/kg, while the manufacturing of a composite rotor requires only about 15 MJ/kg. Based on these figures, the manufacturing of a steel rotor and a composite rotor contributes 90% and 37% to the total manufacturing energy for the steel rotor FESS and the composite rotor FESS, respectively. Along with its large weight, the steel rotor has another drawback, energy loss due to friction between the rotor shaft and the bearings. The lifetime energy requirements in the standby mode are 20 GWh (with 2.5% loss) and 8 GWh (with 1% loss) for the steel rotor FESS and the composite rotor FESS, respectively. As shown in Figure 6.3, the difference in energy consumption in the operation phase for the composite rotor FESS with solar and wind is due to the difference in embodied energy for electricity from solar and wind. The energy demand to produce 1 MWh electricity from solar photovoltaics is about 1.8 times the energy requirement for electricity from wind. The energy consumption in transportation is comparable in both systems; the small difference is due to differences in the total mass of the systems. The energy consumption in the steel rotor FESS EOL phase is higher than for the composite rotor FESS mainly because of the large amount of steel to be recycled from the steel rotor. EOL energy consumed in dismantling contributes 2.50% for a steel rotor FESS and 0.88% for a composite rotor FESS. Landfilling has an insignificant contribution.

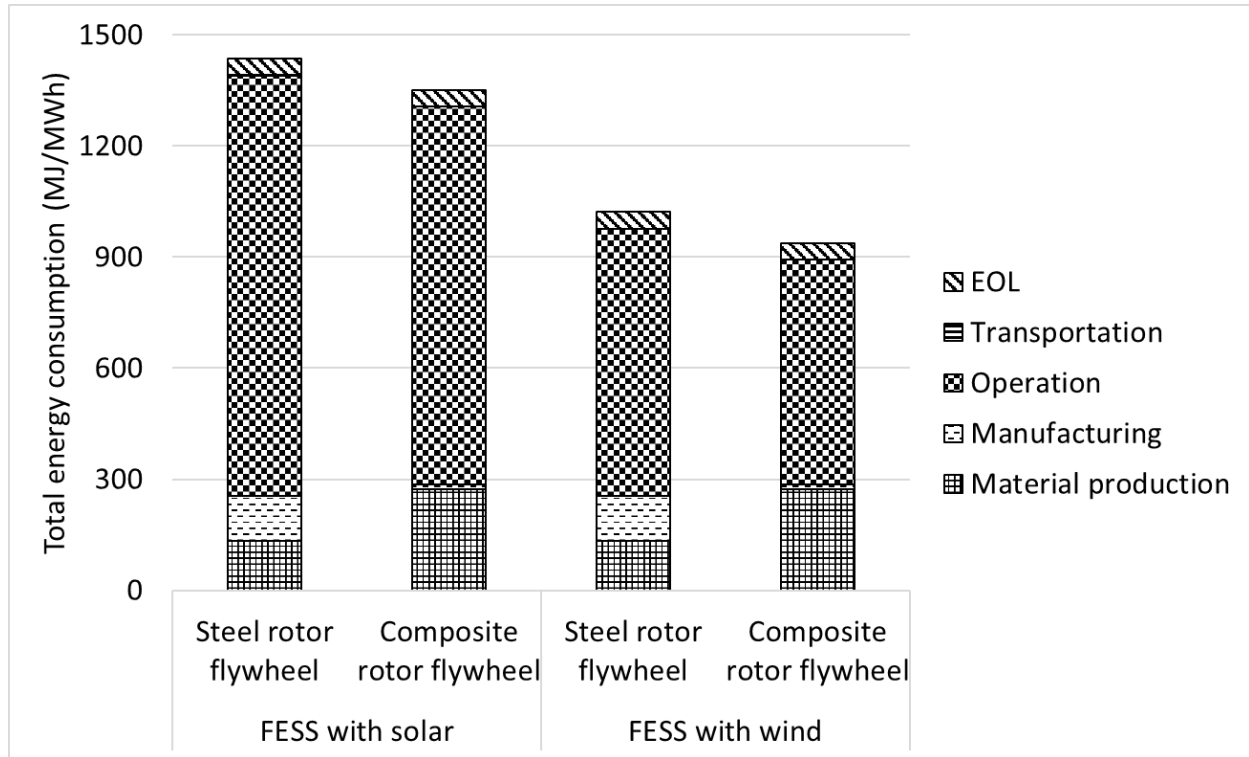


Figure 6.3: Life cycle energy requirements for FESSs

6.3.2. Life cycle GHG emissions

The comparative life cycle GHG emissions of the steel rotor FESS and the composite rotor FESS are shown in Figure 6.4. The composite rotor FESS offers better environmental performance with lower GHG emissions than the steel rotor FESS. The life cycle GHG emissions of the steel rotor FESS and composite rotor FESS are 121.4 kg-CO₂eq/MWh and 95.0 kg-CO₂eq/MWh, respectively, when electricity from solar energy is used for charging. When the charging electricity comes from wind energy, life cycle GHG emissions are 75.2 kg-CO₂eq/MWh and 48.9 kg-CO₂eq/MWh for the steel rotor FESS and composite rotor FESS, respectively. The difference is due to the upstream GHG emissions in solar and wind-based electricity, 48 kg-CO₂eq/MWh for solar and 11 kg-CO₂eq/MWh for wind [442]. Although electricity from solar and wind was considered for charging in the base case, additional results are provided for different electricity

mixes used in four Canadian provinces. Figure E.1 in Appendix E shows the life cycle GHG emissions when electricity for charging comes from the grid.

As Figure 6.4 shows, the operation phase is the largest contributor to GHG emissions: 60-75% for the steel rotor FESS and 54-76% for the composite rotor FESS. This includes the upstream emissions from charging and emissions due to the electricity use in standby mode. The standby mode contributes 34-70% and 17-48%, respectively, to the total GHG emissions in the operation phase of the steel rotor FESS and the composite rotor FESS. In standby mode, the GHG emissions for the steel rotor FESS are about 19 kg-CO₂eq/MWh higher than for the composite rotor FESS due to higher electricity requirements to compensate for the loss. GHG emissions in the material production phase are 7.7 kg-CO₂eq/MWh and 17.9 kg-CO₂eq/MWh for the steel rotor FESS and the composite rotor FESS, respectively. The higher GHG emissions in the case of the composite rotor FESS are due to the energy-intensive composite material production process. To produce one kg of carbon fiber composite, about 36% more GHGs are emitted than for the 4340 steel alloy. The GHG emissions in the manufacturing phase are 19.1 and 1.7 kg-CO₂eq/MWh, respectively, for the steel rotor FESS and the composite rotor FESS. The manufacturing phase of the steel rotor FESS is more GHG-intensive than that of the composite rotor FESS. About 92% of the manufacturing GHG emissions are from the manufacturing of the steel rotor; the manufacturing of the composite rotor makes up 47% of the manufacturing GHG emissions. The contribution of transportation is negligible. The EOL includes dismantling, recycling, and landfilling. Most of the GHG emissions in this phase are from energy use in the recycling of metals. The GHG emissions in the EOL for the steel rotor FESS and the composite rotor FESS are 3.1 kg-CO₂eq/MWh and 2.9 kg-CO₂eq/MWh, respectively. The steel rotor FESS has slightly higher emissions because of the heavy weight of the steel rotor. The EOL contributes 3-6% to the life cycle GHG emissions.

Electricity is the main source of energy used in material production, manufacturing, and other life cycle stages. The GHG emissions in electricity use contribute 82-89% to the total life cycle GHG emissions for steel rotor FESSs, while this contribution for composite rotor FESSs is 52-75%. Alberta grid mix electricity was considered in this study. Alberta's electricity emission factor is high (590 kg-CO₂eq/MWh) because coal and natural gas are the main sources of energy [367]. The overall GHG emissions could be lower if high renewable shares are considered. For example, when the provinces of British Columbia and Manitoba are considered, GHG emissions could be reduced by 18.7 kg-CO₂eq/MWh and 1.3 kg-CO₂eq/MWh for the steel rotor FESS and the composite rotor FESS, respectively. The reduction is much lower for the composite rotor FESS because of its relatively lower energy consumption in the manufacturing phase. Slight adjustments in the model are required to reflect the GHG emissions for other locations. The electricity emission factors for Canadian provinces can be found in Table E.4 of Appendix E.

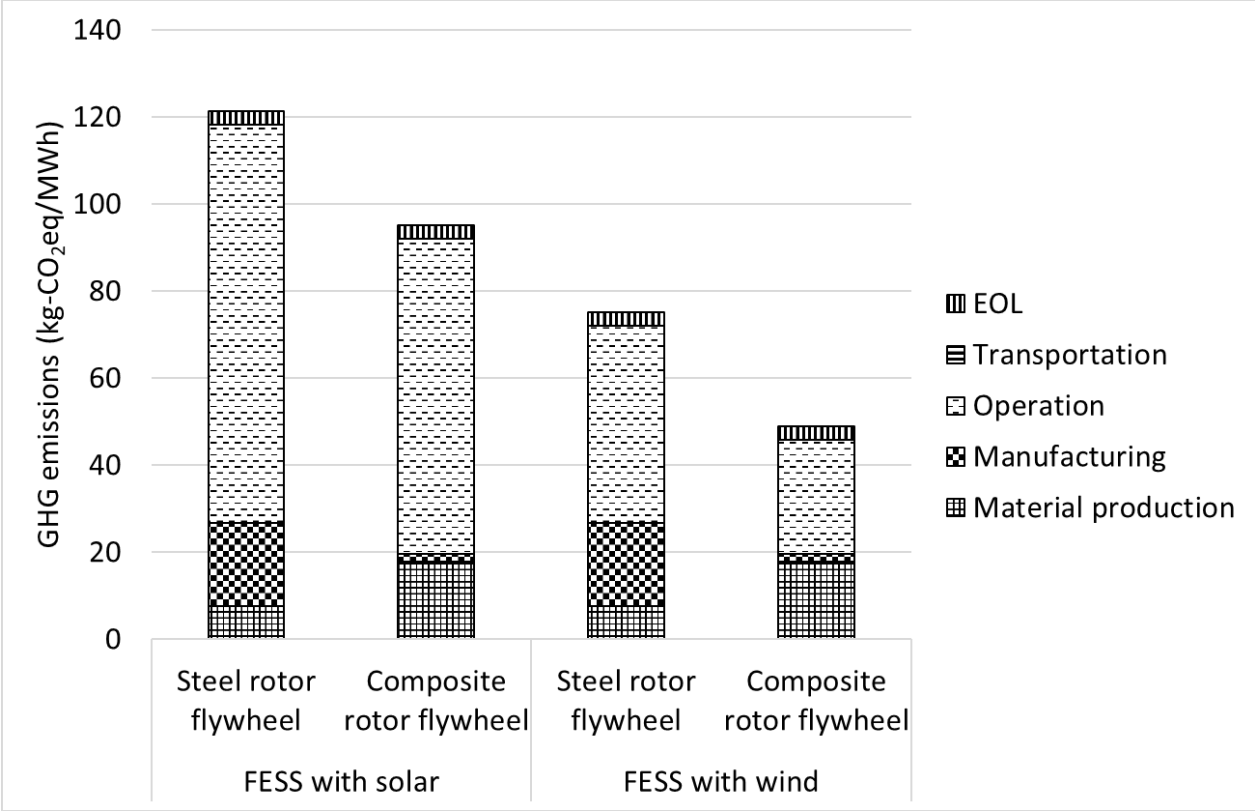


Figure 6.4: Life cycle GHG emissions of FESSs

The GHG emissions of FESSs were compared with the emissions of other storage technologies for similar applications. The GHG emissions in the operation phase depend on the source of electricity, which differs depending on the location of the storage plant. Instead, we compared the GHG emissions from cradle-to-gate (excluding operation) to provide insight into the performance of different ESSs. Figure 6.5 shows a comparison of the cradle-gate GHG emissions of different ESSs in frequency regulation. Most of the LCA studies assessed mature technologies, such as pumped hydro, compressed air, and thermal energy storage systems. Few considered electro-chemical ESSs. Among ESSs, electro-chemical ESSs are suitable for frequency regulation. Although a few studies evaluated the life cycle GHG emissions of different electro-chemical ESSs, only Hiremath et al. [258] provided cradle-to-gate separate results, which we used for comparison.

FESSs have lower GHG emissions than electro-chemical ESSs in frequency regulation applications with 15 min discharge. The main problem with electro-chemical ESSs is their short lifetime. Hiremath et al. give a lifetime of 8.5-11.5 years. For the same application, a FESS has a lifetime of 20 years. Another important reason for lower GHGs in FESSs is that they use mostly metal and composite materials, though the batteries use several GHG-intensive chemicals, such as cathode material (comprised of nickel, cobalt, and manganese) for lithium-ion (Li-ion), β -alumina for sodium-sulfur (Na-S), and V_2O_5 for vanadium redox flow battery (VRFB). For example, the GHG emissions in Li-ion cathode production are 5 times higher compared to the emissions in steel production. It makes steel rotor FESSs less GHG-intensive than Li-ion [488]. Among the electro-chemical ESSs, Li-ion and Na-S have lower GHGs than PbA because of their longer cycle lives. The cycle lives of Na-S and Li-ion are 2.6 and 8.2 times longer than those of PbA batteries [258].

Although FESSs are cleaner than electro-chemical ESSs, they have some challenges including energy loss due to friction and high composite material cost. The development and commercialization of composite materials are crucial in reducing the overall system cost. Research is being conducted to reduce friction loss and improve the discharge duration of flywheels. Amber Kinetics developed a FESS that can discharge for 4 h which will allow it to be used for energy applications [331].

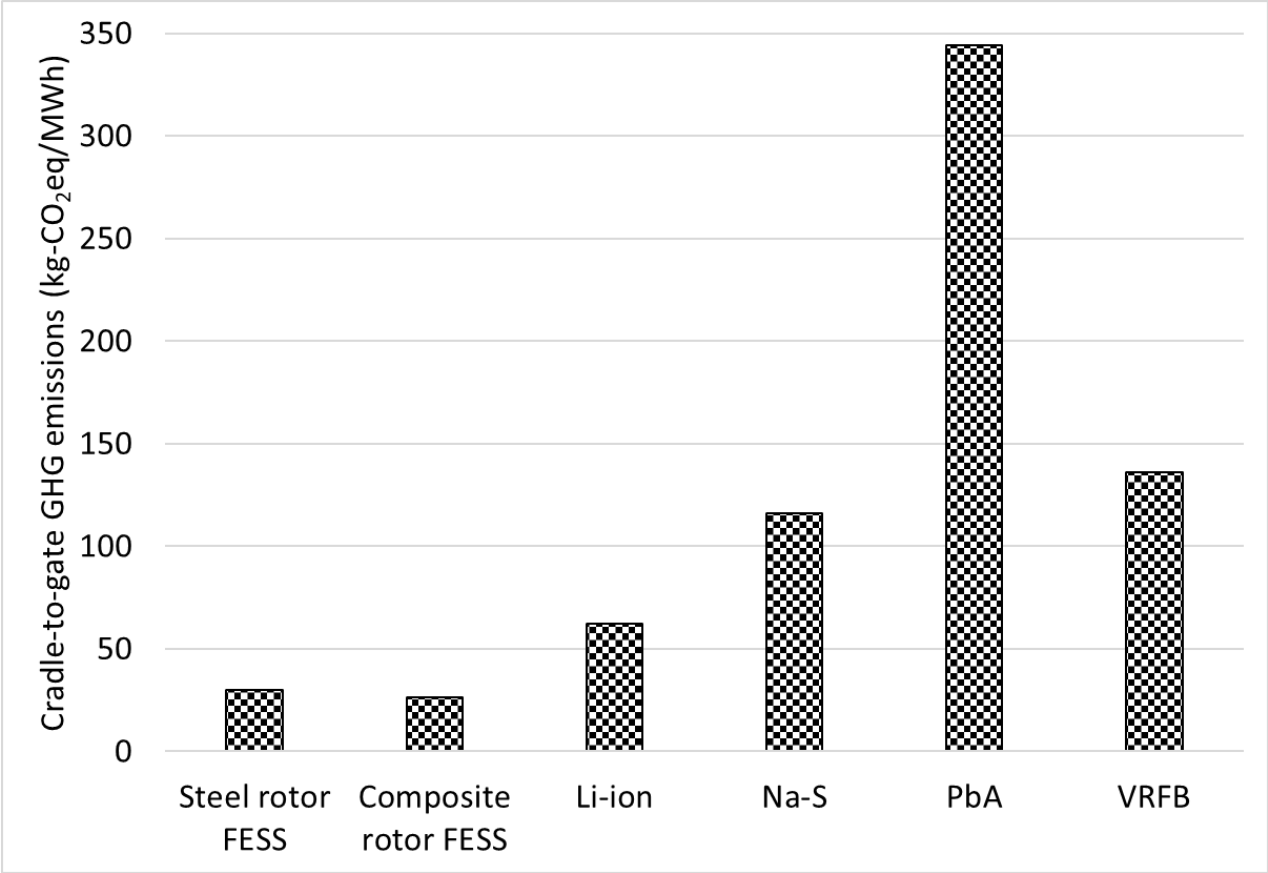


Figure 6.5: Cradle-to-gate GHG emissions for various energy storage technologies used for frequency regulation.

[Note: FESS: flywheel energy storage system, Li-ion: lithium-ion, Na-S: sodium-sulfur, PbA: lead-acid, and VRFB: vanadium redox flow battery]

6.3.3. Sensitivity and uncertainty analyses

The results discussed in the previous sections were based on default inputs and assumptions. To evaluate the uncertainties in the assumptions and data used, a range for each input was considered in the sensitivity and uncertainty analyses. We identified the most influential input parameters in the sensitivity analysis and used these parameters in the uncertainty analysis to obtain the probable

ranges of NER and life cycle GHG emissions. The results of sensitivity and uncertainty analyses are discussed in this section.

In the Morris sensitivity analysis, the parameters with high mean and standard deviation have the largest impact on the results. The most influential parameters for the NER of a steel rotor FESS are standby loss, the number of cycles, and energy demand for solar/wind plants. This is obvious, as all of these parameters are related to the operation phase, which contributes greatly to the life cycle energy use. The efficiency of the PCS, tensile strength of rotor material, and safety factor have a moderate impact on the NER. Other parameters such as energy requirements in landfilling and transportation distance are considered non-influential because of their low mean and standard deviation in the Morris analysis. A similar trend was found for the composite rotor FESS's NER. For the GHG emissions of a FESS, the influential parameters are the electricity emission factors (grid, solar, and wind), standby loss, number of cycles, flywheel and PCS efficiency, and safety factor. An example of sensitivity analysis for life cycle GHG emissions is shown in Figure E.2 in Appendix E.

The uncertainty analysis was performed using the minimum, most likely (defaults in the model), and the maximum values of each input variable (see Table E.5 in Appendix E). Figures 6.6 and 6.7 show the uncertainty analysis results for the NER and life cycle GHG emissions, respectively. The NERs of a steel rotor FESS range from 1.6 to 3.2 and 2.1-5.0, respectively, with solar and wind electricity. The corresponding values for a composite rotor FESS are 1.7-3.5 and 2.3-6.0. Because of the overlaps in the NERs of a steel rotor FESS and a composite rotor FESS, it is not possible to say which one has better performance, however, the mean values indicate that a composite rotor FESS has a slightly higher NER. Energy demand in solar and wind plants is the

most influential parameter in the uncertainty analysis of the NER. The other influential parameters are standby power loss, the number of cycles, the factor of safety, and efficiency of the PCS.

The GHGs of a steel rotor FESS range from 70.7 to 196.3 kg-CO₂eq/MWh and 30.0-100.1 kg-CO₂eq/MWh, respectively, with solar and wind electricity (Figure 6.7). The corresponding values for a composite rotor FESS are 69.2-181.1 kg-CO₂eq/MWh and 31.5-75.5 kg-CO₂eq/MWh. There are overlaps in the GHG emissions of the FESSs, which makes the selection of a system difficult. The overlaps are mainly from the upstream electricity emission factors in the operation phase. The emission factors of solar and wind range from 26 to 183 kg-CO₂eq/MWh and 3-45 kg-CO₂eq/MWh, respectively. The grid emission factor also influences the results. The third most sensitive parameter is the standby energy consumption in a steel rotor FESS. This parameter alone can change the emissions from 114.2 to 138.2 kg-CO₂eq/MWh and 49.8-73.5 kg-CO₂eq/MWh, respectively, for a steel rotor FESS using solar and wind. For the composite rotor, however, along with solar, wind, and grid emission factors, the safety factor, number of cycles, and flywheel and PCS efficiencies can influence the results. If the mean values (yellow dots) are considered, a composite rotor FESS has comparatively lower life cycle GHG emissions.

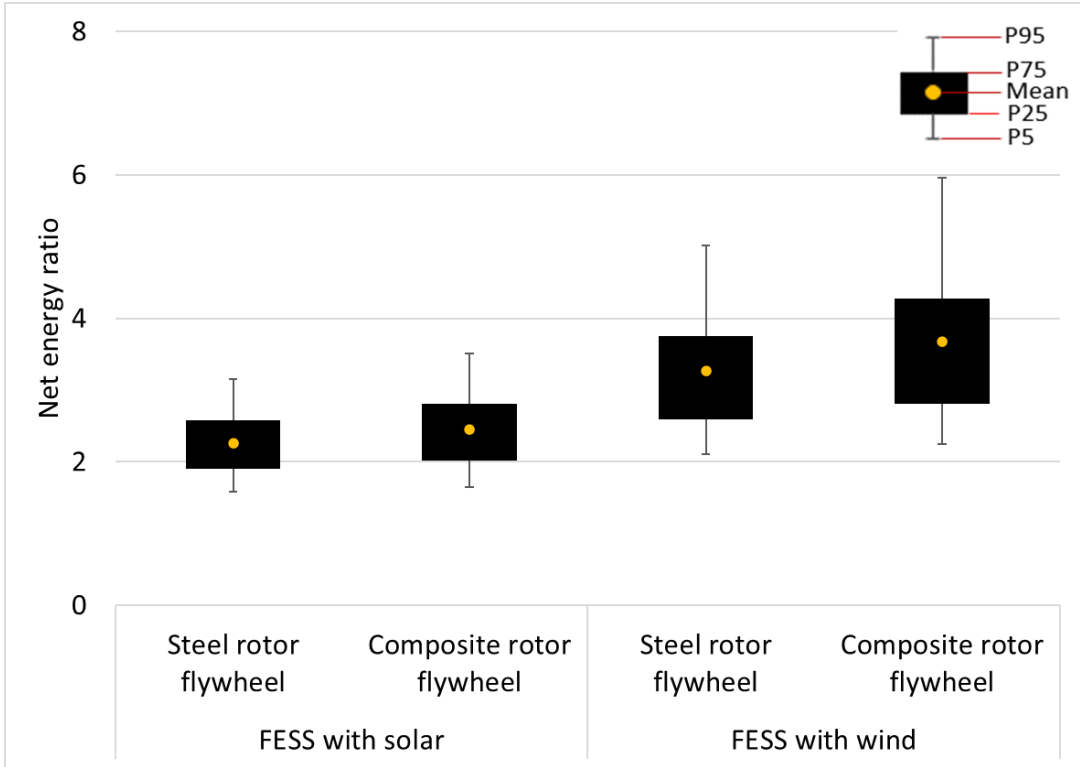


Figure 6.6: Uncertainty analysis for the net energy ratio

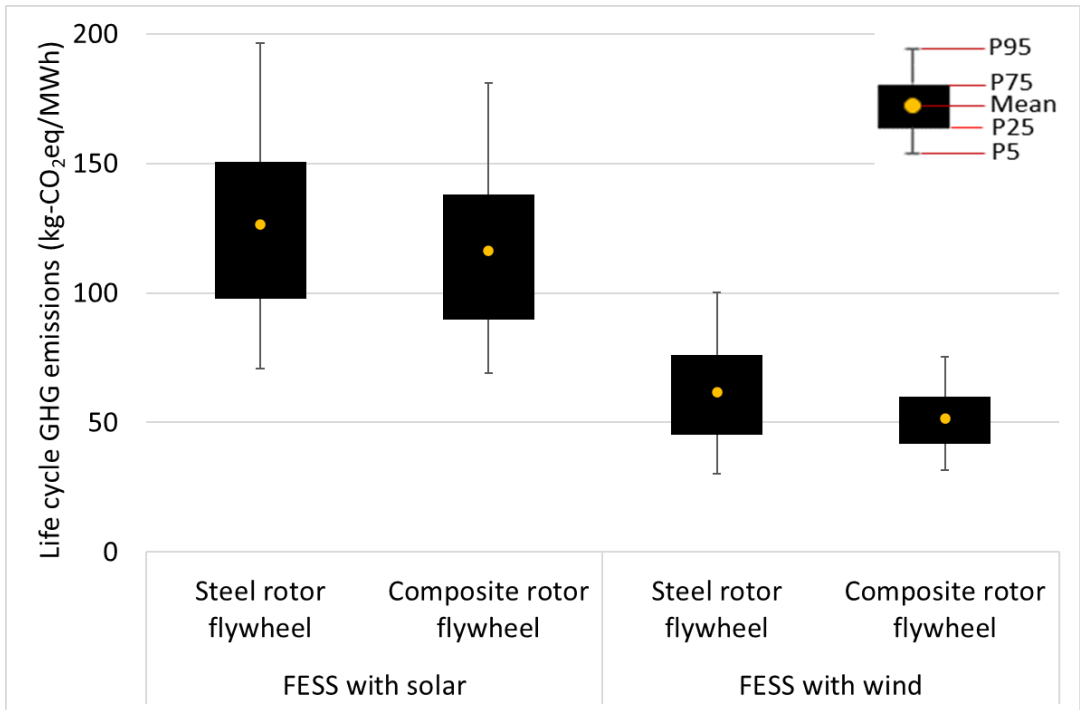


Figure 6.7: Uncertainty analysis for the life cycle GHG emissions

6.4. Conclusion

Environmental and energy performance indicators are an important part of the investment decisions prior to the deployment of utility-scale flywheel energy storage systems. There are no published studies on the environmental footprints of FESSs that investigate all the life cycle stages from cradle-to-grave. This study quantifies the net energy ratio and life cycle GHG emissions of two configurations of FESS, steel rotor and composite rotor, for utility applications of 20 MW capacity and 15 min discharge. A data-intensive model was developed to design the system components and to develop material and energy inventories for the life cycle stages from material production to end-of-life. Then, the material and energy inventories were translated to the NER and life cycle GHG emissions using the appropriate energy and emission factors. Finally, sensitivity and uncertainty analyses were conducted to handle the variability in the model.

Depending on the electricity source, the net energy ratios of steel rotor and composite rotor flywheel energy storage systems are 2.5-3.5 and 2.7-3.8, respectively, and the life cycle GHG emissions are 75.2-121.4 kg-CO₂eq/MWh and 48.9-95.0 kg-CO₂eq/MWh, respectively. The base case results show that the composite rotor FESS has lower GHG emissions than the steel rotor FESS. The use of composite material reduces the overall GHG emissions, however, the life cycle cost of the composite rotor FESS is higher than steel rotor FESS, which results from the high cost of composite material.

Operation is the most energy- and GHG-intensive stage. GHG emissions in this phase are higher in a steel rotor FESS because of its comparatively higher standby loss. The second largest contribution comes from manufacturing for a steel rotor FESS and material production for a composite rotor FESS. The emission factors of solar, wind, and grid, the number of cycles, and the factor of safety are among the few sensitive parameters that can impact GHG emissions. This

study provides information to understand the environmental performances of FESSs that could be useful for their integration into electricity networks. In addition, this study facilitates the comparison of various short-duration energy storage technologies.

Chapter 7: The development of a techno-economic model for assessment of cost of energy storage for vehicle-to-grid applications in a cold climate¹⁰

7.1. Introduction

Renewable energy systems are increasingly replacing fossil fuel-based power generators in an effort to decarbonize the power sector [338]. Policy initiatives undertaken by many countries have helped electric vehicles (EVs) replace conventional vehicles run by carbon-based fuels [493, 494]. In recent years, the number of EVs has increased substantially, from 1.2 million in 2016 to 6.8 million in 2020 [495]. It is projected that the EV market will reach about 120 million by 2030 [32]. This drastic increase will put a significant load on electricity grids, impacting their daily operations, and, as a result, electricity costs will increase [33]. The combined effects of increased renewable penetration and a large number of EVs in electricity networks will result in a power imbalance between demand and supply [34]. Therefore, problems such as frequency variation and voltage fluctuation will occur, which can harm an electricity network's economic and stability performances [35, 36]. One way to manage these problems is to use EVs as aggregated energy storage systems (ESSs), transforming them from electric loads to energy resources. Robledo et al. found that 95% of the time, EVs are in parking lots [496], and therefore they can be used to sell their energy to the electricity network [497]. An EV can be used as energy storage to provide several services to the electricity network including frequency regulation [17], energy arbitrage [18], load-leveling [19], etc. The connection between the grid and EVs can be facilitated through vehicle-to-grid (V2G) technology.

¹⁰ A version of this chapter has been submitted as Rahman MM, Gemechu E, Oni AO, Kumar A. The development of a techno-economic model for assessment of cost of energy storage for vehicle-to-grid applications in a cold climate to Energy.

V2G allows bi-directional flows of energy from an EV to the grid and from the grid to an EV [498]. An EV can receive energy from the grid to charge its batteries and can discharge electricity back to the grid when required through a bi-directional power converter. In recent years, with the development of the EV industry, V2G has become a prominent research area. Numerous studies have been conducted on different aspects: V2G chargers with bi-directional power flow capabilities [499, 500], power management and optimization [501, 502], and the influence of V2Gs on the electricity network [503]. These studies are important to understand the technical parameters and design of V2G systems and their operations. However, techno-economic feasibility studies are necessary from the EV owner's and utility company's perspectives to make informed decisions regarding the use of V2G systems.

To understand the techno-economic feasibility of V2G technology, three key research questions should be addressed: What is the minimum selling price of electricity considering all the incurred costs? What are the important parameters that affect the economic performance of the V2G system and to what extent? How does the V2G system compare with different stationary battery storage systems? A few studies attempted to answer these questions. Noori et al. [37] assessed the emissions reduction potential and net revenue of a V2G system for five independent system operators in the United States. Zhao et al. [38] considered the same system operators and evaluated the V2G's net present revenue and greenhouse gas (GHG) emissions savings. Both studies evaluated revenues for regulation services and found that EVs can be profitable. Huda et al. [504] performed techno-economic and GHG emissions assessments of V2G integration in an Indonesian grid for a load-leveling service and found such the integration to be profitable. A V2G feasibility assessment was conducted by Gough et al. [33]. The authors estimated the return on investment and net present worth of the V2G system for several grid applications. Rodríguez-Molina et al.

[39] developed a cost-benefit model for a V2G system and found that EVs can generate revenue by selling electricity to the grid. The economic impact of applying a V2G system in a microgrid setting was studied by Koubaa et al. [505]. The authors considered only the costs associated with battery degradation and found that microgrid operation costs could be reduced by implementing a V2G system. Ríos et al. [506] built a net cash flow model to assess the net cost of a fleet of trucks connected to the grid using a V2G system. Although current research provides some information on various cost items, including battery degradation cost, V2G infrastructure cost, and overall profit/loss, there are several limitations.

First, most studies conducted regional assessments by calculating the revenue generated from selling electricity to specific locations/grids. The results of these studies are limited in application because each location has a different electricity rate structure. Therefore, even if V2G generates a profit by selling electricity in a specific location, it does not necessarily mean a similar system in another location would also generate profit. In addition, there is no common indicator that can be used to compare the economic performances of V2G applications with stationary battery storage systems. The levelized cost of storage (LCOS), an economic performance indicator, needs to be developed for V2G technology. The advantage of this indicator is that it does not use any location-specific profit/loss function but indicates a price that should be applied to cover all the expenses over the lifetime of a system and can be used as a location-independent performance indicator [11, 331]. It also facilitates the comparison of V2G with other widely used battery storage systems.

Second, the impact of extremely cold weather on the V2G system's economic performance has not been evaluated in these earlier studies. According to Donkers et al. [40] and Yuksel and Michalek [41], extremely cold weather can adversely influence an EV's performance. This is mainly because cold temperatures reduce battery capacity significantly, thus reducing battery

efficiency and increasing energy consumption (to heat the vehicle cabin). To the best of the author's knowledge, no study considers extreme cold weather conditions to evaluate the LCOS for V2G applications.

Finally, the impacts of various design and economic parameters on the results have not been fully studied even though existing studies used a wide range of data and assumptions. For example, due to market competition and reduction in raw material cost, the lithium-ion (Li-ion) battery price is expected to decline rapidly, therefore this aspect should be considered as the battery replacement cost is an important factor that influences the overall system cost. Similarly, battery life and efficiency can vary widely by manufacturer and type [435], and this can influence the findings. Therefore, instead of point estimates, a probable distribution of outputs needs to be presented considering the uncertainties in input parameters.

To address these concerns, we developed a spreadsheet-based model to evaluate the techno-economic feasibility of V2G technology. A case study for Canada, which has a colder climate, was conducted. A performance indicator, LCOS, was calculated for cold weather conditions in four Canadian provinces, Alberta, Ontario, British Columbia, and Quebec. Two grid applications, energy arbitrage and frequency regulation, were assessed given their importance in electricity grids. Although Canada's cold climate conditions are considered as a base case, the model used a wide range of ambient temperatures to study the impact of the LCOS. The specific objectives of this research are to:

- Evaluate the amount of electricity available for vehicle-to-grid applications;
- Develop a data-intensive techno-economic model to estimate the levelized cost of storage in energy arbitrage and frequency regulation;
- Study the impact of ambient temperature on the performance of vehicle-to-grid technology;

- Compare the levelized cost of storage of vehicle-to-grid technology with that of other electro-chemical energy storage systems; and
- Conduct sensitivity and uncertainty analyses to understand the impacts of various input parameters on the levelized cost of storage.

7.2. Methods

Figure 7.1 shows the four-stage methodological framework developed in this study. Vehicle-to-grid technical analysis requires first defining the V2G technology and its applications in the electricity network. The energy available in the EV batteries for the V2G applications was calculated in this stage using the battery capacity and energy required for a daily commute. All cost items, such as capital, charging, and battery degradation costs, were estimated using the technical and cost parameters presented in Figure 7.1. All of these cost items were used in a discounted cash flow (DCF) analysis to calculate the levelized cost of storage. The techno-economic model developed in this study handles a large amount of data from various sources. To increase the reliability of the model, we conducted sensitivity and uncertainty analyses to identify the most influential input parameters and provide a probable distribution of the LCOS. The following section discusses each stage of the framework in detail.

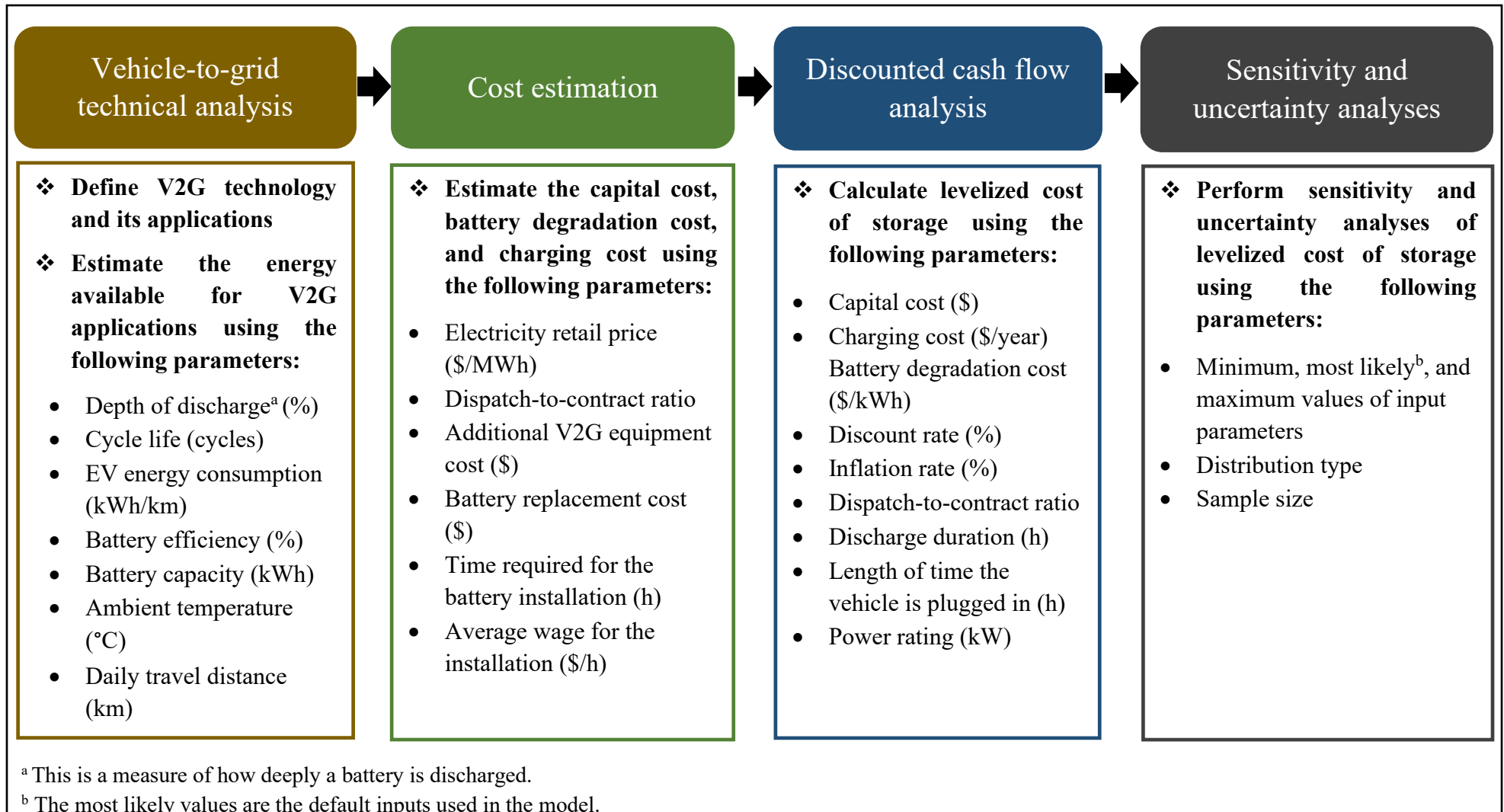


Figure 7.1: Vehicle-to-grid (V2G) techno-economic assessment framework

7.2.1. Vehicle-to-grid technical analysis

V2G systems are becoming increasingly popular with the increased use of EVs. As shown in Figure 7.2, V2G technology allows for bi-directional energy flow between the EV and the grid. The amount of energy remaining in the EV battery after a daily commute can be sold to the electricity grid during periods of high demand. In this way, an EV can be transformed into an energy resource for a grid operator. When electricity demand is low (i.e., during the night), an EV can be charged to its available battery capacity. There are three components required for V2G integration: a metering system to trace the flow of electricity, a power connection to the electricity grid, and a control unit that allows communications between the vehicle and the grid [507]. A bi-directional power converter alters alternating current to direct current to charge the batteries and direct current to alternating current to supply electricity to the grid.

Similar to stationary electro-chemical battery storage systems, an EV can be used for long- and short-duration applications as a mobile ESS [507, 508]. Usually, short-duration applications have a discharge duration of less than 15 minutes, while long-duration applications can have 4 or more hours of discharge [28]. Because energy arbitrage and frequency regulation are among the most popular long- and short-duration grid applications, respectively, we considered those applications to assess the techno-economic feasibility for the V2G system. Energy arbitrage involves charging the batteries when electricity demand is low and discharging them during high demand. The short-duration application, frequency regulation, is used to maintain the frequency of the grid by matching load and electricity production for a short period.

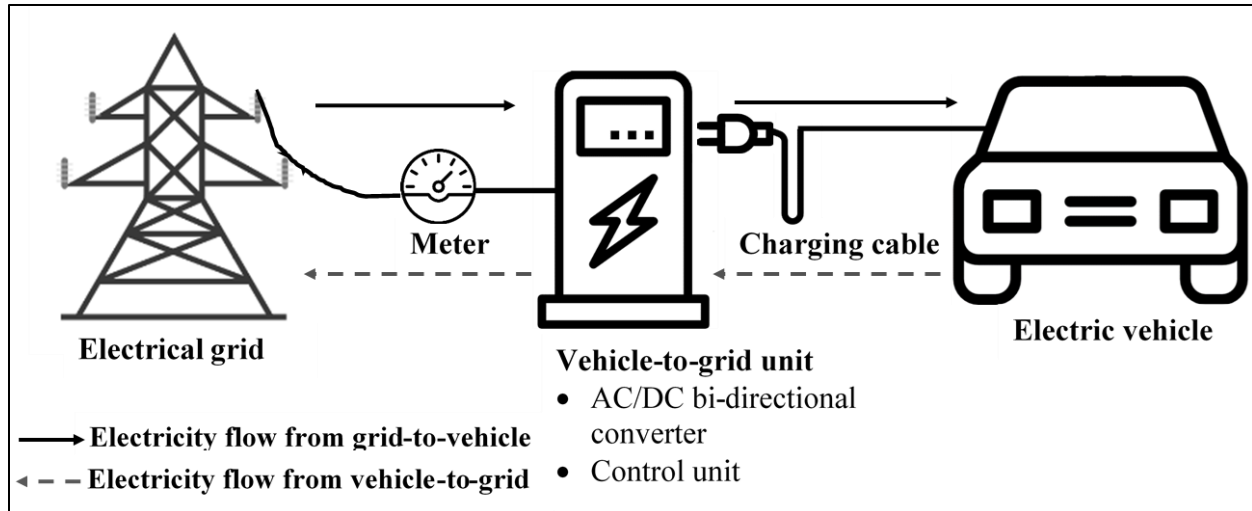


Figure 7.2: Schematic of a vehicle-to-grid system

The energy available for V2G applications depends on the remaining energy in the EV batteries after a daily commute. In Canada, drivers travel on average about 50 km/day [509]. Another important factor in determining the available energy is the depth of discharge (DOD). The DOD is a measure of how deep a battery can be discharged. To limit degradation, batteries are usually discharged at less than 100% of their capacity. The amount of energy available in EV batteries for V2G applications can be calculated using Equation 7.1, adapted from Gough et al. [33]:

$$E_{V2G} = E_B - E_B(1 - DOD) - (E_D D) \quad (7.1)$$

where E_{V2G} is the energy available for V2G applications (kWh), E_B is the EV battery capacity (kWh), DOD is the depth of discharge (%), E_D is the EV energy consumption (kWh/km), and D is the average distance driven (km).

An EV's energy consumption depends on weather conditions. The energy consumption data were taken from a study by Yuksel and Michalek [41] that considered actual vehicle performance under

different driving conditions. The ambient temperature plays an important role in determining the EV energy consumption because of its impact on both battery capacity and heating/cooling requirements inside the vehicle. Road and driving conditions also depend on the ambient temperature.

Table 7.1 presents the EV battery capacity, ambient temperature, and other technical parameters used for the techno-economic modeling. There is a wide variation in temperature throughout the year in Canadian provinces. Figure 7.3 shows the average temperature ranges in four Canadian provinces from 2010-2019. Although the average temperatures in each province were used for the base case, the minimum and maximum temperatures were also considered in the sensitivity and uncertainty analyses to study the impact of temperature on system performance.

Table 7.1: Technical parameters used for the techno-economic assessment

Parameter	Value	Source/comment
EV battery capacity (kWh)	24	Nissan Leaf’s battery capacity [510]. This vehicle has V2G capability.
Average distance travelled (km/day)	50	Canadians drive 50 km/day on an average [509].
DC-to-AC conversion efficiency	93%	Battery-to-grid efficiency [511].
AC-to-DC conversion efficiency	90%	Grid-to-battery efficiency [37].
Depth of discharge	80%	This can limit the degradation of the battery to an acceptable level [512, 513].
Total number of days of operation in a year	365	It was considered that the vehicle will discharge electricity every day [514].
Charging level	Level 2	Level 2 charging stations are commonly used in public parking and residential settings [515].

Parameter	Value	Source/comment
Discharge duration for energy arbitrage (h)	4	A reasonable assumption based on Alberta's on-peak and off-peak hours, and the availability of the vehicle.
Power capacity of V2G for energy arbitrage (kW)	2.2	Calculated from the energy available for V2G and the discharge duration.
Dispatch-to-contract ratio for frequency regulation	0.1	A ratio of energy dispatched to the multiplication of the contracted capacity and duration [507, 514].
Duration of the vehicle plugged in for frequency regulation (h)	6.3	Calculated from the energy available for V2G, the power delivered from V2G, and the dispatch-to-contract ratio.
Power capacity of V2G for frequency regulation (kW)	14.4	This is the contracted power, which is limited by the power of the connection line in the charging station, calculated from the current and voltage in the line. The voltage and current are 240 V and 60 A, respectively [516].

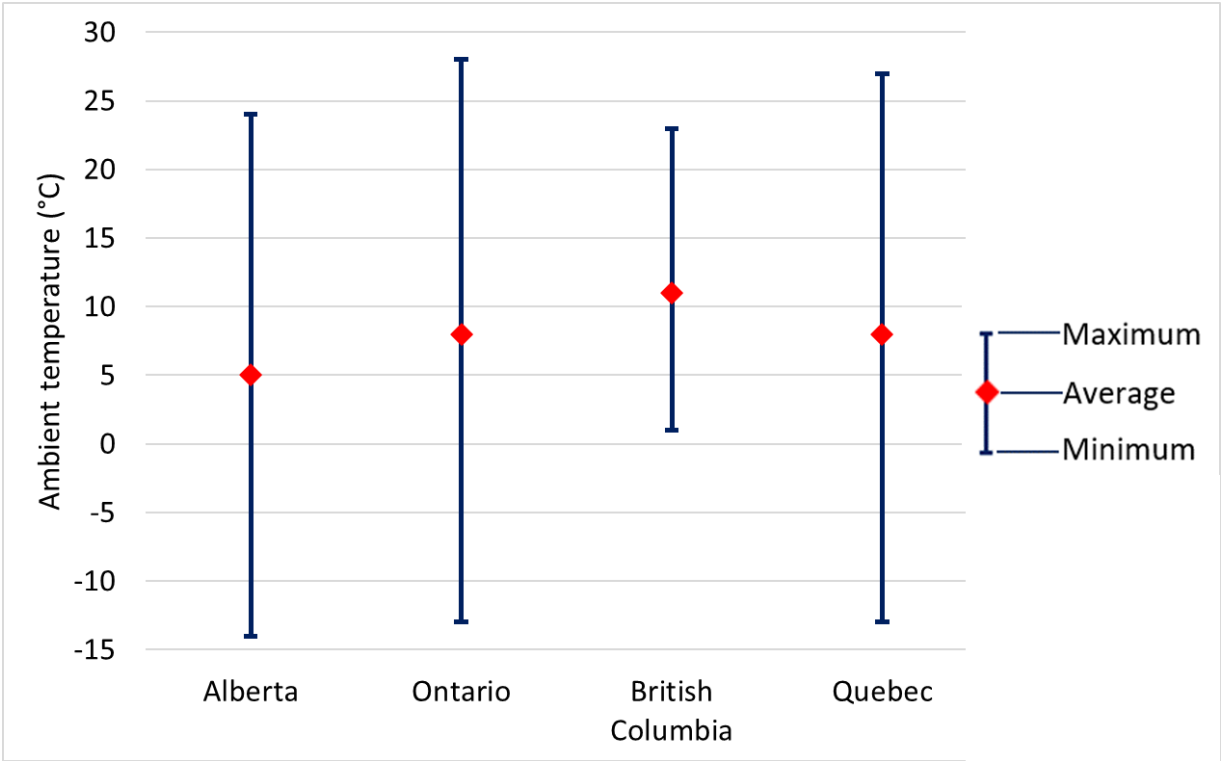


Figure 7.3: Temperature ranges in four Canadian provinces throughout the year. Values were estimated using information from a database [517]

7.2.2. Cost estimation

The main cost components of V2G storage are battery degradation, charging, and additional equipment capital costs. The parameters used to calculate these costs are given in Table 7.2. When an EV is used for V2G operations, the batteries degrade quickly because of this extra use in addition to transportation. Hence, batteries need to be replaced, and the frequency depends on the number of cycles the batteries go through for driving and V2G use. The degradation cost can be calculated using Equation 7.2, adapted from Tomić and Kempton [507]:

$$C_D = \frac{C_B + (W * t)}{L_C * E_B * DOD} \quad (7.2)$$

where C_D is the battery degradation cost (\$/kWh), C_B is the battery capital cost (\$), W average hourly wage for battery replacement (\$), t is the installation time (h), L_C is the number of cycles a battery can operate in its lifetime (calculated using Equation 7.3 [518]), E_B is the battery capacity (kWh), and DOD is the depth of discharge (%) used to calculate the L_C .

$$L_C = -5440.35 * \ln(DOD) + 1191.54 \quad (7.3)$$

An additional capital cost is incurred for the V2G equipment upgrade. This includes onboard power electronics, metering, and communication system upgrades [507]. The V2G capital cost for energy arbitrage was taken as \$571 (adjusted for 2021) for additional equipment [511]. For energy arbitrage, the revenue depends solely on the amount of electricity sold to the grid. The revenue generated from the frequency regulation service has two components: payments from selling energy and power (capacity). Therefore, maximizing power supply generates more revenue. In addition to onboard system upgrades, wiring upgrades are required for frequency regulation to deliver electricity at higher power. The total capital cost for the V2G equipment upgrade in the case of frequency regulation is \$2714 [511] (see Table 7.2 for details). Another cost component is the charging cost. We assumed that the batteries will be charged during the night using low-cost electricity. The charging cost was estimated from the electricity retail price and the charging efficiency. The average electricity prices from 2016-2020 in Alberta, Ontario, British Columbia, and Quebec were considered \$100, \$103, \$89, and \$57 per MWh, respectively¹¹ [519]. The charging cost can be calculated using Equation 7.4, adapted from our earlier study [331]:

$$C_C = \frac{E_P}{\eta_C} \quad (7.4)$$

¹¹ Edmonton, Ottawa, Vancouver, and Montreal are the cities considered for electricity prices in Alberta, Ontario, British Columbia, and Quebec, respectively.

where C_C is the charging cost (\$/kWh), E_P is the electricity price (\$/kWh), and η_C is the charging efficiency (%).

Table 7.2: Parameters used to calculate various cost items

Parameter	Value	Source/comment
Base year	2021	All the cost numbers were adjusted to 2021 USD.
Analysis period (years)	10	A typical lifetime of an electric vehicle [33, 520].
Discount rate	10%	Based on values reported for energy storage projects [31, 338].
Inflation rate	2%	Average inflation rate in Canada [338, 436].
Li-ion battery cost (\$/kWh)	139.74	Inflation adjusted value. The average price in 2020 was \$137/kWh. This price includes the battery cell and packs [521].
Installation time for battery replacement (h)	8	The installation time ranges from 8 to 10 h [514, 522]. The range was considered in the sensitivity and uncertainty analyses.
Average wage (\$/h)	31.76	The average hourly wage of an electrician in Alberta [523].
Capital cost for additional V2G equipment for energy arbitrage (\$)	571.30	Onboard additional cost due to power electronics, connections, communication system, and metering upgrades [514].
Capital cost for V2G additional equipment for frequency regulation (\$)	2713.67	Onboard additional costs and cost of wiring upgrade for a plug capacity of 15 kW [514]. This study used a line power of 14.4 kW (see Table 7.1).

7.2.3. Techno-economic model development

Once degradation, charging, and capital costs are estimated, a discounted cash flow analysis is performed to calculate the LCOS. The LCOS is the minimum electricity selling price to cover all the costs incurred throughout the analysis period [31]. The discount rate, inflation rate, and project lifetime used in the analysis are given in Table 7.2. The cost items used in the analysis include V2G equipment capital cost, which is a one-time fixed cost, and battery degradation and charging costs. We calculated annual degradation and charging costs, which can be expressed in \$/year. These two cost items were summed to calculate the total annual cost. The total annual cost for energy arbitrage and frequency regulation can be calculated using Equations 7.5 and 7.6, respectively:

$$\text{For energy arbitrage:} \quad T_{AC} = (C_D + C_C) * P_V * t_E \quad (7.5)$$

$$\text{For frequency regulation:} \quad T_{AC} = (C_D + C_C) * R_D * P_{FR} * t_F \quad (7.6)$$

where T_{AC} is the total annual cost (\$/year), P_V is the power delivered from the EV for energy arbitrage (kW), t_E is the total time of electricity delivery for energy arbitrage (h/year), R_D is the dispatch-to-contract ratio for the frequency regulation, $P_{FR}=P_{line}$ is the power capacity of V2G for frequency regulation (kW), and t_F is the total time the vehicle is plugged in (h/year).

A general expression for the LCOS was developed using the cost items discussed above and is shown in Equation 7.7:

$$LCOS = \frac{ECC * \frac{i(1+i)^n}{(1+i)^n - 1} + T_{AC}}{E_{out}} \quad (7.7)$$

where i is the real discount rate ($i = \frac{1+d}{1+f} - 1$), d is the nominal discount rate, f is the inflation rate, n is the project lifetime (year), ECC is the additional V2G equipment capital cost, and E_{out} is the amount of electricity delivered to the grid (kWh/year).

7.2.4. Sensitivity and uncertainty analyses

The techno-economic model developed in the study handles a range of input data. Some published studies show a wide range of data. Assumptions are made during model development; these differ from project to project and also on the location. To handle these variations, and to make a model reliable, sensitivity and uncertainty analyses are required. Sensitivity analysis can identify the parameters that most affect the results. The Morris method is a useful way to identify the key parameters that affect the results. The advantage of this method is that it accounts for interactions among the input parameters and considers their non-linear effects. Therefore, in this study, we used the Morris method to identify the most influential inputs. When the inputs have a range, it is necessary to predict a probable range for the outputs. To do that, a Monte Carlo simulation was conducted to present a probable distribution of the LCOS. Random samples were selected within the distribution of the input parameters and iterated 100,000 times to get the output distribution of the LCOS. The Morris sensitivity and Monte Carlo uncertainty analyses were carried out using a methodology developed in an earlier study [285]. Table 7.3 shows the inputs and their ranges used in the sensitivity and uncertainty analyses.

Table 7.3: The maximum and minimum values of the input parameters used in the sensitivity and uncertainty analyses

Input parameter	Unit	Minimum value	Maximum value
Average distance traveled	km/day	46 [524]	60 [524]
Battery round-trip efficiency	(%)	85 [106]	98 [106]
Depth of discharge	(%)	50 [522]	100 [507]
Ambient temperature	°C	-9 [517]	22 [517]
DC-to-AC conversion efficiency	%	90 [525]	95 [526]
Battery cycle life	Cycles	1500 [522]	4500 [513]
Electricity price	\$/MWh	55.7 [519]	127.3 [519]
Dispatch-to-contract ratio for frequency regulation	Dimensionless	0.08 [514]	0.1 [514]
Nominal discount rate	(%)	8 [338]	12 [338]
Inflation rate	(%)	0.94 [338]	2.91 [338]
Li-ion battery cost	(\$/kWh)	58 ^a [521]	150 [527]
Installation time for battery replacement	(h)	8 [514]	10 [514]
Average hourly wage for battery installation	(\$/h)	30.82 [523]	34.91 [523]

^a Predicted value for 2030 [521].

7.3. Results and discussion

This section presents and discusses the results of the techno-economic analysis of a V2G system. The effect of ambient temperature on the overall performance of V2G applications followed by the results of sensitivity and uncertainty analyses are also discussed.

7.3.1. Economic analysis

The annual life cycle costs, in \$/year, for energy arbitrage and frequency regulation are presented in Figure 7.4. The values range from \$594.02 (Québec) to \$782.35 (Ontario) and from \$911.04 (Québec) to \$1099.37 (Ontario) for energy arbitrage and frequency regulation, respectively. The annualized V2G equipment capital costs for energy arbitrage and frequency regulation are \$84.54/year and \$401.56/year, respectively. While both applications need power electronics, communication systems, and metering upgrades, an additional cost is incurred for frequency regulation because of wiring upgrades to supply electricity at comparatively higher power. For frequency regulation, it is desirable to achieve the highest possible power in the line because the revenue not only depends on the amount of electricity sold but also on the power the EV will supply. The battery degradation and charging costs depend on how much electricity is available in the EV batteries for the V2G applications, which ultimately depends on the weather conditions and the distance traveled by the vehicle. Considering a daily average travel of 50 km, the energy available in the EV batteries for the V2G applications is from 9.43-10.31 kWh, depending on the province where the vehicle is used. Moreover, when an EV is used for a V2G application, the batteries degrade faster because of this extra use in addition to transportation. The life of a battery depends on how deeply it is discharged. For an 80% depth of discharge, the number of cycles an EV battery can operate was calculated to be 2406 (see Equation 7.3). Usually, EV batteries are good for about 10 years [33]; however, because of the extra use for V2G applications, the lifetime is reduced to 6 years. Therefore, batteries need to be replaced more frequently. Battery degradation thus leads to battery capital and labor costs. Considering battery capital and installation costs, the replacement cost is \$3353.76. The battery degradation cost was estimated to be 8.4 cents/kWh with a lifetime electricity throughput of 42.95 MWh. The charging cost has a significant influence

on the overall economic performance of the V2G system. Although the EV batteries are used for transportation and V2G, we only considered charging the portion of batteries used for the V2G application. This is because transportation is not within the scope of this study, and including the transportation portion of the charging would lead to a higher charging cost. The charging cost varies widely depending on the electricity retail price, which depends on the electricity mix. In Canada, each province has its own electricity mix, and prices vary. Of the four major Canadian provinces considered in this study, Ontario has the highest electricity price at \$103.70/MWh and Quebec the lowest at \$56.74/MWh [519]. The base case total annual life cycle cost in Figure 7.4 is for Alberta with an electricity price of \$100.83/MWh [519]. The positive error bar represents the total annual life cycle cost considering the charging cost in Ontario. The negative error bar represents the total annual life cycle cost considering the charging cost in Quebec.

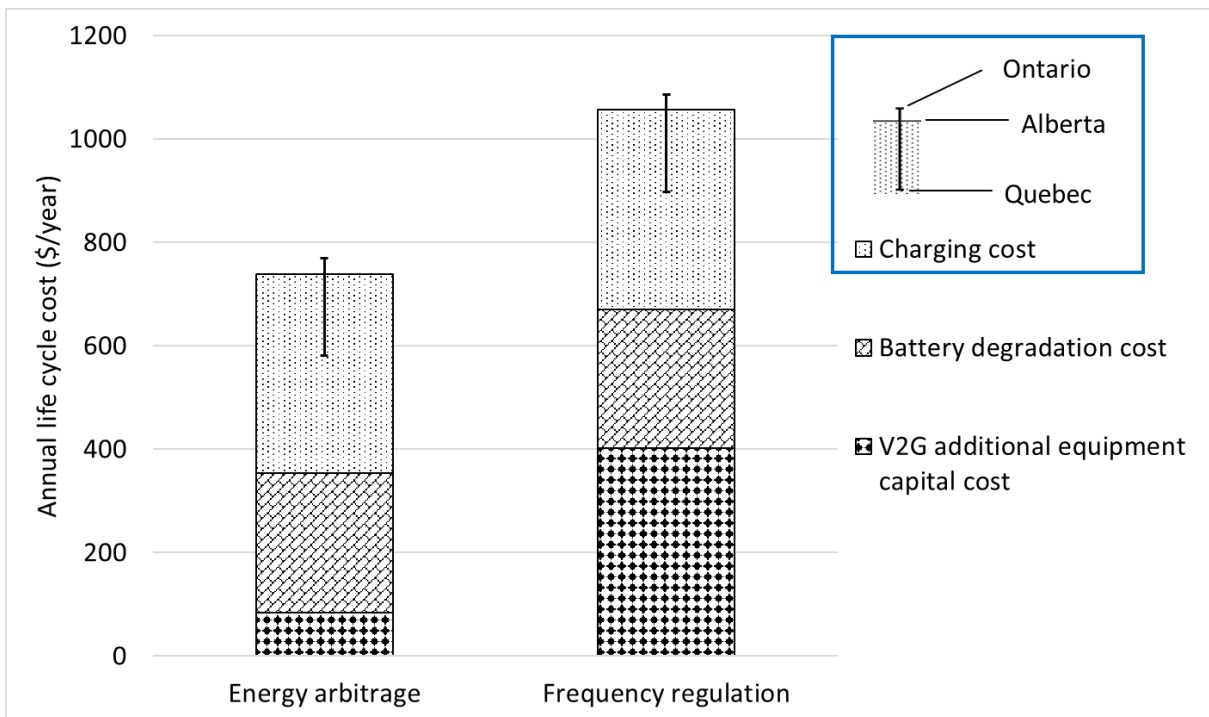


Figure 7.4: Annual life cycle costs for V2G applications

A common performance metric is necessary to compare a V2G system’s economic performance with other energy storage technologies. The levelized cost of storage is a widely used indicator against which energy storage systems’ performances are measured. It can be calculated from the annual life cycle cost and the amount of electricity delivered per year. Figure 7.5 shows the LCOS values for the two V2G applications in four Canadian provinces. The LCOS values range from \$176.97/MWh in Quebec to \$233.08/MWh in Ontario when the V2G system is used for energy arbitrage. When the V2G system is used for frequency regulation, the LCOS values range from \$271.42/MWh in Quebec to \$329.93/MWh in Ontario. The LCOS for frequency regulation is higher than energy arbitrage because of the higher V2G equipment capital cost. The LCOS varies by province mainly because of differences in electricity price and average ambient temperature (see Figure 7.3).

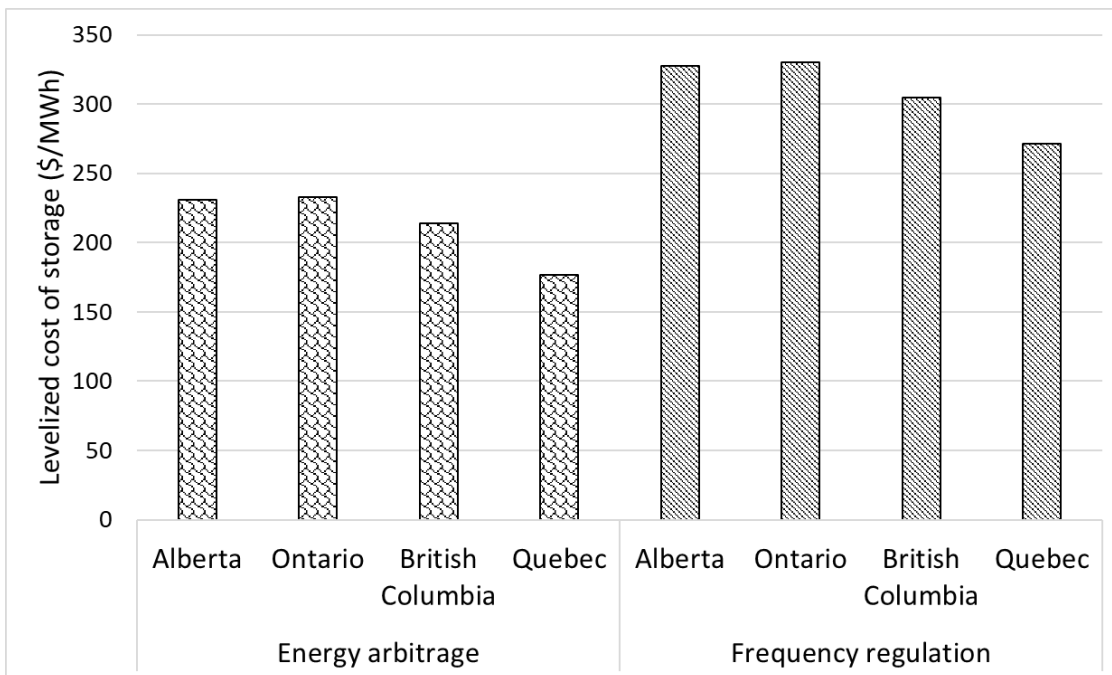


Figure 7.5: Levelized cost of storage in four provinces in Canada

The results obtained in this study were validated against the numbers presented in earlier studies. To the best of the author's knowledge, none of the earlier studies evaluated the LCOS for V2G applications. However, a few estimated the costs of V2G systems, which were used for comparison. The degradation cost estimated in this study is 8.4 cents/kWh, which is in the range reported by Shang and Sun [508] of 6.45-26.25 cents/kWh, depending on the cycles a battery operates in its lifetime. The battery degradation costs reported by Gough et al. [33] are 14-25 cents/kWh. This range is higher than ours mainly because of the difference in battery capital cost. Gough et al. considered £160/kWh (equivalent to \$219/kWh), which is much higher than the value we considered (see Table 7.2). The Li-ion battery price has dropped significantly recently, to \$150/kWh in 2019 [527] and \$137/kWh in 2020 [521]. The annual V2G equipment cost for energy arbitrage in this study was estimated to be \$84.54/year, which is close to the value reported by White and Zhang [522] of \$90/year. The charging cost solely depends on the electricity retail price, which is set by electricity operators and can vary widely by jurisdiction. In this study, we estimated the LCOS of Li-ion-based V2G applications' energy arbitrage and frequency regulation. In a recent study, we assessed similar applications for five stationary electro-chemical energy storage systems [338]. Figure 7.6 shows a comparison of the LCOS for V2G and stationary battery storage systems. The V2G system in this study uses a Li-ion-based vehicle [338]; therefore, the battery capital cost is based on the Li-ion battery price. As shown in Figure 7.6, there is not much difference in the LCOS values for V2G, Li-ion, and sodium-sulfur (Na-S) ESSs. Na-S and Li-ion have similar capital costs and cycle lives [338, 435]. V2G is economically more attractive than valve-regulated lead-acid, nickel-cadmium, and vanadium redox flow ESSs. These battery technologies have comparatively higher battery capital costs [338].

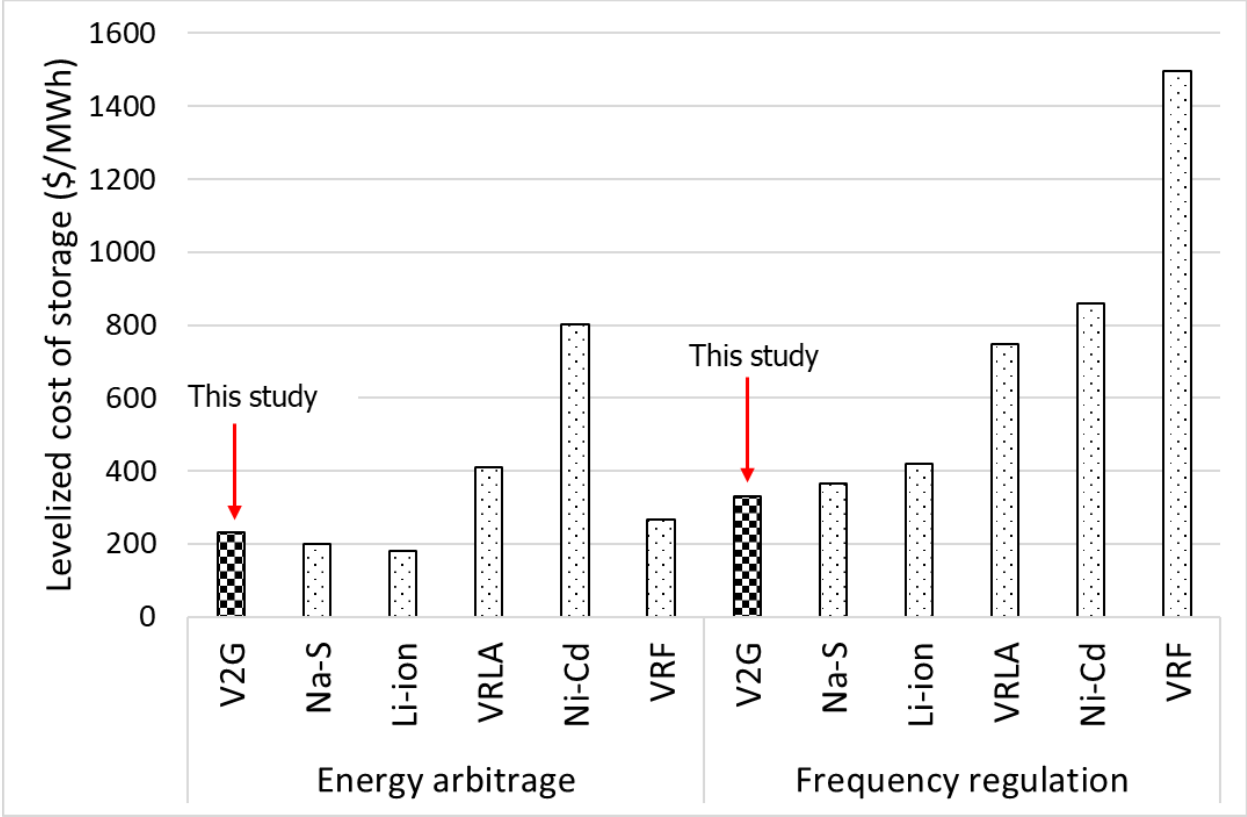


Figure 7.6: Levelized cost of storage for several battery energy storage technologies

(Note: V2G: vehicle-to-grid, Na-S: sodium-sulfur, Li-ion: lithium-ion, VRLA: valve-regulated lead-acid, Ni-Cd: nickel-cadmium, and VRF: vanadium redox flow)

7.3.2. Effect of ambient temperature on available energy

The effect of ambient temperature was studied for a wide range, from -30°C to 30°C. Although we considered cold weather conditions in four Canadian provinces, the framework developed in this study is valid for other jurisdictions. Ambient temperature has an impact on the battery capacity and electricity required for daily driving. The energy consumption per km depends on road conditions, cabin heating/cooling requirements, and battery efficiency. Extreme cold weather reduces battery efficiency significantly and increases energy consumption in the electric heater, which reduces the range of an EV. For example, at -30°C, 0.34 kWh electricity is required to travel

1 km, while only 0.17 kWh is required at 20°C. After 20°C, electricity consumption increases because of the cooling requirement in the vehicle cabin that is supplied by the vehicle air conditioner. Figure 7.7 shows the variation in available energy for V2G applications at ambient temperature. Although the base case results in this study represent a temperature range of 5°C to 11°C (the average temperature range in the selected Canadian provinces), we developed an equation to predict the available energy for V2G applications in various climate conditions. Equation 7.8 was developed to predict the electricity available for the V2G applications based on the ambient temperature. The equation has an R^2 value of 0.9963. When the temperature is extremely low, the LCOS decreases significantly because of a drastic reduction in energy delivered to the grid. For example, in the energy arbitrage scenario, the LCOS increases from \$227.35/MWh to \$311.61/MWh when the ambient temperature decreases from 20°C to -30°C in Alberta.

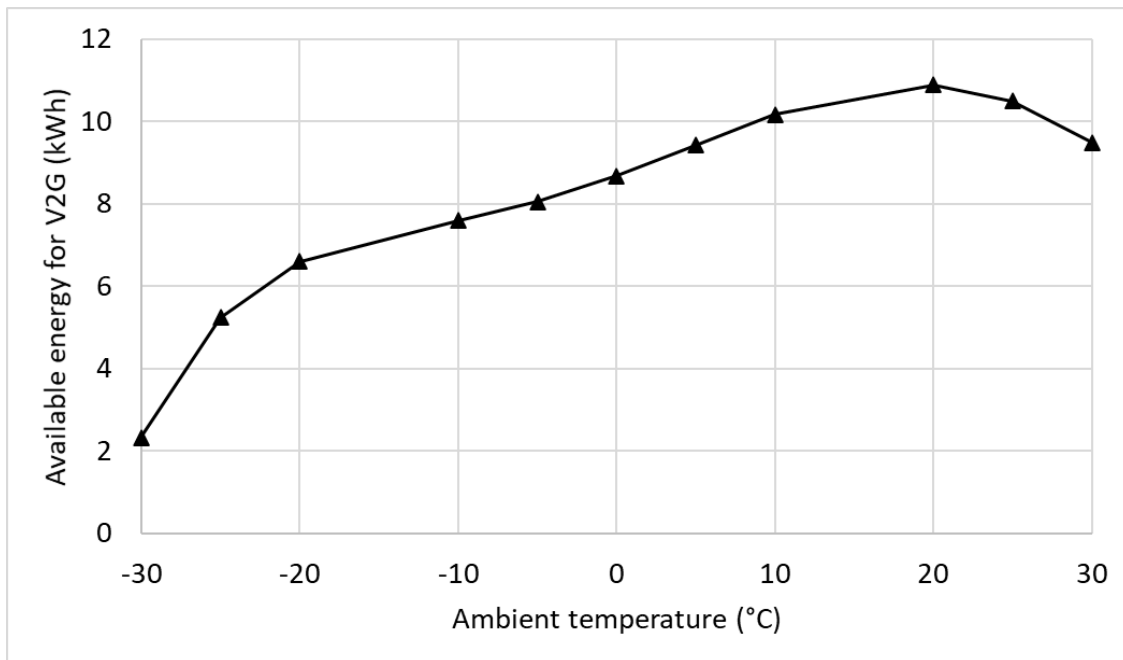


Figure 7.7: Effect of ambient temperature on electricity available for the V2G applications

$$E_{V2G}(T) = -6 * 10^{-6}T^4 + 8 * 10^{-6}T^3 + 0.0028T^2 + 0.1083T + 8.6761 \quad (7.8)$$

Here, E_{V2G} is the amount of energy available after the daily commute (kWh) and T is the ambient temperature ($^{\circ}\text{C}$).

7.3.3. Sensitivity and uncertainty analyses' results

Figure 7.8 shows the results of the Morris sensitivity analysis. The location of a parameter in the figure indicates how sensitive it is to the LCOS. The higher the Morris mean, the higher the sensitivity of the parameter to the LCOS. The Morris mean shows the change in the LCOS due to the change in the input from its minimum to its maximum value. The Morris standard deviation, on the other hand, indicates the interaction of an input with other inputs and its non-linear effects. The parameters with high Morris mean and Morris standard deviations, such as ambient temperature, battery cycle life, electricity price, distance traveled, and depth of discharge, have significant influence on the LCOS. Decreasing the ambient temperature and increasing the distance traveled both reduce the amount of energy available, and, hence, the LCOS increases. Although increasing the depth of discharge increases the energy available for V2G, the degradation cost increases because with a deeper discharge the lifetime of a battery decreases. Battery capital cost and cycle life, as well as electricity price, have a large influence on the LCOS. The parameters with lower mean and standard deviation, such as discount rate, inflation rate, and battery installation time, have an insignificant effect on the LCOS. Therefore, the effects of these parameters can be ignored. Figure 7.8 shows the sensitivity results for energy arbitrage; the frequency regulation sensitivity analysis shows similar trends.

The impact of the most influential parameters can be estimated through uncertainty analysis. A Monte Carlo simulation was performed using the input parameter values in Table 7.3 to provide a probable LCOS range. Figure 7.9 shows the results of uncertainty analysis. The LCOSs are from \$145.96/MWh to \$279.13/MWh for energy arbitrage and from \$250.06/MWh to \$434.17/MWh

for frequency regulation. Among the input parameters, depth of discharge and electricity price influence the distribution of the LCOS the most. For example, if the electricity price changes from \$55.70/MWh to \$127.30/MWh, the LCOS increases to \$248.20/MWh from \$166.0/MWh for energy arbitrage. This increase in LCOS is obvious because an increase in electricity price increases the overall annual life cycle cost, and, hence, the LCOS increases. Battery capital cost has also an influence on the LCOS. In recent years, the Li-ion battery price has decreased substantially. If the capital cost of Li-ion battery becomes \$58/kWh (projected value for 2030), keeping the other parameters the same, the LCOS can be reduced to \$182.10/MWh for energy arbitrage.

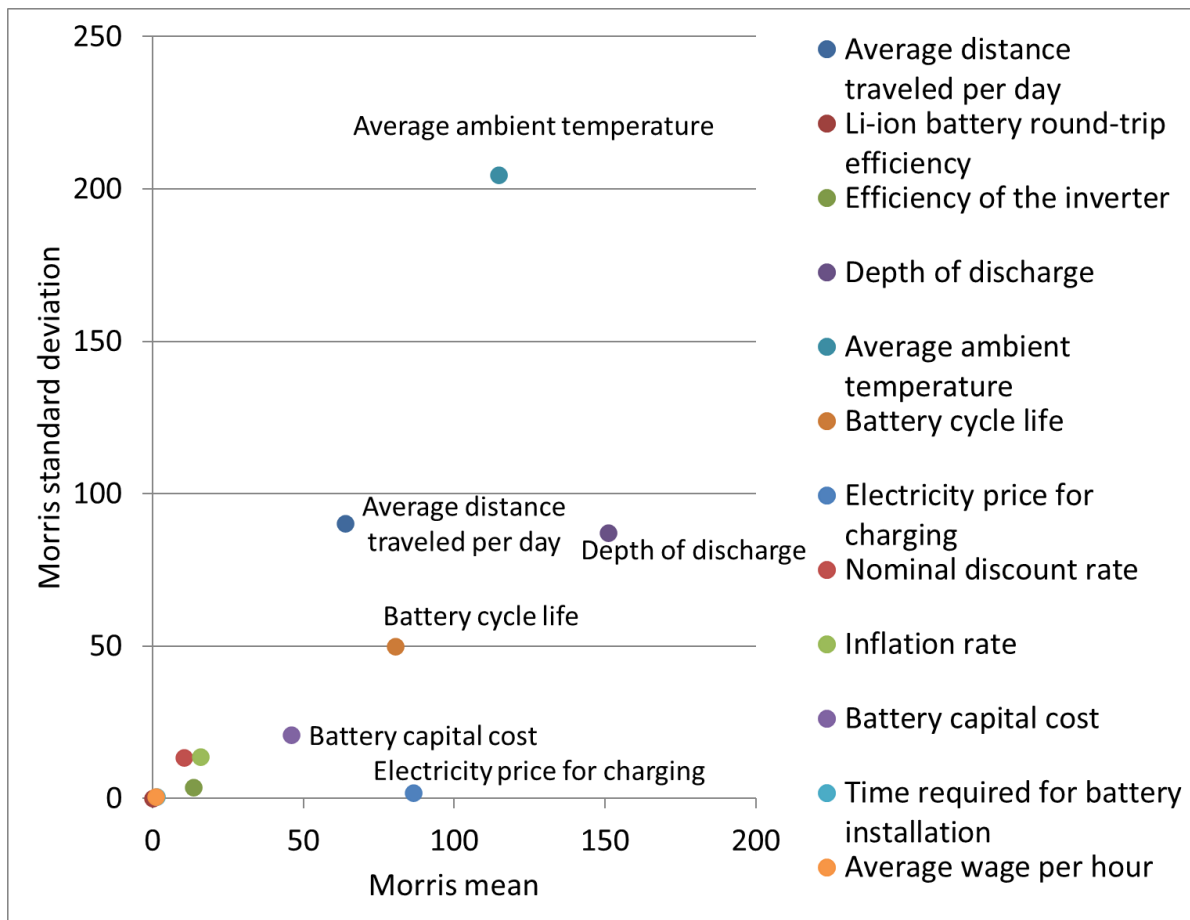


Figure 7.8: Sensitivity analysis for the levelized cost of storage for energy arbitrage

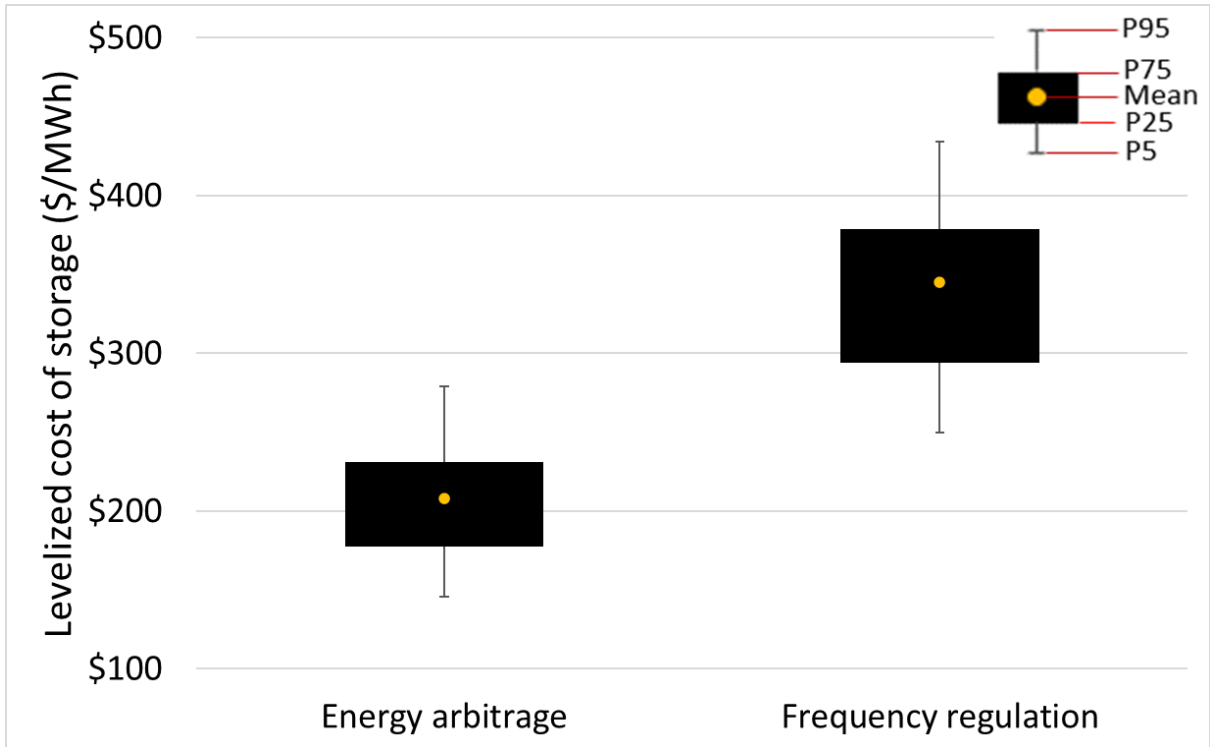


Figure 7.9: Levelized cost of storage uncertainty analysis

7.4. Conclusion

With increased renewable penetration in electricity grids, it seems obvious to use energy storage systems to handle the problems associated with high renewable fractions. Modern electricity networks use different types of stationary ESSs for a wide number of applications, such as energy arbitrage and ancillary services. Additional investment and maintenance are required for these storage systems. Because EVs are increasing significantly in the transportation sector, they can be used to provide services similar to what stationary energy storage provides to electricity networks. V2G is a system through which an EV can supply electricity to the grid when there is a need. A V2G system's economic performance needs to be measured against the commercial energy storage systems' performance to make informed decisions regarding its implementation. The LCOS and annual life cycle cost are critical performance indicators used to measure the economic

performance of energy storage systems. There is limited research on these indicators for a V2G system. In addition, the impact of ambient temperature and other critical parameters, i.e., battery depth of discharge on the overall system performance, has not been extensively studied. Therefore, to fill the gaps in the current research, we developed a techno-economic assessment model to calculate the LCOS for two important energy storage applications, energy arbitrage and frequency regulation. The amount of electricity available for the V2G applications was determined and then several costs, i.e., battery degradation cost, V2G equipment capital cost, and charging cost, were determined. The developed techno-economic model was used to calculate the annual life cycle cost and the LCOS. Detailed sensitivity and uncertainty analyses were performed to understand the impact of each input parameter on the LCOS and to estimate a probable distribution of LCOS. The LCOS values are \$230.88/MWh for energy arbitrage and \$329.93/MWh for frequency regulation based on the most likely inputs. The LCOS for frequency regulation is comparatively higher because of its higher capital cost due to V2G system upgrades. Ambient temperature has a significant impact on the amount of energy available for V2G applications. In extremely cold weather conditions, the available energy drops drastically because of the effect of low temperature on battery efficiency and cabin heating requirement. When the ambient temperature falls to -20°C from 10°C , the amount of energy available for V2G applications drops from 10.17 kWh to 6.60 kWh. The Morris sensitivity analysis shows that in addition to ambient temperature, battery cycle life, distance traveled per day, depth of discharge, battery capital cost, and electricity price are the parameters that most affect the LCOS. Reducing the price of Li-ion batteries will reduce the LCOS further in the near future. When we considered the uncertainty in the input parameters, we found the probable distribution of the LCOS to be \$146-\$279/MWh for energy arbitrage and \$250-\$434/MWh for frequency regulation. We found that the V2G storage system is economically

competitive with lithium-ion and sodium-sulfur energy storage systems. The results of this research will help to understand the techno-economic feasibility of the V2G system and to make a reasonable comparison of the economic performance of various energy storage systems for grid applications.

Chapter 8: Conclusions and recommendations for future research

8.1. Conclusions

Which energy storage system to use for a stationary application depends largely on its techno-economic and environmental performance. There are few evaluations of the techno-economic and environmental feasibility of electro-chemical and flywheel energy storage systems for utility-scale stationary applications. A systematic literature review of techno-economic assessments and LCAs of stationary energy storage systems was conducted to determine the economic and environmental feasibility of energy storage systems and identify research gaps, limitations, and areas for further investigation. Inconsistencies were found in defining the system boundary for cost and emissions assessment in the literature, which makes it difficult to make a reasonable comparison among energy storage technologies. There is very limited information on scale factors for electro-chemical and flywheel energy storage systems. In addition, generic databases were used for LCAs; no product-specific inventories were developed. The development of comprehensive scientific-principles-based techno-economic and LCA models was suggested to make a reasonable comparison of costs and environmental footprints of various ESSs. Bottom-up techno-economic and LCA models were developed for seven energy storage technologies: sodium-sulfur, lithium-ion, valve-regulated lead-acid, nickel-cadmium, vanadium redox flow, steel rotor flywheel, and composite rotor flywheel. The stationary application scenarios assessed in this study are bulk energy storage, transmission and distribution investment deferral, frequency regulation, and support of voltage regulation. A special case of an electro-chemical energy storage system, vehicle-to-grid, was also investigated to evaluate its techno-economic feasibility in Canadian cold weather conditions. The system components were designed, then cost functions were developed. This was followed by a discounted cash flow analysis to calculate the levelized cost of storage

(LCOS) in the techno-economic assessment. The LCA involves designing the system, building material and energy inventory, and translating material and energy to environmental impacts. The environmental impacts quantified in this study are the net energy ratio (NER) and life cycle GHG emissions. To improve the reliability of the models and results, detailed sensitivity and uncertainty analyses were performed to identify the most influential parameters and provide a probable range of results. Techno-economic and LCA models were developed such that they satisfy deficits in the literature or address the limitations associated with current research. Each chapter makes novel contributions in its research context. The key outcomes of this thesis are discussed in the following sections.

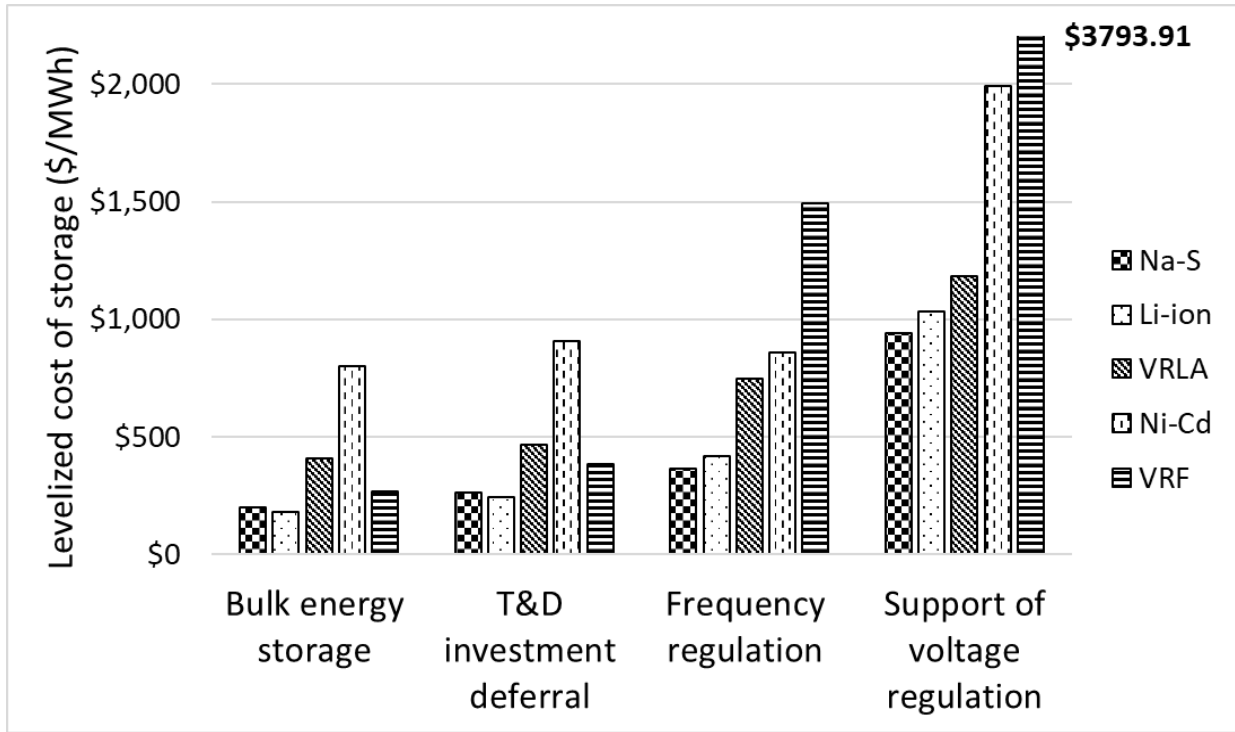
8.1.1. Techno-economic and life cycle assessment of electro-chemical energy storage systems

Bottom-up techno-economic and life cycle assessment models were developed to assess the economic and environmental feasibility of five electro-chemical ESSs in four stationary application scenarios. The life cycle costs and environmental footprints were calculated for the base case capacities of 50 MW for bulk energy storage (Scenario 1), 10 MW for transmission and distribution investment deferral (Scenario 2), 50 MW for frequency regulation (Scenario 3), and 15 MW for support of voltage regulation (Scenario 4). The scenarios were developed based on the operational characteristics of batteries, such as rated power, duration of discharge, and number of cycles. After that, systems components were sized using engineering principles. Once the system components were sized, the technical model was integrated with the economic model. The economic model consists of the cost metrics, e.g., capital cost, operation and maintenance cost, charging cost, etc. The developed techno-economic models estimate the levelized cost of storage. The LCOS ranges from \$179.69/MWh for the Li-ion to \$801.61/MWh for the Ni-Cd in S1, \$242.79/MWh for the Li-ion to \$907.41/MWh for the Ni-Cd in S2, \$365.83/MWh for the Na-S to

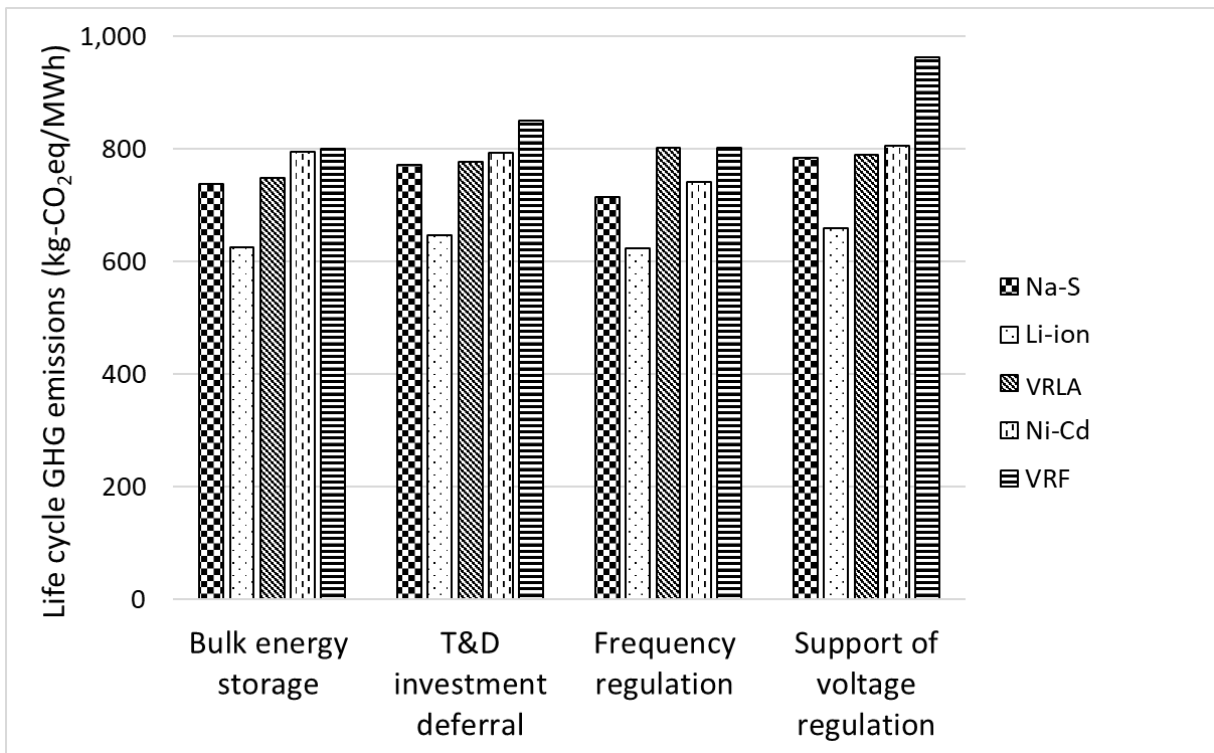
\$1494.83/MWh for the VRF in S3, and \$941.42/MWh for the Na-S to \$3793.91/MWh for the VRF in S4. In addition, scale factors were developed for the ESSs with discharge durations of 1 to 8 hours. The developed scale factors are 0.77, 0.74, 0.82, 0.91, and 0.46 for the sodium-sulfur, lithium-ion, valve-regulated lead-acid, nickel-cadmium, and vanadium redox flow, respectively. The cycle life and battery capital cost mainly determine the relative ranking of storage technologies. Having a longer cycle life and lower capital cost, lithium-ion and sodium-sulfur energy storage systems outperform other battery storage technologies.

After developing the application scenarios and sizing the components, the next step in the life cycle assessment is goal and scope definition (setting the system boundary and functional unit), inventory analysis, and translation of the inventory data to NER and GHG emissions. The functional unit is 1 MWh electricity delivered. The life cycle system boundary includes material production, manufacturing, operation, dismantling. The material and energy inputs and outputs at all the life cycle stages in the system boundary were calculated in the inventory analysis. Then, the inventory is translated into NER and GHG emissions. The NERs range from 0.50 for the Ni-Cd to 0.69 for the Li-ion for S1, 0.47 for the VRF to 0.65 for the Li-ion for S2, 0.50 for the VRLA to 0.70 for the Li-ion for S3, and 0.38 for the VRF to 0.63 for the Li-ion for S4. The life cycle GHG emissions range from 624.96 kg-CO₂eq/MWh for the Li-ion to 800.19 kg-CO₂eq/MWh for the VRF in S1, from 646.23 kg-CO₂eq/MWh for the Li-ion to 849.42 kg-CO₂eq/MWh for the VRF in S2, from 624.43 kg-CO₂eq/MWh for the Li-ion to 802.81 kg-CO₂eq/MWh for the VRLA in S3, and from 658.77 kg-CO₂eq/MWh for the Li-ion to 963.37 kg-CO₂eq/MWh for the VRF in S4. The total GHG emissions are highly dominated by the operation phase. The contributions of material production and manufacturing are 3-25% and 1-10%, respectively, depending on the technology and application. ESSs with high efficiency, long cycle life, and high energy density are preferable,

as they need less electricity for charging and less energy in material production. Thus, the Li-ion and Na-S ESSs are superior to other technologies based on life cycle GHG emissions.



(a)



(b)

Figure 8.1: Comparative reassessment of five electro-chemical energy storage systems' (a) levelized cost of storage and (b) life cycle GHG emissions

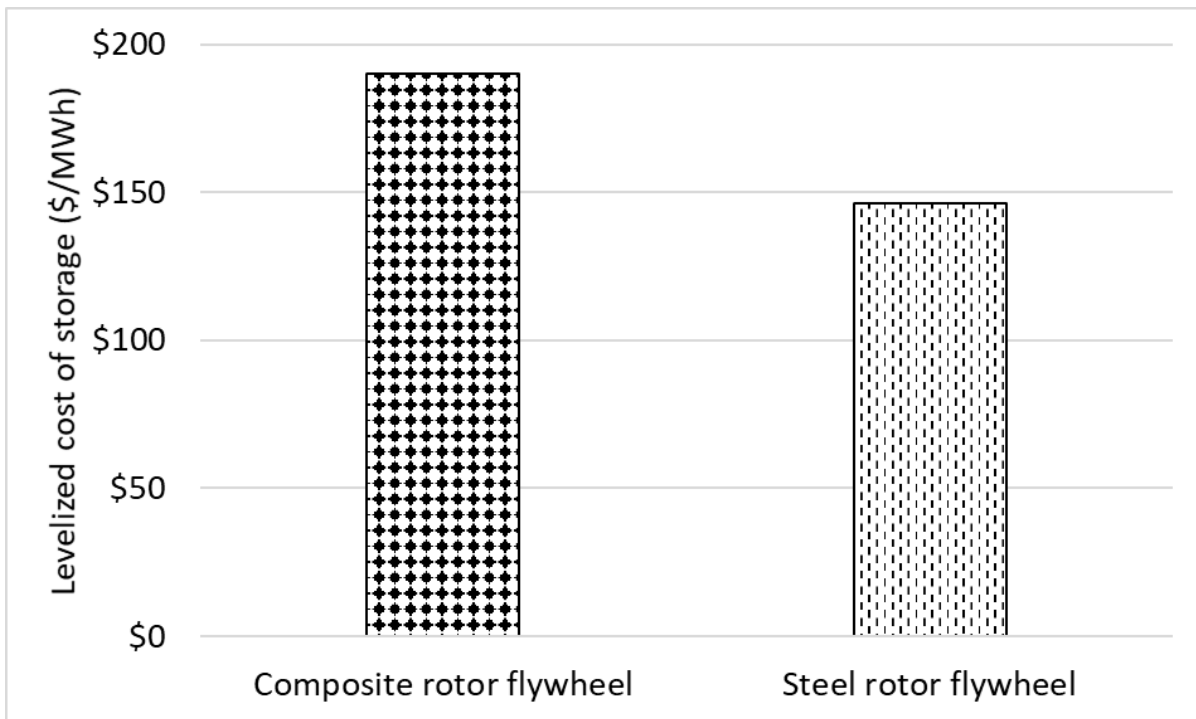
8.1.2. Techno-economic and life cycle assessment of flywheel energy storage systems

Bottom-up techno-economic and life cycle assessment models were developed to design system components and evaluate the levelized cost of storage and life cycle GHG emissions of flywheel energy storage systems for a capacity of 20 MW/5 MWh for frequency regulation. Two rotor configurations were considered: composite rotor and steel rotor flywheel. In the system design, the storage plant capacity was determined, and flywheel components were sized. The number of flywheels required was calculated from the plant capacity and the capacity of each flywheel. After determining the size and capacities of different components, the cost functions were developed for individual pieces of equipment to determine techno-economic performance using the levelized cost of storage. The LCOS for the composite rotor and steel rotor flywheel storage systems are

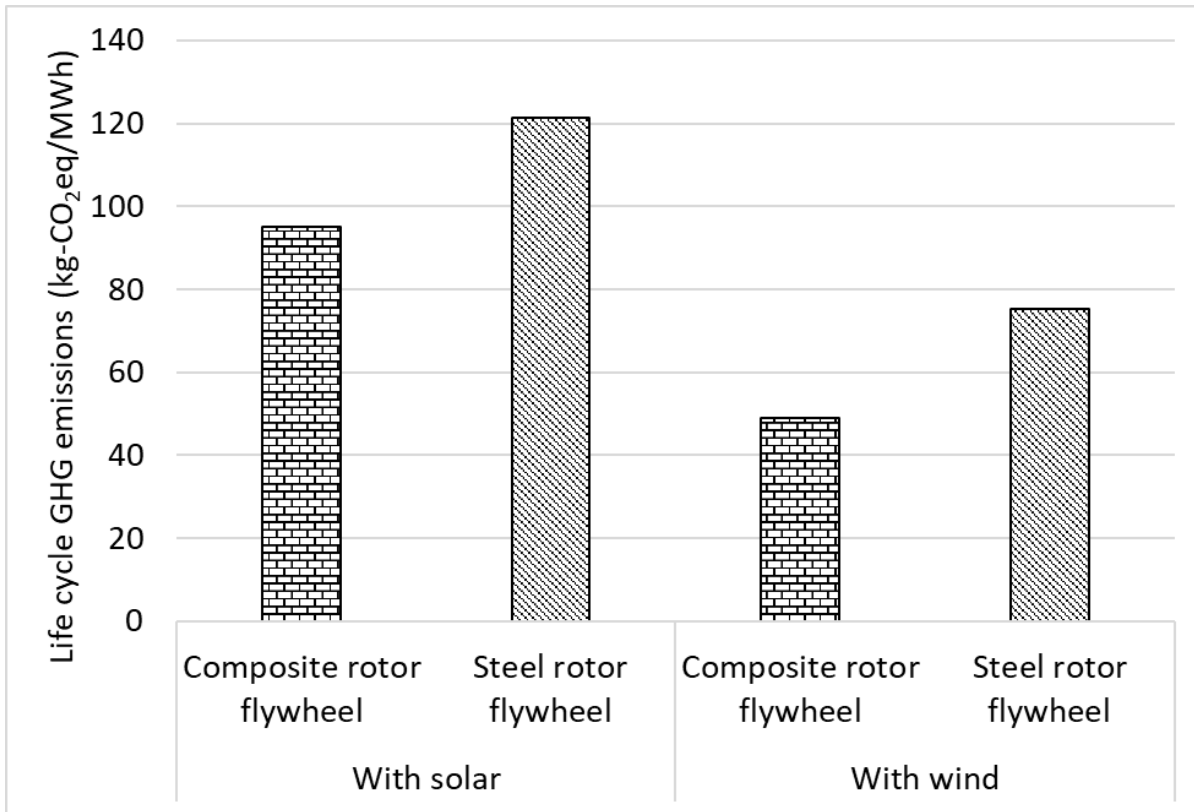
\$189.94/MWh and \$146.41/MWh, respectively. The total investment cost (TIC) makes the largest contribution to the LCOS, followed by the charging cost and the O&M cost. The rotor cost is a key contributor to the TIC. The composite rotor costs more because of the higher material and manufacturing costs; the material and manufacturing costs of a composite rotor are \$36,786 and \$19,392 for a steel rotor. Composite materials are still in the research and development stage and therefore cost more than steel. The manufacturing cost is also higher for the composite rotor because of the complex composite fiber manufacturing process. A scale factor was developed in this study using the total investment costs at different capacities. The value of the scale factor was calculated to be 0.93. This means that the rate at which the TIC increases is lower than the rate of increase in the rated power of the storage plant. The sensitivity and uncertainty results show that factor of safety, tensile strength of the rotor material, number of cycles per year, discount rate, and rotor material cost are the critical parameters and have significant impacts on the LCOS.

The first stage in the LCA is the goal and scope definition, which involves stating the purpose of the study, developing a consistent system boundary that includes all the life cycle stages for the selected systems, and defining the functional unit for a base of comparison. A consistent system boundary was considered with the life cycle stages of material production, operation, transportation, and end-of-life. The emissions were translated into GHG emissions (CO₂ equivalents) per functional unit. The NER was evaluated from the total energy produced and the total primary energy consumed during the lifetime of the systems. Electricity from solar and wind was considered separately in the operation phase. The NERs of the composite rotor FESSs are 2.7 and 3.8 for solar and wind, respectively. The corresponding values for steel rotor FESSs are 2.5 and 3.5. The life cycle greenhouse gas emissions of the composite rotor and steel rotor flywheel energy storage systems are 48.9-95.0 kg-CO₂eq/MWh and 75.2-121.4 kg-CO₂eq/MWh,

respectively, depending on the electricity source. The operation phase is the largest contributor to GHG emissions: 54-76% for the composite rotor FESS and 60-75% for the steel rotor FESS. This includes the upstream emissions from charging and emissions due to the electricity use in standby mode. GHG emissions in this phase are higher in a steel rotor FESS because of its comparatively higher standby loss. While emissions from material production are higher for the composite rotor FESS, the steel rotor FESS has higher manufacturing emissions. The most influential parameters for the life cycle GHG emissions are the electricity emission factors (grid, solar, and wind), standby loss, number of cycles, flywheel and PCS efficiency, and factor of safety.



(a)



(b)

Figure 8.2: Comparative assessment of flywheel energy storage systems' (a) levelized cost of storage and (b) life cycle GHG emissions

8.1.3. Assessment of vehicle-to-grid systems

With the rapidly growing number of electric vehicles, vehicle-to-grid technology can play an important role in stabilizing electricity grids. An electric vehicle could be used as a tiny energy storage system that provides economically viable services to the grid. An engineering principles-based techno-economic model was developed to estimate the levelized cost of storage of vehicle-to-grid technology for energy arbitrage and frequency regulation for Canadian weather conditions. The energy available in the EV batteries for the V2G applications was calculated using the battery capacity and energy required for a daily commute. All cost items, i.e., capital cost, charging cost,

and battery degradation cost, were estimated using various technical and cost parameters. A discounted cash flow analysis was carried out to calculate the LCOS. The LCOS values vary from \$176.97/MWh for Quebec to \$233.08/MWh for Ontario when the V2G system is used for energy arbitrage. When the V2G system is used for frequency regulation, the LCOS values vary from \$271.42/MWh for Quebec to \$329.93/MWh for Ontario (see Figure 8.3). The LCOS for frequency regulation is higher than for energy arbitrage because of the higher V2G equipment capital cost. The LCOS varies by province mainly because of differences in electricity prices and average ambient temperatures. The sensitivity analysis result shows that the most influential parameters are ambient temperature, battery cycle life, distance traveled per day, battery depth of discharge, battery capital cost, and electricity price. Ambient temperature has a significant impact on the amount of energy available for V2G applications. With extremely cold weather conditions, the available energy drops drastically because of the impacts of low temperature on the battery efficiency and the cabin heating requirement. When the ambient temperature falls to -20°C from 10°C , the amount of energy available for V2G applications drops from 10.17 kWh to 6.60 kWh.

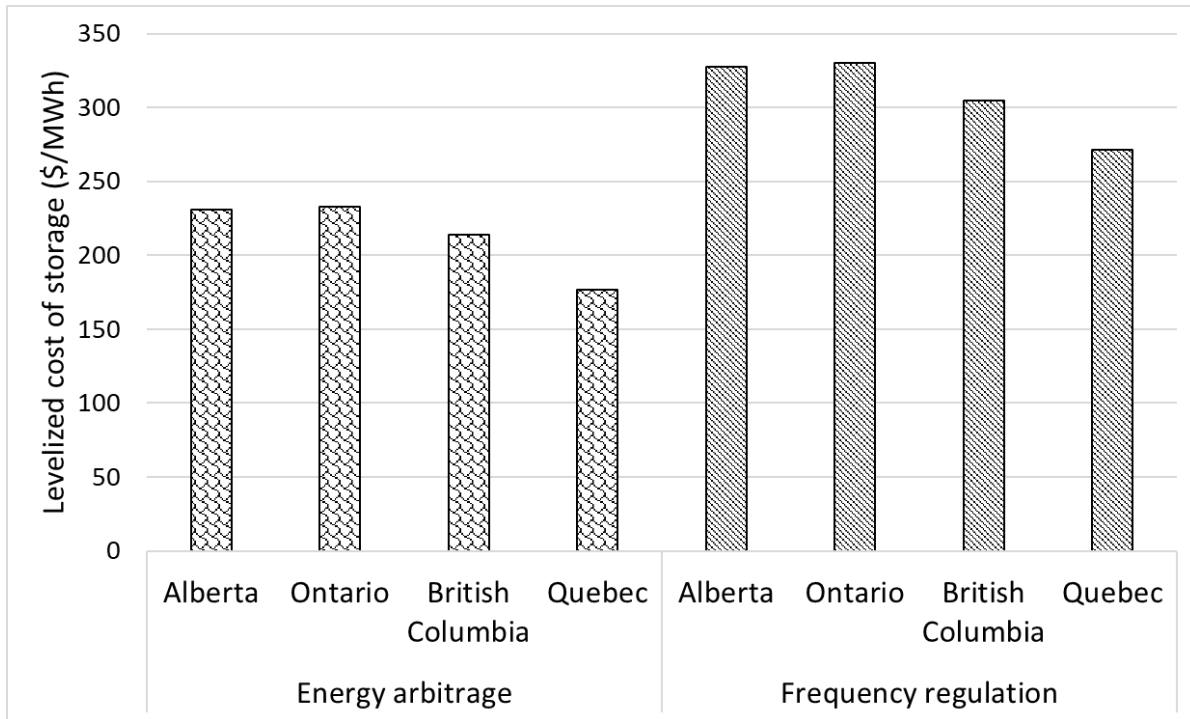


Figure 8.3: Levelized cost of storage in four provinces in Canada

8.2. Recommendations for future work

The following recommendations could be considered to advance the research.

8.2.1. Assessment of alternative and emerging energy storage systems

Although this thesis covers a wide range of energy storage systems, future research should include liquid air, supercapacitor, lithium-sulfur, and solid-state batteries. These technologies are predicted to dominate the future energy storage market with the rapidly increased renewable share in electricity production. Limited availability of the technical and energy use data is one of the main challenges in carrying out techno-economic assessments and LCA. Understanding the economic and environmental performances of these emerging technologies in their early stages of

development would offer opportunities to make design adjustments to minimize cost and environmental burdens.

8.2.2. Life cycle assessment model enhancement

Because of the worldwide effects of global warming, this thesis focuses on net energy ratio and GHG emissions. Other environmental impacts such as acidification, eutrophication, human toxicity, and resource depletion could be included in the assessment to provide a broader representation of the overall environmental impact of energy storage systems. To understand the end-of-life impact of an energy storage system, in-depth research should be conducted on material recycling. Recycling can reduce the overall burden by displacing virgin materials. This topic is not sufficiently addressed because of limited data availability. Additional work should be done to estimate the increase or decrease in the overall emissions due to material recycling.

8.2.3. Life cycle sustainability assessment

The techno-economic and life cycle assessments carried out for different energy storage systems addressed in this research could be complemented with a life cycle sustainability assessment (LCSA). LCSA integrates life cycle cost, environmental footprints, and social impacts to address sustainability-related questions. There are few life cycle sustainability assessments of large-scale energy storage systems. This is an opportunity to understand the social perception of energy storage systems and evaluate their overall sustainability.

8.2.4. Assessment of second-life batteries

Electric vehicle (EV) batteries discarded after use can be used for stationary energy storage systems because they have around 80% of their initial capacity [528]. It is expected that large quantities of EV batteries with different capacities will be available in the market because of the increased number of EVs around the globe. It is important to understand the techno-economic and

environmental feasibility of second-life batteries before their deployment in the electricity network for short- or long-term applications.

8.2.5. Techno-economic model enhancement

With the growing number of battery applications, we could see supply shortages of raw materials in the future. The production of raw materials is environmentally harmful because of the excessive use of energy. Because of limited data availability and lack of reliability, we did not include recycling and decommissioning costs in our current models. However, with the rapid development of battery recycling, it is expected that more data will be available in the future. The cost of recovering and recycling battery materials should be included to understand the role of battery recycling in the circular economy. Material recycling can reduce the overall cost by displacing virgin materials, which are more costly.

Bibliography

- [1] Centre for Climate and Energy Solutions. Global Emissions. Available from: [https://www.c2es.org/content/international-emissions/#targetText=Notes,%25\)%20and%20manufacturing%20\(12%25](https://www.c2es.org/content/international-emissions/#targetText=Notes,%25)%20and%20manufacturing%20(12%25) (Accessed October 03 2019).
- [2] Bloomberg NEF. Global electricity demand to increase 57% by 2050. Available from: <https://about.bnef.com/blog/global-electricity-demand-increase-57-2050/> (Accessed October 03 2019).
- [3] Rogelj J, Den Elzen M, Höhne N, Fransen T, Fekete H, Winkler H, et al. Paris Agreement climate proposals need a boost to keep warming well below 2 C. *Nature*. 2016;534(7609):631.
- [4] International Renewable Energy Agency. Renewable Energy Statistics 2019. Available from: https://www.irena.org/-/media/Files/IRENA/Agency/Publication/2019/Jul/IRENA_Renewable_energy_statistics_2019.pdf (Accessed September 23 2019).
- [5] United Nations Climate Change. Renewables growth must double to achieve Paris goals - IEA. Available from: <https://unfccc.int/news/renewables-growth-must-double-to-achieve-paris-goals-ia> (Accessed February 12 2022).
- [6] Hadjipaschalis I, Poullikkas A, Efthimiou V. Overview of current and future energy storage technologies for electric power applications. *Renewable and Sustainable Energy Reviews*. 2009;13(6-7):1513-22.
- [7] Schäfer B, Beck C, Aihara K, Witthaut D, Timme M. Non-Gaussian power grid frequency fluctuations characterized by Lévy-stable laws and superstatistics. *Nature Energy*. 2018;3(2):119.
- [8] Beaudin M, Zareipour H, Schellenberglobe A, Rosehart W. Energy storage for mitigating the variability of renewable electricity sources: An updated review. *Energy for Sustainable Development*. 2010;14(4):302-14.
- [9] Arbabzadeh M, Sioshansi R, Johnson JX, Keoleian GA. The role of energy storage in deep decarbonization of electricity production. *Nature Communications*. 2019;10(1):3413.
- [10] Chen H, Cong TN, Yang W, Tan C, Li Y, Ding Y. Progress in electrical energy storage system: a critical review. *Progress in Natural Science*. 2009;19(3):291-312.
- [11] Rahman MM, Oni AO, Gemechu E, Kumar A. Assessment of energy storage technologies: A review. *Energy Conversion and Management*. 2020;223:113295.

- [12] DOE Global Energy Storage Database. Available from: http://www.energystorageexchange.org/projects/data_visualization (Accessed July 03 2018).
- [13] Stettner P. Hydropower and pumped storage. Available from: https://www3.eurelectric.org/media/366039/stettner_andritz.pdf (Accessed September 23 2019).
- [14] Gür TM. Review of electrical energy storage technologies, materials and systems: challenges and prospects for large-scale grid storage. *Energy & Environmental Science*. 2018;11(10):2696-767.
- [15] Denholm P, Kulcinski GL. Life cycle energy requirements and greenhouse gas emissions from large scale energy storage systems. *Energy Conversion and Management*. 2004;45(13-14):2153-72.
- [16] Ramadan O, Omer S, Jradi M, Sabir H, Riffat S. Analysis of compressed air energy storage for large-scale wind energy in Suez, Egypt. *International Journal of Low-Carbon Technologies*. 2016;11(4):476-88.
- [17] Meesenburg W, Thingvad A, Elmegaard B, Marinelli M. Combined provision of primary frequency regulation from Vehicle-to-Grid (V2G) capable electric vehicles and community-scale heat pump. *Sustainable Energy, Grids and Networks*. 2020;23:100382.
- [18] Srithapon C, Ghosh P, Siritaratiwat A, Chatthaworn R. Optimization of electric vehicle charging scheduling in urban village networks considering energy arbitrage and distribution Cost. *Energies*. 2020;13(2):349.
- [19] Damiano A, Gatto G, Marongiu I, Porru M, Serpi A. Vehicle-to-grid technology: State-of-the-art and future scenarios. *Journal of Energy and Power Engineering*. 2014;8:152-65.
- [20] Grand View Research. Flywheel energy storage system market size, share & trends analysis report by application (UPS, distributed energy generation, transport, data centers), by region, and segment forecasts, 2020 - 2027. Available from: <https://www.grandviewresearch.com/industry-analysis/flywheel-energy-storage-market?fbclid=IwAR3eXKdFiEcUCk7Zxr-LOD9e1Yh0uaYvqjqtBTFTPGMlzY0uANsIyinBhCw#:~:text=The%20global%20flywheel%20energy%20storage,the%20flywheel%20is%20energy%20storage> (Accessed November 06 2020).
- [21] Cision PR Newswire. Global \$552.1 million flywheel energy storage system markets, analysis 2016-2019 & forecasts 2020-2027. Available from: <https://www.prnewswire.com/news-releases/global-552-1-million-flywheel-energy-storage-system-markets-analysis-2016-2019--forecasts-2020-2027-->

[301133961.html#:~:text=The%20global%20flywheel%20energy%20storage,7.4%25%20over%20the%20forecast%20period.](#) (Accessed November 06 2020).

[22] Nikolaidis P, Poullikkas A. Cost metrics of electrical energy storage technologies in potential power system operations. *Sustainable Energy Technologies and Assessments*. 2018;25:43-59.

[23] Schmidt O, Melchior S, Hawkes A, Staffell I. Projecting the future levelized cost of electricity storage technologies. *Joule*. 2019;3(1):81-100.

[24] Mostafa MH, Abdel Aleem SHE, Ali SG, Ali ZM, Abdelaziz AY. Techno-economic assessment of energy storage systems using annualized life cycle cost of storage (LCCOS) and levelized cost of energy (LCOE) metrics. *Journal of Energy Storage*. 2020;29:101345.

[25] Schoenung S. Energy storage systems cost update: A study for the DOE energy storage systems program. Available from: <https://prod-ng.sandia.gov/techlib-noauth/access-control.cgi/2011/112730.pdf> (Accessed April 02 2019).

[26] Schoenung SM, Eyer J. Benefit/cost framework for evaluating modular energy storage: A study for the DOE energy storage systems program. Report prepared for Sandia National Laboratories. Available: <https://prod-ng.sandia.gov/techlib-noauth/access-control.cgi/2008/080978.pdf> [Accessed April 2 2019].

[27] Abrams A, Fioravanti R, Harrison J, Katzenstein W, Kleinberg M, Lahiri S, et al. Energy storage cost-effectiveness methodology and preliminary results. California, USA: DNV KEMA Energy and Sustainability, California Energy Commission. Available from: https://www.wisconsin.gov/library/storage/EnergyStorageCostEffectiveness_Report-KEMA.pdf (Accessed September 23 2019).

[28] Zakeri B, Syri S. Electrical energy storage systems: a comparative life cycle cost analysis. *Renewable and Sustainable Energy Reviews*. 2015;42:569-96.

[29] Li Y, Miao S, Luo X, Yin B, Han J, Wang J. Dynamic modelling and techno-economic analysis of adiabatic compressed air energy storage for emergency back-up power in supporting microgrid. *Applied Energy*. 2020;261:114448.

[30] Peters JF, Baumann M, Zimmermann B, Braun J, Weil M. The environmental impact of Li-Ion batteries and the role of key parameters – A review. *Renewable and Sustainable Energy Reviews*. 2017;67:491-506.

[31] Kapila S, Oni AO, Kumar A. The development of techno-economic models for large-scale energy storage systems. *Energy*. 2017;140:656-72.

- [32] Bank of Canada. Outlook for electric vehicles and implications for the oil market. Available from: https://publications.gc.ca/collections/collection_2019/banque-bank-canada/FB3-7-2019-19-eng.pdf (Accessed September 2 2021).
- [33] Gough R, Dickerson C, Rowley P, Walsh C. Vehicle-to-grid feasibility: A techno-economic analysis of EV-based energy storage. *Applied Energy*. 2017;192:12-23.
- [34] Li S, Gu C, Zeng X, Zhao P, Pei X, Cheng S. Vehicle-to-grid management for multi-time scale grid power balancing. *Energy*. 2021;234:121201.
- [35] Abazari A, Dozein MG, Monsef H. An optimal fuzzy-logic based frequency control strategy in a high wind penetrated power system. *Journal of the Franklin Institute*. 2018;355(14):6262-85.
- [36] Nasir M, Khan HA, Niazi KAK, Jin Z, Guerrero JM. Dual-loop control strategy applied to PV/battery-based islanded DC microgrids for swarm electrification of developing regions. *The Journal of Engineering*. 2019;2019(18):5298-302.
- [37] Noori M, Zhao Y, Onat NC, Gardner S, Tatari O. Light-duty electric vehicles to improve the integrity of the electricity grid through Vehicle-to-Grid technology: Analysis of regional net revenue and emissions savings. *Applied Energy*. 2016;168:146-58.
- [38] Zhao Y, Noori M, Tatari O. Vehicle to grid regulation services of electric delivery trucks: Economic and environmental benefit analysis. *Applied Energy*. 2016;170:161-75.
- [39] Rodríguez-Molina J, Castillejo P, Beltran V, Martínez-Núñez M. A model for cost-benefit analysis of privately owned vehicle-to-grid solutions. *Energies*. 2020;13(21):5814.
- [40] Donkers A, Yang D, Viktorović M. Influence of driving style, infrastructure, weather and traffic on electric vehicle performance. *Transportation Research Part D: Transport and Environment*. 2020;88:102569.
- [41] Yuksel T, Michalek JJ. Effects of regional temperature on electric vehicle efficiency, range, and emissions in the United States. *Environmental Science & Technology*. 2015;49(6):3974-80.
- [42] Akinyele DO, Rayudu RK. Review of energy storage technologies for sustainable power networks. *Sustainable Energy Technologies and Assessments*. 2014;8:74-91.
- [43] Atherton J, Sharma R, Salgado J. Techno-economic analysis of energy storage systems for application in wind farms. *Energy*. 2017;135:540-52.
- [44] Weber S, Peters JF, Baumann M, Weil M. Life cycle assessment of a vanadium redox flow battery. *Environmental Science & Technology*. 2018;52(18):10864-73.

- [45] Salgado Delgado MA, Usai L, Ellingsen LA-W, Pan Q, Hammer Strømman A. Comparative life cycle assessment of a novel Al-Ion and a Li-Ion battery for stationary applications. *Materials*. 2019;12(19):3270.
- [46] Mostert C, Ostrander B, Bringezu S, Kneiske TM. Comparing electrical energy storage technologies regarding their material and carbon footprint. *Energies*. 2018;11(12):3386.
- [47] Zhao S, You F. Comparative life-cycle assessment of li-ion batteries through process-based and integrated hybrid approaches. *ACS Sustainable Chemistry & Engineering*. 2019;7(5):5082-94.
- [48] Carvalho ML, Temporelli A, Girardi P. Life cycle assessment of stationary storage systems within the Italian electric network. *Energies*. 2021;14(8):2047.
- [49] Ryan NA, Lin Y, Mitchell-Ward N, Mathieu JL, Johnson JX. Use-phase drives lithium-ion battery life cycle environmental impacts when used for frequency regulation. *Environmental Science & Technology*. 2018;52(17):10163-74.
- [50] Jones C, Gilbert P, Stamford L. Assessing the climate change mitigation potential of stationary energy storage for electricity grid services. *Environmental Science & Technology*. 2020;54(1):67-75.
- [51] Baumann M, Peters J, Weil M, Grunwald A. CO₂ footprint and life-cycle costs of electrochemical energy storage for stationary grid applications. *Energy Technology*. 2017;5(7):1071-83.
- [52] Oliveira L, Messagie M, Mertens J, Laget H, Coosemans T, Van Mierlo J. Environmental performance of electricity storage systems for grid applications, a life cycle approach. *Energy Conversion and Management*. 2015;101:326-35.
- [53] Chowdhury JI, Balta-Ozkan N, Goglio P, Hu Y, Varga L, McCabe L. Techno-environmental analysis of battery storage for grid level energy services. *Renewable and Sustainable Energy Reviews*. 2020;131:110018.
- [54] Torell W. Lifecycle carbon footprint analysis of batteries vs. flywheels. Available from: https://download.schneider-electric.com/files?p_enDocType=White+Paper&p_File_Name=VAVR-9KZQVW_R0_EN.pdf&p_Doc_Ref=SPD_VAVR-9KZQVW_EN (Accessed May 16 2020).

- [55] Active Power. Improving sustainability with flywheel UPS. Available from: <https://powersafe.ca/wp-content/uploads/2019/01/wp120-improving-sustainability-with-flywheel-ups.pdf> (Accessed May 16 2020).
- [56] Fioravanti R, Enslin J. Emissions comparison for a 20 MW flywheel-based frequency regulation power plant Available from: https://jointventure.org/images/stories/pdf/kema_flywheel_report_co2_reductions.pdf (Accessed May 20 2020).
- [57] International Organization for Standardization. ISO 14040: Environmental management — Life cycle assessment — Principles and framework. Available: <https://www.iso.org/standard/37456.html>.
- [58] Baky MAH, Rahman MM, Islam AS. Development of renewable energy sector in Bangladesh: Current status and future potentials. *Renewable and Sustainable Energy Reviews*. 2017;73:1184-97.
- [59] Perera F. Pollution from fossil-fuel combustion is the leading environmental threat to global pediatric health and equity: Solutions exist. *International Journal of Environmental Research and Public Health*. 2017;15(1):16.
- [60] Patel M, Zhang X, Kumar A. Techno-economic and life cycle assessment on lignocellulosic biomass thermochemical conversion technologies: A review. *Renewable and Sustainable Energy Reviews*. 2016;53:1486-99.
- [61] Patel M, Kumar A. Production of renewable diesel through the hydroprocessing of lignocellulosic biomass-derived bio-oil: A review. *Renewable and Sustainable Energy Reviews*. 2016;58:1293-307.
- [62] Rahman MM, Canter C, Kumar A. Well-to-wheel life cycle assessment of transportation fuels derived from different North American conventional crudes. *Applied Energy*. 2015;156:159-73.
- [63] Rahman MM, Canter C, Kumar A. Greenhouse gas emissions from recovery of various North American conventional crudes. *Energy*. 2014;74:607-17.
- [64] Rahman MM, Khan MM-U-H, Ullah MA, Zhang X, Kumar A. A hybrid renewable energy system for a North American off-grid community. *Energy*. 2016;97:151-60.
- [65] Aneke M, Wang M. Energy storage technologies and real life applications—A state of the art review. *Applied Energy*. 2016;179:350-77.

- [66] Serra R, Niknia I, Paré D, Titus B, Gagnon B, Laganière J. From conventional to renewable natural gas: can we expect GHG savings in the near term? *Biomass and Bioenergy*. 2019;131:105396.
- [67] Gulagi A, Ram M, Solomon AA, Khan M, Breyer C. Current energy policies and possible transition scenarios adopting renewable energy: A case study for Bangladesh. *Renewable Energy*. 2020;155:899-920.
- [68] Renewables 2016: Global status report. REN21 Renewable Energy Policy Network/Worldwatch Institute. Available from: http://www.ren21.net/wp-content/uploads/2016/05/GSR_2016_Full_Report_lowres.pdf (Accessed May 15 2020).
- [69] Luo X, Wang J, Dooner M, Clarke J. Overview of current development in electrical energy storage technologies and the application potential in power system operation. *Applied Energy*. 2015;137:511-36.
- [70] Ourahou M, Ayir W, El Hassouni B, Haddi A. Review on smart grid control and reliability in presence of renewable energies: Challenges and prospects. *Mathematics and Computers in Simulation*. 2020;167:19-31.
- [71] Bajaj M, Singh AK. Grid integrated renewable DG systems: A review of power quality challenges and state-of-the-art mitigation techniques. *International Journal of Energy Research*. 2020;44(1):26-69.
- [72] Sinsel SR, Riemke RL, Hoffmann VH. Challenges and solution technologies for the integration of variable renewable energy sources—a review. *Renewable Energy*. 2020;145:2271-85.
- [73] Basit MA, Dilshad S, Badar R, Sami ur Rehman SM. Limitations, challenges, and solution approaches in grid-connected renewable energy systems. *International Journal of Energy Research*. 2020;44(6):4132-62.
- [74] Colmenar-Santos A, Linares-Mena A-R, Molina-Ibáñez E-L, Rosales-Asensio E, Borge-Diez D. Technical challenges for the optimum penetration of grid-connected photovoltaic systems: Spain as a case study. *Renewable Energy*. 2020;145:2296-305.
- [75] Abbey C, Joos G. Supercapacitor energy storage for wind energy applications. *IEEE Transactions on Industry Applications*. 2007;43(3):769-76.
- [76] Lu M-S, Chang C-L, Lee W-J, Wang L. Combining the wind power generation system with energy storage equipment. *IEEE Transactions on Industry Applications*. 2009;45(6):2109-15.

- [77] Barton JP, Infield DG. Energy storage and its use with intermittent renewable energy. *IEEE Transactions on Energy Conversion*. 2004;19(2):441-8.
- [78] Yekini Suberu M, Wazir Mustafa M, Bashir N. Energy storage systems for renewable energy power sector integration and mitigation of intermittency. *Renewable and Sustainable Energy Reviews*. 2014;35:499-514.
- [79] Headley AJ, Copp DA. Energy storage sizing for grid compatibility of intermittent renewable resources: A California case study. *Energy*. 2020;198:117310.
- [80] Guney MS, Tepe Y. Classification and assessment of energy storage systems. *Renewable and Sustainable Energy Reviews*. 2017;75:1187-97.
- [81] Baker J, Collinson A. Electrical energy storage at the turn of the millennium. *Power Engineering Journal*. 1999;13(3):107-12.
- [82] Walawalkar R, Apt J, Mancini R. Economics of electric energy storage for energy arbitrage and regulation in New York. *Energy Policy*. 2007;35(4):2558-68.
- [83] Braeuer F, Rominger J, McKenna R, Fichtner W. Battery storage systems: An economic model-based analysis of parallel revenue streams and general implications for industry. *Applied Energy*. 2019;239:1424-40.
- [84] Killer M, Farrokhsersht M, Paterakis NG. Implementation of large-scale Li-ion battery energy storage systems within the EMEA region. *Applied Energy*. 2020;260:114166.
- [85] Weinstock IB. Recent advances in the US Department of Energy's energy storage technology research and development programs for hybrid electric and electric vehicles. *Journal of Power Sources*. 2002;110(2):471-4.
- [86] Koot M, Kessels JT, De Jager B, Heemels W, Van den Bosch P, Steinbuch M. Energy management strategies for vehicular electric power systems. *IEEE Transactions on Vehicular Technology*. 2005;54(3):771-82.
- [87] Hemmati R, Saboori H. Emergence of hybrid energy storage systems in renewable energy and transport applications – A review. *Renewable and Sustainable Energy Reviews*. 2016;65:11-23.
- [88] Mehrjerdi H. Dynamic and multi-stage capacity expansion planning in microgrid integrated with electric vehicle charging station. *Journal of Energy Storage*. 2020;29:101351.

- [89] Lazzeroni P, Olivero S, Repetto M, Stirano F, Vallet M. Optimal battery management for vehicle-to-home and vehicle-to-grid operations in a residential case study. *Energy*. 2019;175:704-21.
- [90] Poullikkas A. A comparative overview of large-scale battery systems for electricity storage. *Renewable and Sustainable Energy Reviews*. 2013;27:778-88.
- [91] Díaz-González F, Sumper A, Gomis-Bellmunt O, Villafáfila-Robles R. A review of energy storage technologies for wind power applications. *Renewable and Sustainable Energy Reviews*. 2012;16(4):2154-71.
- [92] Ibrahim H, Ilinca A, Perron J. Energy storage systems—characteristics and comparisons. *Renewable and Sustainable Energy Reviews*. 2008;12(5):1221-50.
- [93] May GJ, Davidson A, Monahov B. Lead batteries for utility energy storage: A review. *Journal of Energy Storage*. 2018;15:145-57.
- [94] Amirante R, Cassone E, Distaso E, Tamburrano P. Overview on recent developments in energy storage: Mechanical, electrochemical and hydrogen technologies. *Energy Conversion and Management*. 2017;132:372-87.
- [95] Yang Y, Bremner S, Menictas C, Kay M. Battery energy storage system size determination in renewable energy systems: A review. *Renewable and Sustainable Energy Reviews*. 2018;91:109-25.
- [96] Palizban O, Kauhaniemi K. Energy storage systems in modern grids—Matrix of technologies and applications. *Journal of Energy Storage*. 2016;6:248-59.
- [97] Bucciarelli M, Giannitrapani A, Paoletti S, Vicino A, Zarrilli D. Sizing of energy storage systems considering uncertainty on demand and generation. *IFAC-PapersOnLine*. 2017;50(1):8861-6.
- [98] Fossati JP, Galarza A, Martín-Villate A, Fontán L. A method for optimal sizing energy storage systems for microgrids. *Renewable Energy*. 2015;77:539-49.
- [99] Soloveichik GL. Battery technologies for large-scale stationary energy storage. *Annual review of chemical and biomolecular engineering*. 2011;2:503-27.
- [100] Kousksou T, Bruel P, Jamil A, El Rhafiki T, Zeraoui Y. Energy storage: applications and challenges. *Solar Energy Materials and Solar Cells*. 2014;120:59-80.

- [101] Mahlia TMI, Saktisahdan TJ, Jannifar A, Hasan MH, Matseelar HSC. A review of available methods and development on energy storage; technology update. *Renewable and Sustainable Energy Reviews*. 2014;33:532-45.
- [102] Yan T, Wang R, Li T, Wang L, Fred IT. A review of promising candidate reactions for chemical heat storage. *Renewable and Sustainable Energy Reviews*. 2015;43:13-31.
- [103] Zidar M, Georgilakis PS, Hatziaargyriou ND, Capuder T, Škrlec D. Review of energy storage allocation in power distribution networks: applications, methods and future research. *IET Generation, Transmission & Distribution*. 2016;10(3):645-52.
- [104] Figgenger J, Stenzel P, Kairies K-P, Linßen J, Haberschusz D, Wessels O, et al. The development of stationary battery storage systems in Germany – A market review. *Journal of Energy Storage*. 2020;29:101153.
- [105] Battke B, Schmidt TS, Grosspietsch D, Hoffmann VH. A review and probabilistic model of lifecycle costs of stationary batteries in multiple applications. *Renewable and Sustainable Energy Reviews*. 2013;25:240-50.
- [106] Koochi-Fayegh S, Rosen MA. A review of energy storage types, applications and recent developments. *Journal of Energy Storage*. 2020;27:101047.
- [107] ISO 14044: 2006- Environmental management - Life cycle assessment - Requirements and guidelines. The Organization for Standardization. Available: <https://www.iso.org/standard/38498.html>.
- [108] Longo S, Antonucci V, Cellura M, Ferraro M. Life cycle assessment of storage systems: the case study of a sodium/nickel chloride battery. *Journal of Cleaner Production*. 2014;85:337-46.
- [109] Sullivan JL, Gaines L. Status of life cycle inventories for batteries. *Energy Conversion and Management*. 2012;58:134-48.
- [110] Van den Bossche P, Vergels F, Van Mierlo J, Matheys J, Van Autenboer W. SUBAT: An assessment of sustainable battery technology. *Journal of Power Sources*. 2006;162(2):913-9.
- [111] Yu Y, Wang X, Wang D, Huang K, Wang L, Bao L, et al. Environmental characteristics comparison of Li-ion batteries and Ni–MH batteries under the uncertainty of cycle performance. *Journal of Hazardous Materials*. 2012;229:455-60.
- [112] Rahman MM, Alam CS, Ahsan T. A life cycle assessment model for quantification of environmental footprints of a 3.6 kW p photovoltaic system in Bangladesh. *International Journal of Renewable Energy Development*. 2019;8(2).

- [113] Pellow MA, Ambrose H, Mulvaney D, Betita R, Shaw S. Research gaps in environmental life cycle assessments of lithium ion batteries for grid-scale stationary energy storage systems: End-of-life options and other issues. *Sustainable Materials and Technologies*. 2020;23:e00120.
- [114] Molina MG. Dynamic modelling and control design of advanced energy storage for power system applications. *Dynamic Modelling*, Alisson V. Brito, IntechOpen, DOI: 10.5772/7092, 2010. Available: <https://www.intechopen.com/books/dynamic-modelling/dynamic-modelling-and-control-design-of-advanced-energy-storage-for-power-system-applications> [Accessed April 02 2019].
- [115] Zhao H, Wu Q, Hu S, Xu H, Rasmussen CN. Review of energy storage system for wind power integration support. *Applied Energy*. 2015;137:545-53.
- [116] Evans A, Strezov V, Evans TJ. Assessment of utility energy storage options for increased renewable energy penetration. *Renewable and Sustainable Energy Reviews*. 2012;16(6):4141-7.
- [117] Li G, Hwang Y, Radermacher R, Chun H-H. Review of cold storage materials for subzero applications. *Energy*. 2013;51:1-17.
- [118] Wang J, Lu K, Ma L, Wang J, Dooner M, Miao S, et al. Overview of compressed air energy storage and technology development. *Energies*. 2017;10(7):991.
- [119] Akhil AA, Huff G, Currier AB, Kaun BC, Rastler DM, Chen SB, et al. DOE/EPRI electricity storage handbook in collaboration with NRECA. Available from: <https://prod-ng.sandia.gov/techlib-noauth/access-control.cgi/2015/151002.pdf> (Accessed April 10 2019).
- [120] Sebastián R, Peña-Alzola R, Quesada J, Colmenar A. Sizing and simulation of a low cost flywheel based energy storage system for wind diesel hybrid systems. *Energy Conference and Exhibition (ENERGYCON), 2012 IEEE International*. IEEE, p. 495-500.
- [121] Sebastián R, Alzola RP. Flywheel energy storage systems: Review and simulation for an isolated wind power system. *Renewable and Sustainable Energy Reviews*. 2012;16(9):6803-13.
- [122] Karpinski A, Makovetski B, Russell S, Serenyi J, Williams D. Silver–zinc: status of technology and applications. *Journal of Power Sources*. 1999;80(1-2):53-60.
- [123] Wall S, McShane D. A strategy for low-cost utility connection of battery energy storage systems. *Journal of Power Sources*. 1997;67(1-2):193-200.
- [124] Ferreira HL, Garde R, Fulli G, Kling W, Lopes JP. Characterisation of electrical energy storage technologies. *Energy*. 2013;53:288-98.

- [125] Daryl RB, Chvala D. Flywheel energy storage: An alternative to batteries for uninterruptible power supply systems. Available from: <https://www.tandfonline.com/doi/abs/10.1080/01998590509509440> (Accessed May 16 2020).
- [126] Leadbetter J, Swan LG. Selection of battery technology to support grid-integrated renewable electricity. *Journal of Power Sources*. 2012;216:376-86.
- [127] Tamyurek B, Nichols DK, Demirci O. The NAS battery: a multifunction energy storage system. *Power Engineering Society General Meeting, 2003, IEEE*, vol. 4. IEEE, p. 1991-6.
- [128] Takashima K, Ishimaru F, Kunimoto A, Kagawa H, Matsui K, Nomura E, et al. A Plan for a 1MW/8MWH sodium-sulfur battery energy storage plant. *Energy Conversion Engineering Conference, 1990 IECEC-90 Proceedings of the 25th Intersociety*, vol. 3. IEEE, p. 367-71.
- [129] Stackpool F, Auxer W, McNamee M, Mangan M. Sodium sulphur battery development. *Energy Conversion Engineering Conference, 1989 IECEC-89, Proceedings of the 24th Intersociety*. IEEE, p. 2765-8.
- [130] Emirates Energy Award 2015 Winners. Supreme Council of Energy. Available from: http://www.emiratesenergyaward.com/images/EEA_Mag_PRINT_FIN_2.pdf (Accessed August 29 2018).
- [131] Thaker S, Oni AO, Kumar A. Techno-economic evaluation of solar-based thermal energy storage systems. *Energy Conversion and Management*. 2017;153:423-34.
- [132] Comodi G, Carducci F, Sze JY, Balamurugan N, Romagnoli A. Storing energy for cooling demand management in tropical climates: A techno-economic comparison between different energy storage technologies. *Energy*. 2017;121:676-94.
- [133] Socaciu LG. Thermal energy storage: an overview. *ACTA Technica Napocensis-Series: Applied Mathematics, Mechanics, and Engineering*. 2012;55(4).
- [134] Zalba B, Marin JM, Cabeza LF, Mehling H. Review on thermal energy storage with phase change: materials, heat transfer analysis and applications. *Applied Thermal Engineering*. 2003;23(3):251-83.
- [135] Geth F, Brijs T, Kathan J, Driesen J, Belmans R. An overview of large-scale stationary electricity storage plants in Europe: Current status and new developments. *Renewable and Sustainable Energy Reviews*. 2015;52:1212-27.
- [136] Castillo A, Gayme DF. Grid-scale energy storage applications in renewable energy integration: A survey. *Energy Conversion and Management*. 2014;87:885-94.

- [137] Faias S, Santos P, Sousa J, Castro R. An overview on short and long-term response energy storage devices for power systems applications. Available from: <http://www.icrepq.com/icrepq-08/327-faias.pdf> [Accessed August 29 2018].
- [138] Kaldellis J, Zafirakis D. Optimum energy storage techniques for the improvement of renewable energy sources-based electricity generation economic efficiency. *Energy*. 2007;32(12):2295-305.
- [139] Schoenung SM. Characteristics and technologies for long-vs. short-term energy storage: a study by the DOE energy storage systems program. Available from: <https://www.osti.gov/servlets/purl/780306> (Accessed July 15 2018).
- [140] Kazempour SJ, Moghaddam MP, Haghifam M, Yousefi G. Electric energy storage systems in a market-based economy: Comparison of emerging and traditional technologies. *Renewable Energy*. 2009;34(12):2630-9.
- [141] Lipman TE, Ramos R, Kammen DM. An assessment of battery and hydrogen energy storage systems integrated with wind energy resources in California. Available from: <https://trid.trb.org/view/1376938> (Accessed July 10 2018).
- [142] Ries G, Neumueller H-W. Comparison of energy storage in flywheels and SMES. *Physica C: Superconductivity*. 2001;357:1306-10.
- [143] McDowall J. Integrating energy storage with wind power in weak electricity grids. *Journal of Power Sources*. 2006;162(2):959-64.
- [144] Parker CD. Lead–acid battery energy-storage systems for electricity supply networks. *Journal of Power Sources*. 2001;100(1-2):18-28.
- [145] Baker J. New technology and possible advances in energy storage. *Energy Policy*. 2008;36(12):4368-73.
- [146] Rydh CJ. Environmental assessment of vanadium redox and lead-acid batteries for stationary energy storage. *Journal of Power Sources*. 1999;80(1-2):21-9.
- [147] Pickard WF, Shen AQ, Hansing NJ. Parking the power: Strategies and physical limitations for bulk energy storage in supply–demand matching on a grid whose input power is provided by intermittent sources. *Renewable and Sustainable Energy Reviews*. 2009;13(8):1934-45.
- [148] Aifantis KE, Hackney SA, Kumar RV. High energy density lithium batteries: materials, engineering, applications: John Wiley & Sons, 2010.

- [149] Kondoh J, Ishii I, Yamaguchi H, Murata A, Otani K, Sakuta K, et al. Electrical energy storage systems for energy networks. *Energy Conversion and Management*. 2000;41(17):1863-74.
- [150] Saft Batteries. Available from: <https://www.saftbatteries.com/> (Accessed September 05 2018).
- [151] Du Pasquier A, Plitz I, Menocal S, Amatucci G. A comparative study of Li-ion battery, supercapacitor and nonaqueous asymmetric hybrid devices for automotive applications. *Journal of Power Sources*. 2003;115(1):171-8.
- [152] Adachi K, Tajima H, Hashimoto T, Kobayashi K. Development of 16 kWh power storage system applying Li-ion batteries. *Journal of Power Sources*. 2003;119:897-901.
- [153] Clark N, Doughty D. Development and testing of 100 kW/1 min Li-ion battery systems for energy storage applications. *Journal of Power Sources*. 2005;146(1-2):798-803.
- [154] Kawakami N, Iijima Y, Fukuhara M, Bando M, Sakanaka Y, Ogawa K, et al. Development and field experiences of stabilization system using 34MW NAS batteries for a 51MW wind farm. *IEEE International Symposium on Industrial Electronics*. IEEE, p. 2371-6.
- [155] Beck F, Rüetschi P. Rechargeable batteries with aqueous electrolytes. *Electrochimica Acta*. 2000;45(15-16):2467-82.
- [156] Yamamura T, Wu X, Ohta S, Shirasaki K, Sakuraba H, Satoh I, et al. Vanadium solid-salt battery: solid state with two redox couples. *Journal of Power Sources*. 2011;196(8):4003-11.
- [157] Wen Z, Cao J, Gu Z, Xu X, Zhang F, Lin Z. Research on sodium sulfur battery for energy storage. *Solid State Ionics*. 2008;179(27-32):1697-701.
- [158] Smith SC, Sen P, Kroposki B. Advancement of energy storage devices and applications in electrical power system. *Power and Energy Society General Meeting-Conversion and Delivery of Electrical Energy in the 21st Century, 2008 IEEE*. IEEE, p. 1-8.
- [159] Van der Linden S. Bulk energy storage potential in the USA, current developments and future prospects. *Energy*. 2006;31(15):3446-57.
- [160] Hall PJ, Bain EJ. Energy-storage technologies and electricity generation. *Energy Policy*. 2008;36(12):4352-5.
- [161] Smith W. The role of fuel cells in energy storage. *Journal of Power Sources*. 2000;86(1-2):74-83.
- [162] De-Boer P, Raadschelders J. Flow batteries. Leonardo Energy, briefing paper. Available from: <http://www.leonardo-energy.org/> (Accessed April 02 2019).

- [163] Benitez LE, Benitez PC, Van Kooten GC. The economics of wind power with energy storage. *Energy Economics*. 2008;30(4):1973-89.
- [164] Li P. Energy storage is the core of renewable technologies. *IEEE Nanotechnology Magazine*. 2008;2(4).
- [165] Liu M, Tay NS, Bell S, Belusko M, Jacob R, Will G, et al. Review on concentrating solar power plants and new developments in high temperature thermal energy storage technologies. *Renewable and Sustainable Energy Reviews*. 2016;53:1411-32.
- [166] International Renewable Energy Agency. Electricity storage and renewables: costs and markets to 2030 Available from: https://www.irena.org/-/media/Files/IRENA/Agency/Publication/2017/Oct/IRENA_Electricity_Storage_Costs_2017.pdf (Accessed May 16 2020).
- [167] International Renewable Energy Agency. Electricity storage valuation framework: Assessing system value and ensuring project viability. Available from: <https://www.irena.org/publications/2020/Mar/Electricity-Storage-Valuation-Framework-2020> (Accessed May 06 2020).
- [168] Kittner N, Schmidt O, Staffell I, Kammen DM. Chapter 8 - Grid-scale energy storage. In: Junginger M, Louwen A, editors. *Technological Learning in the Transition to a Low-Carbon Energy System*: Academic Press; 2020. p. 119-43.
- [169] Eckroad S, Gyuk I. EPRI-DOE handbook of energy storage for transmission & distribution applications. Available from: <https://www.sandia.gov/ess-ssl/publications/ESHB%201001834%20reduced%20size.pdf> (Accessed June 03 2019).
- [170] Tan X, Li Q, Wang H. Advances and trends of energy storage technology in Microgrid. *International Journal of Electrical Power & Energy Systems*. 2013;44(1):179-91.
- [171] Hittinger E, Whitacre JF, Apt J. What properties of grid energy storage are most valuable? *Journal of Power Sources*. 2012;206:436-49.
- [172] Kintner-Meyer MC, Balducci PJ, Jin C, Nguyen TB, Elizondo MA, Viswanathan VV, et al. Energy storage for power systems applications: A regional assessment for the northwest power pool (NWPP). Available from: https://www.pnnl.gov/main/publications/external/technical_reports/PNNL-19300.pdf (Accessed May 22 2019).

- [173] Das HS, Dey A, Tan CW, Yatim A. Feasibility analysis of standalone PV/wind/battery hybrid energy system for rural Bangladesh. *International Journal of Renewable Energy Research (IJRER)*. 2016;6(2):402-12.
- [174] Kapila S. Techno-economic and life cycle assessment of large energy storage systems [M.Sc. thesis]. University of Alberta; 2018.
- [175] Obi M, Jensen SM, Ferris JB, Bass RB. Calculation of levelized costs of electricity for various electrical energy storage systems. *Renewable and Sustainable Energy Reviews*. 2017;67:908-20.
- [176] Jülch V. Comparison of electricity storage options using levelized cost of storage (LCOS) method. *Applied Energy*. 2016;183:1594-606.
- [177] Cui B, Wang S, Sun Y. Life-cycle cost benefit analysis and optimal design of small scale active storage system for building demand limiting. *Energy*. 2014;73:787-800.
- [178] Gupta R, Soini MC, Patel MK, Parra D. Levelized cost of solar photovoltaics and wind supported by storage technologies to supply firm electricity. *Journal of Energy Storage*. 2020;27:101027.
- [179] Schmidt O, Hawkes A, Gambhir A, Staffell I. The future cost of electrical energy storage based on experience rates. *Nature Energy*. 2017;2(8):17110.
- [180] Wu S, Zhou C, Doroodchi E, Moghtaderi B. Techno-economic analysis of an integrated liquid air and thermochemical energy storage system. *Energy Conversion and Management*. 2020;205:112341.
- [181] Kintner-Meyer M, Jin C, Balducci P, Elizondo M, Guo X, Nguyen T, et al. Energy storage for variable renewable energy resource integration—a regional assessment for the Northwest Power Pool (NWPP). 2011 IEEE/PES Power Systems Conference and Exposition. IEEE, p. 1-7.
- [182] Locatelli G, Palerma E, Mancini M. Assessing the economics of large energy storage plants with an optimisation methodology. *Energy*. 2015;83:15-28.
- [183] Karellas S, Tzouganatos N. Comparison of the performance of compressed-air and hydrogen energy storage systems: Karpathos island case study. *Renewable and Sustainable Energy Reviews*. 2014;29:865-82.
- [184] Brownson DAC, Kampouris DK, Banks CE. An overview of graphene in energy production and storage applications. *Journal of Power Sources*. 2011;196(11):4873-85.

- [185] Ould Amrouche S, Rekioua D, Rekioua T, Bacha S. Overview of energy storage in renewable energy systems. *International Journal of Hydrogen Energy*. 2016;41(45):20914-27.
- [186] Zobaa AF, Afifi SN, Aleem SH, Ribeiro PF. *Energy storage at different voltage levels: technology, integration, and market aspects*: Institution of Engineering & Technology, 2018.
- [187] Connolly D. *The integration of fluctuating renewable energy using energy storage* [PhD thesis]. University of Limerick; 2010.
- [188] Kleinberg M. Battery energy storage study for the 2017 IRP. Available from: https://www.pacificorp.com/content/dam/pcorp/documents/en/pacificorp/energy/integrated-resource-plan/2017-irp/2017-irp-support-and-studies/10018304_R-01-D_PacifiCorp_Battery_Energy_Storage_Study.pdf (Accessed May 16 2020).
- [189] Mongird K, Viswanathan VV, Balducci PJ, Alam MJE, Fotedar V, Koritarov VS, et al. *Energy storage technology and cost characterization report*. Available from: <https://energystorage.pnnl.gov/pdf/PNNL-28866.pdf> (Accessed November 06 2020).
- [190] Flueckiger SM, Iverson BD, Garimella SV. Simulation of a concentrating solar power plant with molten-salt thermocline storage for optimized annual performance. *ASME 2013 7th International Conference on Energy Sustainability American Society of Mechanical Engineers*, p. V001T03A11-VT03A11.
- [191] Buiskikh D, Zakeri B, Syri S, Kauranen P. Economic feasibility of flow batteries in grid-scale applications. *2018 15th International Conference on the European Energy Market (EEM)*. p. 1-5.
- [192] Hameer S, van Niekerk JL. A review of large-scale electrical energy storage. *International Journal of Energy Research*. 2015;39(9):1179-95.
- [193] Pei Y, Cavagnino A, Vaschetto S, Chai F, Tenconi A. Flywheel energy storage systems for power systems application. *2017 6th International Conference on Clean Electrical Power (ICCEP)*. p. 492-501.
- [194] Masebinu SO, Akinlabi ET, Muzenda E, Aboyade AO. Techno-economic analysis of grid-tied energy storage. *International Journal of Environmental Science and Technology*. 2018;15(1):231-42.
- [195] Staffell I, Rustomji M. Maximising the value of electricity storage. *Journal of Energy Storage*. 2016;8:212-25.

- [196] Generation of electricity and district heating, energy storage and energy carrier generation and conversion: technology data for energy plants. Available from: <https://ens.dk/en/our-services/projections-and-models/technology-data/technology-data-generation-electricity-and> (Accessed July 10 2018).
- [197] Caralis G, Christakopoulos T, Karellas S, Gao Z. Analysis of energy storage systems to exploit wind energy curtailment in Crete. *Renewable and Sustainable Energy Reviews*. 2019;103:122-39.
- [198] Kale V, Secanell M. A comparative study between optimal metal and composite rotors for flywheel energy storage systems. *Energy Reports*. 2018;4:576-85.
- [199] Silva-Saravia H, Pulgar-Painemal H, Mauricio JM. Flywheel energy storage model, control and location for improving stability: The Chilean case. *IEEE Transactions on Power Systems*. 2017;32(4):3111-9.
- [200] Cardenas R, Pena R, Asher G, Clare J. Control strategies for enhanced power smoothing in wind energy systems using a flywheel driven by a vector-controlled induction machine. *IEEE Transactions on Industrial Electronics*. 2001;48(3):625-35.
- [201] Kailasan A. Preliminary design and analysis of an energy storage flywheel [PhD thesis]. University of Virginia; 2013.
- [202] Amber Kinetics Inc. Smart grid demonstration program. Available from: https://www.smartgrid.gov/files/documents/Amber_Kinetics_Final_Technical_Report.pdf (Accessed May 16 2020).
- [203] Amiryar ME, Pullen KR. A review of flywheel energy storage system technologies and their applications. *Applied Sciences*. 2017;7(3):286.
- [204] Rupp A, Baier H, Mertiny P, Secanell M. Analysis of a flywheel energy storage system for light rail transit. *Energy*. 2016;107:625-38.
- [205] Brown DR, Chvala WD. Flywheel energy storage: An alternative to batteries for UPS systems. *Energy engineering*. 2005;102(5):7-26.
- [206] Sioshansi R, Denholm P, Jenkin T. A comparative analysis of the value of pure and hybrid electricity storage. *Energy Economics*. 2011;33(1):56-66.
- [207] Rastler D. Electricity energy storage technology options: a white paper primer on applications, costs and benefits. Available from: <http://large.stanford.edu/courses/2012/ph240/doshay1/docs/EPRI.pdf> (Accessed May 05 2019).

- [208] Auer J, Keil J, Stobbe A, AG DB, Mayer T. State-of-the-art electricity storage systems. Available from: https://papers.ssrn.com/sol3/papers.cfm?abstract_id=2882202 (Accessed May 16 2020).
- [209] Kaun B, Chen S. Cost-effectiveness of energy storage in California. Available from: <http://large.stanford.edu/courses/2013/ph240/cabrera1/docs/3002001162.pdf> (Accessed May 16 2020).
- [210] Zhou Q, He Q, Lu C, Du D. Techno-economic analysis of advanced adiabatic compressed air energy storage system based on life cycle cost. *Journal of Cleaner Production*. 2020;265:121768.
- [211] Beacon Power. Carbon fiber flywheels. Available from: <https://beaconpower.com/carbon-fiber-flywheels/> (Accessed May 13 2020).
- [212] Belderbos A, Delarue E, Kessels K, D'Haeseleer W. Levelized cost of storage — Introducing novel metrics. *Energy Economics*. 2017;67:287-99.
- [213] Schmidt TS, Beuse M, Zhang X, Steffen B, Schneider SF, Pena-Bello A, et al. Additional emissions and cost from storing electricity in stationary battery systems. *Environmental Science & Technology*. 2019;53(7):3379-90.
- [214] Dufo-López R, Bernal-Agustín JL. Techno-economic analysis of grid-connected battery storage. *Energy Conversion and Management*. 2015;91:394-404.
- [215] Steward D, Saur G, Penev M, Ramsden T. Lifecycle cost analysis of hydrogen versus other technologies for electrical energy storage. Available from: <https://www.nrel.gov/docs/fy10osti/46719.pdf> (Accessed May 15 2019).
- [216] Mantz RJ, De Battista H. Hydrogen production from idle generation capacity of wind turbines. *International Journal of Hydrogen Energy*. 2008;33(16):4291-300.
- [217] Bernal-Agustín JL, Dufo-López R. Hourly energy management for grid-connected wind–hydrogen systems. *International Journal of Hydrogen Energy*. 2008;33(22):6401-13.
- [218] Anderson D, Leach M. Harvesting and redistributing renewable energy: on the role of gas and electricity grids to overcome intermittency through the generation and storage of hydrogen. *Energy Policy*. 2004;32(14):1603-14.
- [219] Aguado M, Ayerbe E, Azcárate C, Blanco R, Garde R, Mallor F, et al. Economical assessment of a wind–hydrogen energy system using WindHyGen® software. *International Journal of Hydrogen Energy*. 2009;34(7):2845-54.

- [220] Zafirakis DP. 2 - Overview of energy storage technologies for renewable energy systems. In: Kaldellis JK, editor. Stand-Alone and Hybrid Wind Energy Systems: Woodhead Publishing; 2010. p. 29-80.
- [221] Parra D, Patel MK. Techno-economic implications of the electrolyser technology and size for power-to-gas systems. *International Journal of Hydrogen Energy*. 2016;41(6):3748-61.
- [222] Preuster P, Alekseev A, Wasserscheid P. Hydrogen storage technologies for future energy systems. *Annual Review of Chemical and Biomolecular Engineering*. 2017;8(1):445-71.
- [223] Ferrero D, Gamba M, Lanzini A, Santarelli M. Power-to-gas hydrogen: Techno-economic assessment of processes towards a multi-purpose energy carrier. *Energy Procedia*. 2016;101:50-7.
- [224] Marocco P, Ferrero D, Gandiglio M, Ortiz MM, Sundseth K, Lanzini A, et al. A study of the techno-economic feasibility of H₂-based energy storage systems in remote areas. *Energy Conversion and Management*. 2020;211:112768.
- [225] Nguyen T, Abdin Z, Holm T, Mérida W. Grid-connected hydrogen production via large-scale water electrolysis. *Energy Conversion and Management*. 2019;200:112108.
- [226] Ahmed N, Elfeky KE, Lu L, Wang QW. Thermal and economic evaluation of thermocline combined sensible-latent heat thermal energy storage system for medium temperature applications. *Energy Conversion and Management*. 2019;189:14-23.
- [227] Poghosyan V, Hassan MI. Techno-economic assessment of substituting natural gas based heater with thermal energy storage system in parabolic trough concentrated solar power plant. *Renewable Energy*. 2015;75:152-64.
- [228] Rea JE, Oshman CJ, Olsen ML, Hardin CL, Glatzmaier GC, Siegel NP, et al. Performance modeling and techno-economic analysis of a modular concentrated solar power tower with latent heat storage. *Applied Energy*. 2018;217:143-52.
- [229] Boudaoud S, Khellaf A, Mohammedi K, Behar O. Thermal performance prediction and sensitivity analysis for future deployment of molten salt cavity receiver solar power plants in Algeria. *Energy Conversion and Management*. 2015;89:655-64.
- [230] Seitz M, Johnson M, Hübner S. Economic impact of latent heat thermal energy storage systems within direct steam generating solar thermal power plants with parabolic troughs. *Energy Conversion and Management*. 2017;143:286-94.

- [231] Xu B, Li P, Chan C. Application of phase change materials for thermal energy storage in concentrated solar thermal power plants: A review to recent developments. *Applied Energy*. 2015;160:286-307.
- [232] Schoenung S. Economic analysis of large-scale hydrogen storage for renewable utility applications. Available from: <https://prod-ng.sandia.gov/techlib-noauth/access-control.cgi/2011/114845.pdf> (Accessed May 16 2020).
- [233] Medina P, Bizuayehu AW, Catalão JP, Rodrigues EM, Contreras J. Electrical energy storage systems: technologies' state-of-the-art, techno-economic benefits and applications analysis. 47th Hawaii International Conference on System sciences IEEE, p. 2295-304.
- [234] Gracia L, Casero P, Bourasseau C, Chabert A. Use of hydrogen in off-grid locations, a techno-economic assessment. *Energies*. 2018;11(11):3141.
- [235] Guandalini G, Campanari S, Romano MC. Power-to-gas plants and gas turbines for improved wind energy dispatchability: Energy and economic assessment. *Applied Energy*. 2015;147:117-30.
- [236] Jafari M, Armaghan D, Seyed Mahmoudi SM, Chitsaz A. Thermoeconomic analysis of a standalone solar hydrogen system with hybrid energy storage. *International Journal of Hydrogen Energy*. 2019;44(36):19614-27.
- [237] Petrollese M, Arena S, Cascetta M, Casti E, Cau G. Techno-economic comparison of different thermal energy storage technologies for medium-scale CSP plants. *AIP Conference Proceedings*. 2019;2191(1):020128.
- [238] Rodríguez JM, Sánchez D, Martínez GS, Bennouna EG, Ikken B. Techno-economic assessment of thermal energy storage solutions for a 1MWe CSP-ORC power plant. *Solar Energy*. 2016;140:206-18.
- [239] Andika R, Kim Y, Yoon SH, Kim DH, Choi JS, Lee M. Techno-economic assessment of technological improvements in thermal energy storage of concentrated solar power. *Solar Energy*. 2017;157:552-8.
- [240] Bayon A, Bader R, Jafarian M, Fedunik-Hofman L, Sun Y, Hinkley J, et al. Techno-economic assessment of solid-gas thermochemical energy storage systems for solar thermal power applications. *Energy*. 2018;149:473-84.

- [241] European Commission. SOLGATE: Solar Hybrid Gas Turbine Electric Power System. Available from: <https://publications.europa.eu/en/publication-detail/-/publication/e4f88dd1-74ac-4416-aba0-3868cc8ea5ca> (Accessed May 10 2018).
- [242] Heller L, Gauche P. Modeling of the rock bed thermal energy storage system of a combined cycle solar thermal power plant in South Africa. *Solar Energy*. 2013;93:345-56.
- [243] Strasser MN, Selvam RP. A cost and performance comparison of packed bed and structured thermocline thermal energy storage systems. *Solar Energy*. 2014;108:390-402.
- [244] Nithyanandam K, Pitchumani R. Cost and performance analysis of concentrating solar power systems with integrated latent thermal energy storage. *Energy*. 2014;64:793-810.
- [245] Hayward J, Graham P. Electricity generation technology cost projections: 2017-2050. Available from: <https://publications.csiro.au/rpr/download?pid=csiro:EP178771&dsid=DS2> (Accessed May 16 2020).
- [246] Lazard. Lazard's levelized cost of storage analysis, Version 3.0. Available from: <https://www.lazard.com/media/450338/lazard-levelized-cost-of-storage-version-30.pdf> (Accessed May 16 2020).
- [247] Cole WJ, Frazier A. Cost projections for utility-scale battery storage. Available: <https://www.nrel.gov/docs/fy19osti/73222.pdf>.
- [248] Nykvist B, Nilsson M. Rapidly falling costs of battery packs for electric vehicles. *Nature Climate Change*. 2015;5(4):329-32.
- [249] Keck F, Lenzen M, Vassallo A, Li M. The impact of battery energy storage for renewable energy power grids in Australia. *Energy*. 2019;173:647-57.
- [250] Gröger O, Gasteiger HA, Suchsland J-P. Review—Electromobility: Batteries or fuel cells? *Journal of The Electrochemical Society*. 2015;162(14):A2605-A22.
- [251] Hawkins TR, Gausen OM, Strømman AH. Environmental impacts of hybrid and electric vehicles—a review. *The International Journal of Life Cycle Assessment*. 2012;17(8):997-1014.
- [252] Nealer R, Hendrickson TP. Review of recent lifecycle assessments of energy and greenhouse gas emissions for electric vehicles. *Current Sustainable/Renewable Energy Reports*. 2015;2(3):66-73.
- [253] Abdon A, Zhang X, Parra D, Patel MK, Bauer C, Worlitschek J. Techno-economic and environmental assessment of stationary electricity storage technologies for different time scales. *Energy*. 2017;139:1173-87.

- [254] Burkhardt JJ, Heath G, Turchi C. Life cycle assessment of a model parabolic trough concentrating solar power plant with thermal energy storage. ASME 2010 4th International Conference on Energy Sustainability. American Society of Mechanical Engineers, p. 599-608.
- [255] Wang Q, Liu W, Yuan X, Tang H, Tang Y, Wang M, et al. Environmental impact analysis and process optimization of batteries based on life cycle assessment. *Journal of Cleaner Production*. 2018;174:1262-73.
- [256] Kapila S, Oni AO, Gemechu ED, Kumar A. Development of net energy ratios and life cycle greenhouse gas emissions of large-scale mechanical energy storage systems. *Energy*. 2019;170:592-603.
- [257] Bouman EA, Øberg MM, Hertwich EG. Environmental impacts of balancing offshore wind power with compressed air energy storage (CAES). *Energy*. 2016;95:91-8.
- [258] Hiremath M, Derendorf K, Vogt T. Comparative life cycle assessment of battery storage systems for stationary applications. *Environmental Science & Technology*. 2015;49(8):4825-33.
- [259] Oró E, Gil A, De Gracia A, Boer D, Cabeza LF. Comparative life cycle assessment of thermal energy storage systems for solar power plants. *Renewable Energy*. 2012;44:166-73.
- [260] Ellingsen LA-W, Hung CR, Strømman AH. Identifying key assumptions and differences in life cycle assessment studies of lithium-ion traction batteries with focus on greenhouse gas emissions. *Transportation Research Part D: Transport and Environment*. 2017;55:82-90.
- [261] McManus MC. Environmental consequences of the use of batteries in low carbon systems: The impact of battery production. *Applied Energy*. 2012;93:288-95.
- [262] Vandepaer L, Cloutier J, Bauer C, Amor B. Integrating batteries in the future Swiss electricity supply system: A consequential environmental assessment. *Journal of Industrial Ecology*. 2019;23(3):709-25.
- [263] Elzein H, Dandres T, Levasseur A, Samson R. How can an optimized life cycle assessment method help evaluate the use phase of energy storage systems? *Journal of Cleaner Production*. 2019;209:1624-36.
- [264] Thomassen MA, Dalgaard R, Heijungs R, de Boer I. Attributional and consequential LCA of milk production. *The International Journal of Life Cycle Assessment*. 2008;13(4):339-49.
- [265] Ekvall T, Azapagic A, Finnveden G, Rydberg T, Weidema BP, Zamagni A. Attributional and consequential LCA in the ILCD handbook. *The International Journal of Life Cycle Assessment*. 2016;21(3):293-6.

- [266] Kua HW, Kamath S. An attributional and consequential life cycle assessment of substituting concrete with bricks. *Journal of Cleaner Production*. 2014;81:190-200.
- [267] Masruroh NA, Li B, Klemeš J. Life cycle analysis of a solar thermal system with thermochemical storage process. *Renewable Energy*. 2006;31(4):537-48.
- [268] Heath G, Turchi C, Decker T, Burkhardt J, Kutscher C. Life cycle assessment of thermal energy storage: two-tank indirect and thermocline. *ASME 2009 3rd International Conference on Energy Sustainability collocated with the Heat Transfer and InterPACK09 Conferences*. American Society of Mechanical Engineers, p. 689-90.
- [269] Peters J, Buchholz D, Passerini S, Weil M. Life cycle assessment of sodium-ion batteries. *Energy & Environmental Science*. 2016;9(5):1744-51.
- [270] Sternberg A, Bardow A. Power-to-What? – Environmental assessment of energy storage systems. *Energy & Environmental Science*. 2015;8(2):389-400.
- [271] Thaker S, Oni AO, Gemechu E, Kumar A. Evaluating energy and greenhouse gas emission footprints of thermal energy storage systems for concentrated solar power applications. *Journal of Energy Storage*. 2019;26:100992.
- [272] Torres O. Life cycle assessment of a pumped storage power plant: Institutt for Energi-og Prosessteknikk. Available from: https://brage.bibsys.no/xmlui/bitstream/handle/11250/234503/455355_FULLTEXT01.pdf?sequence=2&isAllowed=y (Accessed May 17 2020).
- [273] Majeau-Bettez G, Hawkins TR, Strømman AH. Life cycle environmental assessment of lithium-ion and nickel metal hydride batteries for plug-in hybrid and battery electric vehicles. *Environmental Science & Technology*. 2011;45(10):4548-54.
- [274] Zackrisson M, Avellán L, Orlenius J. Life cycle assessment of lithium-ion batteries for plug-in hybrid electric vehicles – Critical issues. *Journal of Cleaner Production*. 2010;18(15):1519-29.
- [275] Troy S, Schreiber A, Reppert T, Gehrke H-G, Finsterbusch M, Uhlenbruck S, et al. Life cycle assessment and resource analysis of all-solid-state batteries. *Applied Energy*. 2016;169:757-67.
- [276] Arbabzadeh M, Johnson JX, Keoleian GA. Parameters driving environmental performance of energy storage systems across grid applications. *Journal of Energy Storage*. 2017;12:11-28.
- [277] Swain B. Recovery and recycling of lithium: A review. *Separation and Purification Technology*. 2017;172:388-403.

- [278] Brandt AR, Dale M, Barnhart CJ. Calculating systems-scale energy efficiency and net energy returns: A bottom-up matrix-based approach. *Energy*. 2013;62:235-47.
- [279] Goedkoop M. A damage oriented method for life cycle impact assessment. Available from: <https://ci.nii.ac.jp/naid/10011909509/> (Accessed May 16 2020).
- [280] Stougie L, Del Santo G, Innocenti G, Goosen E, Vermaas D, van der Kooi H, et al. Multi-dimensional life cycle assessment of decentralised energy storage systems. *Energy*. 2019;182:535-43.
- [281] Goedkoop M, Heijungs R, Huijbregts M, Schryver A, Struijs J, Zelm R. Report I: Characterisation, ReCiPe 2008: A life cycle impact assessment method which comprises harmonised category indicators at the midpoint and the endpoint level. Ministry of Housing, Spatial planning and the Environment (VROM), The Netherlands. 2009.
- [282] Hsu DD, O'Donoghue P, Fthenakis V, Heath GA, Kim HC, Sawyer P, et al. Life cycle greenhouse gas emissions of crystalline silicon photovoltaic electricity generation. *Journal of Industrial Ecology*. 2012;16(s1):S122-S35.
- [283] Dolan SL, Heath GA. Life cycle greenhouse gas emissions of utility-scale wind power: Systematic review and harmonization. *Journal of Industrial Ecology*. 2012;16:S136-S54.
- [284] Rahman MM, Salehin S, Ahmed SSU, Sadrul Islam AKM. Chapter two - Environmental impact assessment of different renewable energy resources: A recent development. In: Rasul MG, Azad Ak, Sharma SC, editors. *Clean Energy for Sustainable Development*: Academic Press; 2017. p. 29-71.
- [285] Di Lullo G, Gemechu E, Oni AO, Kumar A. Extending sensitivity analysis using regression to effectively disseminate life cycle assessment results. *The International Journal of Life Cycle Assessment*. 2020;25(2):222-39.
- [286] Jülch V, Telsnig T, Schulz M, Hartmann N, Thomsen J, Eltrop L, et al. A holistic comparative analysis of different storage systems using levelized cost of storage and life cycle indicators. *Energy Procedia*. 2015;73:18-28.
- [287] Fernandez-Marchante CM, Millán M, Medina-Santos JI, Lobato J. Environmental and preliminary cost assessments of redox flow batteries for renewable energy storage. *Energy Technology*. n/a(n/a):1900914.

- [288] Mastro C. Behind-the-meter battery storage: technical and market assessment. Available from: <https://www.nyscrda.ny.gov/-/media/Files/Publications/Research/Electric-Power-Delivery/Behind-Meter-Battery-Storage.pdf> (Accessed May 04 2019).
- [289] Immendoerfer A, Tietze I, Hottenroth H, Viere T. Life-cycle impacts of pumped hydropower storage and battery storage. *International Journal of Energy and Environmental Engineering*. 2017;8(3):231-45.
- [290] Renewable Energy Statistics 2019. Available from: <https://www.irena.org/publications/2019/Jul/Renewable-energy-statistics-2019> (Accessed September 23 2019).
- [291] International Renewable Energy Agency. Global energy transformation. Available from: https://www.irena.org/-/media/Files/IRENA/Agency/Publication/2018/Apr/IRENA_Report_GET_2018.pdf (Accessed September 23 2019).
- [292] Denholm P, Ela E, Kirby B, Milligan M. Role of energy storage with renewable electricity generation. Available from: <https://www.osti.gov/biblio/972169> (Accessed September 23 2019).
- [293] Eyer J, Corey G. Energy storage for the electricity grid: Benefits and market potential assessment guide. Available from: https://smartgrid.gov/files/sandia_energy_storage_report_sand2010-0815.pdf (Accessed April 10 2019).
- [294] Bozzolani E. Techno-economic analysis of compressed air energy storage systems [M.Sc. thesis]. Cranfield University; 2010.
- [295] Liu C, Xu Y, Hu S, Chen H. Techno-economic analysis of compressed air energy storage power plant. *Energy Storage Science and Technology*. 2015;4(2):158-68.
- [296] Minke C, Kunz U, Turek T. Techno-economic assessment of novel vanadium redox flow batteries with large-area cells. *Journal of Power Sources*. 2017;361:105-14.
- [297] Poonpun P, Jewell WT. Analysis of the cost per kilowatt hour to store electricity. *IEEE Transactions on Energy Conversion*. 2008;23(2):529-34.
- [298] Dufo-López R, Bernal-Agustín JL, Domínguez-Navarro JA. Generation management using batteries in wind farms: Economical and technical analysis for Spain. *Energy Policy*. 2009;37(1):126-39.

- [299] Rodrigues E, Osório G, Godina R, Bizuayehu A, Lujano-Rojas J, Matias J, et al. Modelling and sizing of NaS (sodium sulfur) battery energy storage system for extending wind power performance in Crete Island. *Energy*. 2015;90:1606-17.
- [300] Utility Dive. Energy storage will disrupt transmission and distribution investments. Available from: [https://www.utilitydive.com/news/energy-storage-will-disrupt-transmission-and-distribution-investments/506945/#targetText=Energy%20storage%20systems%20\(ESSs\)%20providing,development%20of%20new%20business%20models.&targetText=T%26D%20systems%20adapt%20to%20end,the%20placement%20of%20generation%20assets](https://www.utilitydive.com/news/energy-storage-will-disrupt-transmission-and-distribution-investments/506945/#targetText=Energy%20storage%20systems%20(ESSs)%20providing,development%20of%20new%20business%20models.&targetText=T%26D%20systems%20adapt%20to%20end,the%20placement%20of%20generation%20assets). (Accessed September 18 2019).
- [301] Manz D, Keller J, Miller N. Value propositions for utility-scale energy storage. 2011 IEEE/PES Power Systems Conference and Exposition. IEEE, p. 1-10.
- [302] ABB. Energy storage solutions- EssPro™ energy storage power conversion system (PCS). Available from: https://library.e.abb.com/public/a9b8ede76a664383b8ecffaad161730b/EssPro-PCS_Brochure.pdf (Accessed December 02 2019).
- [303] Akinyele D, Belikov J, Levron Y. Battery storage technologies for electrical applications: impact in stand-alone photovoltaic systems. *Energies*. 2017;10(11):1760.
- [304] Kaldellis J, Zafirakis D, Kavadias K. Techno-economic comparison of energy storage systems for island autonomous electrical networks. *Renewable and Sustainable Energy Reviews*. 2009;13(2):378-92.
- [305] Gaillac L. Tehachapi wind energy storage project. Available from: https://www.sandia.gov/ess-ssl/docs/pr_conferences/2014/Friday/Session10/02_Gaillac_Loic_SCEdison_Tehachapi.pdf (Accessed May 15 2019).
- [306] Jackson N. Battery technologies for small scale embedded generation. Available from: <http://www.ee.co.za/wp-content/uploads/2018/10/Norman-Jackson-SAESA-presentation.pdf> (Accessed May 15 2019).
- [307] Dassisti M, Mastrorilli P, Rizzuti A, Cozzolino G, Chimienti M, Olabi A-G, et al. Vanadium: a transition metal for sustainable energy storing in redox flow batteries. Reference Module in Materials Science and Materials Engineering: Elsevier BV; 2016.

- [308] Liao Q, Sun B, Liu Y, Sun J, Zhou G. A techno-economic analysis on NaS battery energy storage system supporting peak shaving. *International Journal of Energy Research*. 2016;40(2):241-7.
- [309] Hussien ZF, Lee WC, Siam MF, Ismail AB. Modeling of sodium sulfur battery for power system applications. *Elektrika Journal of Electrical Engineering*. 2007;9(2):66-72.
- [310] Albright G, Edie J, Al-Hallaj S. A comparison of lead acid to lithium-ion in stationary storage applications. Available from: <https://www.batterypoweronline.com/wp-content/uploads/2012/07/Lead-acid-white-paper.pdf> (Accessed June 10 2019).
- [311] Mallon K, Assadian F, Fu B. Analysis of on-board photovoltaics for a battery electric bus and their impact on battery lifespan. *Energies*. 2017;10(7):943.
- [312] Discover Battery. OPzS (flooded) and OPzV (gel) tubular plate batteries. Available from: <https://www.harrisbattery.com/sites/default/files/literature/Discover-Energy-Storage-OPzS-OPzV-batteries.pdf> (Accessed June 10 2019).
- [313] Discover Battery. Energy CUB. Available from: <https://discoverbattery.com/EN/products/energy-cub> (Accessed May 10 2019).
- [314] Ehnberg J, Liu Y, Grahn M. Grid and storage. Available from: <https://core.ac.uk/download/pdf/70609990.pdf> (Accessed May 20 2019).
- [315] SAFT. Ni-Cd block battery technical manual. Available from: <https://us.v-cdn.net/6024911/uploads/attachments/379/4108.pdf> (Accessed June 20 2019).
- [316] Zimmerman N. Vanadium redox flow battery: sizing of VRB in electrified heavy construction equipment [M.Sc. thesis]. Mälardalen University; 2014.
- [317] Droege P. *Urban energy transition: From fossil fuels to renewable power*. Australia: Elsevier, 2011.
- [318] Discover Battery. Advanced tubular batteries: OPzS/OPzV tubular batteries. Available from: <https://discoverbattery.com/en/products/advanced-tubular-batteries/> (Accessed 2019 May 15).
- [319] Rongke Power. Products and Service. Available from: <http://www.rongkepower.com/chuneng?lang=en> (Accessed February 17 2020).
- [320] Viswanathan V, Crawford A, Stephenson D, Kim S, Wang W, Li B, et al. Cost and performance model for redox flow batteries. *Journal of Power Sources*. 2014;247:1040-51.

- [321] Verma A, Nimana B, Olateju B, Rahman MM, Radpour S, Canter C, et al. A techno-economic assessment of bitumen and synthetic crude oil transport (SCO) in the Canadian oil sands industry: Oil via rail or pipeline? *Energy*. 2017;124:665-83.
- [322] Gyuk I, Eckroad S, Key T, Kamath H. EPRI-DOE handbook supplement of energy storage for grid connected wind generation applications. Available from: <https://www.sandia.gov/ess-ssl/publications/EPRI-DOE%20ESHB%20Wind%20Supplement.pdf> (Accessed April 16 2019).
- [323] AESO. AESO 2017 annual market statistics. Available from: <https://www.aeso.ca/download/listedfiles/2017-Annual-Market-Stats.pdf> (Accessed May 15 2019).
- [324] Inflation.eu. Worldwide inflation data. Available from: <https://www.inflation.eu/inflation-rates/canada/historic-inflation/cpi-inflation-canada-2018.aspx> (Accessed May 09 2019).
- [325] Fu R, Remo TW, Margolis RM. 2018 US utility-scale photovoltaics-plus-energy storage system costs benchmark. Available from: <https://www.nrel.gov/docs/fy19osti/71714.pdf> (Accessed April 23 2019).
- [326] Aquino T, Zuelch C, Koss C. Energy storage technology assessment Available from: <https://www.pnm.com/documents/396023/1506047/11-06-17+PNM+Energy+Storage+Report+-+Draft+-+RevC.pdf/04ca7143-1dbe-79e1-8549-294be656f4ca/> (Accessed May 10 2019).
- [327] Viswanathan V, Kintner-Meyer M, Balducci P, Jin C. National assessment of energy storage for grid balancing and arbitrage phase II volume 2: cost and performance characterization. Available from: https://energyenvironment.pnnl.gov/pdf/National_Assessment_Storage_PHASE_II_vol_2_final.pdf (Accessed May 15 2019).
- [328] Carnegie R, Gotham D, Nderitu D, Preckel PV. Utility scale energy storage systems, benefits, application, and technologies, by State Utility Forecasting Group, June 2013. Available from: <https://www.purdue.edu/discoverypark/sufg/docs/publications/SUFG%20Energy%20Storage%20Report.pdf> (Accessed June 12 2019).
- [329] Kintner-Meyer M, Balducci P, Colella W, Elizondo M, Jin C, Nguyen T, et al. National assessment of energy storage for grid balancing and arbitrage: phase: II: WECC, ERCOT, EIC, volume 1: technical analysis. Available from:

https://energyenvironment.pnnl.gov/pdf/National_Assessment_Storage_PHASE_II_vol_1_final.pdf (Accessed May 18 2019).

[330] BloombergNEF. A behind the scenes take on lithium-ion battery prices. Available from: <https://about.bnef.com/blog/behind-scenes-take-lithium-ion-battery-prices/> (Accessed September 27 2019).

[331] Rahman MM, Gemechu E, Oni AO, Kumar A. The development of a techno-economic model for the assessment of the cost of flywheel energy storage systems for utility-scale stationary applications. *Sustainable Energy Technologies and Assessments*. 2021;47:101382.

[332] Dowling JA, Rinaldi KZ, Ruggles TH, Davis SJ, Yuan M, Tong F, et al. Role of long-duration energy storage in variable renewable electricity systems. *Joule*. 2020;4(9):1907-28.

[333] Saranya G, Ramachandra TV. Life cycle assessment of biodiesel from estuarine microalgae. *Energy Conversion and Management: X*. 2020;8:100065.

[334] Mahmud MAP, Huda N, Farjana SH, Lang C. Comparative life cycle environmental impact analysis of lithium-ion (LiIo) and nickel-metal hydride (NiMH) batteries. *Batteries*. 2019;5(1):22.

[335] Accardo A, Dotelli G, Musa ML, Spessa E. Life cycle assessment of an NMC battery for application to electric light-duty commercial vehicles and comparison with a sodium-nickel-chloride battery. *Applied Sciences*. 2021;11(3):1160.

[336] Li R, Zhang H, Chen H, Zhang Y, Li Z, Zhao J, et al. Hybrid techno-economic and environmental assessment of adiabatic compressed air energy storage system in China-Situation. *Applied Thermal Engineering*. 2021;186:116443.

[337] Ni Z, Wang Y, Wang Y, Chen S, Xie M, Grotenhuis T, et al. Comparative life-cycle assessment of aquifer thermal energy storage integrated with in situ bioremediation of chlorinated volatile organic compounds. *Environmental Science & Technology*. 2020;54(5):3039-49.

[338] Rahman MM, Oni AO, Gemechu E, Kumar A. The development of techno-economic models for the assessment of utility-scale electro-chemical battery storage systems. *Applied Energy*. 2021;283:116343.

[339] Cready E, Lippert J, Pihl J, Weinstock I, Symons P, Jungst RG. Final report technical and economic feasibility of applying used EV batteries in stationary applications. Available: <https://www.osti.gov/servlets/purl/809607>.

- [340] Butler P, Miller JL, Taylor PA. Energy storage opportunities analysis phase ii final report a study for the doe energy storage systems program. Available: <https://www.sandia.gov/ess-ssl/publications/SAND2002-1314.pdf>.
- [341] Spanos C, Turney DE, Fthenakis V. Life-cycle analysis of flow-assisted nickel zinc-, manganese dioxide-, and valve-regulated lead-acid batteries designed for demand-charge reduction. *Renewable and Sustainable Energy Reviews*. 2015;43:478-94.
- [342] Stan A, Świerczyński M, Stroe D, Teodorescu R, Andreasen SJ. Lithium ion battery chemistries from renewable energy storage to automotive and back-up power applications — An overview. 2014 International Conference on Optimization of Electrical and Electronic Equipment (OPTIM). p. 713-20.
- [343] Sudworth JL. 8 - High temperature cells. In: Vincent CA, Scrosati B, editors. *Modern Batteries (Second Edition)*. Oxford: Butterworth-Heinemann; 1997. p. 243-74.
- [344] European Association for Storage for Energy. Sodium-sulphur (NaS) battery. Available from: http://ease-storage.eu/wp-content/uploads/2018/09/2018.07_EASE_Technology-Description_NaS.pdf (Accessed April 23 2020).
- [345] Brost R. Valve-regulated lead-acid batteries in automotive applications—a vehicle manufacturer's perspective. *Valve-regulated lead-acid batteries*: Elsevier; 2004. p. 327-96.
- [346] Discover. Tubular gel (OPZV) batteries - stationary & renewable energy applications. Available from: <https://discoverbattery.com/assets/dropbox/Resources/Brochures/en/Tubular-Gel-OPzV-Batteries-Brochure.pdf> (Accessed April 12 2020).
- [347] Omar N, Firouz Y, Monem MA, Samba A, Gualous H, Coosemans T, et al. Analysis of nickel-based battery technologies for hybrid and electric vehicles. *Reference Module in Chemistry, Molecular Sciences and Chemical Engineering*: Elsevier; 2014.
- [348] Fan X, Liu B, Liu J, Ding J, Han X, Deng Y, et al. Battery technologies for grid-level large-scale electrical energy storage. *Transactions of Tianjin University*. 2020;26(2):92-103.
- [349] Sullivan J, Gaines L. A review of battery life-cycle analysis: state of knowledge and critical needs. Available from: <https://publications.anl.gov/anlpubs/2010/11/68455.pdf> (Accessed December 10 2019).
- [350] GREET 2. Argonne National Laboratory. Available: <https://greet.es.anl.gov/greet.models>.
- [351] Rydh CJ, Karlström M. Life cycle inventory of recycling portable nickel–cadmium batteries. *Resources, Conservation and Recycling*. 2002;34(4):289-309.

- [352] Saft. Safety data sheet. Available from: <https://cellpacksolutions.co.uk/wp-content/uploads/2015/06/saft-nicd-safety-data-sheet.pdf> (Accessed December 10 2019).
- [353] Indrivetec. Power conversion systems for energy storage. Available from: <https://www.eseexpo.de/vis-content/event-energy2018/exh-energy2018.2565909/Energy-Storage-Europe-2018-INDRIVETEC-AG-Paper-energy2018.2565909-71ymsoNDToiEwLEBZjL0iQ.pdf> (Accessed March 10 2020).
- [354] Meksan Transformer. Main dimensions of the 300-2500 kVA standard transformers with oil expansion tanks. Available from: <http://www.meksantrafo.com.tr/en/node/15> (Accessed March 05 2020).
- [355] Dunn JB, Gaines L, Barnes M, Sullivan JL, Wang M. Material and energy flows in the materials production, assembly, and end-of-life stages of the automotive lithium-ion battery life cycle. Available: <https://publications.anl.gov/anlpubs/2014/11/109509.pdf>.
- [356] Energy Storage. BASF ‘enters energy market’ with NGK NAS battery partnership. Available from: <https://www.energy-storage.news/news/basf-enters-energy-market-with-ngk-nas-battery-partnership> (Accessed February 24 2020).
- [357] Rydh CJ, Sandén BA. Energy analysis of batteries in photovoltaic systems. Part I: Performance and energy requirements. *Energy Conversion and Management*. 2005;46(11):1957-79.
- [358] Breeze P. Chapter 10 - Power system energy storage technologies. In: Breeze P, editor. *Power Generation Technologies (Third Edition)*: Newnes; 2019. p. 219-49.
- [359] Carbon Footprint. 2019 grid electricity emissions factors v1.0 – June 2019. Available from: https://www.carbonfootprint.com/docs/2019_06_emissions_factors_sources_for_2019_electricity.pdf (Accessed March 08 2020).
- [360] Dougher C. Breaking down the lithium-ion cell manufacturing supply chain in the U.S. to identify key barriers to growth [Masters thesis]. Duke University; 2018.
- [361] Climate Leadership. Emissions factors for greenhouse gas inventories. Available from: https://www.epa.gov/sites/production/files/2018-03/documents/emission-factors_mar_2018_0.pdf (Accessed December 10 2019).
- [362] East Penn. Manufacturing plant and battery technology. Available from: <http://www.eastpenncanada.com/phone/manufacturing.html> (Accessed December 03 2019).

- [363] Mudgal S, Guern Y, Tinetti B, Chanoine A, Pahal S, Witte F. Comparative life-cycle assessment of nickel-cadmium (NiCd) batteries used in Cordless Power Tools (CPTs) vs. their alternatives nickel-metal hydride (NiMH) and lithium-ion (Li-ion) batteries. Final Report of European Commission. Bio Intelligence Service, Paris, France. Available from: https://ec.europa.eu/environment/waste/batteries/pdf/report_12.pdf (Accessed December 10 2019).
- [364] Debra F. Vanadium flow battery companies. Available from: <http://www.altenergystocks.com/archives/2019/06/vanadium-flow-battery-companies/> (Accessed December 03 2019).
- [365] Tschümperlin L, Stolz P, Wyss F, Frischknecht R. Life cycle assessment of low power solar inverters (2.5 to 20 kW). Available from: http://treeze.ch/fileadmin/user_upload/downloads/Publications/Case_Studies/Energy/174-Update_Inverter_IEA_PVPS_v1.1.pdf (Accessed March 02 2020).
- [366] Burger Mansilha M, Brondani M, Farret FA, Cantorski da Rosa L, Hoffmann R. Life cycle assessment of electrical distribution transformers: Comparative study between aluminum and copper coils. *Environmental Engineering Science*. 2019;36(1):114-35.
- [367] Davis M, Moronkeji A, Ahiduzzaman M, Kumar A. Assessment of renewable energy transition pathways for a fossil fuel-dependent electricity-producing jurisdiction. *Energy for Sustainable Development*. 2020;59:243-61.
- [368] Portworld. Distance calculator. Available from: <https://www.portworld.com/map> (Accessed December 05 2019).
- [369] Morris MD. Factorial sampling plans for preliminary computational experiments. *Technometrics*. 1991;33(2):161-74.
- [370] Nuss P, Eckelman MJ. Life cycle assessment of metals: a scientific synthesis. *PLOS ONE*. 2014;9(7):e101298.
- [371] Kalair A, Abas N, Saleem MS, Kalair AR, Khan N. Role of energy storage systems in energy transition from fossil fuels to renewables. *Energy Storage*. 2021;3(1):e135.
- [372] Gielen D, Boshell F, Saygin D, Bazilian MD, Wagner N, Gorini R. The role of renewable energy in the global energy transformation. *Energy Strategy Reviews*. 2019;24:38-50.
- [373] Mehrjerdi H, Hemmati R. Stochastic model for electric vehicle charging station integrated with wind energy. *Sustainable Energy Technologies and Assessments*. 2020;37:100577.

- [374] Beltran H, Harrison S, Egea-Álvarez A, Xu L. Techno-economic assessment of energy storage technologies for inertia response and frequency support from wind farms. *Energies*. 2020;13(13):3421.
- [375] Chen T, Jin Y, Lv H, Yang A, Liu M, Chen B, et al. Applications of lithium-ion batteries in grid-scale energy storage systems. *Transactions of Tianjin University*. 2020;26(3):208-17.
- [376] Mahmoud M, Ramadan M, Olabi A-G, Pullen K, Naher S. A review of mechanical energy storage systems combined with wind and solar applications. *Energy Conversion and Management*. 2020;210:112670.
- [377] Mousavi G SM, Faraji F, Majazi A, Al-Haddad K. A comprehensive review of Flywheel Energy Storage System technology. *Renewable and Sustainable Energy Reviews*. 2017;67:477-90.
- [378] Arani AAK, Karami H, Gharehpetian GB, Hejazi MSA. Review of flywheel energy storage systems structures and applications in power systems and microgrids. *Renewable and Sustainable Energy Reviews*. 2017;69:9-18.
- [379] Soomro A, Amiryar ME, Nankoo D, Pullen KR. Performance and loss analysis of squirrel cage induction machine based flywheel energy storage system. *Applied Sciences*. 2019;9(21):4537.
- [380] Ruddell AJ. 11 - Flywheel energy storage technologies for wind energy systems. In: Kaldellis JK, editor. *Stand-Alone and Hybrid Wind Energy Systems*: Woodhead Publishing; 2010. p. 366-92.
- [381] Mittelstedt M, Hansen C, Mertiny P. Design and multi-objective optimization of fiber-reinforced polymer composite flywheel rotors. *Applied Sciences*. 2018;8(8):1256.
- [382] Andriollo M, Benato R, Tortella A. Design and modeling of an integrated flywheel magnetic suspension for kinetic energy storage systems. *Energies*. 2020;13(4):847.
- [383] Yuan Y, Sun Y, Xiang Q. Design and analysis of a magnetic bearings with three degrees of freedom. *Chinese Journal of Mechanical Engineering*. 2019;32(1):3.
- [384] Li Y, Zhu C, Wu L, Zheng Y. Multi-objective optimal design of high-speed surface-mounted permanent magnet synchronous motor for magnetically levitated flywheel energy storage system. *IEEE Transactions on Magnetics*. 2019;55(7):1-8.

- [385] Maksimov N, Savosteenko N, Semenova K, Belov N. Optimization of flywheel for starter-generator based on the differential electric drive. IOP Conference Series: Materials Science and Engineering, vol. 919. IOP Publishing, p. 062065.
- [386] Esen H, Inalli M, Esen M. A techno-economic comparison of ground-coupled and air-coupled heat pump system for space cooling. Building and Environment. 2007;42(5):1955-65.
- [387] Sadeghi S, Ahmadi P. Thermo-economic optimization of a high-performance CCHP system integrated with compressed air energy storage (CAES) and carbon dioxide ejector cooling system. Sustainable Energy Technologies and Assessments. 2021;45:101112.
- [388] Krishan O, Suhag S. An updated review of energy storage systems: Classification and applications in distributed generation power systems incorporating renewable energy resources. International Journal of Energy Research. 2019;43(12):6171-210.
- [389] Amber Kinetics Inc. Technical report (final): smart grid demonstration program. Available from: https://www.smartgrid.gov/files/documents/Amber_Kinetics_Final_Technical_Report.pdf (Accessed June 10 2020).
- [390] Li X, Anvari B, Palazzolo A, Wang Z, Toliyat H. A utility-scale flywheel energy storage system with a shaftless, hubless, high-strength steel rotor. IEEE Transactions on Industrial Electronics. 2018;65(8):6667-75.
- [391] Richman R. Flywheel energy storage. Electric Power Research Institute TR-108378. 1997.
- [392] Beacon Power. Flywheel energy storage systems. Available from: https://beaconpower.com/wp-content/themes/beaconpower/inc/beacon_power_brochure_032514.pdf (Accessed November 02 2020).
- [393] Parfomak PW. Energy storage for power grids and electric transportation: A technology assessment, congressional research service. Available: <https://fas.org/sgp/crs/misc/R42455.pdf>.
- [394] Rojas A. Flywheel energy matrix systems—today’s technology, tomorrow’s energy storage solution. Available from: <http://spec-instalacije.etf.rs/flywheel.pdf> (Accessed June 20 2020).
- [395] Sabihuddin S, Kiprakis AE, Mueller M. A numerical and graphical review of energy storage technologies. Energies. 2015;8(1):172-216.
- [396] Miller P, Kumar A. Techno-economic assessment of hydrogenation-derived renewable diesel production from canola and camelina. Sustainable Energy Technologies and Assessments. 2014;6:105-15.

- [397] EIA. Battery storage in the United States: An update on market trends. Available from: https://www.eia.gov/analysis/studies/electricity/batterystorage/pdf/battery_storage.pdf (Accessed November 03 2020).
- [398] Energy. World's largest flywheel energy storage system. Available from: <https://www.energydigital.com/smart-energy/worlds-largest-flywheel-energy-storage-system> (Accessed 2020 November 03).
- [399] Better World Solutions. Smart grid energy storage: Flywheels. Available from: <https://www.betterworldsolutions.eu/smart-grid-energy-storage-flywheels/> (Accessed April 30 2020).
- [400] Kirk JA, Studer PA. Flywheel energy storage—II: Magnetically suspended superflywheel. *International Journal of Mechanical Sciences*. 1977;19(4):233-45.
- [401] Bender D. Flywheels. *Storing energy*: Elsevier; 2016. p. 183-201.
- [402] Headifen R. Flywheel energy storage for wind turbines. *Intersociety Energy Conversion Engineering Conference*, 29 th, Monterey, CA. p. 1374-9.
- [403] Active Power. Understanding flywheel energy storage: does high-speed really imply a better design? Available from: <http://www.edsenerji.com.tr/userfiles/files/WP%20112%20Flywheel%20Energy%20Storage.pdf> (Accessed June 20 2020).
- [404] Olivier J-C, Bernard N, Mendoza L, Bourguet S. Techno-economic optimization of flywheel storage system in transportation. Available from: <https://hal.archives-ouvertes.fr/hal-01065180/document> (Accessed June 20 2020).
- [405] Bolund B, Bernhoff H, Leijon M. Flywheel energy and power storage systems. *Renewable and Sustainable Energy Reviews*. 2007;11(2):235-58.
- [406] Starbuck JM, Hansen JG. Safety assessment of PowerBeam flywheel technology. Available from: <https://info.ornl.gov/sites/publications/files/Pub21756.pdf> (Accessed April 20 2020).
- [407] Kalaiselvam S, Parameshwaran R. *Thermal energy storage technologies for sustainability: systems design, assessment and applications*: Elsevier, 2014.
- [408] Sanjai V, Hejazi M, Abhishek N. Design optimization of flywheel based energy storage system. Available from: https://designinformaticslab.github.io/_teaching//designopt/projects/2015/desopt_2015_05.pdf (Accessed June 18 2020).

- [409] Krack M, Secanell M, Mertiny P. Rotor design for high-speed flywheel energy storage systems. *Energy Storage in the Emerging Era of Smart Grids*. 2011:41.
- [410] Caprio M, Herbst J, Thelen R. MW 130 kWh Flywheel Energy Storage System. Available from: https://www.sandia.gov/ess-ssl/EESAT/2003_papers/Caprio.pdf (Accessed June 20 2020).
- [411] National Energy Strategy. Efficiency of energy conversion. Available from: <https://personal.ems.psu.edu/~radovic/Chapter4.pdf> (Accessed July 12 2020).
- [412] Wang R-M, Zheng S-R, Zheng YG. *Polymer matrix composites and technology*: Elsevier, 2011.
- [413] Peña-Alzola R, Sebastián R, Quesada J, Colmenar A. Review of flywheel based energy storage systems. 2011 International Conference on Power Engineering, Energy and Electrical Drives. p. 1-6.
- [414] Xinda Green Energy Co. Limited. Available from: http://www.xindaenergy.com/e_products/?big_id=18 (Accessed December 16 2020).
- [415] Atlas Corpo. Available from: <https://atlascompoccompressorstore.com/> (Accessed August 20 2019).
- [416] Haghghat Mamaghani A, Avella Escandon SA, Najafi B, Shirazi A, Rinaldi F. Techno-economic feasibility of photovoltaic, wind, diesel and hybrid electrification systems for off-grid rural electrification in Colombia. *Renewable Energy*. 2016;97:293-305.
- [417] Salehin S, Ferdaous MT, Chowdhury RM, Shithi SS, Rofi MSRB, Mohammed MA. Assessment of renewable energy systems combining techno-economic optimization with energy scenario analysis. *Energy*. 2016;112:729-41.
- [418] Nisingizwe E. Investigating renewable energy potential for rural electrification in Rwanda: technical and economic viability [M.Sc. thesis]. University of Nairobi; 2018.
- [419] Raji AK. Techno-economic feasibility study of autonomous hybrid AC/DC microgrid system. *System Reliability*. 2017:299.
- [420] Twaha S, Idris MH, Anwari M, Khairuddin A. Applying grid-connected photovoltaic system as alternative source of electricity to supplement hydro power instead of using diesel in Uganda. *Energy*. 2012;37(1):185-94.
- [421] AESO. AESO 2019 annual market statistics. Available from: <https://www.aeso.ca/market/market-and-system-reporting/annual-market-statistic-reports/> (Accessed September 20 2020).

- [422] Stefani F, Perrone A, Ratto L, Francesconi R. Comparative analysis of bearings for micro-GT: an innovative arrangement. *Bearing Technology*. 2017:1-26.
- [423] Rossow M. Flywheels for use in uninterruptible power supply systems. Available from: <https://www.cedengineering.com/userfiles/Flywheels%20for%20Use%20in%20UPS%20System.s.pdf> (Accessed November 02 2020).
- [424] Johnson T. Highly redundant inverter architecture. Available from: https://www.nrel.gov/pv/assets/pdfs/2014_pvmrw_23_johnson.pdf (Accessed November 03 2020).
- [425] Kaldellis JK. Stand-alone and hybrid wind energy systems: technology, energy storage and applications: Elsevier, 2010.
- [426] ABB. EssPro™ PCS. Available from: [https://new.abb.com/power-converters-inverters/energy-storage-grid-stabilization/energy-storage-power-conversion-system-\(pcs\)/esspro-pcs](https://new.abb.com/power-converters-inverters/energy-storage-grid-stabilization/energy-storage-power-conversion-system-(pcs)/esspro-pcs) (Accessed April 26 2020).
- [427] DeTeresa SJ. Materials for advanced flywheel energy-storage devices. *MRS bulletin*. 1999;24(11):51-6.
- [428] NeoNickel. 4340 alloy steel. Available from: <https://www.neonickel.com/alloys/alloy-steels/4340-alloy-steel/> (Accessed November 04 2020).
- [429] Raj R, Suman R, Ghandehariun S, Kumar A, Tiwari MK. A techno-economic assessment of the liquefied natural gas (LNG) production facilities in Western Canada. *Sustainable Energy Technologies and Assessments*. 2016;18:140-52.
- [430] Wang R-M, Zheng S-R, Zheng Y-P. 2 - Reinforced materials. In: Wang R-M, Zheng S-R, Zheng Y-P, editors. *Polymer Matrix Composites and Technology*: Woodhead Publishing; 2011. p. 29-548.
- [431] Agbor E, Oyedun AO, Zhang X, Kumar A. Integrated techno-economic and environmental assessments of sixty scenarios for co-firing biomass with coal and natural gas. *Applied Energy*. 2016;169:433-49.
- [432] Chiao E. Amber Kinetics. Available from: <https://www.energy.gov/sites/prod/files/ESS%202012%20Peer%20Review%20-%20Amber%20Kinetics%20Flywheel%20Energy%20Storage%20Demo%20-%20Ed%20Chiao,%20Amber%20Kinetics.pdf> (Accessed November 11 2020).

- [433] Amber Kinetics. A revolution in energy storage. Available from: https://www.energy-cast.com/assets/amberkinetics_2018.pdf (Accessed December 20 2020).
- [434] International Renewable Energy Agency. Global energy transformation: A roadmap to 2050. Available from: <https://www.irena.org/publications/2019/Apr/Global-energy-transformation-A-roadmap-to-2050-2019Edition> (Accessed July 20 2020).
- [435] Rahman MM, Gemechu E, Oni AO, Kumar A. The greenhouse gas emissions' footprint and net energy ratio of utility-scale electro-chemical energy storage systems. *Energy Conversion and Management*. 2021;244:114497.
- [436] Thaker S, Olufemi Oni A, Kumar A. Techno-economic evaluation of solar-based thermal energy storage systems. *Energy Conversion and Management*. 2017;153:423-34.
- [437] Choudhury S. Flywheel energy storage systems: A critical review on technologies, applications, and future prospects. *International Transactions on Electrical Energy Systems*. 2021(n/a):e13024.
- [438] Olabi AG, Wilberforce T, Abdelkareem MA, Ramadan M. Critical review of flywheel energy storage system. *Energies*. 2021;14(8):2159.
- [439] Beacon Power. Carbon fiber flywheels. Available from: <https://beaconpower.com/carbon-fiber-flywheels/> (Accessed April 18 2020).
- [440] Grand View Research. Flywheel energy storage market size worth \$479.3 million by 2025. Available from: <https://www.grandviewresearch.com/press-release/global-flywheel-energy-storage-market> (Accessed July 20 2020).
- [441] Grand View Research. Flywheel energy storage market size, industry report, 2019-2025. Available from: <https://www.grandviewresearch.com/industry-analysis/flywheel-energy-storage-market?fbclid=IwAR3eXKdFiEcUCk7Zxr-LOD9e1Yh0uaYvqjqtBTFTPGMlZY0uANsIyinBhCw#:~:text=The%20global%20flywheel%20energy%20storage,the%20flywheel%20is%20energy%20storage> (Accessed July 20 2020).
- [442] Bruckner T, Fulton L, Hertwich E, McKinnon A, Perczyk D, Roy J, et al. Annex III: Technology-specific Cost and Performance Parameters. Available from: https://www.ipcc.ch/site/assets/uploads/2018/02/ipcc_wg3_ar5_annex-iii.pdf (Accessed June 12 2020).

- [443] Lusny T, Osborne G. 2 MW Minto flywheel facility: market impact case study. Available from: <http://nrstor.com/wp-content/uploads/2019/11/2-MW-Minto-Flywheel-Facility-Case-Study.pdf> (Accessed April 23 2020).
- [444] Carberry W. Airplane recycling efforts benefit Boeing operators. Available from: http://www.phantomworks.org/commercial/aeromagazine/articles/qtr_4_08/pdfs/AERO_Q408_article02.pdf (Accessed May 15 2020).
- [445] Li X, Anvari B, Palazzolo A, Wang Z, Toliyat H. A utility-scale flywheel energy storage system with a shaftless, hubless, high-strength steel rotor. IEEE Transactions on Industrial Electronics. 2017;65(8):6667-75.
- [446] Zhang X-P. 15 - Development of European Energy Internet and the role of Energy Union. In: Su W, Huang AQ, editors. The Energy Internet: Woodhead Publishing; 2019. p. 347-67.
- [447] Arseneaux J. 20 MW Flywheel frequency regulation plant. Available from: <https://www.osti.gov/servlets/purl/1351296> (Accessed March 10 2020).
- [448] Canadian Consulting Engineer. Flywheel energy storage. Available from: <https://www.canadianconsultingengineer.com/features/flywheel-energy-storage/> (Accessed May 02 2020).
- [449] gtm. Flywheel energy storage lives on at Beacon Power. Available from: <https://www.greentechmedia.com/articles/read/Flywheel-Energy-Storage-Lives-On-at-Beacon-Power> (Accessed April 30 2020).
- [450] Bender D. Flywheels. Available from: <https://www.sandia.gov/ess-ssl/publications/SAND2015-3976.pdf> (Accessed May 21 2020).
- [451] Kailasan A. Preliminary design and analysis of an energy storage flywheel [PhD thesis] [PhD thesis]. University of Virginia, Charlottesville, VA, USA; 2013.
- [452] Headifen R. Flywheel energy storage for wind turbines. 29th Intersociety Energy Conversion Engineering Conference, Monterey, CA. 1994:1374-9.
- [453] Genta G. Kinetic energy storage: theory and practice of advanced flywheel systems. first ed: Butterworth-Heinemann, 1985.
- [454] Amber Kinetics Inc. Technical report (final): smart grid demonstration program. Available from: https://www.smartgrid.gov/files/documents/Amber_Kinetics_Final_Technical_Report.pdf (Accessed May 10 2020).

- [455] Caprio M, Herbst J, Thelen R. 2 MW 130 kWh flywheel energy storage system. Available from: https://www.sandia.gov/ess-ssl/EESAT/2003_papers/Caprio.pdf (Accessed June 21 2020).
- [456] Stefani F, Perrone A, Ratto L, Francesconi R. Comparative analysis of bearings for micro-GT: an innovative arrangement. In: Darji PH, editor. Bearing Technology: IntechOpen; 2017. p. 1-26.
- [457] Krack M, Secanell M, Mertiny P. Rotor design for high-speed flywheel energy storage systems. In: Carbone R, editor. Energy Storage in the Emerging Era of Smart Grids. London, UK: IntechOpen; 2011. p. 41-68.
- [458] Sanjai VV, Hejazi M, Abhishek N. Design optimization of flywheel based energy storage system Available from: https://designinformaticslab.github.io/teaching//designopt/projects/2015/desopt_2015_05.pdf (Accessed May 13 2020).
- [459] National Energy Strategy. Efficiency of energy conversion. Available from: <https://personal.ems.psu.edu/~radovic/Chapter4.pdf> (Accessed July 12 2020).
- [460] Beacon Power. Flywheel energy storage systems. Available from: https://beaconpower.com/wp-content/themes/beaconpower/inc/beacon_power_brochure_032514.pdf (Accessed May 13 2020).
- [461] Rossow M. Flywheels for use in uninterruptible power supply systems. Available from: <https://www.cedengineering.com/userfiles/Flywheels%20for%20Use%20in%20UPS%20Systems.pdf> (Accessed April 10 2020).
- [462] Johnson T. Highly redundant inverter architecture. Available from: https://www.nrel.gov/pv/assets/pdfs/2014_pvmrw_23_johnson.pdf (Accessed May 05 2020).
- [463] Hebner R, Beno J, Herbst J. Composite flywheels for energy storage-design considerations. Available from: https://www.sandia.gov/ess-ssl/EESAT/2002_papers/00009.pdf (Accessed May 15 2020).
- [464] Hansen JG, O'Kain DU. An assessment of flywheel high power energy storage technology for hybrid vehicles. Available from: <https://trid.trb.org/view/1246779> (Accessed May 15 2020).
- [465] Rogers S. Advanced power electronics and electric motors R&D. Available from: https://www.energy.gov/sites/prod/files/2014/03/f13/ape00a_rogers_2013_o.pdf (Accessed May 15 2020).

- [466] AST. Bearing materials - ceramics, chrome steels, stainless steels, and plastics. Available from: <https://www.astbearings.com/bearing-materials.html> (Accessed April 18 2020).
- [467] Timken. Timken ball bearings catalog. Available from: https://www.timken.com/wp-content/uploads/2018/04/Timken-Ball-Bearing-Catalog_10734.pdf (Accessed May 15 2020).
- [468] Post R. Passive magnetic bearings for vehicular electromechanical batteries. Available from: <https://www.osti.gov/servlets/purl/10139868> (Accessed May 15 2020).
- [469] Werfel F, Floegel-Delor U, Riedel T, Rothfeld R, Wippich D, Goebel B, et al. 250 kW flywheel with HTS magnetic bearing for industrial use. *Journal of Physics: Conference Series*. 2008;97(1):012206.
- [470] Tantau M. Active magnetic bearing for ultra precision flexible electronics production system [M.Sc. thesis] [M.Sc. thesis]. Cranfield University; 2015.
- [471] Travani Pumps USA. Single stage medium/high vacuum pumps. Available from: <http://www.travaini.com/PDF/Datasheet/SingleStageVariPorted/TRVA%2065-300,450.pdf> (Accessed June 10 2020).
- [472] Tuthill. Liquid ring vacuum pumps. Available from: <https://www.tuthillvacuumblower.com/dam/357.pdf> (Accessed May 15 2020).
- [473] Pfeiffer. Pascal 2005, SD version, 3-Phase motor, 342–460 V, 50 Hz | 342–520 V, 60 Hz, CE/UL/CSA. Available from: <https://static.pfeiffer-vacuum.com/productPdfs/205SDTHEM.en.pdf> (Accessed May 15 2020).
- [474] Nimana B, Verma A, Di Lullo G, Rahman MM, Canter CE, Olateju B, et al. Life cycle analysis of bitumen transportation to refineries by rail and pipeline. *Environmental Science & Technology*. 2017;51(1):680-91.
- [475] Mason J, Fthenakis V, Hansen T, Kim H. Energy payback and life-cycle CO₂ emissions of the BOS in an optimized 3· 5 MW PV installation. *Progress in Photovoltaics: Research and Applications*. 2006;14(2):179-90.
- [476] PV Powered. PVP75kW/100kW inverter installation & operation manual. Available from: http://www.dot.state.oh.us/Divisions/Planning/SPR/Research/reportsandplans/Reports/2012/Structures/426835_App_D/O_M/A_PV%20System/PV%20Powered/75-100_pvp_Manual.pdf (Accessed May 15 2020).

- [477] Yu S, Liu Y, Li L. Comparative life cycle assessment of servo press and flywheel press. In: Nee A, Song B, Ong SK, editors. Re-engineering Manufacturing for Sustainability: Springer; 2013. p. 515-21.
- [478] Brosius D. IACMI baseline cost and energy metrics. Available from: <https://iacmi.org/wp-content/uploads/2017/12/IACMI-Baseline-Cost-and-Energy-Metrics-March-2017.pdf> (Accessed May 15 2020).
- [479] Boluk MY, Aktik M, Bilgen E. Energy requirements and cost in polymer curing processes. Energy. 1990;15(9):811-20.
- [480] Zhao G, Hou C, Qiao J, Cheng X. Energy consumption characteristics evaluation method in turning. Advances in Mechanical Engineering. 2016;8(11):1687814016680737.
- [481] Ecoinvent 3.6. Available from: <https://v36.ecoquery.ecoinvent.org/Search/Index> (Accessed April 19 2020).
- [482] Ekdahl Å. Life cycle assessment on SKF's spherical roller bearing. Available from: <http://citeseerx.ist.psu.edu/viewdoc/download?doi=10.1.1.201.9437&rep=rep1&type=pdf> (Accessed July 20 2020).
- [483] Koehler B-U, Denk J, Van Maanen G, Lang M. Applying standard industrial components for active magnetic bearings. Actuators. 2017;6(1):8.
- [484] Tschümperlin L, Stolz P, Frischknecht R. Life cycle assessment of low power solar inverters (2.5 to 20 kW). Available from: https://treeze.ch/fileadmin/user_upload/downloads/Publications/Case_Studies/Energy/174-Update_Inverter_IEA_PVPS_v1.1.pdf (Accessed July 20 2020).
- [485] Parfomak PW. Energy storage for power grids and electric transportation: A technology assessment. Available from: <http://abaque.com.br/wp-content/uploads/2017/07/R42455.pdf> (Accessed June 10 2020).
- [486] Rojas A. Flywheel energy matrix systems—today's technology, tomorrow's energy storage solution. Available from: <http://spec-instalaciije.etf.rs/flywheel.pdf> (Accessed June 10 2020).
- [487] Manfredi S, Tonini D, Christensen TH, Scharff H. Landfilling of waste: accounting of greenhouse gases and global warming contributions. Waste Management & Research. 2009;27(8):825-36.
- [488] GREET 2. Argonne National Laboratory. Available from: <https://greet.es.anl.gov/greet.models> (Accessed June 10 2020).

- [489] Materials. Available from: <http://www.dartmouth.edu/~cushman/books/Numbers/Chap1-Materials.pdf> (Accessed December 05 2019).
- [490] Nylund N-O, Erkkilä K. Heavy-duty truck emissions and fuel consumption simulating real-world driving in laboratory conditions. Available from: https://www.energy.gov/sites/prod/files/2014/03/f9/2005_deer_erkkila.pdf (Accessed June 10 2020).
- [491] Staffell I. The energy and fuel data sheet. Available from: https://www.claverton-energy.com/wordpress/wp-content/uploads/2012/08/the_energy_and_fuel_data_sheet1.pdf (Accessed June 10 2020).
- [492] Greenhouse Gas Protocol. Global warming potential values. Available from: https://www.ghgprotocol.org/sites/default/files/ghgp/Global-Warming-Potential-Values%20%28Feb%2016%202016%29_1.pdf (Accessed June 10 2020).
- [493] Wang L, Sharkh S, Chipperfield A. Optimal coordination of vehicle-to-grid batteries and renewable generators in a distribution system. *Energy*. 2016;113:1250-64.
- [494] Ferro G, Minciardi R, Robba M. A user equilibrium model for electric vehicles: Joint traffic and energy demand assignment. *Energy*. 2020;198:117299.
- [495] Statista. Worldwide number of battery electric vehicles in use from 2016 to 2020. Available from: <https://www.statista.com/statistics/270603/worldwide-number-of-hybrid-and-electric-vehicles-since-2009/> (Accessed September 2 2021).
- [496] Robledo CB, Poorte MJ, Mathijssen HHM, van der Veen RAC, van Wijk AJM. Fuel cell electric vehicle-to-grid feasibility: A technical analysis of aggregated units offering frequency reserves. In: Palensky P, Cvetković M, Keviczky T, editors. *Intelligent Integrated Energy Systems: The PowerWeb Program at TU Delft*. Cham: Springer International Publishing; 2019. p. 167-94.
- [497] Lee C-Y, Jang J-W, Lee M-K. Willingness to accept values for vehicle-to-grid service in South Korea. *Transportation Research Part D: Transport and Environment*. 2020;87:102487.
- [498] Hashim MS, Yong JY, Ramachandaramurthy VK, Tan KM, Mansor M, Tariq M. Priority-based vehicle-to-grid scheduling for minimization of power grid load variance. *Journal of Energy Storage*. 2021;39:102607.
- [499] Tan KM, Padmanaban S, Yong JY, Ramachandaramurthy VK. A multi-control vehicle-to-grid charger with bi-directional active and reactive power capabilities for power grid support. *Energy*. 2019;171:1150-63.

- [500] Tan KM, Ramachandaramurthy VK, Yong JY, Tariq M. Experimental verification of a flexible vehicle-to-grid charger for power grid load variance reduction. *Energy*. 2021;228:120560.
- [501] Alsharif A, Tan CW, Ayop R, Lau KY, Dobi AMd. A rule-based power management strategy for Vehicle-to-Grid system using antlion sizing optimization. *Journal of Energy Storage*. 2021;41:102913.
- [502] Jiao Z, Ran L, Zhang Y, Ren Y. Robust vehicle-to-grid power dispatching operations amid sociotechnical complexities. *Applied Energy*. 2021;281:115912.
- [503] Bibak B, Tekiner-Mogulkoc H. Influences of vehicle to grid (V2G) on power grid: An analysis by considering associated stochastic parameters explicitly. *Sustainable Energy, Grids and Networks*. 2021;26:100429.
- [504] Huda M, Koji T, Aziz M. Techno economic analysis of vehicle to grid (V2G) integration as distributed energy resources in Indonesia power system. *Energies*. 2020;13(5):1162.
- [505] Koubaa R, Yoldas Y, Goren S, Krichen L, Onen A. Implementation of cost benefit analysis of vehicle to grid coupled real Micro-Grid by considering battery energy wear: Practical study case. *Energy & Environment*. 2020:0958305X20965158.
- [506] Ríos ADL, Goentzel J, Nordstrom KE, Siegert CW. Economic analysis of vehicle-to-grid (V2G)-enabled fleets participating in the regulation service market. 2012 IEEE PES Innovative Smart Grid Technologies (ISGT). p. 1-8.
- [507] Tomić J, Kempton W. Using fleets of electric-drive vehicles for grid support. *Journal of Power Sources*. 2007;168(2):459-68.
- [508] Shang D, Sun G. Electricity-price arbitrage with plug-in hybrid electric vehicle: Gain or loss? *Energy Policy*. 2016;95:402-10.
- [509] Alberta Infrastructure. Electric vehicles: Driving the shift to greener transportation. Available from: <https://www.alberta.ca/assets/documents/tr/tr-dtseries09elecveh2018.pdf> (Accessed January 22 2021).
- [510] Electric Vehicle Database. Nissan Leaf 24 kWh. Available from: <https://ev-database.org/car/1019/Nissan-Leaf-24-kWh> (Accessed August 15 2021).
- [511] Kempton W, Tomić J. Vehicle-to-grid power fundamentals: Calculating capacity and net revenue. *Journal of Power Sources*. 2005;144(1):268-79.

- [512] Steward DM. Critical elements of vehicle-to-grid (v2g) economics. National Renewable Energy Lab.(NREL), Golden, CO (United States). Available: <https://www.nrel.gov/docs/fy17osti/69017.pdf>. Available.
- [513] Loisel R, Pasaoglu G, Thiel C. Large-scale deployment of electric vehicles in Germany by 2030: An analysis of grid-to-vehicle and vehicle-to-grid concepts. Energy Policy. 2014;65:432-43.
- [514] Kempton W, Tomic J, Letendre S, Brooks A, Lipman T. Vehicle-to-grid power: battery, hybrid, and fuel cell vehicles as resources for distributed electric power in California. UC Davis: Institute of Transportation Studies. Available: <https://escholarship.org/uc/item/5cc9g0jp>. Available.
- [515] EVTown. Levels of charging. Available from: <http://www.evtown.org/about-ev-town/ev-charging/charging-levels.html> (Accessed January 22 2021).
- [516] Calgary. Homeowners electrical wiring guide. Available from: <https://www.calgary.ca/content/dam/www/pda/pd/documents/brochures/homeowner-electrical-wiring-guide.pdf> (Accessed August 15 2021).
- [517] Weather and Science Facts. Weather averages for Canada. Available from: <https://www.currentresults.com/Weather/Canada/weather-averages-index.php> (Accessed August 19 2021).
- [518] Zia MF, Elbouchikhi E, Benbouzid M. Optimal operational planning of scalable DC microgrid with demand response, islanding, and battery degradation cost considerations. Applied Energy. 2019;237:695-707.
- [519] Hydro Quebec. Comparison of electricity prices in major North American cities. Available from: <https://www.hydroquebec.com/data/documents-donnees/pdf/comparison-electricity-prices.pdf> (Accessed August 19 2021).
- [520] Quinn C, Zimmerle D, Bradley TH. The effect of communication architecture on the availability, reliability, and economics of plug-in hybrid electric vehicle-to-grid ancillary services. Journal of Power Sources. 2010;195(5):1500-9.
- [521] BloombergNEF. Battery pack prices cited below \$100/kWh for the first time in 2020, while market average sits at \$137/kWh. Available from: <https://about.bnef.com/blog/battery-pack-prices-cited-below-100-kwh-for-the-first-time-in-2020-while-market-average-sits-at-137-kwh/> (Accessed January 21 2021).

- [522] White CD, Zhang KM. Using vehicle-to-grid technology for frequency regulation and peak-load reduction. *Journal of Power Sources*. 2011;196(8):3972-80.
- [523] Alberta alis. Occupations in Alberta. Available from: <https://alis.alberta.ca/occinfo/occupations-in-alberta/occupation-profiles/electrician/> (Accessed January 21 2021).
- [524] Plug n Drive. Driving EV uptake in the greater Toronto and Hamilton area. Available from: <https://www.plugndrive.ca/wp-content/uploads/2017/07/EV-Survey-Report.pdf> (Accessed January 21 2021).
- [525] Gerber DL, Vossos V, Feng W, Marnay C, Nordman B, Brown R. A simulation-based efficiency comparison of AC and DC power distribution networks in commercial buildings. *Applied Energy*. 2018;210:1167-87.
- [526] Dustmann CH, Bito A. Secondary batteries – High temperature systems | Safety. In: Garche J, editor. *Encyclopedia of Electrochemical Power Sources*. Amsterdam: Elsevier; 2009. p. 324-33.
- [527] Duffner F, Wentker M, Greenwood M, Leker J. Battery cost modeling: A review and directions for future research. *Renewable and Sustainable Energy Reviews*. 2020;127:109872.
- [528] Faessler B. Stationary, second use battery energy storage systems and their applications: A research review. *Energies*. 2021;14(8):2335.
- [529] Barbour E, Mignard D, Ding Y, Li Y. Adiabatic compressed air energy storage with packed bed thermal energy storage. *Applied Energy*. 2015;155:804-15.
- [530] Hõimoja H. Flywheel energy storage: principles and possibilities. 3rd International Symposium on Actual Problems, vol. 750. p. 89-92.
- [531] Gonçalves de Oliveira J. Power control systems in a flywheel based all-electric driveline [PhD thesis]. *Acta Universitatis Upsaliensis*; 2011.
- [532] Samineni S, Johnson BK, Hess HL, Law JD. Modeling and analysis of a flywheel energy storage system with a power converter interface. *International Conference on Power Systems Transients (IPST)*, New Orleans, USA.
- [533] Parfomak PW. Energy storage for power grids and electric transportation: a technology assessment. *Congressional Research Service*. 2012;42455.
- [534] Bakay L, Dubois M, Viarouge P, Ruel J. Mass-losses relationship in an optimized 8-pole radial AMB for long term flywheel energy storage. *Africon. IEEE*, p. 1-5.
- [535] McLarnon FR, Cairns EJ. Energy storage. *Annual Review of Energy*. 1989;14(1):241-71.

- [536] Ter-Gazarian A. Energy storage for power systems: Peter Peregrinus Ltd, 1994.
- [537] Linden D. Handbook of batteries and fuel cells. New York: McGraw-Hill Book Co., 1984.
- [538] Winter M, Brodd RJ. What are batteries, fuel cells, and supercapacitors? Chemical Reviews. 2004;104:4245–70.
- [539] Bullock KR. Lead/acid batteries. Journal of Power Sources. 1994;51(1-2):1-17.
- [540] Horiba T. Lithium-ion battery systems. Proceedings of the IEEE. 2014;102(6):939-50.
- [541] Scrosati B, Hassoun J, Sun Y-K. Lithium-ion batteries. A look into the future. Energy & Environmental Science. 2011;4(9):3287-95.
- [542] Wakihara M. Recent developments in lithium ion batteries. Materials Science and Engineering: R: Reports. 2001;33(4):109-34.
- [543] Bruce PG. Energy storage beyond the horizon: Rechargeable lithium batteries. Solid State Ionics. 2008;179(21-26):752-60.
- [544] Dhameja S. Electric vehicle battery systems. 1st Edition: Elsevier, 2001.
- [545] Zaghbi K, Dontigny M, Guerfi A, Charest P, Rodrigues I, Mauger A, et al. Safe and fast-charging Li-ion battery with long shelf life for power applications. Journal of Power Sources. 2011;196(8):3949-54.
- [546] Fergus JW. Recent developments in cathode materials for lithium ion batteries. Journal of Power Sources. 2010;195(4):939-54.
- [547] Broussely M, Pistoia G. Industrial applications of batteries: from cars to aerospace and energy storage. 1st Edition: Elsevier, 2007.
- [548] NGK Insulators Ltd. Available from: <https://www.ngk-insulators.com/en/index.html> (Accessed August 29 2018).
- [549] Sakaebe H. Zebra batteries. Encyclopedia of Applied Electrochemistry: Springer; 2014. p. 2165-9.
- [550] Sudworth J. The sodium/nickel chloride (ZEBRA) battery. Journal of Power Sources. 2001;100(1-2):149-63.
- [551] Zelinsky M, Fetcenko M, Kusay J, Koch J. Storage-integrated PV systems using advanced NiMH battery technology. Fifth International Renewable Energy Storage Conference (IRES 2010) Berlin, Germany. p. 424-9.
- [552] Morioka Y, Narukawa S, Itou T. State-of-the-art of alkaline rechargeable batteries. Journal of Power Sources. 2001;100(1-2):107-16.

- [553] Shukla A, Ravikumar M, Balasubramanian T. Nickel/iron batteries. *Journal of Power Sources*. 1994;51(1-2):29-36.
- [554] Lei D, Lee D-C, Magasinski A, Zhao E, Steingart D, Yushin G. Performance enhancement and side reactions in rechargeable nickel–iron batteries with nanostructured electrodes. *ACS applied Materials & Interfaces*. 2016;8(3):2088-96.
- [555] Scamman DP, Reade GW, Roberts EP. Numerical modelling of a bromide–polysulphide redox flow battery: Part 1: Modelling approach and validation for a pilot-scale system. *Journal of Power Sources*. 2009;189(2):1220-30.
- [556] Ponce de León C, Frías-Ferrer A, González-García J, Szánto DA, Walsh FC. Redox flow cells for energy conversion. *Journal of Power Sources*. 2006;160(1):716-32.
- [557] Olateju B, Kumar A. Techno-economic assessment of hydrogen production from underground coal gasification (UCG) in Western Canada with carbon capture and sequestration (CCS) for upgrading bitumen from oil sands. *Applied Energy*. 2013;111:428-40.
- [558] Friedmann SJ, Upadhye R, Kong F-M. Prospects for underground coal gasification in carbon-constrained world. *Energy Procedia*. 2009;1(1):4551-7.
- [559] Prabu V, Jayanti S. Underground coal-air gasification based solid oxide fuel cell system. *Applied Energy*. 2012;94:406-14.
- [560] Hossain M, Charpentier P. Hydrogen production by gasification of biomass and opportunity fuels. *Compendium of Hydrogen Energy: Elsevier*; 2015. p. 137-75.
- [561] Parthasarathy P, Narayanan KS. Hydrogen production from steam gasification of biomass: Influence of process parameters on hydrogen yield – A review. *Renewable Energy*. 2014;66:570-9.
- [562] Olateju B, Kumar A. Hydrogen production from wind energy in Western Canada for upgrading bitumen from oil sands. *Energy*. 2011;36(11):6326-39.
- [563] Olateju B, Monds J, Kumar A. Large scale hydrogen production from wind energy for the upgrading of bitumen from oil sands. *Applied Energy*. 2014;118:48-56.
- [564] Sherif SA, Barbir F, Veziroglu T. Wind energy and the hydrogen economy—review of the technology. *Solar Energy*. 2005;78(5):647-60.
- [565] Varkaraki E, Lymberopoulos N, Zoulias E, Guichardot D, Poli G. Hydrogen-based uninterruptible power supply. *International Journal of Hydrogen Energy*. 2007;32(10-11):1589-96.

- [566] Conte M, Iacobazzi A, Ronchetti M, Vellone R. Hydrogen economy for a sustainable development: state-of-the-art and technological perspectives. *Journal of Power Sources*. 2001;100(1-2):171-87.
- [567] Shaw S, Peteves E. Exploiting synergies in European wind and hydrogen sectors: a cost-benefit assessment. *International Journal of Hydrogen Energy*. 2008;33(13):3249-63.
- [568] Korpås M, Greiner CJ. Opportunities for hydrogen production in connection with wind power in weak grids. *Renewable Energy*. 2008;33(6):1199-208.
- [569] Ruwa TL, Adun HH, Abbasoglu S. Thermal energy storage for solar power plant applications. *Proceedings of the HONET-ICT*. IEEE, p. 170-4.
- [570] Sharma A, Tyagi VV, Chen C, Buddhi D. Review on thermal energy storage with phase change materials and applications. *Renewable and Sustainable Energy Reviews*. 2009;13(2):318-45.
- [571] Dunn R, Lovegrove K, Burgess G. A review of ammonia-based thermochemical energy storage for concentrating solar power. *Proceedings of the IEEE*. 2012;100(2):391-400.
- [572] Luzzi A, Lovegrove K, Filippi E, Fricker H, Schmitz-Goeb M, Chandapillai M, et al. Techno-economic analysis of a 10 MWe solar thermal power plant using ammonia-based thermochemical energy storage. *Solar Energy*. 1999;66(2):91-101.
- [573] Schoenung SM. Characteristics and technologies for long-vs. short-term energy storage. Available from: <https://prod-ng.sandia.gov/techlib-noauth/access-control.cgi/2001/010765.pdf> (Accessed July 15 2018).
- [574] Akhil AA, Huff G, Currier AB, Kaun BC, Rastler DM, Chen SB, et al. DOE/EPRI 2013 electricity storage handbook in collaboration with NRECA. Available from: <http://www.emnrd.state.nm.us/ECMD/RenewableEnergy/documents/SNL-ElectricityStorageHandbook2013.pdf> (Accessed April 10 2019).
- [575] Kishinevsky Y. Long island bus sodium sulfur battery storage project. Available from: https://www.sandia.gov/ess-ssl/docs/pr_conferences/2006/kishinevsky.pdf (Accessed June 06 2019).
- [576] Deep cycle batteries. Available from: <https://www.solar-wind.co.uk/deep-cycle-batteries-gel-agm?q=Categories-2V+Cells/Brand-Fiamm> (Accessed June 06 2019).
- [577] Rumsey DJ. How to calculate a confidence interval for a population mean when you know its standard deviation. Available from: <https://www.dummies.com/education/math/statistics/how->

[to-calculate-a-confidence-interval-for-a-population-mean-when-you-know-its-standard-deviation/](#) (Accessed October 10 2019).

[578] Bitto A. Overview of the sodium-sulfur battery for the IEEE stationary battery committee. IEEE Power Engineering Society General Meeting, 2005. IEEE, p. 1232-5.

[579] Sapkota K, Oni AO, Kumar A, Linwei M. The development of a techno-economic model for the extraction, transportation, upgrading, and shipping of Canadian oil sands products to the Asia-Pacific region. Applied Energy. 2018;223:273-92.

[580] Whitford F, Baalman K, Hawkins S, Flanders J, Smith K. Fiberglass tanks for storage, transport, and application. Available from: <https://www.extension.purdue.edu/extmedia/ppp/ppp-93.pdf> (Accessed March 10 2020).

[581] Vanderwerf P. Concrete floor slabs. Available from: https://www.concreteconstruction.net/how-to/construction/concrete-cement-floor-slabs_o#targetText=Standard%20concrete%20floor%20slab%20thickness,allow%20for%20the%20slab%20thickness (Accessed Decemebr 03 2019).

[582] Sjunnesson J. Life cycle assessment of concrete [M.Sc. thesis]. Lund University; 2005.

[583] Freightfinders. 40 feet ISO container measurements, weight, volume, area and transport. Available from: <https://freightfinders.com/container-transport/40-feet-iso-container/> (Accessed December 03 2019).

[584] Mason JE, Fthenakis VM, Hansen T, Kim HC. Energy payback and life-cycle CO2 emissions of the BOS in an optimized 3.5 MW PV installation. Progress in Photovoltaics: Research and Applications. 2006;14(2):179-90.

[585] Weidmann. Insulation in Transformers. Available from: https://site.ieee.org/gms-pes/files/2016/05/IEEE-GMS-PES-Presentation_Mod.pdf (Accessed March 02 2020).

[586] Fthenakis V, Kim H, Frischknecht R, Raugei M, Sinha P, Stucki M. Life cycle inventories and life cycle assessment of photovoltaic systems. Available from: http://www.iea-pvps.org/fileadmin/dam/public/report/technical/IEA-PVPS_Task_12_LCI_LCA.pdf (Accessed March 10 2020).

[587] Singh M, Ganguli T. Materials used in transformers. Available from: <https://www.accessengineeringlibrary.com/binary/mheaeworks/6a7c7f5a14004caf/8b758ca402410aa845ab9ec1ee806100cd049c09599a617a7badd8d39193239b/materials-used-in->

[transformers.pdf?implicit-login=true&sigma-token=DtuTXwwlj0aOzDtp2gT-zDNFLFmkiLOZVI_OIoX_huI](#) (Accessed March 10 2020).

[588] Sullivan D, Morse T, Patel P, Patel S, Bondar J, Taylor L. Life-cycle energy analyses of electric vehicle storage batteries. Available: <https://www.osti.gov/servlets/purl/6655795>.

[589] GREET 1. Argonne National Laboratory. Available: <https://greet.es.anl.gov/greet.models>.

[590] Materials. Available from: <http://www.dartmouth.edu/~cushman/books/Numbers/Chap1-Materials.pdf> (Accessed December 05 2019).

[591] Nylund N, Erkkila K. Heavy-duty truck emissions and fuel consumption simulating real-world driving in laboratory conditions. Available from: https://www.energy.gov/sites/prod/files/2014/03/f9/2005_deer_erkkila.pdf (Accessed April 10 2020).

[592] Moore C, Kraft T. Metallic rotor sizing and performance model for flywheel systems. Available from: <https://ntrs.nasa.gov/archive/nasa/casi.ntrs.nasa.gov/20130000784.pdf> (Accessed June 10 2020).

[593] Moore CJ, Kraft TG. Metallic rotor sizing and performance model for flywheel systems. Available from: <https://ntrs.nasa.gov/archive/nasa/casi.ntrs.nasa.gov/20130000784.pdf> (Accessed June 10 2020).

[594] AZO Materials. AISI 52100 alloy steel. Available from: <https://www.azom.com/article.aspx?ArticleID=6704> (Accessed April 18 2020).

[595] Ihm P, Krarti M. Design optimization of energy efficient residential buildings in Tunisia. Building and Environment. 2012;58:81-90.

[596] EPA. Emission factors for greenhouse gas inventories. Available from: https://www.epa.gov/sites/production/files/2015-07/documents/emission-factors_2014.pdf (Accessed July 20 2020).

[597] GREET 1. Argonne National Laboratory. Available from: <https://greet.es.anl.gov/greet.models> (Accessed June 10 2020).

[598] Better World Solutions. Smart grid energy storage: Flywheels. Available from: <https://www.betterworldsolutions.eu/smart-grid-energy-storage-flywheels/> (Accessed April 30 2020).

[599] NeoNickel. 4340 alloy steel. Available from: <https://www.neonickel.com/alloys/alloy-steels/4340-alloy-steel/> (Accessed July 20 2020).

- [600] California Environmental Protection Agency. Method for estimating greenhouse gas emission reductions from recycling. Available from: https://ww3.arb.ca.gov/cc/protocols/localgov/pubs/recycling_method.pdf (Accessed June 10 2020).
- [601] Johnson MC, Sullivan JL. Lightweight materials for automotive application: an assessment of material production data for magnesium and carbon fiber. Available from: <https://publications.anl.gov/anlpubs/2014/09/107574.pdf> (Accessed June 21 2020).
- [602] Asdrubali F, Baldinelli G, D'Alessandro F, Scrucca F. Life cycle assessment of electricity production from renewable energies: Review and results harmonization. *Renewable and Sustainable Energy Reviews*. 2015;42:1113-22.
- [603] Hsu DD, O'Donoghue P, Fthenakis V, Heath GA, Kim HC, Sawyer P, et al. Life cycle greenhouse gas emissions of crystalline silicon photovoltaic electricity generation: systematic review and harmonization. *Journal of Industrial Ecology*. 2012;16:S122-S35.

Appendix A

A.1. Basics of energy storage technologies

A.1.1. Pumped hydro storage

A pumped hydro storage (PHS) system stores energy in the form of hydraulic power when there is a surplus of electricity, for instance during off-peak hours. The system pumps water from the lower to the upper reservoir, converting electricity into hydraulic potential energy. During peak hours when the electricity demand is high, water is released from the upper reservoir to run the hydraulic turbine that converts the potential energy of water into electricity using an electrical generator. The power output (P) from the PHS system is proportional to the head available (H) between the reservoirs and the volume flow rate (Q) of water flowing through the turbine, as indicated by Equation A.1 [31]:

$$P = \eta \cdot Q \cdot \gamma \cdot H \quad (\text{A.1})$$

where η and γ are the efficiency of the plant and the specific weight of water, respectively.

The important components of the PHS system are the hydraulic turbine, pump, reservoirs, penstock, valves, and surge chamber.

A.1.2. Compressed air energy storage

A compressed air energy storage system (CAES) stores electricity in the form of the potential elastic energy of air. CAES plants can be classified into two types: adiabatic compressed air storage and conventional compressed air storage. When electricity demand is low, the air is compressed to high pressure (usually 4-8 MPa) using multi-stage compressors and stored in large volume air storage systems [10]. When electricity demand is high, the stored air is released from the storage medium and used in a gas-fired turbine to produce mechanical power, which is subsequently

converted to electricity using an electrical generator. Underground rock caverns, natural salt caverns, and depleted oil or gas fields are low-cost options for compressed air storage [166]. To increase the efficiency of a conventional compressed air storage plant, heat exchangers are used to preheat the air before it enters the combustor using the energy from the exhaust gas stream that comes from the turbine. An adiabatic compressed air storage system, on the other hand, uses a heat storage fluid (usually oil, water, or a molten salt solution) to capture the heat generated during the air compression process, and this heat is used to heat the compressed air that is released through the turbine to generate electricity without combustion [182, 529].

A.1.3. Flywheel energy storage

Flywheel energy storage (FES) is a rapidly growing technology that stores energy in the form of rotational kinetic energy. The main components of a FES system are the flywheel rotor, bi-directional converter, mechanical/magnetic bearings, motor/generator, and vacuum enclosure [203, 530]. Energy is taken from an electrical energy source and converted to mechanical energy using a rotating mass. This mechanical energy is converted back to electrical energy using a motor-generator during the discharge [121]. The amount of kinetic energy (E_k) stored in the flywheel depends on the moment of inertia (I) of the rotating mass and its angular speed (ω), as indicated by Equation A.2 [531, 532]:

$$E_k = \frac{1}{2} \cdot I \cdot \omega^2 \quad (\text{A.2})$$

The moment of inertia is a function of the mass and shape of the rotating mass. The flywheels can be of different shapes, e.g., cylindrical (solid or hollow), drum type, disk type, etc. [533, 534]. The moment of inertia can be calculated using Equation A.3:

$$I = \int r^2 dm \quad (\text{A.3})$$

where r represents the distance of each differential mass dm from the axis around which the mass rotates.

A.1.4. Electro-chemical energy storage

Electro-chemical batteries are one of the oldest electrical storage devices used to store electricity in the form of electro-chemical energy [81, 535]. Several battery cells are connected in parallel, in a series, or in parallel and series combination; the connection determines the output voltage, current, and capacity of the system [6]. The main components of a battery cell are an anode, a cathode, and an electrolyte that could be solid, liquid, or paste [536]. When the electric loads are applied to the battery cell's terminal, because of the chemical reactions inside the cell, electrons flow through the external circuit between the anode and the cathode. During charging, reversible reactions occur when an electromotive force is applied across the positive and negative electrodes [10, 537, 538].

A.1.4.1. Lead-acid battery

Among the rechargeable electro-chemical storage devices, lead-acid (Pb-A) batteries are the oldest [10]. The anode and cathode of lead-acid batteries are made of lead metal (Pb) and lead oxide (PbO₂), respectively. In these batteries, 37% sulfuric acid (H₂SO₄) is used as the electrolyte [10, 99, 144]. According to the reactions shown in Equations A.4 and A.5, both electrodes are transformed into a white crystalline solid lead sulfate (PbSO₄) during discharge. Charging allows the electrodes to come back to the initial state. Equations A.4 and A.5, found in a paper by Bullock [539], represent the chemical reactions that occur at the cathode and the anode, respectively.





A.1.4.2. Lithium-ion battery

Lithium metal oxides, such as LiCoO_2 , LiNiO_2 , LiMO_2 , etc., are used as the cathode, and graphite carbon (C) is used as the anode in lithium-ion (Li-ion) batteries [540]. The electrolytes are made up of lithium salts (e.g., LiPF_6), organic solvents, and different additives [540, 541]. During charging, the lithium ions transfer to the anode from the cathode through the electrolyte solution [542, 543]. The reverse reactions occur during discharge. Equations A.6 and A.7, adapted from Dhameja [544], represent the reactions at the anode and cathode of the lithium-ion cell, respectively. Manganese, cobalt, and phosphate are the main types of lithium-ion batteries used in commercial applications [545, 546].



A.1.4.3. Sodium-based battery

The sodium-sulfur (Na-S) battery is a promising high-temperature battery technology used in large-scale energy storage systems. The battery cell consists of sodium (Na) and sulfur (S) as electrodes and solid ceramic beta alumina (Al_2O_3) as the electrolyte [157]. The batteries need to be kept at a high temperature, around 350°C , for the reactions to initiate [547]. When the batteries are discharged, sodium ions are released from sodium metal and move toward the sulfur electrode through the Al_2O_3 electrolyte. Sodium ions are combined with sulfur ions to produce sodium polysulfide (NaS_x). While charging, reverse reactions occur to produce sodium and sulfur from NaS_x [91]. The overall reaction is shown by Equation A.8. These low-cost batteries are mainly manufactured by NGK Insulators, a Japanese company [548].



Another sodium-based battery, sodium nickel chloride, also known as ZEBRA (Zeolite Battery Research Africa), was invented by Johan Coetzer at the Council for Scientific and Industrial Research in South Africa [549]. Like sodium-sulfur batteries, ZEBRA batteries use liquid sodium as a negative electrode, but the positive electrode is made up of nickel chloride (NiCl_2). A second electrolyte, sodium chloroaluminate, is used in the batteries for the rapid transportation of sodium ions [550]. Equation A.9, from Sudworth's work, describes the overall chemical reaction [550]:



A.1.4.4. Nickel-based battery

The nickel-cadmium (Ni-Cd) battery is the most mature and popular nickel-based battery technology [10]. The positive and negative electrodes of Ni-Cd batteries are made of nickel oxyhydroxide and metallic cadmium, respectively [551]. Alkaline electrolyte, such as potassium hydroxide (KOH), is used as a transport medium for ions [552]. During the discharge process, hydroxide ions and nickel hydroxide are produced at the positive electrode. The negative electrode produces cadmium hydroxide [543]. The process is reversed when the battery is charged. Equation A.10, from Chen et al., shows the overall reaction of the process [10]. There are two types of Ni-Cd batteries, sealed and vented. The only difference between them is that the vented type releases the gases through the valves when the battery is overcharged or rapidly discharged [543].



Another nickel-based battery technology is the nickel-iron battery, which uses nickel oxyhydroxide and iron at the positive and negative electrodes, respectively, with potassium

hydroxide as the electrolyte [553, 554]. The governing equation for the overall reaction, adapted from Shukla et al., is shown by Equation A.11 [553]:



A.1.4.5. Flow battery

Although flow battery technology is relatively new, the batteries are commercially available for utility-scale energy storage systems [9]. A flow battery consists of two separate reservoirs for storing two different solutions of electrolytes; pumps for circulating the electrolytic solutions; and electrodes, membrane, and cells [296]. The electricity is converted to chemical energy in the electro-chemical cells and stored in the electrolytic fluids in the external reservoirs [160, 555]. Vanadium redox and zinc-bromine are the most used large-scale flow battery technologies. The energy rating of these battery technologies depends on the volume of the electrolytes in the tanks; however, the number of cells and size of the electrodes determine the power rating [10].

The vanadium redox flow battery (VRFB) is the most widely used flow battery. These batteries use $\text{V}^{2+}/\text{V}^{3+}$ electrolytes in the anolytic tank and $\text{V}^{4+}/\text{V}^{5+}$ electrolytes in the catholytic tank in sulfuric acid solutions [146, 556]. During the charging or discharging processes, hydrogen ions (H^+) are switched through the polymer membrane between the two reservoirs. The reactions at the positive and negative electrodes are shown by Equations A.12 and A.13, respectively:



The membrane of zinc-bromine batteries (Zn-Br) is made of microporous polyolefin, which separates the carbon-plastic electrodes [556]. The reservoirs contain two different electrolytic solutions based on zinc (Zn) and bromine (Br) [91]. When the battery is being charged, zinc

bromide is formed and, as a result, the densities of both Zn^{2+} and Br-ion are increased in the reservoirs. During the charging process, metallic Zn is stored on one side of the electrode. Equations A.14 and A.15, from Chen et al., describe the reactions at the positive and negative electrodes, respectively [10].



A.1.5. Hydrogen storage

Hydrogen can be produced from the gasification of coal [557-559] and biomass [560, 561], as well as the electrolysis of renewable energy sources, i.e., solar, wind, and hydro [562, 563]. When there is excess solar or wind energy during periods of low demand, electricity from wind can be used in electrolyzers (e.g., alkaline electrolyzers and polymer electrolytic membrane electrolyzers) to produce hydrogen and oxygen from water [564]. The produced hydrogen can be stored in tanks made of metals or composite materials, such as polymer and carbon fiber [565, 566]. A fuel cell is used to produce electricity and water from hydrogen and oxygen during high electricity demand [567, 568].

A.1.6. Thermal storage

In a sensible heat thermal energy storage (TES) system, the heat transfer fluid does not change its phase during heating or cooling processes. The heat is stored in the molten salt during low-demand periods. When demand is high, the heat transfer fluid extracts heat from the molten salt to produce superheated steam, which is then used to produce electricity using the steam turbines.

In latent heat TES systems, the heat transfer medium changes phases. When heat is absorbed by the heat transfer material, it is converted to liquid, and when heat is released, it is converted back

to a solid from a liquid. This heat is used in steam turbines to produce steam for electricity generation.

Thermo-chemical storage is designed based on the exothermic and endothermic reactions resulting from the forming and breaking of chemical bonds in a reversible reaction [569, 570]. The working fluid (for instance, ammonia) is heated through solar insolation and then dissociated in a dissociation reactor. Then the hydrogen (H₂) and nitrogen (N₂) mixture is cooled and stored in a two-phase tank [571]. A synthesis reactor is used to produce ammonia again from preheated H₂ and N₂ in the presence of a catalyst. This reaction is exothermic and releases a large quantity of heat to produce steam to be used in steam turbines to generate electricity [572]. The chemical formulas, from Thaker et al. [131], are represented by Equations A.16 and A.17:



where ΔH is the reaction heat.

A.2. Cost components of an energy storage system

The costs of various components of an ESS, such as power conversion system (PCS), storage unit (SU), and balance of plant (BOP), should be considered in a techno-economic analysis of a storage system as total capital cost (TCC) and life cycle cost (LCC). The TCC is the sum of the PCS, SU, and BOP costs, as shown in Equation A.18:

$$\text{TCC (\$)} = C_{\text{PCS}} + C_{\text{SU}} + C_{\text{BOP}} \quad (\text{A.18})$$

The unit cost of a PCS is expressed per unit of power capacity as \$/kW, while the cost per unit of energy delivered (\$/kWh) is used for the SU. The BOP is usually expressed as \$/kW, but \$/kWh is also applicable, as the BOP capital cost varies with the energy stored or delivered. Sometimes,

BOP costs are considered fixed costs based on the storage technology used [573]. It is difficult to estimate the BOP costs due to a lack of data.

The PCS, SU, and BOP capital costs can be expressed using Equations A.19, A.20, and A.21, respectively:

$$C_{PCS} (\$) = C_{PCSU} * P \quad (A.19)$$

$$C_{SU} (\$) = C_{SUU} * P * h / \eta \quad (A.20)$$

$$C_{BOP} (\$) = C_{BOPU} * P * h \quad (A.21)$$

where C_{PCSU} is the PCS unit cost (\$/kW), P is the power capacity of the system (kW), C_{SUU} is the SU unit cost (\$/kWh), h is the length of each discharge cycle (hour), C_{BOPU} is the BOP unit cost (\$/kWh), and η is the round-trip efficiency of the system.

The LCC is defined as the annual payment to cover the upfront expenditures including the investment cost, annual operation and maintenance (O&M) costs, replacement costs if any, and fuel costs (e.g., electricity, natural gas, etc.) [28]. From a decision-making perspective, the LCC is a more powerful indicator than TCC when comparing ESSs as it includes cost components such as operation and maintenance (O&M) costs, replacement costs, and decommissioning and recycling costs. The LCC calculations include the amortization of the TCC over the lifetime of a project using the capital recovery factor (CRF) based on the discount rate, as shown by Equation A.22, found in Kapila et al. [31]:

$$CRF = \frac{i * (1 + i)^n}{(1 + i)^n - 1} \quad (A.22)$$

where i is the discount rate and n is the project lifetime.

The annual LCC can be calculated using Equation A.23, found in Kapila et al. [31]:

$$LCC_{\text{annual}} (\$/\text{yr}) = (TCC * CRF + O\&M_{\text{cost}} + \text{Fuel}/\text{Electricity}_{\text{cost}} * N * \text{Fuel}_{\text{consumed}}) \quad (\text{A.23})$$

where N is the number of cycles in a year.

The levelized cost of electricity (LCOE), expressed in $\$/\text{kWh}$, can be defined as the electricity price set by the ESS operator to cover all the costs over the lifetime of a system. Kapila et al. estimated the LCOE using the following equation [31]:

$$LCOE = \frac{TCC * CRF + O\&M + \text{Fuel}/\text{Electricity}_{\text{price}} * N * \text{Fuel}/\text{Electricity}_{\text{consumed}}}{N * E_{\text{produced}}} \quad (\text{A.24})$$

where E_{produced} is the amount of electricity generated in one cycle. In addition to the LCOE, sometimes the term levelized cost of storage (LCOS) is used when the cost of charging electricity is not included in the analysis. The LCOS can be calculated by subtracting the fuel cost (i.e., charging cost) from the LCOE and is shown through the following equation [31]:

$$LCOS = LCOE - \frac{\text{Price of charging fuel}}{\eta} \quad (\text{A.25})$$

where η is the overall efficiency of the system.

Appendix B

B.1. Definitions of the stationary applications considered

Bulk energy storage: Energy time-shift is considered a bulk energy service [119]. It involves charging an energy storage system (ESS) when demand is low and discharging when demand is high [24, 574]. The discharge duration for this application is usually 2-8 hours [293].

Transmission and distribution investment deferral: An ESS can be used for 3-6 hours to defer and/or avoid investing in transmission and distribution infrastructure including lines and substations [105, 293, 574].

Frequency regulation maintains the frequency of the grid within permissible limits by balancing differences in energy generation and consumption for a short duration, usually 0.25-1 hour [24, 105, 207].

Support of voltage regulation: In this application, an ESS injects or absorbs power to support the control of reactance in the transmission and distribution (T&D) grid to maintain the voltage within the specific limits [105]. The discharge duration for this application is typically 0.25-1 hour [207].

B.2. Components of an energy storage system

An electro-chemical storage system consists of a power conversion system (PCS), a storage section (battery and enclosure), and the balance of plant (BOP). The PCS converts an alternating current (AC) to a direct current (DC) before electricity is stored in the battery and converts DC back to AC before the electricity is injected into the electrical grid network. In some cases, a separate PCS is used to convert AC to DC and DC to AC [28]. A battery is an electro-chemical device that can store electricity in the form of chemical energy [10]. An electro-chemical battery consists of one

or more cells connected in different configurations to supply the desired voltage and capacity. Each battery cell is comprised of an anode, a cathode, an electrolyte, and separators [6]. Any item not included in the PCS or storage section such as heating, ventilation, and air conditioning (HVAC), grid connection, monitoring and control systems, installation, etc., can be considered BOP items [28].

B.3. Cycle life

For electro-chemical batteries, cycle life depends on the depth of discharge (DOD). The deeper the battery is discharged during an operational cycle, the more its cycle life reduces. Data for cycle life corresponding to the DOD were obtained from the Discover Battery brochure [318] and Eckroad and Gyuk [169] for valve-regulated lead-acid (VRLA) and nickel-cadmium (Ni-Cd) batteries, respectively. From the plot of cycle life vs. DOD, best-fit curves were drawn, and equations were obtained that were used in the techno-economic models. Figures B.1 and B.2 show the relationship between cycle life and DOD for VRLA and Ni-Cd batteries, respectively.

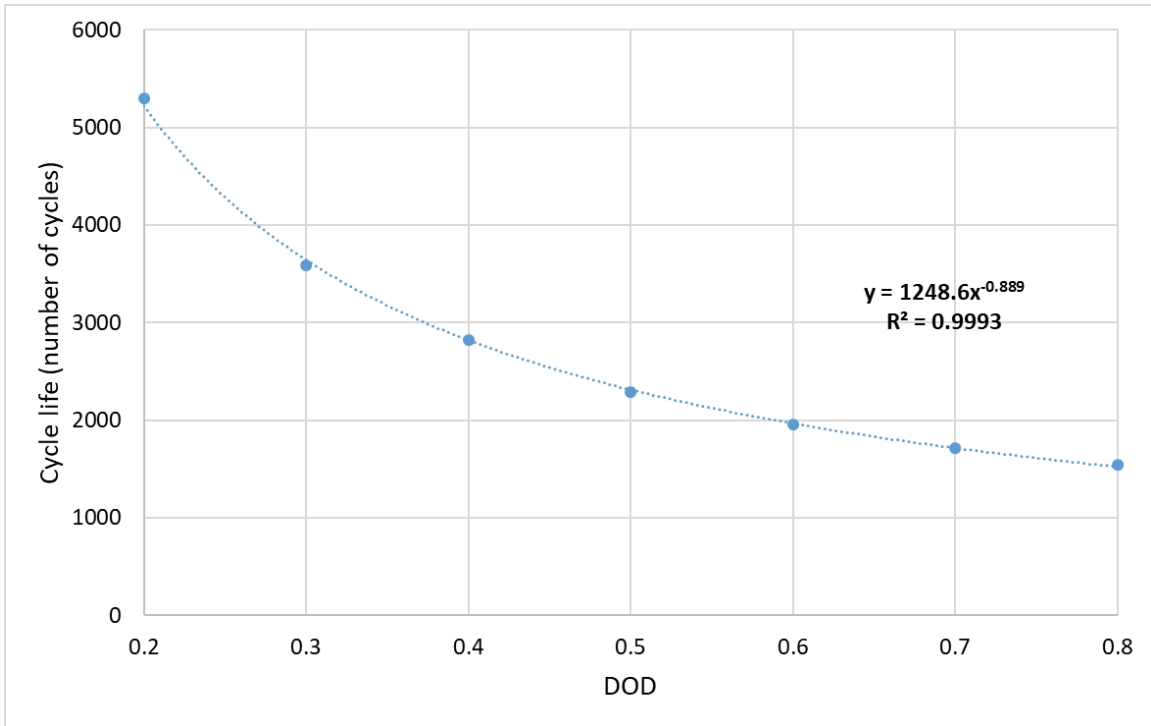


Figure B.1: The plot of cycle life vs. DOD for a VRLA battery

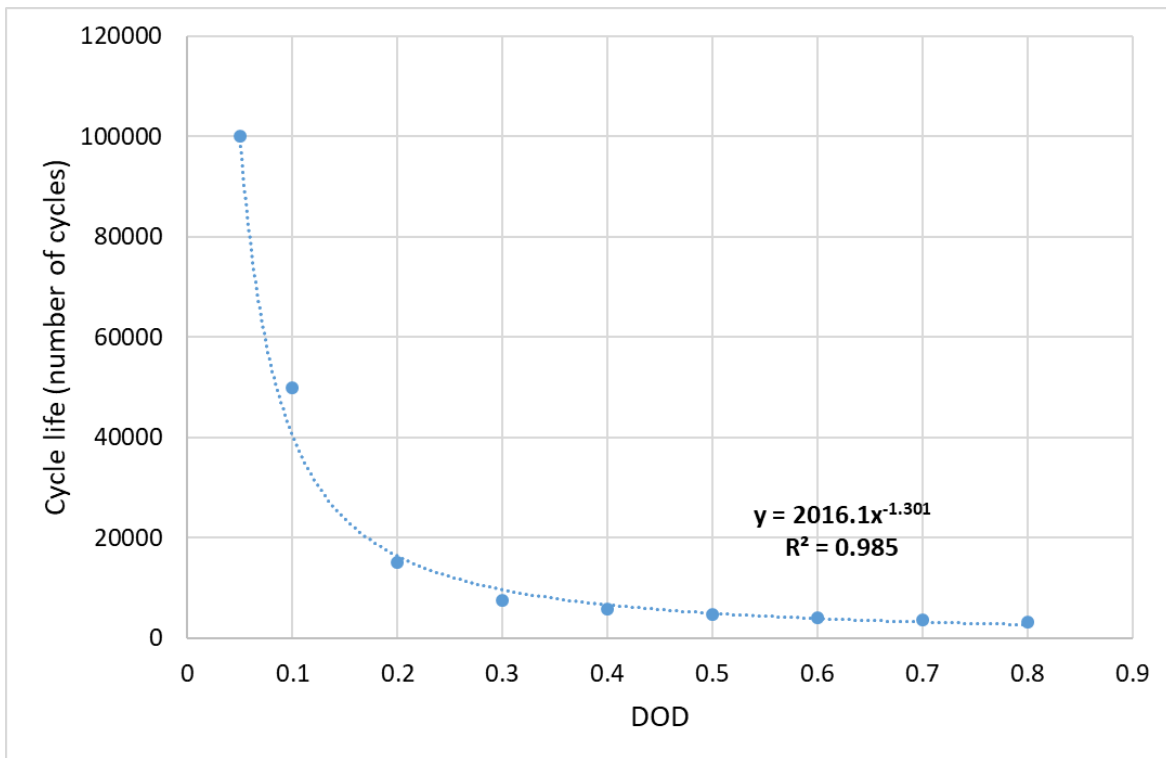


Figure B.2: The plot of cycle life vs. DOD for a Ni-Cd battery

B.4. Pump and heat exchanger design for the vanadium redox system

Pumps and heat exchangers (HXs) are the accessories, along with some piping and fittings (for electrolyte circulation), required for vanadium redox flow (VRF) battery systems. Each tank is connected to a pump to circulate the electrolyte to the stacks. The volume flow rate for pumps was calculated from the molar flow of vanadium (see Equation 3.3 in Chapter 3) and the vanadium concentration in the electrolyte using Equation B.1, adapted from Minke et al. [296]:

$$F_P = \frac{Q_V}{C_V} \quad (\text{B.1})$$

where Q_V is the flow rate of vanadium (mol/s) and C_V is the vanadium concentration (mol/L).

HXs are required to dissipate the heat generated during the system operation. Each MW subsystem needs two heat exchangers. We calculated the heat of reaction from the rated power, average voltage, and open circuit voltage (OCV) using Equation B.2, found in Minke et al. [296]:

$$H = P * \frac{(OCV - V)}{V} \quad (\text{B.2})$$

where H is the heat of reaction (kW), OCV is open circuit voltage (V), and V is average voltage (V). Each electrolyte circuit has an HX that dissipates half the reaction heat. Therefore, the heat flow in the apparatus is $Q_{HX} = 0.5H$. With the thermal resistance (TR) and the mean of the logarithmic temperature difference ($\Delta T_{log-mean}$), we estimated the area of heat exchanger tubes according to Equation B.3:

$$A = Q_{HX} * \frac{TR}{\Delta T_{log-mean}} \quad (\text{B.3})$$

where TR is total thermal resistance (m^2K/W) and $\Delta T_{log-mean}$ is the mean of the logarithmic temperature difference (K).

A 35 m length of the pipeline for the electrolyte circulation from the tank to the stacks for each electrolyte circuit in the system was assumed [296].

B.5. Capital cost of batteries

The capital cost of a sodium-sulfur (Na-S) battery is based on the price of a G50 module [575]. The nominal voltage of a G50 module is 64 V or 128 V depending on the arrangement of the cells. The configuration of cells could be either (8s*5p)*8s or (8s*10p)*4s [575]. Once we estimated the installed capacity of a Na-S storage system, we calculated the number of G50 modules required. In this study, \$84,913.45 (inflation-adjusted for 2019 US dollars) per module was assumed to calculate the total capital cost of a Na-S battery [169].

For a VRLA battery, the cost function was developed with battery prices for several capacity ranges [576]. Figure B.3 shows the cost curve developed in this study.

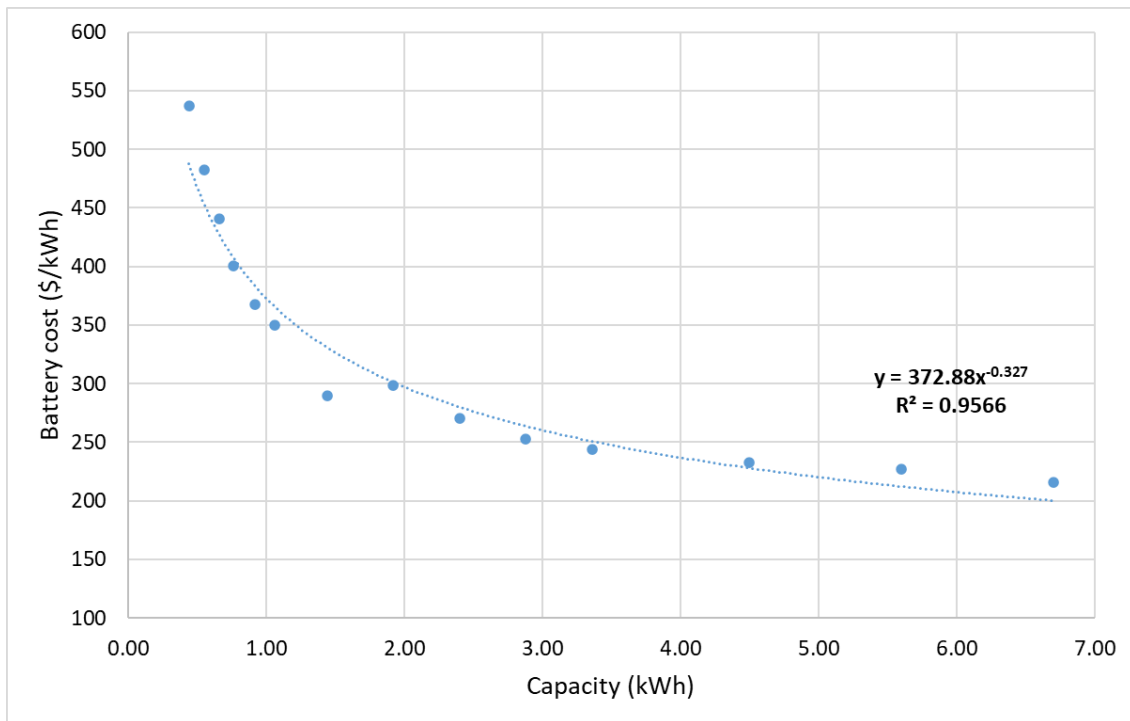


Figure B.3: Capital cost curve for a VRLA battery

B.6. Life cycle costs

Scenario 1 (S1), Scenario 2 (S2), Scenario 3 (S3), and Scenario 4 (S4) represent bulk energy storage, T&D investment deferral, frequency regulation, and support of voltage regulation, respectively.

In this section, additional results for different power capacities for S1-S4 are shown. The discharge duration was considered to be 5 hours for S1 and S2 and 15 minutes for S3 and S4. Table B.1 shows total investment costs (TICs) and replacement costs (RCs). The levelized costs of storage (LCOSs) and levelized costs added by storage (LCASs) can be found in Table B.2. The LCOS and LCAS can be calculated using Equations B.4 and B.5, respectively.

$$LCOS = \frac{\frac{TIC}{(1+i)^{n-1}} + O\&M + E_{in} * E_{price} * N + \left[\frac{RC}{(1+i)^n}, RC * \frac{i(1+i)^n}{(1+i)^{n-1}} \right]}{E_{out} * N} \quad (B.4)$$

$$LCAS = LCOS - \frac{Charging\ cost}{\eta_{overall}} \quad (B.5)$$

In these equations, i is real discount rate ($i = \left[\frac{1+d}{1+f} \right] - 1$), d is the nominal discount rate, f is the inflation rate, n is the lifetime of the project (year), E_{in} is charging electricity in one cycle (MWh), E_{price} is the electricity cost for charging (\$/MWh), N is number of cycles in a year, RC is replacement cost, n, RC is the replacement period (year), E_{out} is electricity discharged in one cycle (MWh), and $\eta_{overall}$ is overall efficiency of the system (%).

As shown in Table B.1, the TIC and RC increase with the increase in rated power. This is obvious, because with the increase in capacity more battery cells and PCS are required to satisfy the power and energy requirements. The LCOS decreases with an increase in rated power because of economies of scale. The LCOS is lower at higher capacities because of the decrease in unit capital cost with an increase in ESS rated capacity.

Table B.1: Total investment cost and replacement cost (million \$) for ESSs of several rated capacities

	Na-S		Li-ion		VRLA		Ni-Cd		VRF	
	TIC	RC	TIC	RC	TIC	RC	TIC	RC	TIC	RC
S1										
5 MW	11.11	8.73	10.17	7.51	15.60	35.23	36.44	61.61	17.71	5.34
25 MW	55.21	43.63	50.47	37.55	77.64	176.13	181.81	308.06	88.20	26.68
75 MW	164.64	130.88	150.37	112.64	231.90	528.39	544.40	924.19	263.61	80.03
100 MW	219.17	174.51	200.11	150.18	308.83	704.52	725.50	1232.26	351.11	106.71
S2										
5 MW	11.11	8.73	10.17	7.51	15.60	23.48	36.44	30.81	17.71	5.34
15 MW	33.20	26.18	30.36	22.52	46.67	70.45	109.17	92.42	53.00	16.01
20 MW	44.21	34.90	40.41	30.03	62.16	93.94	145.50	123.23	70.61	21.34
25 MW	55.21	43.63	50.47	37.55	77.64	117.42	181.81	154.03	88.20	26.68
S3										
5 MW	2.07	0.44	2.14	0.74	2.40	5.28	3.59	3.08	7.84	5.34
25 MW	10.00	2.18	10.35	3.75	11.63	26.42	17.56	15.40	38.82	26.68
75 MW	29.03	6.54	30.03	11.26	33.89	79.26	51.67	46.21	115.43	80.03
100 MW	38.35	8.73	39.67	15.02	44.81	105.68	68.52	61.61	153.55	106.70
S4										
5 MW	2.26	0.44	2.34	0.37	2.60	1.17	3.79	1.54	8.03	5.34
10 MW	4.47	0.87	4.63	0.75	5.14	2.35	7.51	3.08	16.00	10.67
20 MW	8.77	1.75	9.09	1.51	10.12	4.70	14.86	6.16	31.84	21.34

	Na-S		Li-ion		VRLA		Ni-Cd		VRF	
30 MW	13.00	2.62	13.46	2.25	15.01	7.05	22.12	9.24	47.60	32.01

Table B.2: Levelized cost of storage and levelized cost added by storage (\$/MWh) for ESSs of several rated capacities

	Na-S		Li-ion		VRLA		Ni-Cd		VRF	
	LCOS	LCAS	LCOS	LCAS	LCOS	LCAS	LCOS	LCAS	LCOS	LCAS
S1										
5 MW	200.79	178.30	181.08	161.61	411.71	390.34	803.02	781.12	268.15	244.79
25 MW	199.92	177.43	180.21	160.74	410.06	389.43	802.11	780.21	267.26	243.90
75 MW	199.16	176.66	179.39	159.93	409.99	388.62	801.31	779.40	266.48	243.12
100 MW	198.95	176.45	179.17	159.70	409.77	388.40	801.09	779.18	266.26	242.90
S2										
5 MW	267.79	245.30	243.29	223.82	468.03	446.66	907.91	886.01	383.09	359.73
15 MW	266.98	244.49	242.44	222.97	467.18	445.81	907.06	885.16	382.26	358.90
20 MW	266.72	244.23	242.17	222.70	466.91	445.54	906.79	884.89	382.00	358.64
25 MW	266.51	244.02	242.01	222.54	466.69	445.31	906.57	884.66	381.78	358.42
S3										
5 MW	381.69	359.20	433.88	414.42	764.81	743.44	874.54	852.64	1511.56	1488.20
25 MW	371.44	348.95	424.48	405.01	754.08	732.71	863.81	841.90	1501.12	1477.76
75 MW	362.40	339.91	415.01	395.54	744.61	723.24	854.33	832.43	1491.53	1468.16
100 MW	359.93	337.44	412.42	392.95	742.02	720.65	851.75	829.85	1489.11	1465.74

	Na-S		Li-ion		VRLA		Ni-Cd		VRF	
	S4									
5 MW	963.75	941.26	1050.36	1030.89	1204.36	1182.99	2011.21	1989.30	3813.32	3789.96
10 MW	952.60	930.10	1041.61	1022.14	1192.68	1171.30	1999.52	1977.61	3801.95	3778.59
20 MW	938.59	916.09	1026.93	1007.46	1178.00	1156.62	1984.84	1962.94	3787.68	3764.32
30 MW	929.39	906.89	1016.32	996.85	1168.36	1146.99	1975.20	1953.30	3778.30	3754.94

B.7. Sensitivity and uncertainty analyses

The sampling error for the Monte Carlo simulation can be calculated using Equation B.6 [577]:

$$\text{Sampling error} = \frac{z * \sigma}{n^{1/2}} \quad (\text{B.6})$$

where the standard deviation of the mean and the number of samples are σ and n , respectively. The value of z was taken to be 1.96 for a 95% confidence interval.

To perform the Monte Carlo simulations, the statistical distributions of the inputs are required. When there is limited data, triangular distributions were generated; they give conservative results for predictable values with lower standard deviations. When it is hard to predict a reliable value, uniform distribution was used to treat all the inputs equally. Finally, a PERT distribution was used when the inputs did not differ widely to emphasize the most likely value instead of the minimum and maximum values. The minimum and maximum values of input parameters for each ESS for which sensitivity and uncertainty analyses were performed are listed in Table B.3.

Table B.3: The minimum and maximum values of the input parameters for sensitivity and uncertainty analyses

ESS	Parameter	Minimum value	Maximum value
Na-S	Round-trip efficiency (%)	70 [288]	90 [10]
	Depth of discharge (%)	70 [157]	90 [578]
	PCS efficiency (%)	90 [425]	97 [302]
	Nominal discount rate (%)	8 ^a	12 [579]
	Inflation rate (%)	0.94 ^b [324]	2.91 ^c [324]
	Battery cost (\$/kWh)	212 [24]	465 [11]
	Cost of enclosure and foundation (\$/m ²)	198.07 ^d	367.85 ^d
	Yearly fixed O&M cost for the battery (\$/kW-year)	2.61 [28]	22.55 [28]

ESS	Parameter	Minimum value	Maximum value
	Yearly variable O&M cost for the battery (\$/MWh)	0.39 [28]	7.30 [28]
	Fixed O&M cost for the PCS (\$/kW-year)	1.84 ^d	3.42 ^d
	BOP cost (\$/kW)	71.49 [105]	116.62 [181]
	Unit price of electricity (\$/MWh)	11.47 ^e [323]	21.11 ^f [323]
	Contingency cost as a percent of capital cost (%)	1 [207]	5 [207]
Li-ion	Round-trip efficiency (%)	85 [288]	98 [288]
	Depth of discharge (%)	75 ^g	90 ^g
	PCS efficiency (%)	90 [425]	97 [302]
	Nominal discount rate (%)	8 ^a	12 [579]
	Inflation rate (%)	0.94 ^b [324]	2.91 ^c [324]
	Battery cost (\$/kWh)	189 [11]	555 [213]
	Cost of enclosure and foundation (\$/m ²)	198.07 ^d	367.85 ^d
	Yearly fixed O&M cost for the battery (\$/kW-year)	6.21 [326]	14.49 [326]
	Yearly variable O&M cost for the battery (\$/MWh)	0.52 [28]	7.31 [28]
	Fixed O&M cost for the PCS (\$/kW-year)	1.84 ^d	3.42 ^d
	BOP cost (\$/kW)	97.45 [329]	116.62 [181]
	Unit price of electricity (\$/MWh)	11.47 ^e [323]	21.11 ^f [323]
	Contingency cost as a percent of capital cost (%)	5 [207]	10 [207]
VRLA	Round-trip efficiency (%)	80 [288]	90 [288]
	Depth of discharge (%)	50 ^h	70 ^h
	PCS efficiency (%)	90 [425]	97 [302]
	Nominal discount rate (%)	8 ^a	12 [579]
	Inflation rate (%)	0.94 ^b [324]	2.91 ^c [324]
	Battery cost (\$/kWh)	126 [213]	376 [51]
	Cost of enclosure and foundation (\$/m ²)	198.07 ^d	367.85 ^d
	Yearly fixed O&M cost for the battery (\$/kW-year)	4.17 ⁱ [28]	16.94 ⁱ [28]
	Yearly variable O&M cost for the battery (\$/MWh)	0.20 [28]	0.68 [28]
	Fixed O&M cost for the PCS (\$/kW-year)	1.84 ^d	3.42 ^d
	BOP cost (\$/kW)	94.42 [105]	113.40 [28]

ESS	Parameter	Minimum value	Maximum value
	Unit price of electricity (\$/MWh)	11.47 ^e [323]	21.11 ^f [323]
	Contingency cost as a percent of capital cost (%)	5 [207]	10 [207]
Ni-Cd	Round-trip efficiency (%)	70 [314]	90 [314]
	Depth of discharge (%)	70 ^g	85 ^g
	PCS efficiency (%)	90 [425]	97 [302]
	Nominal discount rate (%)	8 ^a	12 [579]
	Inflation rate (%)	0.94 ^b [324]	2.91 ^c [324]
	Battery cost (\$/kWh)	609 [11]	1210 [11]
	Cost of enclosure and foundation (\$/m ²)	198.07 ^d	367.85 ^d
	Yearly fixed O&M cost for the battery (\$/kW-year)	5.21 [28]	31.28 [28]
	Yearly variable O&M cost for the battery (\$/kW-year)	6.16 ^d	11.45 ^d
	Fixed O&M cost for the PCS (\$/kW-year)	1.84 ^d	3.42 ^d
	BOP cost (\$/kW)	75 [215]	125 ^j
	Unit price of electricity (\$/MWh)	11.47 ^e [323]	21.11 ^f [323]
	Contingency cost as a percent of capital cost (%)	5 ^j	10 ^j
VRF	Round-trip efficiency (%)	70 [105]	80 [105]
	PCS efficiency (%)	90 [425]	97 [302]
	Nominal discount rate (%)	8 ^a	12 [579]
	Inflation rate (%)	0.94 ^b [324]	2.91 ^c [324]
	Number of cycles in lifetime	10,000 [28]	13,000 [28]
	Pump cost (\$/m ³ h ⁻¹)	13 [296]	82 [296]
	Heat exchanger cost (\$/m ²)	219 [296]	487 [296]
	V ₂ O ₅ cost (\$/kg)	17.43 [327]	26.14 [327]
	H ₂ SO ₄ cost (\$/kg)	0.05 [327]	0.09 [327]
	Cost of enclosure and foundation (\$/m ²)	198.07 ^d	367.85 ^d
	Yearly fixed O&M cost for the battery (\$/kW-year)	4.59 [28]	23.38 [28]
	Yearly variable O&M cost for the battery (\$/MWh)	0.27 [28]	3.65 [28]
	Fixed O&M cost for the PCS (\$/kW-year)	1.84 ^d	3.42 ^d

ESS	Parameter	Minimum value	Maximum value
	BOP cost (\$/kW)	32.59 [28]	99.10 [105]
	Unit price of electricity (\$/MWh)	11.47 ^e [323]	21.11 ^f [323]
	Contingency cost as a percent of capital cost (%)	5 [119]	7 [119]

^a 20% less than the default value was assumed.

^b Lowest yearly average inflation rate in Canada from 2010-18.

^c Highest yearly average inflation rate in Canada from 2010-18.

^d Varied by 30% from the default value due to the unavailability of data.

^e Lowest yearly average off-peak pool price of electricity in Alberta from 2013-17.

^f Highest yearly average off-peak pool price of electricity in Alberta from 2013-17.

^g Assumed as a realistic range because most studies considered 80%.

^h Assumed as a realistic range because most studies considered 60%.

ⁱ The O&M for a VRLA was assumed to be the same as for a Pb-A.

^j Assumed value.

B.7.1. Sensitivity analysis for the VRF system

The sensitivity results for the VRF system for bulk energy storage are presented in Figures B.4 and B.5 for the TIC and LCOS, respectively.

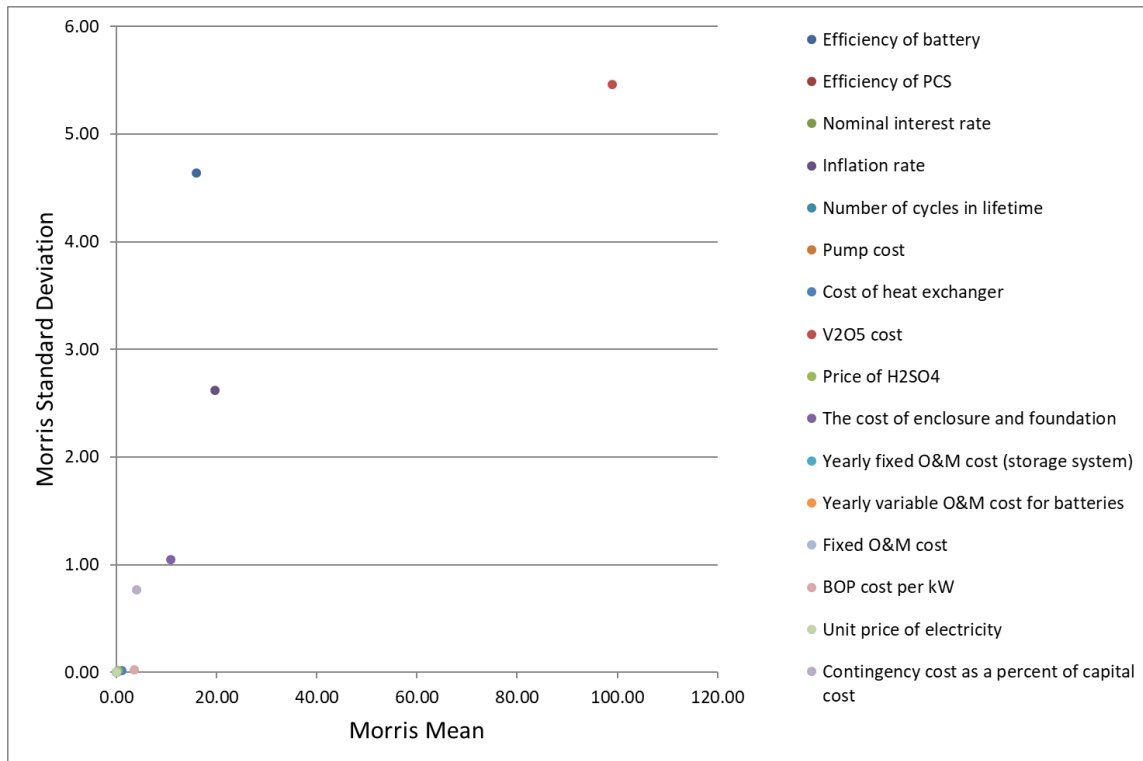


Figure B.4: Sensitivity analysis for the TIC in the VRF ESS for bulk energy storage

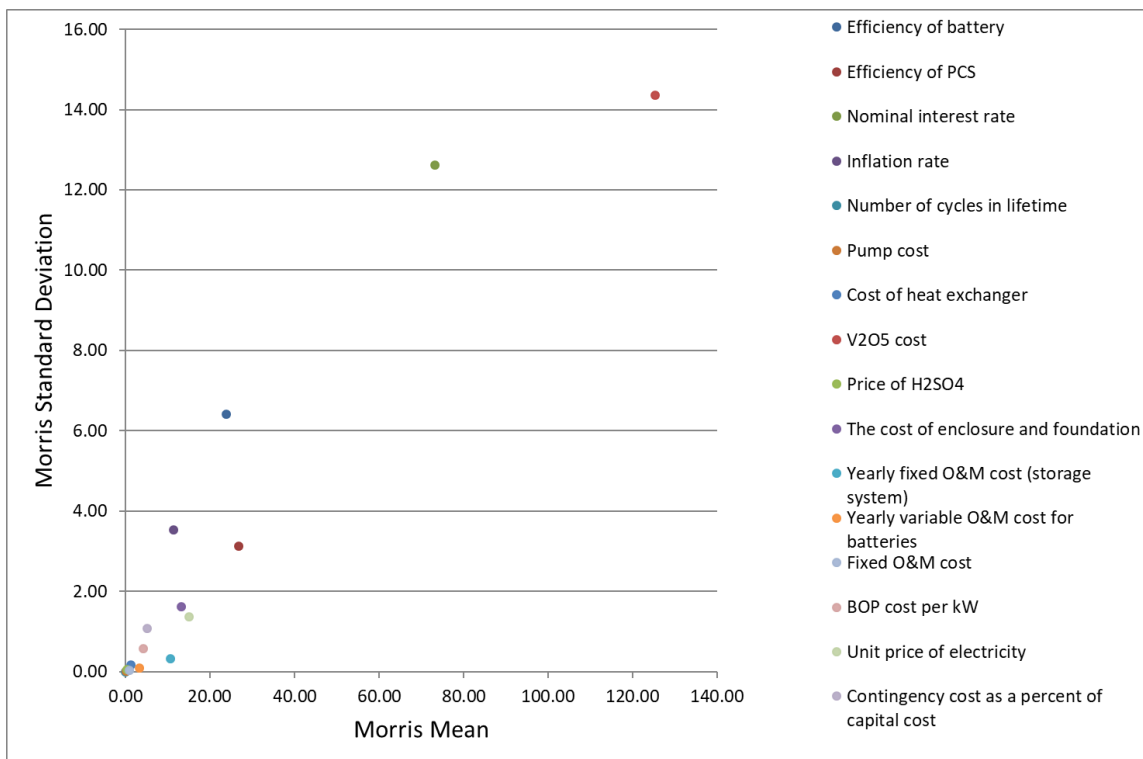


Figure B.5: Sensitivity analysis for the LCOS in the VRF ESS for bulk energy storage

B.7.2. Uncertainty in TIC

The bottom and top of the rectangular boxes in Figures B.6-B.9 represent the 25th and 75th percentiles, respectively, and the bottom and top of the error bars represent the 5th and 95th percentiles, respectively. The dots in the rectangular boxes represent the means.

The uncertainties in LCOS were discussed in Chapter 3. The uncertainty results in TIC are presented in Figures B.6-B.9.

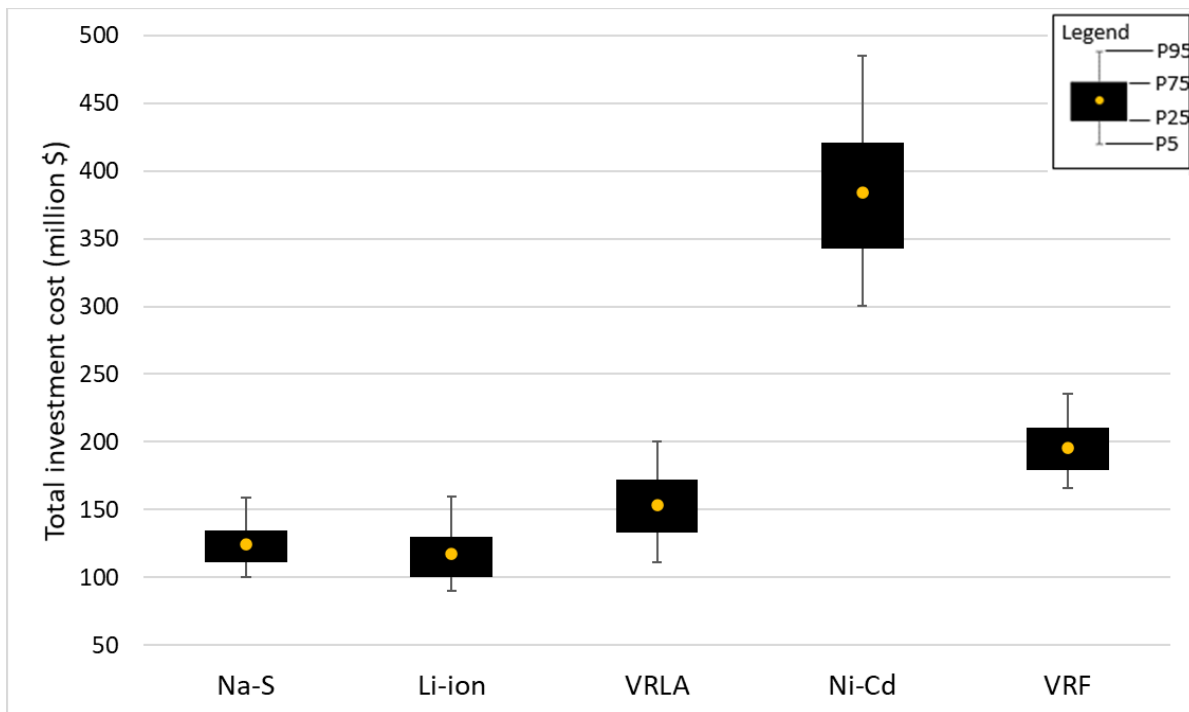


Figure B.6: Uncertainty analysis for the TIC for bulk energy storage

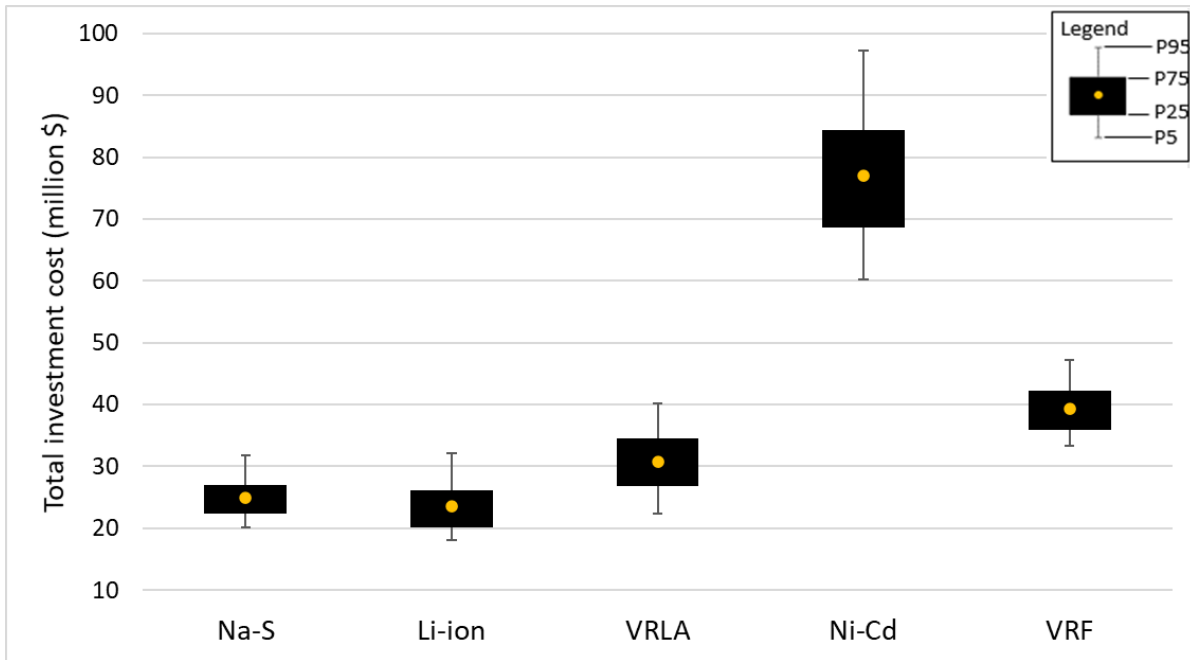


Figure B.7: Uncertainty analysis for the TIC for T&D investment deferral

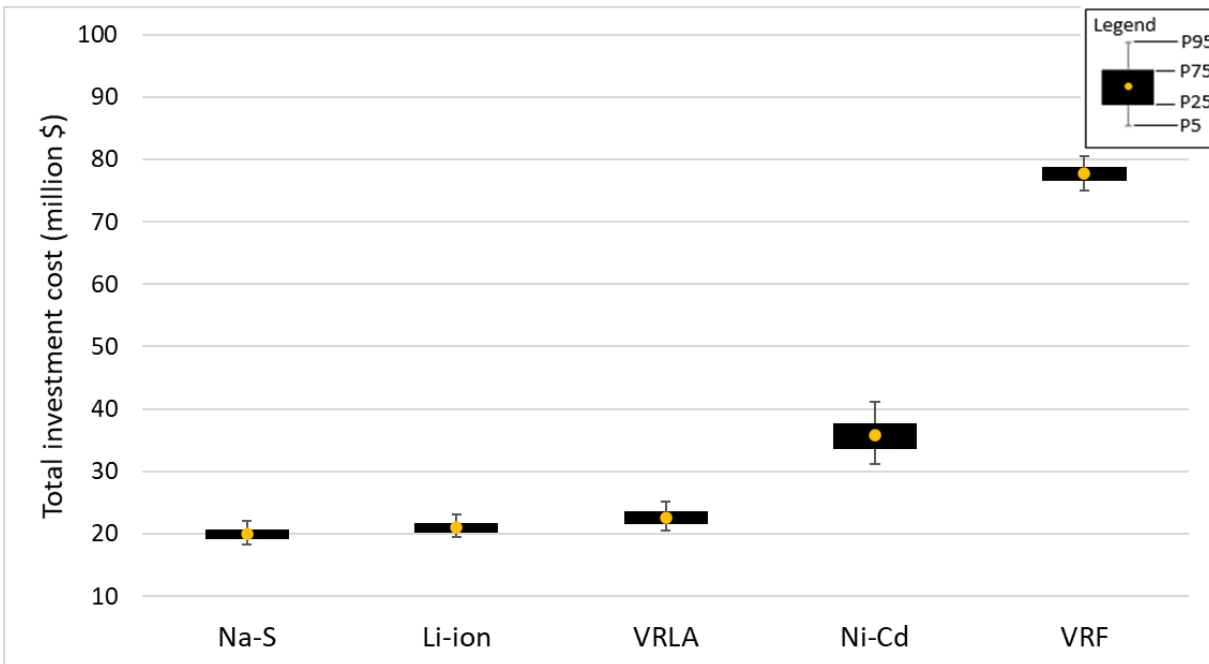


Figure B.8: Uncertainty analysis for the TIC for frequency regulation

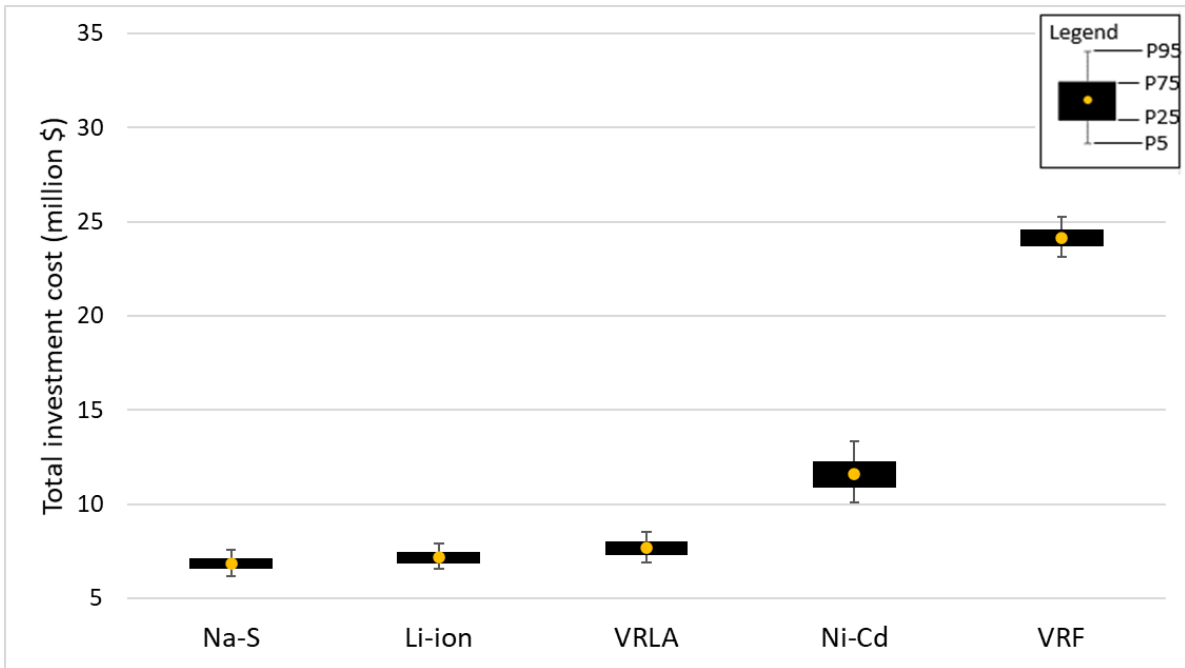


Figure B.9: Uncertainty analysis for the TIC for support for voltage regulation

Appendix C

C.1. The sizing of components of a vanadium redox flow storage system

For the vanadium redox flow (VRF) battery, the electrolyte can operate for 13,000 cycles [258] without degradation [307]. However, the stacks need to be replaced after 10 years [320] as various components are subject to corrosion [44]. The power and energy capacities of the VRF battery are designed independently. While the power comes from the stacks that contain the cells, the energy comes from the electrolyte. The number of stacks required was calculated from the rated power of each stationary application and the power of each stack. The energy is stored in the electrolyte in the VRF battery. The electrolyte volume determines the energy capacity. The amount of electrolyte required and the volume of positive and negative electrolyte tanks were calculated based on the power and duration of discharge (listed in Table 4.1 of Chapter 4). The amount of vanadium pentoxide (V_2O_5) needed for the positive (N_{PE}) and negative (N_{NE}) electrolytes can be estimated using Equation C.1, adapted from Minke et al. [296]:

$$N_{PE} = N_{NE} = N = \frac{P_R * H * 3600}{\eta_b * DOD * V * F} \quad (C.1)$$

where N is the amount of vanadium (mols), P_R is the rated power (W), H is the duration of discharge (h), η_b is the battery efficiency (%), DOD is the depth of discharge (%), V is the average voltage of each cell (V), and F is the Faraday constant.

The volume of positive (V_{PE}) and negative (V_{NE}) electrolytes was calculated using Equation C.2:

$$V_{PE} = V_{NE} = \frac{N}{C_V} \quad (C.2)$$

where C_V is the V_2O_5 concentration in mol/L.

To avoid spillage, some void space is kept in the tanks. It was assumed that the volume of each tank is 1.5 times the electrolyte volume [296]. The electrolyte is a mixture of V_2O_5 , sulfuric acid (H_2SO_4), and water. The volume of H_2SO_4 was calculated using the volume of electrolyte, the molecular mass of H_2SO_4 , and the concentration of H_2SO_4 (see Table C.1). We calculated the amount of water assuming an electrolyte density of 1200 kg/m^3 [316].

The system was considered to be modular, each module having a 1 MW capacity [44]. The advantage of a 1 MW module is that it can be fitted into a standard container (40-foot) [319]. Each 1 MW power subsystem is connected to one positive and one negative electrolyte tank. The volume of each tank was calculated using the rated power of each module and the duration of discharge (see Table 4.1 in Chapter 4). The number of tanks was calculated from the amount of electrolyte required for the rated power of the energy storage system (ESS) and the amount of electrolyte for a 1 MW module for the specified duration of discharge.

Table C.1: Technical inputs used to design the VRF energy storage system

Parameter	Value	Unit
Depth of discharge	90 [316]	%
Battery efficiency	75 [105]	%
Cycle life	13,000 [258]	cycles
Current density	3000 [316]	A/m^2
Active cell area	1 [316]	m^2
Capacity of each stack	250 [296]	kW
Vanadium concentration	1.6 [44]	mol/L
Sulfuric acid concentration	5 [316]	mol/L
Electrolyte density	1200 [316]	kg/m^3
Molecular mass of vanadium	181.90 [316]	g/mol
Average cell voltage	1.19 [316]	V

C.2. Inventory analysis

Table C.2 shows the mass fraction of different materials for the batteries. For a VRF battery, the mass of the pumps, heat exchangers (HXs), pipes, and cables were assumed to be 69.88 kg/MWh, 123.25 kg/MWh, 332 kg/MW, and 177 kg/MW, respectively [44]. The pumps need to be replaced after 10 years [474]. We assumed that the HXs, pipes, and cables are made of stainless steel, steel, and copper, respectively [44], and the pumps of 50% stainless steel and 50% cast iron [474]. Table C.3 shows the material inventory for the five electro-chemical ESSs.

Table C.2: Material composition of different electro-chemical batteries

Na-S [349]		VRLA [341]	
Material	Wt (%)	Material	Wt (%)
Sulfur	12.5	Lead	71
Sodium	8	Calcium	0.03
β - alumina	10.2	Aluminium	0.01
α - alumina	2.3	Tin	0.4
Steel	12.8	Silver	0.01
Aluminium	20.6	Negative electrode additives	0.2
Graphite	2	Fiberglass separator	2.5
Copper	3.4	Copper terminals	0.5
Glass	4.3	H ₂ SO ₄	6.3
Sand	15.2	Water	10.8
Miscellaneous ^a	8.7	Polypropylene	7.5
		Control electronics	0.8
Li-ion [350]			
Chemistry	LMO	NMC	LFP
Material	Wt (%)		
Active material (cathode)	30.75	25.17	23.75
Graphite	12.67	15.75	13.84
Binder (PVDF)	2.28	2.15	1.98

Copper	11.57	11.73	10.41
Wrought aluminum	22.67	23.85	23.08
Electrolyte: LiPF ₆	1.65	1.61	2.45
Electrolyte: Ethylene carbonate	4.61	4.5	6.84
Electrolyte: Dimethyl carbonate	4.61	4.5	6.84
Plastic: Polypropylene	1.11	1.1	0.97
Plastic: Polyethylene	0.35	0.36	0.31
Plastic: Polyethylene terephthalate	0.2	0.21	0.22
Steel	0.61	0.62	0.71
Thermal insulation	0.43	0.49	0.46
Coolant: Glycol	3.41	4.3	5.1
Electronic parts	3.07	3.66	3.03
Ni-Cd [351]		VRF (1 MW power subsystem) [44]	
Material	Wt (%)	Material	Wt (%)
Steel	39.2	Membrane (Nafion)	1.5
Ni	20.5	Electrode (PAN carbon felt)	4.2
Cd	16.4	Bipolar plate ^b (PPG86 composite)	54.8
Ni(OH) ₂	8.1	Current collector (copper)	19.7
H ₂ O	8.0	Cell frame (PVC)	3.1
KOH	3.5	Gaskets (EPDM)	4.3
Polyamide	2.6	Stack frame (steel)	12.5
PVC	1.1		
Co	0.5		
Rubber (polypropylene)	0.3		

For the VRF, the materials for different components are presented in parentheses.

^a Due to the lack of data, polypropylene was assumed to be 8.7% for the miscellaneous items [349].

^b The material requirements/kg of bipolar plates: 0.88 kg of synthetic graphite and 0.14 kg of polypropylene [44].

Table C.3: The amounts of different materials (tonnes) for 250, 50, 12.5, and 3.75 MWh ESSs for S1, S2, S3, and S4, respectively

ESS	Material	Bulk energy storage (S1)	T&D investment deferral (S2)	Frequency regulation (S3)	Support of voltage regulation (S4)
Battery and foundation					
Na-S	Sulfur	864	173	44	13
	Sodium	553	111	27	8
	β -alumina	706	142	35	11
	α -alumina	159	32	8	3
	Steel	885	177	44	14
	Aluminium	1425	285	72	22
	Graphite	138	27	7	2
	Copper	234	47	12	4
	Glass	298	60	15	5
	Sand	1051	210	53	15
	Polypropylene	601	121	30	9
	Concrete (foundation)	3646	729	182	54
Li-ion ^a	Active material (cathode)	1295, 1941, 1609	259, 388, 322	97, 145, 121	19, 29, 24
	Graphite	810, 800, 938	162, 160, 188	61, 60, 71	12, 12, 15
	Binder (PVDF)	111, 144, 134	22, 29, 27	8, 11, 10	2, 2, 2
	Copper	603, 730, 705	121, 146, 141	45, 54, 53	9, 11, 11
	Wrought aluminum	1227, 1431, 1564	245, 286, 313	92, 107, 117	18, 22, 24
	Electrolyte: LiPF ₆	83, 104, 166	16, 21, 34	6, 8, 13	1, 2, 3
	Electrolyte: Ethylene carbonate	231, 291, 464	46, 58, 93	17, 22, 34	4, 5, 7

ESS	Material	Bulk energy storage (S1)	T&D investment deferral (S2)	Frequency regulation (S3)	Support of voltage regulation (S4)
	Electrolyte: Dimethyl carbonate	231, 291, 464	46, 58, 93	17, 22, 34	4, 5, 7
	Plastic: Polypropylene	57, 70, 65	12, 14, 13	5, 5, 5	1, 1, 1
	Plastic: Polyethylene	18, 22, 21	4, 5, 5	2, 2, 2	0.3, 0.4, 0.3
	Plastic: Polyethylene terephthalate	11, 13, 15	2, 3, 3	1, 1, 1	0.2, 0.2, 0.3
	Steel	32, 39, 48	6, 8, 10	3, 3, 4	0.5, 0.6, 0.8
	Thermal insulation	25, 27, 32	5, 5, 6	2, 2, 3	0.4, 0.5, 0.5
	Coolant: Glycol	221, 269, 318	44, 43, 69	16, 16, 26	4, 4, 5
	Concrete (foundation)	1804	361	90	27
VRLA	Lead	41,231	6184	5154	464
	Calcium	17	3	2	0.2
	Aluminium	5	1	1	0.1
	Tin	232	34	29	3
	Silver	5	1	1	0.1
	Fiberglass	1452	218	181	16
	Copper	290	44	36	4
	H ₂ SO ₄	3659	549	457	41
	Polypropylene	4355	653	544	49
	Concrete (foundation)	9592	1919	480	144

ESS	Material	Bulk energy storage (S1)	T&D investment deferral (S2)	Frequency regulation (S3)	Support of voltage regulation (S4)
Ni-Cd	Steel	8353	1114	417	83
	Ni	4368	582	219	44
	Cd	3495	466	175	35
	Ni(OH) ₂	1725	230	86	17
	H ₂ O	1705	228	85	17
	KOH	746	98	37	7
	Polyamide	554	73	28	5
	PVC	234	31	12	3
	Co	106	15	5	1
	Rubber (polypropylene)	64	8	4	1
	Concrete (foundation)	6764	1358	338	102
	VRF	Glass fibre	802	161	112
Vanadium		4225	845	211	64
Sulfuric acid		7119	1423	356	107
Nafion		15	3	15	5
Carbon fiber (CF)		42	8	42	13
Synthetic graphite		484	97	484	145
Polypropylene		77	15	77	23
Copper		206	41	206	62
Steel		142	28	142	43
Stainless steel		48	10	3	1
PVC		31	6	31	9
EPDM		43	8	43	13
Cast iron		17	4	1	0.3

ESS	Material	Bulk energy storage (S1)	T&D investment deferral (S2)	Frequency regulation (S3)	Support of voltage regulation (S4)
	Concrete (foundation)	18,555	3711	828	279
PCS and container					
	Steel	151	30	151	45
	Aluminium	12	3	12	4
	Copper	24	5	24	7
	Plastics	6	1	6	2
	Transformer oil	32	6	32	9
	Pressboard	3	1	4	1
	Paper	1	0.3	1	0.4

^a For a Li-ion battery, the first, second, and third values represent NMC, LMO, and LFP chemistry, respectively.

Table C.4: Parameters used to calculate the inventory for the PCS, PCS container, concrete foundation, and vanadium electrolyte tank

Parameter	Value	Unit
Efficiency of the PCS	95 [169]	%
Lifetime of the PCS	20 [299]	year
Wall thickness of the electrolyte tank	0.016 [580]	m
Thickness in the bottom of the electrolyte tank	0.029 [580]	m
Concrete floor thickness (for heavy loads)	0.127 [581]	m
Density of concrete	2400 [582]	kg/m ³
Mass of the PCS container (40-foot long made of steel)	3740 [583]	kg

The mass of various capacity inverters was found in Indrivetec’s brochure [353]. The data for the transformers was taken from Meksan Transformer’s webpage [354]. From the plots of mass vs. capacity, best-fit curves were drawn. Figures C.1 and C.2 show the plots for the inverter and the transformer, respectively. The material composition of the inverter and the transformer is given in Table C.5. The mass of various materials was calculated from the total mass of the inverter and the transformer and their material composition.

For the inverter, electricity, fuel oil, natural gas, and heat from municipal waste incineration are the assumed energy sources [365]. The energy required from these sources was plotted against the rated power (2.5-20 kW). From the plots of energy required vs. rated power, best-fit curves were drawn, and the equations obtained were used to calculate the amount of energy used for a 5 MW inverter. Equations C.3-C.6 show the energy requirements from electricity, fuel oil, natural gas, and heat from waste incineration, respectively. In these equations, y is the energy required from various sources and x is the rated power (kW). To see the impact of the change in the fuel mix, natural gas instead of fuel oil and municipal waste was considered in sensitivity and uncertainty analyses. The sources of energy to manufacture transformers are electricity and heat from natural gas [366]. The amounts of electricity and natural gas were estimated based on the data provided by Burger Mansilha et al. [366] for a 75 kVA transformer. Table C.6 shows the manufacturing energy requirements for the PCS for the four stationary applications.

$$\text{Electricity (kWh)} \quad y = 5.6856x^{0.68} \quad (\text{C.3})$$

$$\text{Fuel oil (MJ)} \quad y = 0.1211x^{0.68} \quad (\text{C.4})$$

$$\text{Natural gas (MJ)} \quad y = 1.9131x^{0.68} \quad (\text{C.5})$$

$$\text{Heat from waste incineration plant (MJ)} \quad y = 4.9277x^{0.68} \quad (\text{C.6})$$

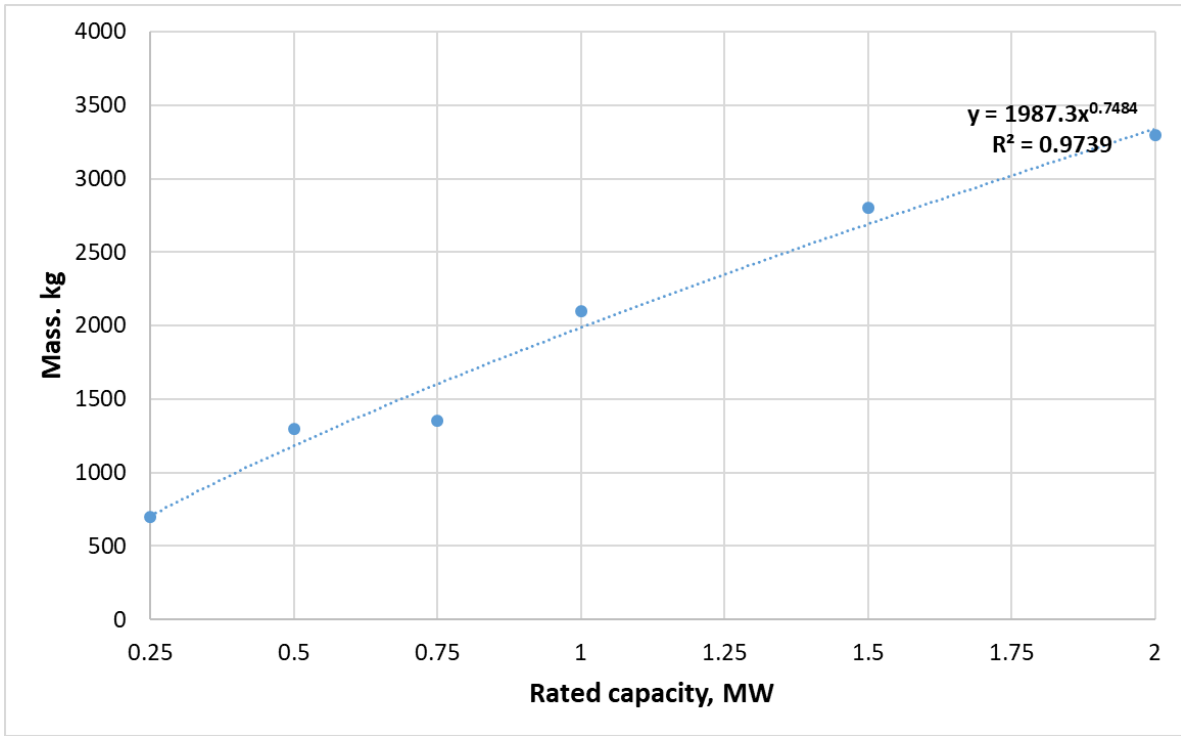


Figure C.1: The plot of mass vs. rated capacity for the inverter

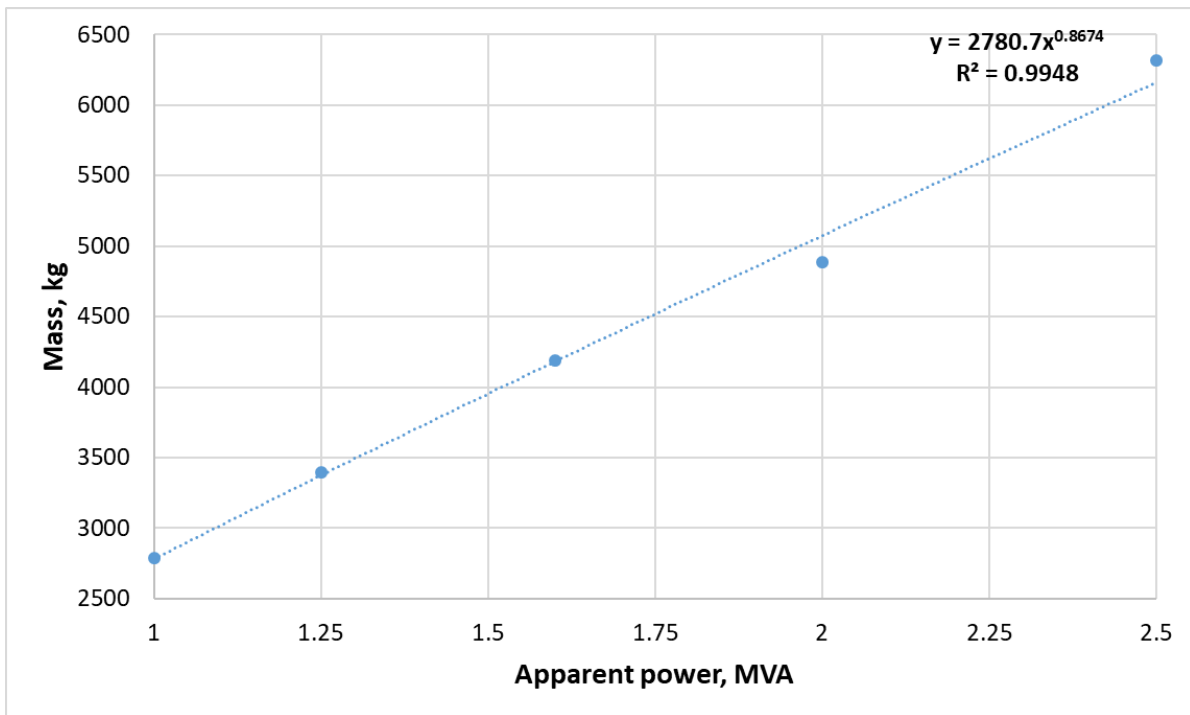


Figure C.2: The plot of mass vs. rated apparent power for the transformer

Table C.5: Material composition of the inverter and the transformer for the PCS

Inverter [584]		Transformer [585]	
Material	Wt (%)	Material	Wt (%)
Steel	60.24	Transformer oil ^b	24
Aluminium	17.74	Steel	56
Copper	12.40	Copper	12
Plastics ^a	9.62	Pressboard	3
		Paper	1
		Other	4

^a Polyamide, injection molding plastic was assumed [586].

^b Mineral oil was assumed for transformer oil [587].

Table C.6: Energy requirements for the manufacturing of inverters and transformers for the PCS

	Source	Bulk energy storage (S1)	T&D investment deferral (S2)	Frequency regulation (S3)	Support of voltage regulation (S4)
Inverter	Electricity (kWh)	18,341	3668	18,341	5502
	Fuel oil (MJ)	395	79	395	118
	Natural gas (MJ)	6299	1260	6299	1890
	Heat from waste (MJ)	16,224	3245	16,224	4867
Transformer	Electricity (kWh)	29,186	5837	29,186	8756
	Natural gas (MJ)	56,397	11,279	56,397	16,919

Table C.7: Recovery rate and specific energy consumption for various materials

Battery type	Materials recycled	Recovery rate (%)	Specific energy consumption (MJ/tonne)	Emission factor (kg-CO₂eq/tonne)
Na-S	Steel	50 [588]	21,028 [589]	1399 [589]
	Copper	50 [588]	14,300 [590]	1070 [590]
	Aluminium	50 [588]	30,697 [589]	1840 [589]
Li-ion	Li manganese oxide	50 (assumed)	34,863 [589]	3144 [589]
	Li nickel cobalt manganese oxide	50 (assumed)	202,981 [589]	13,830 [589]
	Wrought aluminium	50 [588]	26,767 [589]	1608 [589]
	Copper	50 [588]	14,300 [590]	1070 [590]
VRLA	Lead	98.30 [110]	4923 [589]	482 [589]
	Sulfuric acid	90 [110]	160 [44]	36 ^a
Ni-Cd	Steel	50 [588]	21,028 [589]	1399 [589]
	Cadmium	90 [363]	1260 [349]	102 [349]
	Nickel	50 (assumed)	22,441 [589]	1519 [589]
VRF	Electrolyte	95 [44]	160 [44]	36 ^a

^a Calculated from the electricity requirement and Alberta's electricity EFs.

C.3. Sensitivity and uncertainty analyses

A sensitivity analysis was conducted to find the influential input parameters used in the models. An uncertainty analysis was performed to report ranges for the net energy ratio and life cycle GHG emissions. Only the most impactful parameters identified in the sensitivity analysis were used in the uncertainty analysis. Table C.8 shows the ranges of input parameters used for the uncertainty analysis.

Table C.8: Input parameters for the uncertainty analysis

ESS/application	Parameter	Minimum value	Maximum value
Na-S	Round-trip efficiency (%)	70 [288]	90 [10]
	Depth of discharge (%)	70 [157]	90 [578]
	PCS efficiency (%)	90 [425]	97 [302]
	Energy density (Wh/kg)	100 [343]	206 [344]
	Manufacturing energy (MJ/Wh)	0.42 ^a	0.78 ^a
	Concrete floor thickness (m)	0.10 [581]	0.15 [581]
	Truck diesel consumption (L/tonne-km)	0.017 [591]	0.044 [591]
Li-ion	Round-trip efficiency (%)	85 [288]	98 [288]
	Depth of discharge (%)	75 ^b	90 ^b
	PCS efficiency (%)	90 [425]	97 [302]
	Energy density (Wh/kg)	90 [342]	170 [342]
	Manufacturing energy (MJ/Wh)	0.84 ^a	1.56 ^a
	Concrete floor thickness (m)	0.10 [581]	0.15 [581]
	Truck diesel consumption (L/tonne-km)	0.017 [591]	0.044 [591]
VRLA	Round-trip efficiency (%)	80 [288]	90 [288]
	Depth of discharge (%)	50 ^c	70 ^c
	PCS efficiency (%)	90 [425]	97 [302]
	Energy density (Wh/kg)	30 [346]	40 [346]
	Manufacturing energy (MJ/Wh)	0.29 ^a	0.55 ^a
	Concrete floor thickness (m)	0.10 [581]	0.15 [581]
	Truck diesel consumption (L/tonne-km)	0.017 [591]	0.044 [591]
Ni-Cd	Round-trip efficiency (%)	70 [314]	90 [314]
	Depth of discharge (%)	70 ^b	85 ^b
	PCS efficiency (%)	90 [425]	97 [302]
	Energy density (Wh/kg)	50 [347]	75 [348]

ESS/application	Parameter	Minimum value	Maximum value
	Manufacturing energy (MJ/Wh)	1.5 ^a	2.7 ^a
	Concrete floor thickness (m)	0.10 [581]	0.15 [581]
	Truck diesel consumption (L/tonne-km)	0.017 [591]	0.044 [591]
VRF	Round-trip efficiency (%)	70 [105]	90 [105]
	PCS efficiency (%)	90 [425]	97 [302]
	Number of cycles in lifetime	10,000 [28]	13,000 [28]
	Manufacturing energy (MJ/Wh)	0.52 ^a	0.96 ^a
	Concrete floor thickness (m)	0.10 [581]	0.15 [581]
	Truck diesel consumption (L/tonne-km)	0.017 [591]	0.044 [591]
	Tank wall thickness (m)	0.013 [580]	0.019 [580]
	Cell voltage (V)	0.8 [316]	1.55 [316]
	Vanadium concentration (mol/L)	1.5 [320]	2 [320]
Bulk energy storage (S1)	Rated power (MW)	5 [338]	100 [338]
	Discharge duration (h)	4 [28]	8 [28]
	Number of cycles per year	350 [31]	365 [213]
	Alberta electricity emission factor (kg-CO ₂ eq/MWh)	252 ^d [367]	559 ^e [367]
T&D investment deferral (S2)	Rated power (MW)	5 [338]	25 [338]
	Discharge duration (h)	2 [119]	5 [119]
	Number of cycles per year	248 [105]	250 [213]
Frequency regulation (S3)	Rated power (MW)	5 [338]	100 [338]
	Discharge duration (h)	0.25 [119]	1 [119]
	Number of cycles per year	9928 ^f	14,892 ^f
Support of voltage regulation (S4)	Rated power (MW)	5 [338]	30 [338]
	Discharge duration (h)	0.25 [207]	1 [51]
	Number of cycles per year	248 [105]	250 [340]

^a 30% variation from the default value was assumed.

^b Assumed to be a realistic range as most studies considered 80%.

^c Assumed to be a realistic range as most studies considered 60%.

^d Projected value for 2041.

^e 2021 emission factor including upstream emissions.

^f 20% variation from the default value was assumed due to the lack of data.

C.4. Impact of recycling on life cycle GHG emissions

A mix of virgin and recycled materials was assumed for material requirements for each battery technology to assess the impact of recycling. The GHG emissions from material recycling were estimated using the material recovery percentage, specific energy, and emission factors (see Table C.7). Figure C.3 shows the change in GHG emissions when recycling is included in the analysis. The GHG emissions are lower than in the base case without recycling for the ESSs considered. Although recycling adds energy to the life cycle energy use, it reduces the dependence on virgin materials, which are more energy-intensive than the recycled materials. For the Na-S ESS, the most energy-intensive material is β -alumina, and there is no developed process to recycle it. Recycling steel, copper, and aluminium reduces life cycle GHG emissions by only 2-5 kg-CO₂eq/MWh. The reductions in GHG emissions from the recycling of Li-ion and Ni-Cd ESSs are about 3-5 and 11-18 kg-CO₂eq/MWh, respectively, depending on the application. VRLA and VRF ESSs achieve the biggest advantage from recycling. Pb-A batteries are highly recyclable with a high recovery rate of more than 90% for lead and sulfuric acid [110]. With recycling, the life cycle GHG emissions of a VRLA ESS were reduced by 7-9%, depending on the application. For the VRF, V₂O₅ electrolyte production is the main source of energy use and resulting GHG emissions. According to Weber et al. [44], the electrolyte needs only 0.045 kWh/kg electricity for electrolyte re-balancing and recycling. If the electrolyte is recycled, the total GHG emissions can be reduced by 10% and 13% for S1 and S2, respectively, and 6% and 12% for S3 and S4, respectively.

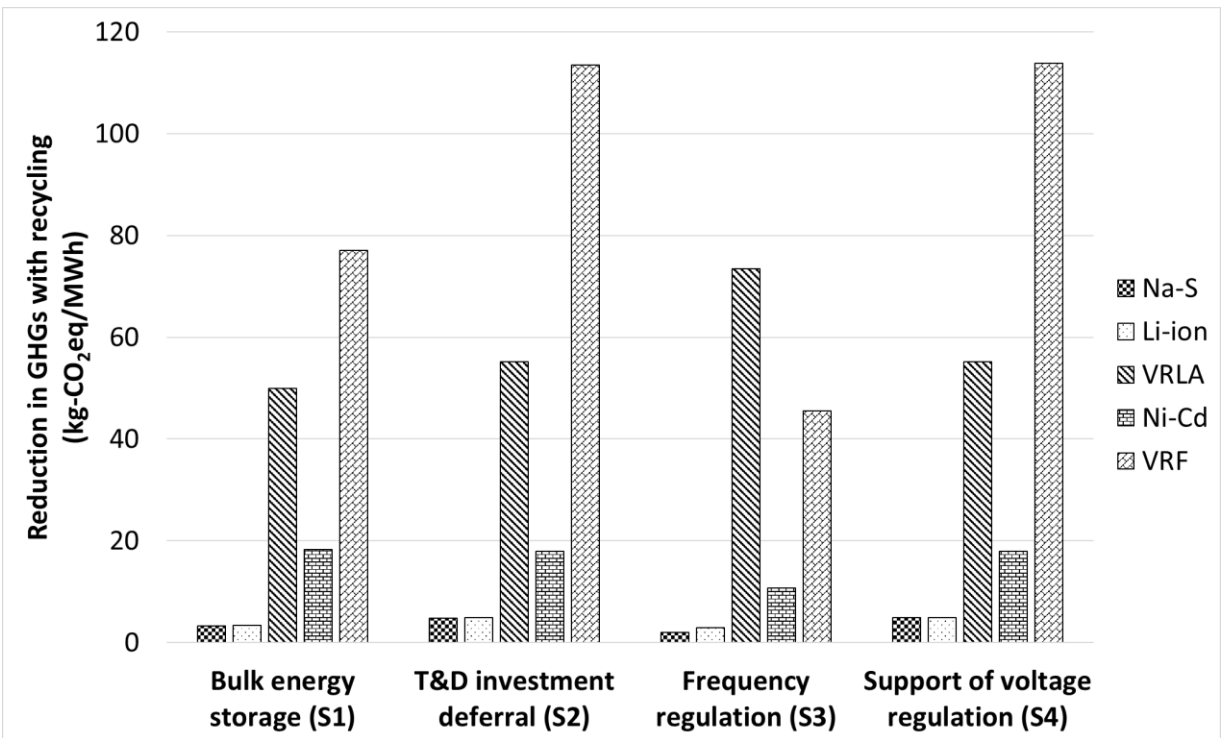


Figure C.3: Reduction of total GHG emissions from the recycling of battery materials

C.5. Additional results

The GHG emissions in the operation stage for the Canadian provinces are presented in Figure C.4, and Figure C.5 shows the sensitivity analysis for the life cycle GHG emissions of the VRF ESS for bulk energy storage.

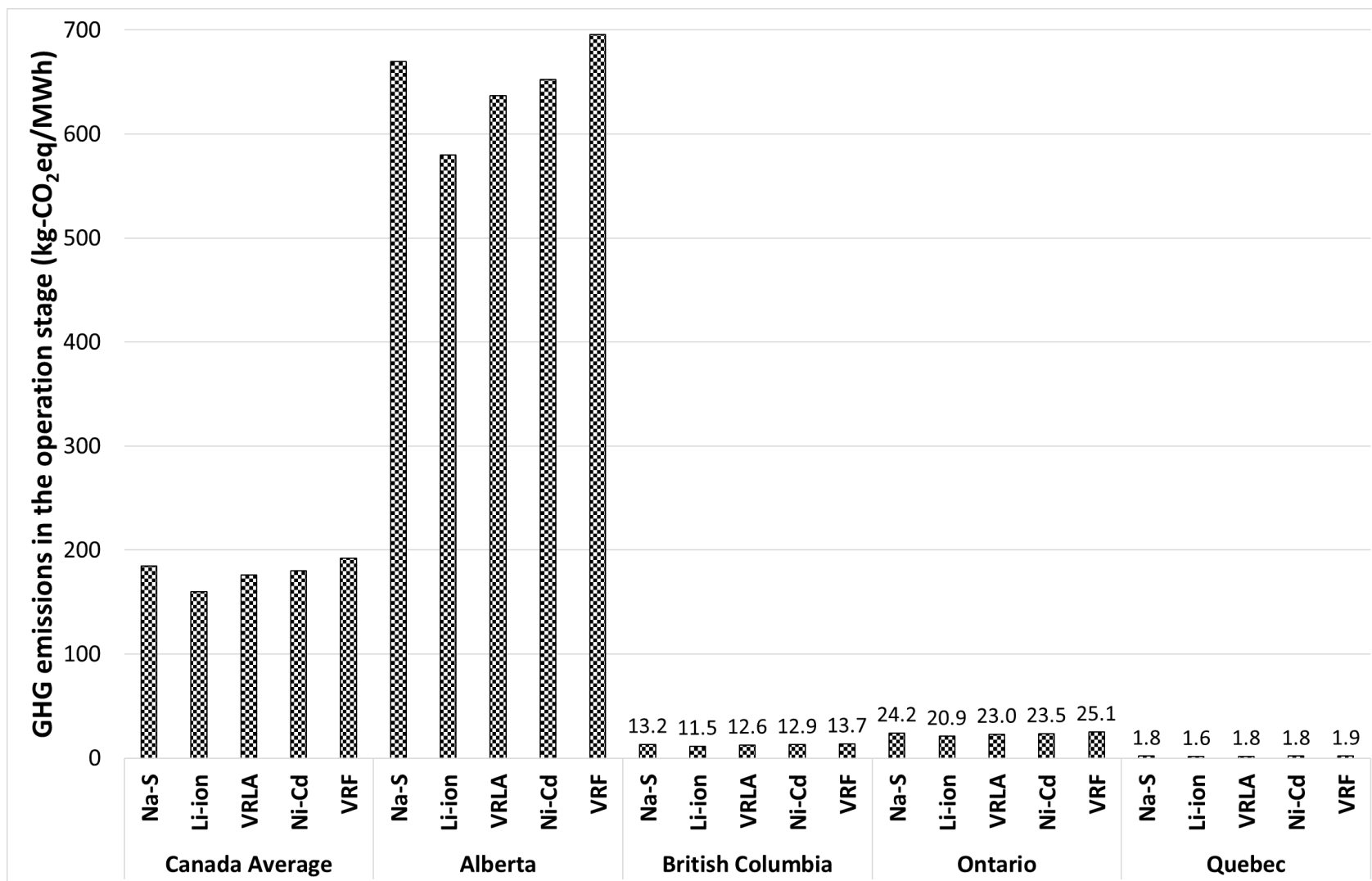


Figure C.4: GHG emissions in the operation stage

[Note: Na-S: sodium-sulfur, Li-ion: lithium-ion, VRLA: valve-regulated lead-acid, Ni-Cd: nickel-cadmium, and VRF: vanadium redox flow].

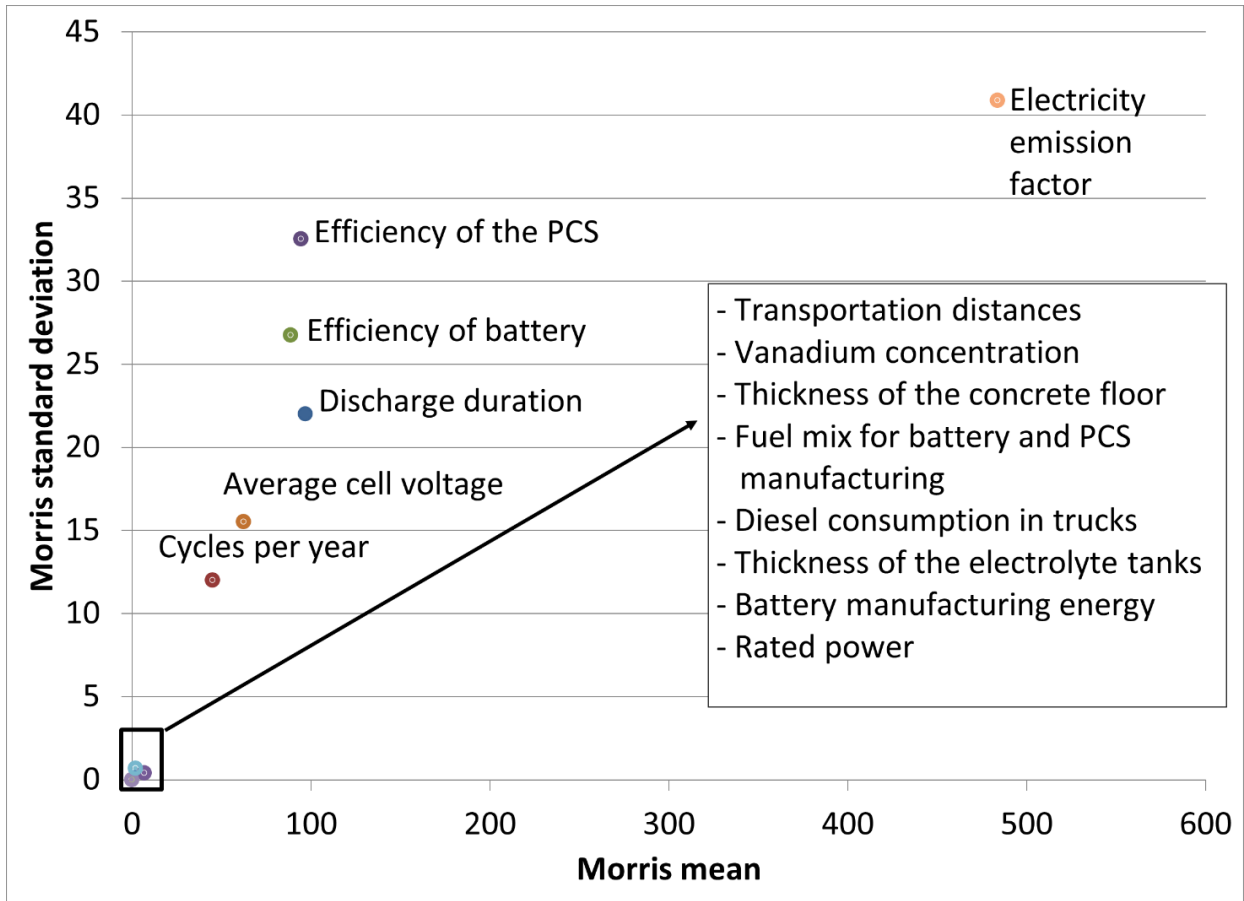


Figure C.5: Sensitivity analysis for the life cycle GHG emissions of the VRF ESS for bulk energy storage (S1)

Appendix D

D.1. Calculation of outer radius

The outer radius of a hollow composite rotor for the composite rotor flywheel energy storage system (FESS) was calculated using Equation D.1, adapted from Kailasan [201]:

$$r_o = \frac{1}{\omega_{max}} \sqrt{\frac{\sigma}{\rho \cdot N}} \quad (D.1)$$

where r_o is the rotor outer radius (m), σ is the tensile strength of the rotor material (Pa), ω_{max} is the maximum angular speed (rad/s), ρ is the density of the rotor material (kg/m³), and N is the safety factor.

The radius of a solid rotor for the steel rotor FESS was calculated using Equation D.2, adapted from Moore and Kraft [592]:

$$r = \frac{1}{\omega_{max}} \sqrt{\frac{8 \cdot \sigma}{\rho \cdot N \cdot (3 + \nu)}} \quad (D.2)$$

where r is the rotor radius (m), σ is the tensile strength of the rotor material (Pa), ω_{max} is the maximum angular speed (rad/s), ρ is the density of the rotor material (kg/m³), N is the safety factor, and ν is Poisson's ratio of the rotor material.

D.2. Additional results

Table D.1: The output cost results for flywheel energy storage systems with rated capacities from 1-40 MW

Storage system	Capacity	TIC (million \$)	RC (million \$)	LCOS (\$/MWh)	LCAS (\$/MWh)
Composite rotor	1 MW	\$1.55	\$0.04	\$217.76	\$183.39
FESS	5 MW	\$7.08	\$0.18	\$203.12	\$168.75
	10 MW	\$13.60	\$0.36	\$197.03	\$162.67
	20 MW	\$25.88	\$0.72	\$189.94	\$155.58
	40 MW	\$49.21	\$1.45	\$183.11	\$148.74
Steel rotor FESS	1 MW	\$1.18	\$0.10	\$175.07	\$140.70
	5 MW	\$5.06	\$0.49	\$156.92	\$122.56
	10 MW	\$9.61	\$0.97	\$151.42	\$117.05
	20 MW	\$18.28	\$1.95	\$146.41	\$112.05
	40 MW	\$34.76	\$3.89	\$141.55	\$107.18

Appendix E

E.1. Flywheel energy storage design

The useful energy stored in the flywheel was calculated using Equation E.1, adapted from Amiryar and Pullen [203]:

$$E = \frac{1}{2} k \pi \rho h (\omega_{max}^2 - \omega_{min}^2) (r_2^4 - r_1^4) \quad (E.1)$$

where E is the useful energy of the flywheel (J), k is the shape factor, ρ is the density of the rotor material (kg/m^3), h is the height of the rotor (m), ω is the angular velocity (rad/s), r_1 is the inner radius (m), and r_2 is the outer radius (m).

For a given speed, the outer radius of a hollow cylindrical composite rotor can be calculated using Equation E.2, adapted from Kailasan [451]:

$$r_2 = \frac{1}{\omega_{max}} \sqrt{\frac{\sigma}{\rho \cdot N}} \quad (E.2)$$

where r_2 is the outer radius (m), ω_{max} is the maximum angular velocity (rad/s), σ is the tensile strength of the material (Pa), ρ is the density of the rotor material (kg/m^3), and N is the factor of safety.

The radius of a solid cylindrical steel rotor can be calculated using Equation E.3, adapted from Moore and Kraft [593]:

$$r = \frac{1}{\omega_{max}} \sqrt{\frac{8 \cdot \sigma}{\rho \cdot N \cdot (3 + \nu)}} \quad (E.3)$$

where r is the radius (m), ω_{max} is the maximum angular velocity (rad/s), σ is the tensile strength of the material (Pa), ρ is the density of the rotor material (kg/m^3), ν is Poisson's ratio for the rotor material, and N is the factor of safety.

E.2. Material composition of 4340 alloy steel and chrome steel

Table E.1 shows the material composition of 4340 alloy steel for the steel rotor and chrome steel for the mechanical bearing.

Table E.1: Composition of 4340 alloy steel and chrome steel

4340 alloy steel [55]		Chrome steel [594]	
Composition	Wt (%)	Composition ^a	Wt (%)
Iron	95.50	Iron	96.91
Nickel	1.83	Chromium	1.45
Chromium	0.80	Carbon	1.04
Manganese	0.70	Manganese	0.35
Carbon	0.40	Silicon	0.45
Molybdenum	0.25		
Silicon	0.20		

^a Given their insignificant contribution, sulfur and phosphorous were not included [594].

E.3. Manufacturing of flywheel components

Table E.2 shows the specific energy requirements for the manufacturing of mechanical bearings. The values were calculated by summing the reported numbers from Ekdahl [482] for each manufacturing process. We assumed that the heat requirement is fulfilled by burning natural gas, as natural gas is widely used for industrial energy consumption. The standard conversion efficiency for heat production from natural gas was taken to be 85% [595].

Table E.2: The specific energy requirements for mechanical bearing manufacturing

Source of energy	Value (MJ/kg)
Electricity	26.12
Heat	8.51
Natural gas	3.18

Source of energy	Value (MJ/kg)
Liquefied petroleum gas	3.05
Fuel oil	2.10
Diesel	0.01
Coal	0.002

Table E.3 shows the energy requirements for the manufacturing of the power conversion system (PCS). The energy requirements for 2.5-20 kW PCSs, from Tschümperlin et al. [484], were used to construct Equations E.4-E.7. These equations were then used to quantify the energy requirements for the PCS systems (108 kW for the steel rotor flywheel and 100 kW for the composite rotor flywheel) used in this study.

Table E.3: The specific energy requirements for power conversion system manufacturing at various capacities

Capacity (kW)	Electricity (kWh)	Fuel oil (MJ)	NG (MJ)	Heat from municipal waste (MJ)
2.5	10.6	0.226	3.57	9.21
5	16.9	0.361	5.72	14.7
10	27.1	0.579	9.17	23.6
20	43.4	0.928	14.7	37.9
108 (calculated)	136.10	2.92	46.31	119.29
100 (calculated)	129.17	2.77	43.95	113.20

$$m = 5.6856x^{0.68} \quad (E.4)$$

$$n = 0.1211x^{0.68} \quad (E.5)$$

$$y = 1.9131x^{0.68} \quad (E.6)$$

$$z = 4.9277x^{0.68} \quad (E.7)$$

m , n , y , and z are the amount of energy from electricity (kWh), fuel oil (MJ), natural gas (MJ), and heat from municipal waste (MJ), respectively, and x is the capacity of the PCS (kW).

E.4. Emission factors

Table E.4: Emission factors used in the model for various energy sources

Energy source	Emission factor	Unit	Reference
Alberta electricity mix	0.59	kg-CO ₂ eq/kWh	[367]
British Columbia electricity mix	0	kg-CO ₂ eq/kWh	[367]
Saskatchewan electricity mix	0.50	kg-CO ₂ eq/kWh	[367]
Manitoba electricity mix	0	kg-CO ₂ eq/kWh	[367]
Ontario electricity mix	0.01	kg-CO ₂ eq/kWh	[367]
Quebec electricity mix	0.01	kg-CO ₂ eq/kWh	[367]
Canada average electricity mix	0.14	kg-CO ₂ eq/kWh	[367]
Municipal solid waste	1017	kg-CO ₂ eq/tonne	[596]
Natural gas	0.07	kg-CO ₂ eq/MJ	[597]
Fuel oil	0.09	kg-CO ₂ eq/MJ	[597]
Diesel for heating	0.08	kg-CO ₂ eq/MJ	[597]
Bunker fuel	0.08	kg-CO ₂ eq/MJ	[597]
Coal	0.10	kg-CO ₂ eq/MJ	[597]
Diesel for transportation	0.09	kg-CO ₂ eq/MJ	[597]
Liquefied petroleum gas	0.07	kg-CO ₂ eq/MJ	[597]

E.5. Sensitivity and uncertainty analyses

Table E.5: The input parameters and values for uncertainty analysis

Parameter	Minimum value	Maximum value
Number of cycles per year	3000 [598]	5000 [119, 598]
Flywheel efficiency (%)	85 [43]	95 [460]
Efficiency of the PCS (%)	90 [425]	98 [426]
Factor of safety	3 [451]	5 [451]
Tensile strength of steel (GPa)	0.80 [599]	1.4 [454]
Tensile strength of composite (GPa)	2 [427, 451]	6 [427]
Composite rotor inside-to-outside diameter ratio	0.50 [451]	0.75 [451]
Specific power of the motor/generator (kW/kg)	1.2 [465]	1.6 [465]
Steam generator efficiency (%)	80 [595]	95 [595]
Standby loss for the steel rotor flywheel (%)	1 [205]	5 [395]
Standby loss for the composite rotor flywheel (%)	0.5 [485]	2 [486]
Metal recycling rate (%)	90 [600]	98 [600]
Specific diesel requirement in landfilling (L/tonne)	1 [487]	3 [487]
Specific electricity requirement in landfilling (kWh/tonne)	2 [487]	12 [487]
Specific diesel consumption in transportation (L/tonne-km)	0.017 [490]	0.044 [490]
Electricity grid emission factor (kg-CO ₂ eq/MWh)	0 [367]	590 [367]
Specific energy for composite material production (MJ/kg)	632 [601]	840 [601]
Specific emission factor for composite material production (kg-CO ₂ eq/kg)	42.5 [601]	54.2 [601]
Specific energy consumption in curing of composite rotor (MJ/kg)	4 [479]	11 [479]
Energy demand for solar PV plant (MJ/MWh)	360 [602]	1800 [602]
Energy demand for wind power plant (MJ/MWh)	10 [602]	1200 [602]

Parameter	Minimum value	Maximum value
Emission factor of electricity from solar (kg-CO ₂ eq/MWh)	26 [603]	183 [603]
Emission factor of electricity from wind (kg-CO ₂ eq/MWh)	3 [283]	45 [283]
Transportation distance (km)	50 ^{§§§}	4800 ^{****}

E.6. Additional results

Although electricity from solar and wind was considered for charging in the base case, additional results are provided for different electricity mixes used in four Canadian provinces. Figure E.1 shows the life cycle GHG emissions when electricity for charging comes from the grid. Figure E.2 shows the Morris sensitivity analysis for life cycle GHG emissions of a steel rotor flywheel energy storage system. In this case, electricity is supplied from a solar photovoltaic source. The points in the figure represent the input parameters used in the model. The parameters in zone 1, such as transportation distance, recycling rate of metals, and diesel and electricity requirements in landfilling, are insignificant, with a lower Morris mean and standard deviation. Zone 3 includes the critical input parameters that influence the results significantly. The most influential parameters are standby loss, efficiency of the PCS, Alberta's electricity emission factor, and the electricity emission factor for solar. The parameters in zone 2 are moderately sensitive; these parameters are flywheel efficiency, factor of safety, tensile strength of steel, and the number of cycles.

^{§§§} Assumed distance within Alberta

^{****} Distance from Nova Scotia to Alberta calculated using Google Maps

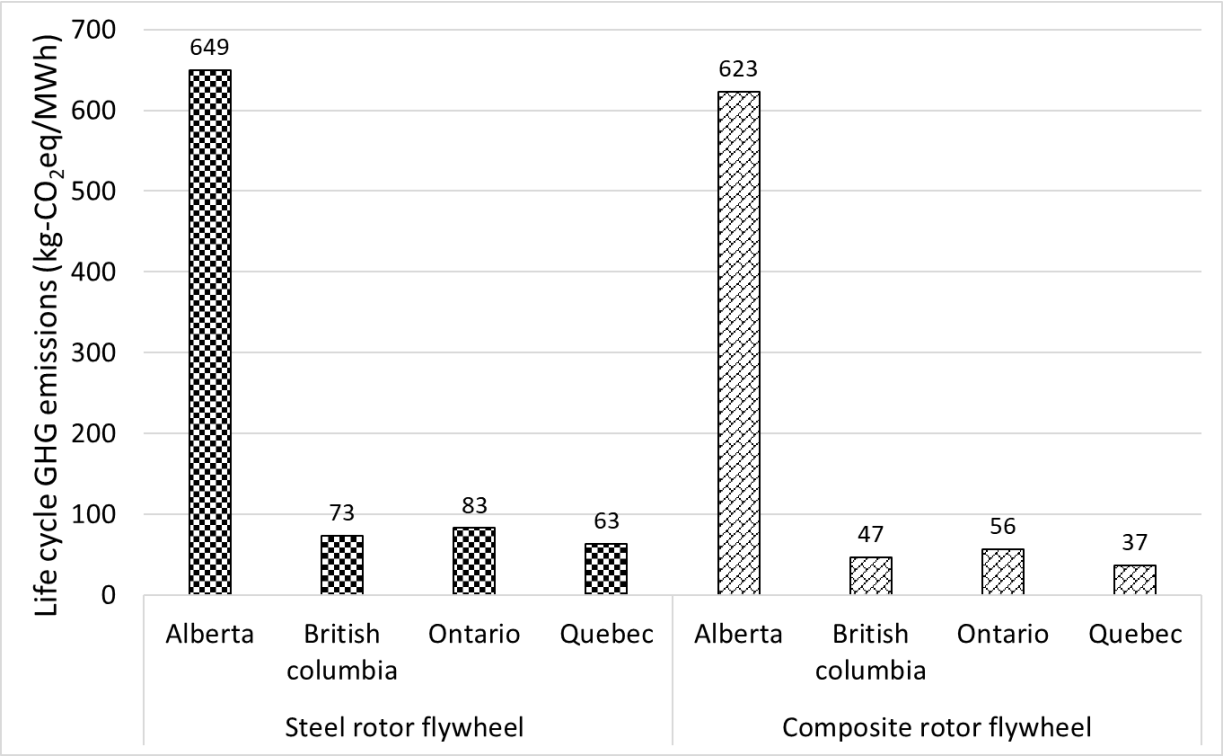


Figure E.1: Life cycle GHG emissions with electricity for charging from different provincial grids

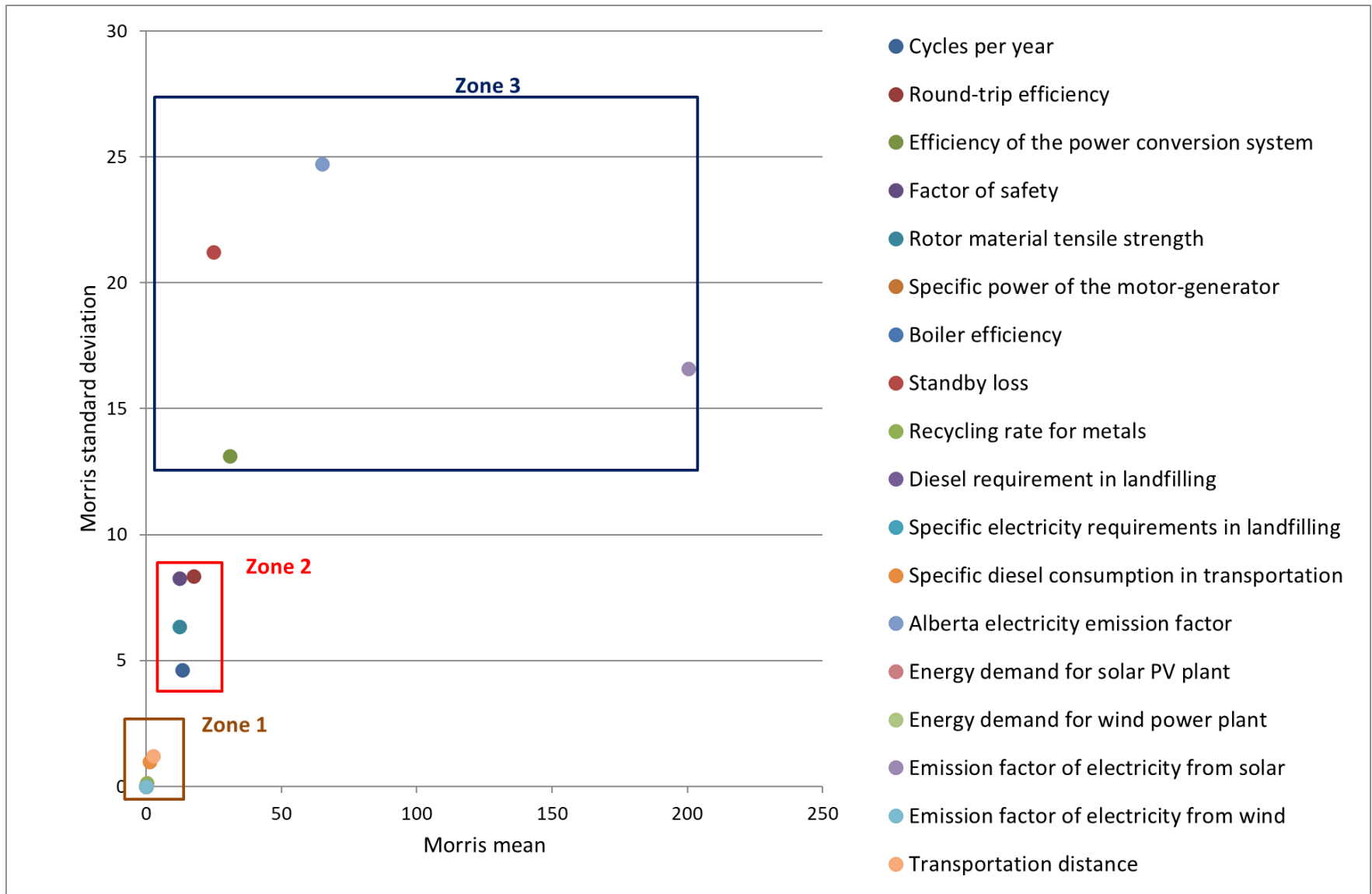


Figure E.2: Sensitivity analysis for the life cycle GHG emissions of a steel rotor flywheel energy storage system

List of publications

Book chapter

1. Rahman MM, Oni AO, Gemechu E, Kumar A. Environmental impact assessments of compressed air energy storage systems: A review. In: Fokaides PA, Morsink-Georgali PZ, Kylili Angeliki, editors. Environmental Assessment of Renewable Energy Conversion Technologies, Elsevier Inc., Amsterdam, The Netherlands, 2022 (In press).

Journal publications

1. Rahman MM, Oni AO, Gemechu E, Kumar A. Assessment of energy storage technologies: A review. *Energy Conversion and Management*. 2020;223:113295.
2. Rahman MM, Oni AO, Gemechu E, Kumar A. The development of techno-economic models for the assessment of utility-scale electro-chemical battery storage systems. *Applied Energy*. 2021;283:116343.
3. Rahman MM, Gemechu E, Oni AO, Kumar A. The greenhouse gas emissions' footprint and net energy ratio of utility-scale electro-chemical energy storage systems. *Energy Conversion and Management*. 2021;244:114497.
4. Rahman MM, Gemechu E, Oni AO, Kumar A. The development of a techno-economic model for the assessment of the cost of flywheel energy storage systems for utility-scale stationary applications. *Sustainable Energy Technologies and Assessments*. 2021;47:101382.
5. Rahman MM, Gemechu E, Oni AO, Kumar A. Energy and environmental footprints of flywheels for utility-scale energy storage applications. *e-Prime*, 2021;1:100020.

6. Rahman MM, Gemechu E, Oni AO, Kumar A. The development of a techno-economic model for assessment of cost of energy storage for vehicle-to-grid applications in a cold climate. Submitted to Energy, Elsevier.